Modelling and Control of Thermal Deflection in Machine Tool Structures

Steven Fraser

A Thesis

in

The Department

of

Mechanical Engineering

Presented in Partial Fulfilment of the Requirements
for the Degree of Master of Applied Science
Concordia University
Montreal, Quebec, Canada

November 1992

ISBN 0-315-87262-4

Canada

ABSTRACT

Modelling and Control of Thermal Deflection
in Machine Tool Structures

Steven Fraser

A significant limitation on the fabrication of precision parts is the inherent inaccuracy of the machining process due to the thermal deformation of the machine tool structure. The problem has begun to receive considerable attention as the threshold for machining tolerances has dropped, and automated machine tools have become widespread. At the present time, the only commercially viable method of reducing the operational thermal deformation of a machine tool structure is fluid showering, a costly and inconvenient process that is only available for exceptional applications.

This thesis presents a technique for reducing thermally induced machining error by measuring the structural deformation of the machine tool while it is in operation, and compensating for it on-line. The structural thermal deformation is indirectly measured by relating it to point temperatures on the structure through a process model. A technique for determining the approximate analytical form for the temperature distribution in the structure will be developed in the thesis.

The thermally induced deflection of the structure is compensated by an array of artificial electric heaters, attached to the surface of the structure, and controlled by a PC based numerical control system. The control system manipulates the artificial heaters to calibrate a deflection pattern in the structure that eliminates the natural deformation at key points.

The performance of the control system is evaluated using a finite-element test model of a simulated machine tool structure. The control system approach tested in this thesis provides a reduction of thermally induced error that is comparable to the commercial method of fluid showering, but at a fraction of the cost and complexity.

ACKNOWLEDGEMENTS

This thesis is respectfully dedicated to my parents for their valuable encouragement and support.

The author also expresses his sincere gratitude to his thesis supervisors Drs. M.O.M. Osman and H. Attia for their patience, support, and guidance. Their knowledge, distinction, and standards of excellence inspired me to strive for my highest potential.

The financial support of the National Science and Research Council is also acknowledged and appreciated.

The author is also grateful to Alexandra Kessoglou-Rossicci and Basil Dane for their help in preparing the manuscript.

TABLE OF CONTENTS

Chapter page

Chapter page

Chapter page

LIST OF FIGURES

LIST OF TABLES

LIST OF SYMBOLS

Symbol	Definition
a	variable = h/(kw)
A	constant
b	constant
c_p	specific heat
d_x	deflection error in x-direction
d_z	deflection error in z-direction
d_1	deflection of lower arm
d_2	deflection of upper arm
e	error
F_1, F_2	variables defining analytical temperature solution
g(t)	Crump summation
g(r,th)	heat generation per unit volume
G(s)	transfer function to IHCP
G_1, G_2	variables defining analytical thermal deflection solution
h	convective heat transfer coefficient
H(s)	forward transfer function to DHCP
$H^*(s)$	transfer function of direct problem minus singularities
I	imaginary component of s
J_0	zeroth order Bessel function
k	thermal conductivity
K	constant
K_*	constant
K_c	PID gain
L	effective delay
n	integer
N	number of iterations
P	magnitude of PID controller
$\underline{q}$	heat generation
q	non-dimensional heat generation
Q(s)	transformed heat generation
Q_{c1}	control heater 1
Q_{c2}	control heater 2

Symbol	Definition
Q_{c3}	control heater 3
Q_d	disturbance heater
r	radius
r_0	radius of generating ring
R	real component of s
s	Laplacian variable
S	error residual
S	maximum slope of step solution
t	time (dummy variable)
T	temperature
T(s)	transformed temperature
T1(s)-T8(s)	thermal deflection transfer function
T^*	absolute temperature
T_{0_*}	unstressed reference temperature
T_0^*	absolute unstressed reference temperature
T_{a_*}	ambient temperature
T_a^*	absolute ambient temperature
T_D	derivative time
T_R	reset time
T_s	temperature step solution
$T_s(s)$	transformed temperature step solution
T_{ss}	steady-state temperature
u	transformation variable = $r\sqrt{(\gamma - a)}$
u	dummy variable
w	thickness of plate
x	space variable
y	space variable
Y	measured temperature
z	transformation variable = (R + a)/b
z	space variable
α	regularization factor
α	diffusivity
α_c	coefficient of thermal expansion
B	gradient constant for steepest descent method
B	Hankel variable
γ	integration constant
δ	deflection error
$d\delta$	differential elongation

Symbol	Definition
ϵ	strain
ϵ	error
θ	rotation about x-axis
Θ	transformed variable
Θ	Hankel transformation
ρ	density
τ	time
ϕ	rotation about y-axis
Φ	step solution to direct temperature problem
ψ	rotation about z-axis
ω	frequency
$\Im$	imaginary component of function
$\Re$	real component of function
$\mathcal{L}$	laplace transform

CHAPTER 1: INTRODUCTION

The development of achievable machining accuracy over the last 100 years has been led by the ever increasing demands of the industrial environment for greater precision in machine tools. The present threshold of achievable dimensional tolerances has been reduced below 0.01 μm for ultra precision machining processes, and is on the order of 5-10 μm for 'normal' machining processes such as precision lathes, grinding machines, and lapping machines. It has been predicted that the ultra precision machining threshold will drop below 0.001 μm by the turn of the century, and the threshold for normal machining processes will be below 1 μm.

Before the turn of the last century, structural imperfections in the machine tools was the primary source of machining error. As production capabilities improved, and normal machining tolerances were reduced, the mechanical effect of static and dynamic deflection came to be the dominant source of machining error. Now as mechanical effects are gradually being reduced, the problem of thermal deflection is receiving more attention. The widespread introduction of automated NC machine tools has aggravated the problem further, because the human operator has traditionally been the primary source of compensation.

Compensating for thermal deflection is a relatively new aspect of machine tool design. The problem can be significantly reduced by designing the structure for optimal thermal stability, and by simple measures like cooling fluid, chip removal, and external location of heat sources. Although the problem can be reduced at the design stage, there will always be some residual thermal deformation of the machine tool and work piece

because of the thermal loading that is inherent to the machining process. When high precision tolerances are required, it becomes necessary to employ active compensation for thermally induced error. The only commercially viable method for actively controlling thermal deformation available today is fluid showering of the machine tool structure and cutting tool. Fluid showering of the structure is expensive and inconvenient. The machine tool must usually be located in a sealed cubicle, and a refrigeration source is required.

There has been a significant amount of research in the area of active measurement and compensation for thermally induced machining error, but the work has not yet led to a practical solution to the problem. The major obstacle to active measurement and compensation is the problem of measuring the thermal deflection of the cutting tool while the machine tool is in operation. Sensitive deflection measurement equipment is easily damaged in the machining environment, and the readings are often obscured by the cutting process. Most attempts at measuring the thermal deflection have focused on the development of process models which relate the thermal deflection error to some other variable which is more easily measured. The problem with modelling a machine tool structure is that the geometry and boundary conditions are complex, and resist accurate modelling. Most of the models that have been developed by the researchers have either been too simple and inaccurate, or too complicated and slow to incorporate into a real time control system. Thermal deflection modelling of the machine tool structure and cutting tool is presently the effective barrier which must be overcome before a commercially viable deflection control system is possible.

The objective of this thesis is to develop a multi-axis feedback control system to reduce structural thermal deflection error in machine tools to a level comparable with fluid showering. The control system must be universal, flexible, applicable to real machine tools of any type, and insensitive to all kinds of measurement and actuation errors. The problem of measuring the deflection error will be solved by developing a process model to relate it to another variable which is more easily measured.

The first part of the thesis focuses on the problem of modelling the thermal deflection in a machine tool structure for control purposes. The model must be accurate and reliable enough to predict the thermal deflection in the structure to an accuracy greater than 1 μm, for an arbitrary load condition. The model must also be computationally simple enough to keep up with a control system with a cycling frequency in excess of 0.1 Hz. These are conflicting requirements that demand a new approach to the modelling process. A new method of determining the approximate analytical form of a model to represent a complex physical process will be developed in this thesis. Once the approximate analytical form of the solution is determined, it serves as the approximate mathematical base on which to curve-fit the solution to the real problem. It will be shown that this method of generalizing an analytical solution is able to meet the stringent requirements of the thermal deflection control model better than any other type of model, including finite-element models, analytical models, and empirical models.

Once the thermal deflection models have been developed, they will be assembled into an operational control system, the effectiveness of which will be tested on a finite-element test model of a simplified machine tool structure. The numerical controller will

be a 486-PC, and compensation will be effected through an array of artificial electric heaters attached to the surface of the structure. The numerical controller generates a deflection field with the artificial heaters that counter-balances the deflection error of the disturbance heat generation, and yields a net deflection error approaching zero at key points on the structure. It will be shown that the accuracy and reliability of the method is comparable to some of the commercially available methods of fluid showering, but at a fraction of the cost and complexity.

A number of original procedures and mathematical derivations will be developed in the course of this thesis. and these are listed here:

-A new method of determining an approximate analytical model for a real process will be developed, called the *generalized analytical solution* method. The generalized model meets the requirements of real time control better than any other type of model for complex real problems.

-In order to implement the generalized analytical method on the structure of a machine tool, the analytical solution for a thin infinite plate with a convective boundary condition on its face, and a circular heat source at its centre, will be derived for the first time in this thesis by the method of the modified Hankel transformation.

-The analytical step solution to the infinite plate model will be transformed to a Laplace system of variables analytically, by complex integration.

-A general numerical procedure will be developed to use the Laplace transformation to solve the inverse problem of heat conduction. The method allows the Laplace method to be extended to complicated and numerically defined functions that do not have an analytical transformation.

-A new method of solving the exponential integral at extreme points will be developed based on methods of variational calculus.

-A new method of numerically transforming complex functions from the Laplace domain to the time domain will be developed. The new method is faster and more reliable than the numerical methods previously available, and it allows for the transformation of singularity functions which do not satisfy the existence theorem of the Laplace Transformation

PART I: THE LITERATURE REVIEW

CHAPTER 2: LITERATURE REVIEW OF THERMAL DEFORMATION IN MACHINE TOOL STRUCTURES

2.1 The Problem of Thermal Deformation of Machine Tool Structures

2.1.1 The Sources of Inaccuracy in Machine Tools

The accuracy of a machine tool is described by its ability to correctly position a cutting tool relative to the work piece, and maintain the correct position during the cutting operation. The sources of inaccuracy derive from *i*) structural imperfections, *ii*) measurement effects, *iii*) mechanical effects, and *iv*) thermal effects:

i) Structural imperfections include deviations in the uniformity of guideways, and the imperfect alignment of the spindles, chucks, and bearings. This is often called kinematic inaccuracy, because it derives from positioning errors that occur in the absence of any thermal or mechanical loading. The accuracy of the machining can be no greater than the accuracy of the machine itself, so much depends on the production capability of the manufacturer.

ii) Measurement effects are the uncertainty in the measured positions of the cutting tool and workpiece. The accuracy of the machine is limited by the ability of the operator to correctly position the cutting tool. This is especially true for numerically controlled machine tools, where the cutting path is programmed from a computer model, and the tool is positioned automatically without any conventional reference point.

iii) Mechanical effects include the static and dynamic compliance of the machine structure and cutting tool, and the wear of the cutting tool. Mechanical effects have

received a considerable amount of attention over the past twenty years, as industry has demanded greater and greater accuracy from the machine tools.

iv) Thermal effects are the changes in the relative position between the cutting tool and work piece that derive from the thermal loading of the machine tool. Thermal effects are an inevitable consequence of the machining process because of the thermal loading and large physical dimensions of the structure. The sources of thermal loading include changes in the ambient temperature, and steady and quasi-static temperature gradients due to internal sources of heat generation. In contrast to the problem of mechanical loading, thermal loading has not been extensively studied, for a number of reasons, primarily [1]:

- A general lack of interest due to inadequate understanding of the problem by the general user.
- The need for no load tests.
- The need for a described 'duty cycle' appropriate to each test.
- The requirement for instrumentation not normally found on the shop floor.

The focus of this thesis will be the problem of the thermal deformation due to the thermal loading of the machine tool. This only addresses part of the inaccuracy problem discussed above, but it is a significant part, especially since researchers and manufacturers have successfully reduced many of the other sources of inaccuracy.

2.1.2 The Sources and Nature of the Thermal deflection Error

There are two principal sources of thermal deflection error: uniform changes in the ambient temperature, and temperature gradients from internal sources of heat generation. There are three predominant places where the deformation occurs: the structural frame of the machine tool, the cutting tool, and the work piece. The deformation of the cutting tool and the work piece is due to the high intensity heat generation at the tip of the cutting tool, and from the chips and cutting fluid [2]. The deformation of the structure is primarily due to internal sources of heat generation, such as bearings, motor, and gearbox [3]. Changes in the ambient temperature can also have a serious effect on structural thermal deformation, but this is much easier to control. The heat of the cutting process and the heat of the drive system are really an inevitable consequence of the machine's operation, but environmental conditions are more easily controlled by air conditioning or air showering, sometimes within a sealed cubicle [4].

2.1.3 The Relative Significance of Thermal Deformation

The significance of thermal deformation as compared to other sources of inaccuracy depends on a number of factors, including the size of the machine tool and the work piece, and the co-efficients of thermal expansion. From an examination of available test data, Attia [1] was unable to find any conventional machine tool with a co-efficient of expansion of less than 0.01 mm/m for a temperature change of $\pm 1^0$ C. Thus, thermal deformation can be a significant problem even in relatively small machine tools, and it is usually a very serious problem in large machine tools [5].

Opitz (cited in [6]) states that the errors caused by thermal deformations have, in many cases, the same order of magnitude or higher than the errors due to kinematic inaccuracy and the static and dynamic compliance. Mottu [7] states that from his experience, 50 to 60% of the errors in precision parts result from thermal errors. As a rule of thumb, Weck (cited in [6]) stated that thermal effects in steel parts become significant at a tolerance of about 2.5 μm. For pieces over 25 cm long the threshold is about 25 μm, and for aluminum pieces it can be as high as 125 μm. Weck is referring to the problem of thermal deformation of the work piece, but in most conventional operations the structural deformation of the machine tool is a greater source of thermal error. For most machine tools of conventional size, thermal deformation is a significant source of error for tolerances below 10 μm.

There is a prevailing ignorance among users and manufacturers of the cost and nature of thermally induced errors [3,8]. While significant progress has been made in understanding and reducing some of the other sources of error, very little progress has been made in the area of thermal deformation. Mottu [7] credits this to the adaptive operator, whose skill and experience allows him to produce an acceptable product in spite of some impossibly bad thermal problems. Indeed, many machine tools are bought and sold with so little attention to their thermal characteristics that the only requirement is that they be warmed up prior to accuracy testing [3].

The situation has been changing however, with the introduction of automated NC machines. Without the skill and judgement of a human operator to compensate for thermal errors, the machine tool manufacturers must resort to other means. At the same

time, high technology fields such as high energy lasers have pushed the threshold of machining tolerances below 0.025 μm. Since thermally induced errors are at least two orders of magnitude higher than that, the problem of thermal deformation cannot be ignored any longer [3].

2.1.4 Minimization of Thermally Induced Error

2.1.4.1 Reducing the Thermally Induced Error at the Design Stage

The internal heat sources of a machine tool are the various elements of the drive and power transmission system, including motors, gears, bearings, pumps, hydraulic oil, and the machining process itself. It has been indicated in [9] that 60% of the power input to a machine tool is dissipated in the drive and power transmission system, inducing machining error by the thermal deformation of the structural frame. The remaining 40% finds its way into the cutting tool and work piece, and into the chips and cutting fluid. The local deformation of the cutting tool is higher than the deformation of the frame because of the extremely high temperature of the cutting tool, but the total deformation is usually less because of the small dimensions [2]. Much of the heat from the cutting process flows back into the structural frame of the machine tool, resulting in additional deformation of the structure.

Much of the thermally induced deformation can be eliminated at the design stage, by methods as simple as proper chip disposal, and cooling the cutting fluid [6]. Other techniques include:

-External location of the major heat sources, like the motor and bearings [10].

-The utilization of thermal symmetry, so that the thermal deformation is symmetric about some point or axis, and the net deflection of the point or axis is zero [3,11].

-The appropriate positioning and attachment of heat sources, so that the deformation in critical directions is minimized [12,13].

-The use of structural materials which are capable of rapid and uniform distribution of heat to minimize temperature gradients.

-Using insulation to control the flow of heat, and direct it away from critical areas [14].

-Direct temperature control of the structure by a shower or bath of cooling fluid [15,16].

2.1.4.2 Compensation for Thermal Deflection at the Design Stage

Optimizing the design of machine tools to protect against thermal error is an important practice, but there will inevitably be some residual thermal deformation. Also, structural redesign is not feasible for existing machine tools, only for new designs. Even at the design stage, it is often preferable to solve a problem electronically rather than by elaborate mechanical solutions, given the advanced state of numerical measurement and control technology.

Compensation schemes for thermal deflection are particularly attractive for numerically controlled machines, because implementing the correction is as simple telling the numerical controller how much to move to compensate. The major obstacle is the problem of measuring the relative deflection between the cutting tool and the work piece

while the machine tool is in operation. It is not practical to measure it directly because the delicate measuring equipment is easily damaged, and chips and cutting fluid would obscure the readings. Most compensation schemes measure the thermal deflection indirectly, by another physical property that is directly related to the thermal deformation but is more easily measured. The most frequently used property is the surface temperature of the structure [17].

2.2 The Measurement of Thermal Deflection

2.2.1 Direct Measurement

Tonshoff et al. [18] studied the problem of direct deflection measurement. They looked at a number of displacement sensors with a resolution less than 1 μm, including touching gauge fingers (resolution 0.5 μm), and non-touching optical sensors (resolution 1 μm). The sensors were applied directly to the machine tool, and used to intermittently sample the relative deflection between the cutting tool and work piece.

Direct measurement establishes the real position of the tool. This allows for the compensation of all sources of inaccuracy, whether or not they are thermally induced. It also eliminates the need to model the structure, as is required for indirect measurement. The disadvantage of direct measurement is that the delicate sensors are easily damaged during the operation of the tool. Also, their presence is intrusive, interfering with the smooth operation of the machine tool. Finally, the presence of chips and cutting fluid in the working environment makes the readings unreliable, especially for optical type sensors. After thoroughly studying the problem, Tonshoff concludes that

"The direct and continuous detection of thermally induced displacements in most machine tools is not possible, because direct working sensors cannot be used during the machining process.".

Tonshoff et al. [18] tested another direct measurement technique using integrating expansion sensors. The sensors are placed at strategic locations on the machine tool structure between the machining table and the cutting tool. The sensors are tightly fixed to the machine structure, and directly measure the thermal expansion. The expansion is integrated in a line from the work to the tool, giving a direct estimation of the thermal deflection in the structure. the weakness in this method is the relatively low resolution of the expansion sensors.

2.2.2 Indirect Measurement of Thermal Deflection from a Thermal Deflection Model

Most compensation schemes utilize an alternate physical property to indirectly measure the thermal deflection, because of the difficulties associated with direct measurement. Sartori, Balsamo, and Marques [19] use a thermal deflection model that divides the structure into a number of simpler components, and use a combination of finite-element equations and polynomial curve-fitting to represent the components. The model expresses the structural thermal deformation as a function of the temperature distribution. The measurement scheme requires more than 100 thermocouples, and the thermal model consists of some 1400 equations. The authors believe that the large number of thermocouples is a minor problem, because of the low cost of sensors and

data acquisition cards. The results showed that 80 to 85% of the deformation could be explained by the model.

The obvious problem with this method is the large number of thermocouples and the complexity of the deflection model. Many of the thermocouples are located in difficult positions, around internal bearings and spindles, and the positioning must be accurate if the model is to yield good results. The control system for the test machine is updated every 5 to 10 minutes. This is a very large time delay for a control system, and it is related to the complexity of the model.

In an on-line process there is a compromise between speed and accuracy. Improving the accuracy of an on-line model may actually cause a deterioration in the performance of the control system if it increases the computation time of the controller, and creates a large time delay between the input sampling and correcting signal. With a 5 to 10 minute time delay, a lot of uncontrolled deformation can occur between changes in the controller output, and the control system is always 5 to 10 minutes behind the present state of deformation.

2.2.3 Indirect Measurement of Thermal Deformation from Limited Temperature Data

The most common methods of indirectly measuring thermal deflection avoid the data acquisition problems associated with measuring the complete temperature distribution. They utilize an empirical transfer function that relates the thermal deflection to a small number of measured temperatures which are representative of the overall temperature distribution and deflection. Chiappulini et al. [20] use five measured

temperatures at five points on the structure, one close to each of the major internal sources of heat in the machine tool. The transfer function relating the measured temperatures to the thermal deformation is based on an empirical polynomial equation of the form:

$$\delta = b_0 + \sum_{i=1}^{k} b_{ii} T_i^2 + \sum_{i<j}^{k} b_{ij} T_i T_j + \ldots \qquad (2.1)$$

The empirical parameters are found by optimizing the fit between the empirical equation and the response of the test structure for a variety of operating conditions. The displacement response of the structure is measured by three displacement transducers mounted on the mandrill nose of the test milling machine.

Chiappulini et al. [20] made the assumption that the sources are independent of one another and the principle of superposition applies. The assumption was necessary to simplify the calibration of the parameters, which would otherwise require multi-variable optimization. This assumption was their largest single source of error because of the practical difficulty of running each of the sources independently in a real machine tool.

Jedrzejewski and Modrzycki [21] used a similar approach and the same empirical transfer function as Chiappulini and Gianotti, except that they use a finite element model of the machine tool structure to curve fit the empirical parameters. The model does not have the same practical limitations as the real structure tested by Chiappulini. The sources can be operated independently, so that the parameters can be linearly curve-fit for each measured temperature. Another advantage is that the model determines the deflection, so it is unnecessary to measure it with a transducer. But the accuracy of the

empirical transfer function depends on the accuracy of the finite-element model of the structure. Real structures are difficult to model, especially in the area of the heat sources, so discrepancies between the transfer function and the real structure are inevitable.

Ichimya et al. [22] used an empirical transfer function to relate discrete temperatures to the thermal deformation of a milling machine structure. The empirical constants are determined separately for each input load condition, so the parameters must be changed each time the loading conditions change. With a continuously variable load, the accuracy of the results deteriorates rapidly.

The major disadvantage of an empirical transfer function is that the form of the empirical equation is not related to the mathematical form of the real solution. The empirical equation can be matched to the physical system for only a small number of test inputs, but the thermal loading of the real structure is infinitely variable. There is no correlation between the physical form of the model and the physical form of the solution, so the response to untested inputs is unpredictable. Increasing the flexibility of the transfer function to accommodate variable loading requires higher order polynomial expressions, making the transfer function cumbersome and the empirical constants difficult to determine.

2.2.4 The Mathematical Justification for the Limited Temperature Data Model

The work of Balsamo et al. [19] is based on a clear physical relationship between the temperature distribution in a solid and its thermal deformation. The work of Chiappulini et al. [20] and Jedrzejewski et al. [21] does not have a mathematical basis,

it is based on empirical observations. Nevertheless, there is a mathematical justification for using discrete temperatures to predict the thermal deformation. The temperature profiles of discrete points in the vicinity of a heat source are uniquely defined by the magnitude of the heat generation. Thus, there is a direct relationship between discrete temperatures profiles in the vicinity of the heat sources and the thermal boundary conditions of the structure. The thermal boundary conditions define the complete temperature distribution, which in turn defines the deflection. Hence, there is a direct physical link between discrete temperatures in the vicinity of the sources and the thermal deflection [23]. The methods proposed above do not attempt to actually define the relationship, they only recognize that it exists, and curve fit a polynomial solution. In this thesis the relationship will be better identified by studying its mathematical basis.

2.2.5 Exact Modelling of Thermal Boundary Conditions to Indirectly Measure Deflection

The limitation of empirical models is that they do not define the physical relationship between the input and output variables. A number of researchers, including Moriwaki [24] and Jedrzejewski et al. [25], have gone another route, attempting to exactly model the thermal and deflection processes which occur in the machine tool structure. This is a tedious process for a real machine tool because the geometry and thermal boundary conditions are complex, and resist exact modelling [26]. The method is used mostly for the analysis of lathes, because the thermally induced error is mainly attributable to the thermal elongation of the main spindle, a phenomenon known as *spindle growth*.

Moriwaki uses the axial symmetry of the main spindle and housing system of a lathe to represent it by a two dimensional finite difference model. The heat generation comes from the thrust and radial bearings supporting the spindle. The greatest obstacle to exact modelling is determining the actual heat generation of the bearings. Jedrzejewski et al. [25] found a discrepancy of a few hundred percent between the power generation actually observed in modern bearing assemblies and those predicted by the existing theories. The large discrepancy is due to the significant improvements is design and manufacture of bearing assemblies that have occurred in the last twenty years. Jedrzejewski et al. [25] also found that the power generation of a bearing depends on a number of parameters, including the speed, the internal mechanical forces, and the operating temperature. Furthermore, they found that the power generation of a bearing depends on its age and its condition. Thus, the relationship between the input parameters and the power generation is not constant over the useful life of the machine tool.

2.2.6 The Difficulties Associated with Exact Modelling Machine Tools

2.2.6.1 Numerical Modelling

Exact modelling of machine tools can only be done numerically, by finite element or finite difference methods because of the extreme complexity of the geometry and boundary conditions. The methods suffer from uncertainty in the boundary conditions, as discussed above, but there are also problems with modelling real elements like spindles and bolted brackets [25,27,28]. In the internal mechanisms of a machine tool, the heat flux is defined by conduction, but also convection and radiation from one part

to another because of the proximity of the mechanical elements. This type of heat flux is difficult to model, even numerically.

Harary (cited in [6]) investigated the finite element method against a number of test structures, and found serious disagreement with respect to the accuracy needed for machine tools. Hicks et al. (cited in [6]) have also had poor results with FEA codes: "The finite element method is a very good means of predicting mechanical stress. However for thermal deformations, we believe that it is only able to predict about 20% of the deformation."

2.2.6.2 Analytical Models

Exact analytical modelling is a difficult, or even impossible solution for most real problems. Exact analytical solutions are only available for some simple geometries like slabs, cylinders, and spheres, for certain prescribed boundary conditions. The models cannot be readily assembled into more complex structures because the boundary conditions at the interfaces of the elements would tend to be complex, and could not be handled analytically.

Sometimes an exact analytical model is used to represent a more complicated problem, even though the shortcomings of the model are recognized, and certain inaccuracies in the solution are expected. The Rosenthal solution for the temperature distribution in a weldment puddle is derived with the assumptions of pure conduction, constant thermal properties, and a single point heat source [29]. Although the assumptions are not correct for a real welding process, the simplified model is widely

used as an approximate solution to the real process. Another familiar example is the lumped heat capacity model of a solid. The exact analytical solution to the lumped model is treated as an approximate solution to a real problem with a small Biot number, where Bi=lh/k [30].

2.2.7 Indirect Measurement By Approximate Analytical Modelling

Analytical models are the most desirable basis for a control algorithm because they are both flexible and computationally efficient. Finite element algorithms are normally too slow for control purposes, and the exact modelling suffers from the limitations discussed in the last subsection [31]. Empirical models are probably the most cumbersome of all, and the solution is only valid for the limited test inputs for which it was derived. While analytical models are the most appealing, they suffer from two major handicaps: the limited number of solved problems, and the difficulty in measuring some analytical parameters.

In their paper on Weldment control, Bates and Hardt [32] employ an analytical model to represent the temperature distribution around the arc in a welded plate. The problem with the analytical model is that two of the analytical parameters defining the temperature distribution cannot be measured or accurately predicted. Bates and Hardt solved the problem by treating the analytical parameters as empirical parameters, and calibrating them on-line to fit the actual solution. Assuming that for some parameter values the model can predict accurate isotherms, they reduce the problem to an on-line method of determining the 'optimal' values of the parameters. The procedure is as

follows: 1) measure the temperature at two points on the plate. 2) Adjust the parameters to get an optimal match between the measured temperatures and those predicted by the analytical model. 3) Using the parameter values to define the analytical solution, predict the entire temperature distribution in the welded plate.

The empirical parameters lose their physical identity, so the optimal values do not correspond to the correct analytical ones. The procedure does more than determine the values of two unknown analytical constants, it finds an optimal fit between the solution to the analytical model and the physical solution, offsetting some of the intrinsic weaknesses of the analytical model. The method can be extended to other physical problems, developing a combination analytical/empirical solution that is custom fit to the physical problem. If the form of the analytical solution is similar to the physical solution, then the analytical/empirical solution can approach the accuracy of fully analytical solution. This is a very powerful method that will be developed further, later on in the thesis.

2.3 Summary of the Thermal Deflection Review

The objective of this thesis is to estimate the thermal deformation of a machine tool structure, and then compensate for the deformation with a numerical control system. The deflection of the structure cannot be measured directly, as discussed in section 2.2.1, so it will have to be measured indirectly by an alternate physical property. The deflection of the structure is directly related to the complete temperature distribution, but it is impractical to measure it directly, and the complexity of the transfer function makes it

unsuitable for on-line control, as discussed in section 2.2.2. Devising a thermal model of the structure in addition to the deflection model limits the scope of the input to the thermal boundary conditions rather than the temperature distribution, as discussed in section 2.2.3. But it is difficult to measure the thermal input directly, because the power generation of the bearings depends on too many parameters and the relationship is unstable over the life of the machine tool, as discussed in section 2.2.5. The most practical input for control purposes is a small number of discrete temperatures at strategic locations on the structure, as proposed in section 2.2.3. The physical justification for a link between discrete nodal temperatures and thermal deformation was given in section 2.2.4, but the mathematical form of this relationship has never been determined. An empirical transfer function based on a polynomial equation was introduced in section 2.2.3, but it must be rejected because it is too awkward, and unreliable for untested inputs. Exact numerical solutions based on finite element and finite difference models, like the ones in section 2.2.6.1, must also be rejected because they are too slow and inaccurate. The best procedure is to determine a combination analytical/empirical solution, by the method discussed in section 2.2.7. The thermal deflection model relates the thermal deflection to simplified thermal boundary conditions, but this still leaves the problem of determining the boundary conditions. This can be done by a similar method to the one given in section 2.2.7. Measure a small number of discrete temperatures in the vicinity of a heat source, and then optimize an empirical parameters of the model so that the model fits the measured temperatures. The general form of this problem is called the *inverse problem* of heat transfer, and it will be treated in detail in the next chapter.

Once the boundary conditions have been identified, the thermal model gives the temperature distribution, and the deflection model gives the thermal deflection.

CHAPTER 3: LITERATURE REVIEW OF THE INVERSE PROBLEM

3.1 Introduction to the Inverse Problem

The *direct problem* in heat conduction involves the determination of either the heat flux or temperature distribution in a structure when the initial and boundary conditions are known. The *inverse heat conduction problem* (IHCP) arises when an unknown boundary condition must be determined on the basis of internal temperature measurements. The determination of boundary conditions is an important element of heat transfer because it is often the first step in the analysis of a real system when the boundary conditions cannot be measured directly. There are other problems that are commonly referred to as inverse problems, including parameter estimation and sensitivity analysis, and the techniques developed to treat those problems are similar [33].

There are a number of inherent difficulties associated with the inverse problem, and these are grouped into three major categories: *i*) the difficulty of expressing the solution in explicit form, *ii*) instability, and *iii*) the non-uniqueness of the solution. These three difficulties will be discussed in the next section. It will be shown that special techniques are required to deal with the problem, because it defies the usual methods of solution. In section 2.2.3, the Stoltz [34] method will be introduced and used as an example to illustrate the difficulties associated with the inverse problem and the special character of the solution. More practical solution techniques will be introduced in the later sections.

3.2 Special Difficulties Associated with the Inverse Problem

3.2.1 The Difficulty with Obtaining an Explicit Solution

With most problems in heat transfer there is a direct and one to one correspondence between the input and output variables [33]. For a fully defined input, such as the heat generation at a boundary, there corresponds a unique temperature distribution, which is the solution to the direct problem. This relationship can be reversed: for a defined temperature distribution there must correspond a boundary condition, which is the solution to the IHCP. A *chiral* problem is one which is mathematically similar in the forward and backward directions. The mathematical expression for a linear spring is chiral because the direct problem $F=kx$, and the inverse problem $x=F/k$, are mathematically similar. A linear differential equation is also chiral if the input is the forcing function.

Most problems in heat transfer are not chiral because there is a preferred orientation for the solution. The basic structure of the heat conduction equation makes it more difficult to obtain an explicit solution for the boundary conditions than for the internal heat or temperature distribution. The boundary conditions are normally applied to the general solution once the differential equation has been solved, so the boundary conditions are integrated into the solution and it is usually not possible to separate them and solve explicitly. Burgraff [35] derived explicit theoretical solutions to the IHCP for a number of basic shapes, including a slab, cylinder, and sphere. Burgraff's method is to define the solution as an infinite series, such that the problem becomes chiral and an explicit solution to the IHCP is possible. Burgraff's procedure is not a practical one

because it only applies to simple shapes and the solution cannot be stabilized by the methods that will be introduced in the following sections. The significance of his work, from the point of view of this thesis, is that it demonstrates that chirality is determined from the method of solution, and is not necessarily an intrinsic element of the problem.

In most of the methods that will be presented, the chirality of the problem makes it impossible to express the boundary conditions as an explicit function of the internal temperature. The problem can only be solved by assuming a functional form for the boundary condition, and then solving the direct problem [36]. The functional form of the boundary condition contains some unknown parameters which are solved explicitly, and this becomes the solution to the IHCP. This creates another problem, because assuming the functional form of the solution in advance means that the functional form of the input is defined by the problem, and so the input cannot be specified in advance. This is the source of the non-uniqueness of the solution which will be discussed shortly.

3.2.2 Instability

The early research done by Stoltz [34] and Burgraff [35] recognized that the solution to an inverse problem suffers from an inherent instability because of the delayed and damped nature of the solution to the direct problem. Attia et al. [37] used the finite-element method to investigate the stability of the IHCP in machine tool structures. Figure 3.1 shows their finite-element model of a simplified machine tool structure, along with the steady-state isotherms for a unit heat generation of a source. The model is exposed to a convective boundary condition on its upper and lower faces. The transient

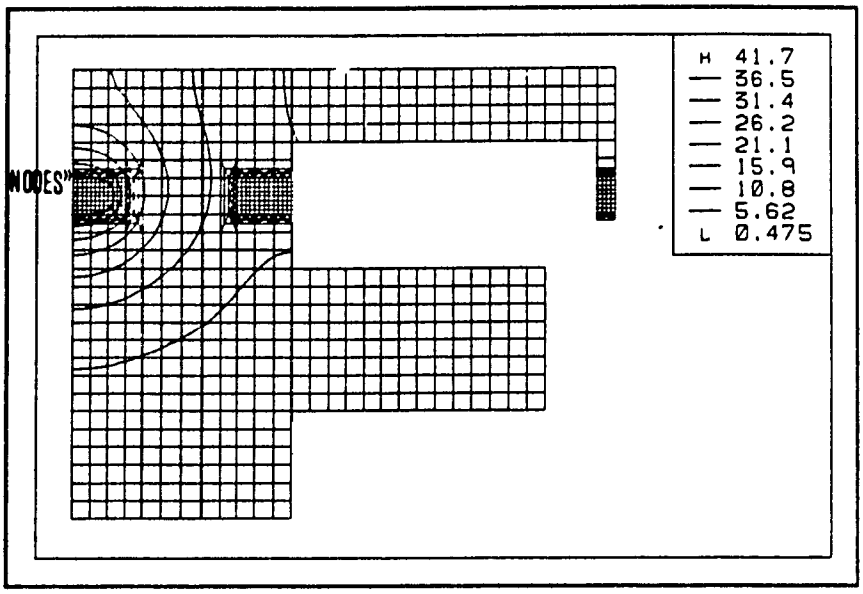

Figure 3.1: Finite-Element Model of Machine Tool Structure Showing Isotherms [37]

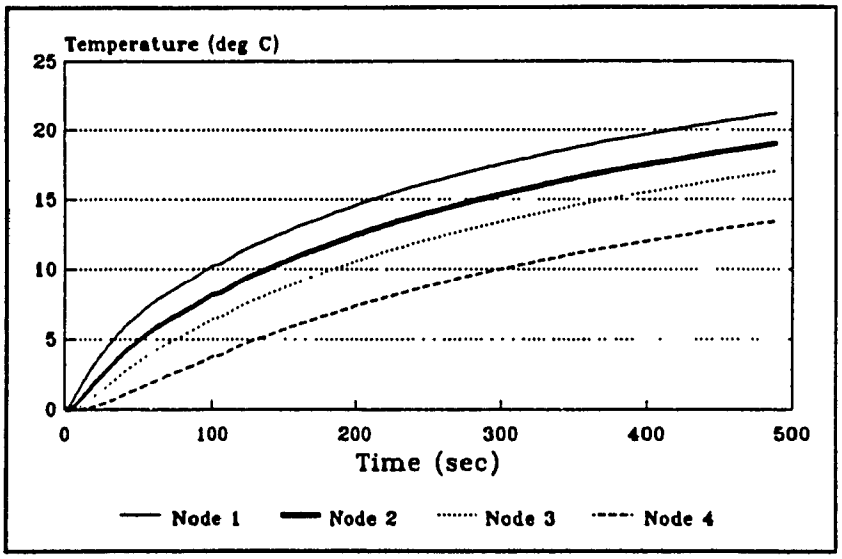

Figure 3.2: Temperature Profiles for Four Nodes in the Proximity of a Heat Source [37].

temperature profiles for four nodes on the surface of the model are given in figure 3.2, when the source is subjected to a unit step heat input at t=0. The distance between the node and the active boundary increases progressively from node 1 through node 4. The greater the distance between the node and the generating boundary, the smaller the temperature rise, but more importantly, the greater the time lag between the step change in the boundary and the response of the temperature profile. This shows that the gain between the input and output for the direct problem approaches zero as $t \to 0$. If the problem is inverted then the gain approaches infinity as $t \to 0$. Small measurement errors can lead to instability because they correspond to large changes in the boundary generation. A solution is said to be unstable when small changes in the input variable x produce significant changes in the output variable y. Mathematically, this is the condition that occurs when:

$$\frac{dy}{y} > \frac{dx}{x} \tag{3.1}$$

or,

$$\frac{dy}{dx} > \frac{y}{x} \tag{3.2}$$

where,

x is the input variable
y is the output variable

Murio et al. [38] demonstrated the instability of the IHCP by taking the Fourrier transformation of a one dimensional infinite slab problem. They showed how the solution to the IHCP multiplies every Fourier frequency component in the input by a factor of $\exp\sqrt{[\omega/2]}$, demonstrating that the IHCP is highly ill-posed for high frequency inputs.

3.2.3 The Non-Uniqueness of the Solution

The solution to the inverse problem is not unique for discrete input data because the mathematical form of the input determines the structure of the solution, and with sampled data the mathematical form is unknown. When solving a direct problem, it is the boundary conditions that determine the form of the governing equation [36]. To illustrate this, consider the one dimensional heat transfer equation for a plate in polar co-ordinates:

$$T'' + \frac{1}{r}T' - aT = \frac{1}{\alpha}\dot{T} \qquad (3.3)$$

If there is no convective boundary on the plate then the last term on the left hand side of the equation drops out. Thus, it is the boundary conditions that determine what mathematical form the solution will take. In a direct problem, the boundary conditions are specified by the problem, so the form of the solution is known in advance. But in an inverse problem the boundary condition is what must be determined so its form is unknown and thus the form of the input is unknown also. This can lead to problems in practical situations where the input is obtained experimentally. Arbitrarily assuming a mathematical form for the output can lead to inaccurate results, because the form of the input can be fundamentally altered in the process.

When solving a direct problem, the input is always defined continuously and uniquely in the time domain [36]. When the input is sampled at discrete intervals, a functional form for the data is always assumed so that the input is defined continuously and there is only one possible solution to the direct problem. The input to the IHCP is

not continuously defined for discrete input data, so there is no unique solution in the sense of a direct problem. This can be understood by reference to figure 3.3. Figure 3.3 shows how more than one continuous functions can be equal to [T] at each T_i. Any [q] which generates a continuous T(t) that matches [T] at each t_i is a solution to the IHCP. This combined with the inherent instability of the inverse problem can lead to an unstable, oscillatory solution. This point will be addressed later in the chapter. In the case of a direct problem, sampled data is used as the basis for a continuous function, say a series of steps or line segments. Since the functional form of the input is defined continuously, the solution is a unique one.

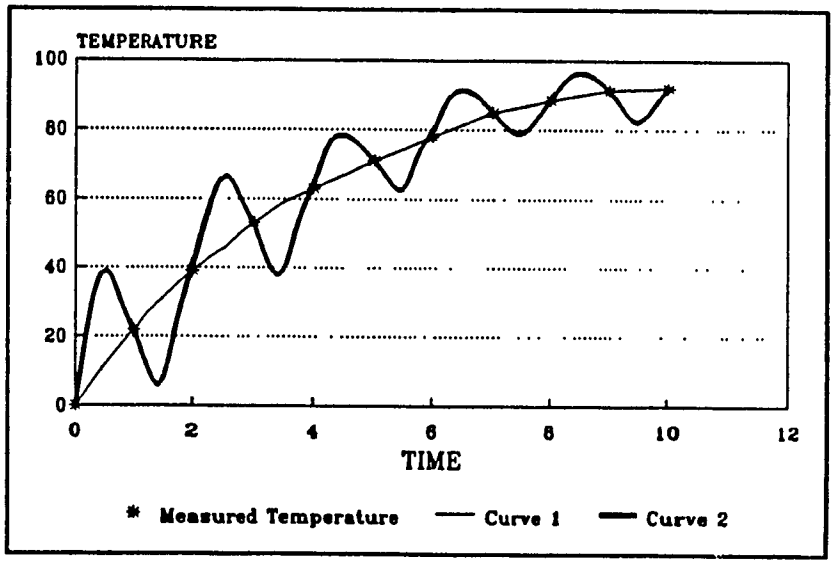

Figure 3.3: Possible Solutions that fit Discrete Temperature Data

3.3 The Stoltz Solution

One of the first general methods to solve the inverse heat conduction problem was developed by Stoltz [34]. His method is based on the Duhammel integral, and is applicable to any linear problem where the geometric conditions do not change. The Duhammel integral states that the solution of any linear system to an arbitrary input can be found through a convolution integral of the input function with the step solution of the system. Mathematically, the Duhammel integral is expressed as follows:

$$T(r, t) = T_0 + \int_0^t q(\tau) \frac{\partial \Phi (r, t-\tau)}{\partial t} d\tau \qquad (3.4)$$

where $\Phi(r,t)$ is the step solution for T(r,t) and q(t) is the input. For the inverse problem, it is T(r,t) that is known and q(t) that must be found. But as is usually the case with the inverse problem, the output variable is not readily available in explicit form. Stoltz assumes the form of the output q(t) to be a series of constant steps, and expresses equation (3.4) in finite-difference form as follows:

$$[T] = [\Phi] [q] \qquad (3.5)$$

where $[\Phi]$ is a transformation matrix, or the finite-difference representation of equation (3.4)
[T] is the matrix of temperatures T_i
[q] is the matrix of step magnitudes q_i

The next step is to invert matrix $[\Phi]$ and solve explicitly for [q]:

$$[q] = [\Phi]^{-1} [T] \qquad (3.6)$$

The inverse matrix $[\Phi]^{-1}$ does not have to be solved because it is an upper triangular matrix. The q_i can be found sequentially starting with q_1, q_2, and so on. Stoltz's derivation does not actually use this matrix formulation, he derives the same sequential algorithm directly from equation (3.4).

Stoltz's procedure is very simple and versatile method for linear inverse problems, but there is no effort to control the inherent instability of the solution. Furthermore, it is only required that [q] be a solution to equation (3.6), whether or not it is the desired solution. At small sampling intervals, random errors in the temperature measurements induce wide oscillations in the q_i values. The accuracy that can be obtained from the method is limited by the inability to reduce the sampling interval.

Stoltz uses a solution to a direct problem to solve the corresponding inverse problem. This is generally true for all of the inverse methods because of the nature of the heat conduction equation, as discussed previously.

3.4 Regularization

3.4.1 Whole Domain Regularization

Since Stoltz's paper in 1960, other researcher have sought ways to increase the stability of inverse problems. There are two specific problems which must be addressed: 1) The inverse problem opens the door to more than one possible solution because the input function is not defined continuously in the time domain, and 2) measurement errors and numerical round off errors lead to instability because of the large output gain for high frequency inputs. Figure 3.4 shows two possible inverse solutions for a hypothetical

heat generation [q]. The solutions were obtained by the Stoltz method for the transient temperature profile in a convecting plate. Both satisfy the input function [T] at each time t_i, but one is relatively stable and the other is oscillatory. The smooth function is probably the correct solution to the physical problem, but an unregulated procedure like the Stoltz method might just as easily produce the oscillatory solution, especially if the sampling interval is small and the measurement data contains errors. A number of Soviet researchers, including Alifanov and Artyukhin [39], and Tikanov [40], developed a method of biasing an algorithm so that it converges to a particular type of solution. This method is called whole domain regularization, and it makes an algorithm much more likely to converge to a stable solution than to an oscillatory one [36,39,40]. The method requires a solution to the direct problem, call it T(t), where T is the temperature at some interior node in a solid, due to a heat input q(t). If $Y(t_i)$ are the measured temperatures

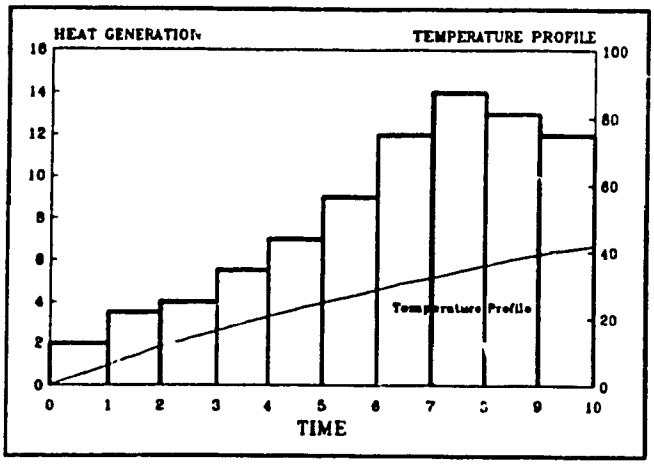

Figure 3.4a: Stable Solution

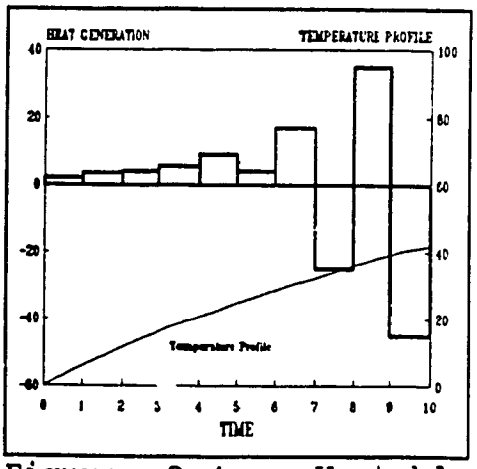

Figure 3.4a: Unstable Solution

Figure 3.4: Possible Solutions for q(t) from Inversion of Temperature Profile

at times t_i, then without regularization the error residual is defined by:

$$S = \sum_{i=1}^{n} (Y_i - T_i)^2 \qquad (3.7)$$

If S is differentiated with respect to q_1, q_2,....q_n, and each equation is equated to zero, a system of n equations is generated for n unknown q_i. If Y(t) is the Duhammel integral, then the solution is equivalent to the Stoltz method and there is exact matching of Y, and T_i [41]. With exact matching, the method suffers from the same stability problems as the Stoltz method. To overcome this problem Tikanov introduced an extra term into the error residual [40]:

$$S = \sum_{i=1}^{n} (Y_i - T_i)^2 + \alpha \sum_{i=1}^{n} q_i^2 \qquad (3.8)$$

The extra term is called the zeroth-order regularization term. By minimizing S with respect to q_1,...q_n, the optimal solution for q_1,...q_n accommodates the condition that the q_i's be as small as possible, as well as minimizing the error residual. Since these are conflicting requirements, the choice of α is critical. If $\alpha=0$, then exact matching between Y_i and T_i is obtained. As $\alpha \to \infty$, the regularization term dominates and q_i is zero for all values of i. A similar method, called first order regularization, minimizes the following residual [36,39,40]:

$$S = \sum_{i=1}^{n} (Y_i - T_i)^2 + \alpha \sum_{i=1}^{n-1} (q_{i+1} - q_i)^2 \qquad (3.9)$$

In this case, there is a compromise between minimizing the error residual, and the first derivative of the solution $q(t_i)$. With both zeroth order and first order regularization, the

algorithm is more likely to converge to a smooth solution like curve 1 in figure 3.3, rather than curve 2. Oscillatory solutions tend to have large magnitudes and abruptly changing slopes. Thus, an algorithm which minimizes these characteristics tends to converge to the more stable solution. On the other hand, with regularization there is no longer exact matching between Y_i and T_i. Second order regularization is biased toward the solution with the smaller second derivative. It is obtained by minimizing S defined by the following equation [36,39,40]:

$$S = \sum_{i=1}^{n} (Y_i - T_i)^2 + \alpha \sum_{i=1}^{n-2} (q_{i+2} - 2q_{i+1} + q_i)^2 \qquad (3.10)$$

Regularization is an extremely powerful technique which can be applied to linear as well as non-linear problems. All that is required is a solution to the direct problem, and the means to solve an nxn system of equations which may or may not be linear. Numerically, the most challenging problem is solving the nxn solution matrix. As the step size is decreased, the size of the matrix increases, and so does the computer time required to solve it. This is especially true when the matrix is non-linear. Although the speed of the algorithm is always significant, it is especially critical for the purpose of real time control because the speed of the algorithm defines the cycle time of the digital controller. An inversion method which increases the accuracy of the solution will not necessarily improve the performance of the control system if it increases the computation time as well.

Alifanov et al. [39] used the regularization method to stabilize a solution to a non-linear inverse problem. The problem is a generalized one-dimensional heat conduction

equation corresponding to heat transfer in a porous object with internal heat and mass evolution. The procedure generates a system of non-linear algebraic equations with a symmetric, five-diagonal, positive definite matrix. The result illustrates the problem with the regularization technique. If the time step is small, then the solution to the system of equations is time consuming.

3.4.2 Sequential Regularization

It is possible to reduce the size of the solution matrix by a method called sequential regularization [41]. The time domain is divided into segments, and a regularized solution for each of the time segments is obtained. In the extreme case where the time segments comprise only one time step t_{i+1}-t_i, then the matrix for each interval is 1x1 and no matrix solver is required. Beck [41] concludes that sequential regularization produces similar results to the whole domain procedure. This statement is true if there is no future information incorporated into the whole domain procedure. As an example, consider again the Stoltz inversion method, based on the Duhammel integral. The solution can be expressed as a linear transformation matrix as in equations (3.6) and (3.7):

$$\begin{aligned} [T] &= [\Phi]\,[q] \\ [\Phi]^{-1}\,[T] &= [q] \end{aligned} \qquad (3.11)$$

Where $[\Phi]$ and $[\Phi]^{-1}$ are lower diagonal matrices. Since the transformation matrix $[\Phi]^{-1}$ is linear and lower diagonal, q_i is a linear function of T_i, T_{i-1},...T_1, but it is independent of the temperature history following t_i, (t_{i+1}, t_{i+2},...t_n). Thus, there is no advantage to be

gained from using a whole domain method rather than a sequential method. In fact, the matrix $[\Phi]^{-1}$ can only be solved in a sequential manner because it is already lower diagonal.

Physically, $[\Phi]$ must be a lower diagonal matrix because the present temperature distribution has to be independent of future changes in the boundary conditions. A machine tool structure cannot anticipate that more heat shall soon be supplied by a heater or convective surface. However, If $[\Phi]$ is a lower diagonal matrix, then $[\Phi]^{-1}$ will also be lower diagonal. Thus, exact methods are sequential by definition. This is not the case however, when regularization is used. Each q_i is chosen such that the residual S is minimized. That implies that some property of the whole solution, either the absolute value, the first derivative, or the second derivative, is minimized also [36,42]. Hence, there is a communication among all of the q_i, past and present. In this case the sequential solution is not equivalent to the whole domain solution. But if the time segments contain more than a few time intervals, then the final results will be similar.

3.5 The Function Specification Method

Another important class of whole domain estimation, called the function specification method, was introduced by Frank [43]. To solve the inverse problem, he represented the boundary condition by a polynomial with unknown co-efficients and then solved the corresponding direct problem. He used a least-squares method to best fit the co-efficients of the direct solution to match arbitrary temperature inputs. These co-efficients define the input boundary condition. This is a powerful method that works on

linear or non-linear problems. The stability of the solution is well controlled because it is guided toward a particular form, as with the regularization method. Another factor contributing to stability is that future information is incorporated into each time step. An inherent weakness in the method is that the accuracy of the solution is dependant on the assumed form of the input. It works best when the form of the solution is known in advance [44].

Raudensky [45] used the function specification method to estimate the heat transfer co-efficient in hot steel surfaces. He assumed that the relationship between temperature and the heat transfer co-efficient is a second order polynomial. The co-efficients were found by minimizing the square of the error residual.

Beck et al. [46] used a function specification method for the analysis of quenching and heat transfer processes. They devised a code, called the QUENCH1D, which can treat one dimensional non linear problems with a variable number of future time steps.

If the problem is linear, then assuming a polynomial input will yield a linear solution matrix. If the assumed functional form is exponential or sinusoidal however, the solution will be non-linear, even if the problem is linear. Hence, the functional form of the input should be chosen with caution. When dealing with linear problems, most researchers prefer to use polynomial expressions. This can become cumbersome when high order polynomials are used to achieve good accuracy. One way to solve this problem is to divide the time domain into segments and apply the function specification method to each of the segments separately [44]. This forms a compromise between a whole domain method and a sequential procedure.

3.6 The Beck Method

In the regularization method and the function specification method, it was seen that the utilization of future information improved the stability of the method. If the algorithm is only looking as far as the next time step, there is a tendency to overcompensate for small perturbations. But if the algorithm is looking several time steps ahead, it is more likely to choose a stable solution rather than an unstable one. Beck [47] proposed a sequential function specification method which incorporates future information, but advances only one time step at a time. The procedure is as follows: the previous heat flux components, $q_1,\ldots q_{m-1}$ are assumed to be known, and the objective is to estimate the next component q_m. In order to include future information into the solution for q_m, a functional form is assumed for q in the region q_m, q_{m+1}, $q_{m+2},\ldots q_{m+r-1}$, such that $q_{m+1},\ldots q_{m+r-1}$ are functions of q_m. The error residual:

$$S=\sum_{i=1}^{r}(Y_{m+i-1}-T_{m+i-1}) \qquad (3.12)$$

is minimized with respect to q_m, and an estimate of q_m is obtained. All of the q values except q_m are discarded, and the procedure is repeated for the next time step. If $r=1$ then no future information is used and exact matching of the measured and experimental values is obtained. If $r>1$ then there is no longer exact matching between T_m and Y_m, but the solution is stabilized because the algorithm sees the whole domain and not just the next time step. Beck recommended a value of about 3 or 4 for r. The simplest application of this method is to assume that $q_{m+1}=q_{m+2}=\ldots=q_{m+r-1}=q_m$.

3.7 The Trial Function Method

Another popular heat inversion technique is called the trial function method. This method combines the function specification method with regularization, and was developed by Twomey [48]. The basic concept is the same as the function specification method, except that regularization terms are included in the residual. The method is useful, especially when higher order polynomials are used to represent q(t) because high order polynomials are prone to instability.

3.8 Iterative Regularization

All of the methods discussed so far arrive at an explicit solution for the unknown boundary condition. The next two procedures are classified as iterative regularization. As before, a method of solving the direct problem is required, but instead of inverting the problem and solving explicitly for the boundary values, successive guesses are tried for the input, and the direct solution is used to evaluate the correctness of the guess [42]. If the solution to the direct problem matches the measured data within some prescribed degree of tolerance, then the solution is found. While the simplicity of the approach seems appealing, the method requires some kind of guidance to direct the approximations in the right direction. If solutions are tested at random it would take a long time to arrive at an acceptable solution [49].

All methods of iterative regularization require a measure of the correctness of the solution. The usual criterion is the error residual:

$$S = \sum_{i=1}^{n} (Y_i - T_i) \qquad (3.13)$$

The second important element to iterative regularization is a mechanism which guides the successive approximations toward the correct solution. Given two successive approximations to the boundary condition, the second approximation will be an improvement on the first if the magnitude of the change in the error residual is negative, that is if $dS = S_2 - S_1 < 0$. If $q_i(t)$ is the i^{th} approximation to the boundary condition and S_i is the error residual corresponding to $q_i(t)$, then a negative magnitude for the derivative:

$$\frac{dS}{dq} = \frac{S_2 - S_1}{q_2(t) - q_1(t)} \qquad (3.14)$$

implies that $q_2(t)$ is a better approximation to the solution than $q_1(t)$ [49]. In order to speed convergence, it is desirable that the derivative in equation (16) be as small as possible. The gradient of a function defines the magnitude and direction of the maximum slope of the function. Therefore, the direction of maximum decrease is in the direction opposite to the gradient of the function. Thus, for an initial guess q_i, a better estimate to q is given by [39,42]:

$$q_{i+1} = q_i - \mathbf{B} \frac{\nabla S_i(q_i)}{\|\nabla S_i(q_i)\|} \qquad (3.15)$$

where,

$\nabla S_i(q_i)$ = *The Gradient of* S_i

$\mathbf{B}$ = *A positive constant*

The gradient of S is an m-dimensional vector, where m is the number of discrete time intervals. That is:

$$q_i(t) = [q_i(t_1), q_i(t_2), q_i(t_3), \ldots . q_i(t_m)] \qquad (3.16)$$

Where integer m defines the dimension of the vector q.

The first method of iterative regularization is called the *steepest descent method.* This is a logical application of the above theory. If the solution to the direct problem is given by:

$$T = \Psi\{q(t)\} \qquad (3.17)$$

then given an initial guess $q_i(t)$, an improved estimate is given by [41]:

$$q_{i+1} = q_i - B_i \nabla_j S(q_i(t_j)) \qquad (3.18)$$

where,

$$B_i = \frac{\|\nabla_j S(q_i(t_j))\|^2}{\|\Psi(\nabla_j S(q_i(t_j)))\|^2} \qquad (3.19)$$

The new estimate is obtained by moving a particular distance in the direction of maximum decrease of the error residual. The displacement of this step is defined by the constant B.

The physical significance of q and ∇q in the steepest descent algorithm is illustrated by figure 3.5. The variables q and ∇q are m-dimensional vectors, where m is defined by the number of time steps t_i. Figure 3.5 shows three hypothetical iterations of the steepest descent method for m=6, along with the exact solution. The first approximation for q(t) is a horizontal line. The gradient is a 6-dimensional vector, a multiple of which is added to the previous approximation. The new approximation is

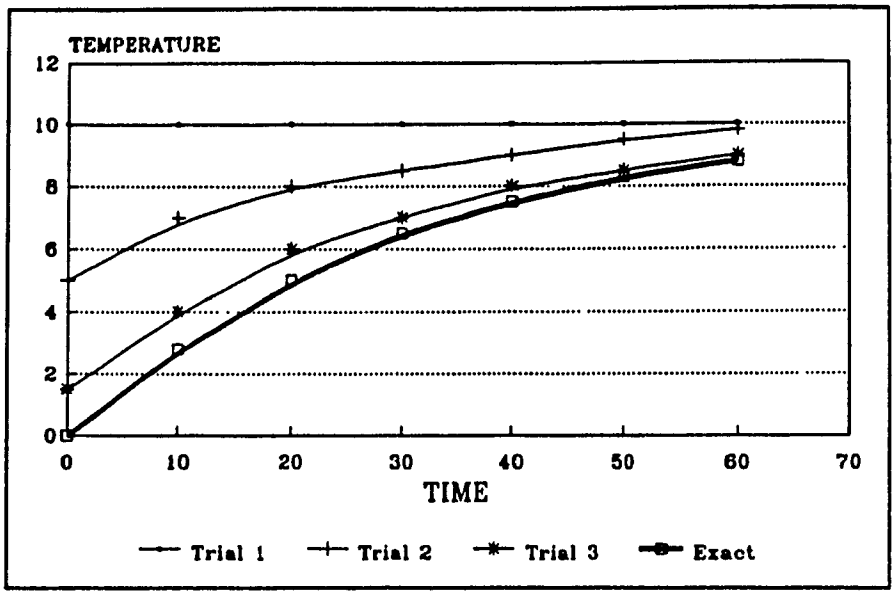

Figure 3.5: Steepest Descent Example showing Three Iterations

closer to the exact solution than was the previous approximation. Similarly, the second approximation is closer than the first. The multiplier B should decrease as the approximation approaches the exact solution.

LeBrizaut [50] used the steepest descent method to calculate the required heating boundary condition for a mould to generate a desired temperature distribution in a thermoplastic material. He uses the finite-element method to solve the direct problem for the inversion algorithm. The solution is accurate, even for discontinuous solutions.

Kang and Zabras [51] used the steepest descent method to estimate the optimal boundary heat flux in a solidification process. The model of the direct problem includes a solid region, a liquid region, and an interface between the two. The algorithm was tested against the exact solution with impressive results. The solution is accurate for a

relatively large time step, and the accuracy improves as the time step is reduced. This is in contrast to unregulated solutions, even exact ones like Burgraff's [35] solutions, where the algorithm becomes unstable for small time steps.

The disadvantage of the steepest descent method is that it requires iteration to reach a solution. This can be time consuming, especially if the solution to the direct problem is very elaborate. The advantage is that it can be used for linear or non-linear problems, and it is particularly useful when there is more than one boundary condition to be found.

Similar to the steepest descent method is the *conjugate gradient method*. It is also an iterative process that utilizes the gradient of the error residual, but it uses a slightly modified algorithm that considers the previous two estimates q_{i-1} and q_{i-2}.

Neto and Özisk [52] used the conjugate gradient method to estimate the strength and location of a plane heat source inside a plate. They used the conjugate gradient method instead of the regularization method or any of the other methods because iterative solutions are particularly useful when more than one parameter is required. They pointed out that regularization is implicitly built into the program, so the procedure is insensitive to perturbations or measurement errors.

Osman et al. [53] used the conjugate gradient method to solve for the thermal boundary conditions in a D-shaped ingot. The TOPAZ3D finite element code for heat transfer was used to solve the direct problem.

3.9 The Space Marching Method

Another inverse method that has become popular is the space marching method. Space marching is a finite difference solution to the heat equation, but instead of solving explicitly for the temperature distribution from known boundary conditions, the space marching technique works by extrapolating interior temperature data to the boundary. Space-marching is a risky procedure because it extrapolates the measured data, and extrapolation is always more hazardous than interpolation. Furthermore, there are a limited number of thermocouples that can be used to determine the temperature distribution within the structure. It is also difficult to apply the method to two-dimensional problems.

Space marching requires temperature data in a structure at distinct space and time intervals. It is important to accurately know the positions of the thermocouples relative the boundary condition that is to be measured. The best methods utilize future time data when space marching toward the boundary. A practical difficulty with space marching is that the space increments must be equal to the distance between the measured temperature nodes. Thus the space increment cannot be reduced below the closest practical separation of the thermocouples.

Raynaud [54] applied the space marching technique to a one-dimensional problem of solidifying metal. He used a combination of central and backward difference expressions to represent the derivatives in the heat equation, resulting in four and six point computational molecules. The mesh size of the finite-difference grid was chosen so that the advancing solidification front crossed only one node per time step. The results

were close to the analytical solution, but a large number of temperature measurements are not convenient in most situations.

The difference between a space marching solution to an inverse problem and a finite-difference solution to a direct problem, is that the space-marching algorithm must extrapolate beyond known data, instead of interpolating between known boundary conditions. Thus the measured temperatures should be as close to the boundary as possible. Collecting more nodal temperatures improves the reliability of the solution, but the data is usually difficult to obtain.

3.10 Direct Numerical Solutions

Finite-element and finite-difference methods are often used in the solution of the inverse problem, frequently as the only possible solution to the direct problem in the iterative regularization methods. These numerical solutions are sometimes the only way to obtain a direct solution to a real life problem, such as welding, casting, or thermal modelling of machine tools. Their application to direct inversion is limited however, since an exhaustive knowledge of the nodal temperatures in the structure would be necessary to directly solve the inverted solution matrix. Finite-difference methods are used however, in the space-marching technique, discussed previously.

3.11 Conclusions of the Inverse Heat Conduction Problem

In section 3.1 it was found that an inverse problem is more difficult than a direct problem because of three factors: 1) the difficulty of expressing the solution in explicit

form, 2) instability, and 3) the non-uniqueness of the solution. In section 3.2.1 it was found that the first factor comes from the chirality of the problem. Furthermore, it was found that the chirality is determined by the method of solution and is not inherent to the problem. In section 3.2.2 it was found that instability is due to the delayed and damped nature of the solution to the direct problem, and is therefore an inherent characteristic of the IHCP. In section 3.2.3 it was found that the non-uniqueness of the solution is a consequence of the solution methods, and is not necessarily inherent to the IHCP. In section 3.3 the Stoltz solution was introduced. The Stoltz method is simple and efficient, but there is no control over the inherent instability of the problem. In section 3.4 methods of regularizing an IHCP were introduced. Regularization is the most widely used method of dealing with the instability of the IHCP. The problem with regularization, from the point of view of this thesis, is that it requires future information and is not readily compatible with classical control theory. In sections 3.5, 3.6, and 3.7, the methods of function specification, the Beck method, and the trial function method were presented as alternatives to regularization. These methods suffer from the same limitations as regularization with regard to control systems. In section 3.8 the methods of iterative regularization were introduced. These methods are most suitable for non-linear problems with more that one unknown boundary condition. The problem with the methods is that they are inherently slow, and therefore not appropriate for real time control purposes. The space marching method presented in section 3.9 is the inverse version of the finite difference method. The problem with the method is that it requires

too many measured nodes, and it is not accurate enough to fulfil the requirements of the control system.

CHAPTER 4: LITERATURE REVIEW OF REAL TIME CONTROL OF THERMAL DEFORMATIONS

4.1 Introduction

A variety of methods of dealing with the problem of thermal deformation in machine tools have already been discussed in chapter 2. The methods fit into three broad categories: *i*) Reducing the propensity for thermal deformation at the design stage, *ii*) passively reducing the thermal inputs while the machine is in operation (ie. proper chip disposal and external temperature control), and *iii*) active measurement and compensation of thermal deformation during machine operation. Optimizing the thermal behaviour of machine tools at the design stage is an essential practice, but it will never entirely eliminate the problem of thermal deformation under general loading conditions [55]. Some of the passive methods of reducing thermal deformation are also indispensable, especially when it is as simple as diverting the chips away from the structure. While sophisticated passive methods like liquid showering are highly effective for specialized applications, it is an extremely awkward and expensive procedure for general purpose applications [6]. In the past, liquid showering was the only possible solution where strict control of thermal deformation was required, such as the precision grinding of ultra-thin quartz wafers [56]. Active methods of reducing thermal deformation have not yet gained commercial acceptance because the accuracy and reliability of the methods are not generally impressive [57,58]. The fundamental difficulty with active compensation is the problem of measuring the thermal deformation while the machine is in operation. Indirect

measurements of deformation rely on tenuous empirical or quasi-empirical relationships that are slow to evaluate and difficult to implement with existing control theory.

There are three important elements to a real time control system: *i*) data acquisition of the input variables, *ii*) the structural configuration of the controller and control system, and *iii*) the mechanism for implementing the control output. Each of these elements will be considered in the following sections.

4.2 Data Acquisition

The problem of data acquisition has already been considered in depth in the preceding chapters, so only the conclusions will be restated here. The direct on-line measurement of thermal deformation is not feasible in a realistic machining environment [18]. The thermal deformation must therefore be measured indirectly, by an alternate physical property or properties that are directly related to the thermal deformation. There are three principal groups of properties which have been used to estimate thermal deformation: *i*) the operating parameters of the machine tool [24,25], *ii*) a large number of thermocouples representing the temperature distribution of the structure [19], and *iii*) a small number of discrete point temperatures [20,21].

Indirect measurement requires mathematical models to relate the input variables to the thermal deformation. The form of these mathematical models defines the form of the control system, because the models are the essential building blocks of the control system [32]. Control system designers will frequently try to gloss over the problem of mathematical modelling, especially when the problem is complex and reliable models are

difficult to obtain. But poorly defined models yield complicated, slow, and cumbersome control systems. When dealing with complicated three dimensional machine structures, the process of mathematical modelling deserves an extraordinary amount of attention. The investment in time and effort will certainly pay off at the next stage, when the models are assembled into a control system.

4.3 The Controller and the Control System

Figure 4.1 shows a schematic drawing of a control system. The input variables are measured on the real structure, and they define the magnitude of the controlled variable δ through a series of mathematical models. The controller is the brains behind the control system. It examines the estimated controlled variable, and then determines an appropriate actuation signal to maintain a predetermined condition of the controlled variable [59]. It is sometimes convenient to think of the controller as encompassing the entire operation between the input variables and the actuating signal, as represented by the dotted box in figure 4.1. The way in which the controller operates on the input variables depends on the nature of the input variables, and on the mathematical relationship between the input variables and the controlled variable.

Much of the classical work on control theory is based on mathematical transfer functions in the s-domain or z-domain. The controller generates a signal based on the proportional plus integral plus derivative (PID) of the difference between the measured and desired values of the controlled variable. PID control is fast and reliable, but it

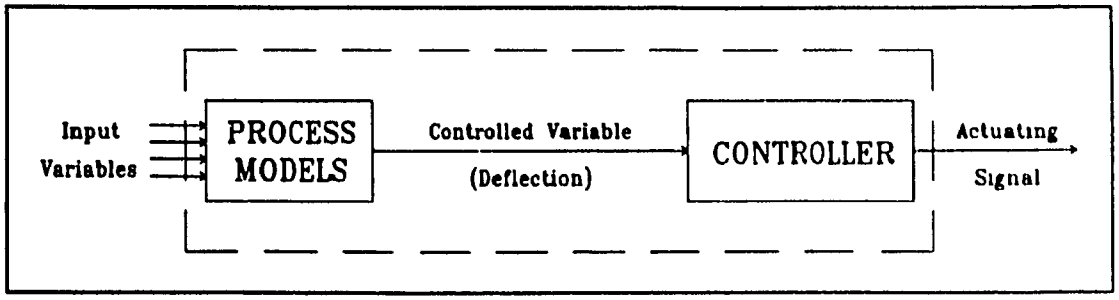

Figure 4.1: Schematic Drawing of the Control System

relies on well defined mathematical transfer functions that can be transformed to the z-domain or to the s-domain [60]. When the mathematical models are not sufficiently reliable, it often becomes necessary to use adaptive control. Adaptive control is the in-process calibration of the system parameters, which means readjusting the constant parameters of the mathematical models (ie. the gains K and the time constants τ) [60]. If mathematical models are not available, or if the number of input variables is large, then classical control theory is not effective and an alternate solution must be found. One of the most powerful methods of dealing with multiple inputs and poorly defined models is with expert systems [61]. An expert system involves a statistical matching of the input to the output variables. One of the most promising new fields in expert systems is the area of fuzzy logic.

Expert systems are revolutionizing the science of control system design in the applications where there is no clear and direct relationship between the input variables and the output, such as pattern recognition [61]. As the availability of these systems has increased, they are frequently applied to more conventional problems, so as to avoid the difficult mathematical modelling of the physical processes. But it is not true that an expert system is always superior to classical control methods. If there is a physically

direct relationship between the variables, then it is far better to identify that relationship with a definite mathematical expression, rather than simulate it with an expert system.

4.3.1 Types of Control Systems

The form of the control system is essentially determined by the form of the mathematical models making up the system. Sata et al. [62] developed a method for controlling the thermal deformation of a machine tool structure by reducing the warm up time to bring the structure to thermal equilibrium. The deformation is related to the heat generation by finite element models of the structure. Finite element models are not compatible with classical control theory because they cannot be transformed to the s-domain. Sata et al. used the method of linear programming to find the optimal actuating signal. Linear programming is a non-conventional method which applies to matrix type problems like this one. The most serious problem with the method is the long computation time for linear programming a large solution matrix.

Balsamo et al. [19] developed a combined empirical- finite element model relating the deformation in a machine tool structure to the measured temperature distribution. Measuring the temperature distribution required more than 100 thermocouples, as discussed in section 2.2.2. This model is incompatible with classical control theory, and Balsamo states that only a control system based on a 'real proper expert system' is capable of handling the complex model for industrial applications.

In their paper on weldment control, Bates and Hardt [63] used a simplified mathematical model to estimate the temperature distribution in an arc welding process

from limited temperature measurements. The simplified model is not adequate to describe the welding process without on-line parameter calibration, requiring an adaptive control system. Nevertheless, the advantages of a direct mathematical model are the relative simplicity of the control system, the reliability of the direct relationship, and the speed and accuracy of the control system.

Ichimiya et al. [64] used a linear transfer function to relate the thermal deformation to a small number of positional temperatures in a machine tool structure. A control system based on this model would depend heavily on adaptive control because the linear constants change with the operating conditions of the machine tool. Ichimiya et al. did not actually build a control system with their model, but the decision to use adaptive control with such a primitive transfer function is questionable. Adaptive control is a powerful method when the form of the transfer function is partially known. Since the mathematical form of their transfer function is completely unknown, an expert control system would certainly yield better results.

Adaptive control adds an extra loop a linear control system for the calibration of the system parameters. Calibration is usually an iterative process and significantly increases the calculation time for the controller [63]. From the point of view of the control system, an ideal model is one which accurately describes the relationship between the variables without the need for parameter calibration. If a problem is inherently linear then there theoretically exists a model which is compatible with classical control theory without adaptive control. The challenge, especially for complex problems, is identifying the form of this ideal model.

4.3.2 Types of Input Parameters

Three types of input parameters were identified in section 4.2 for the thermal deformation problem:

i) The thermal deformation is related to the operating parameters of the machine tool through three mathematical models, as shc .n in figure 4.2. The first model, relating the operating parameters to the heat generation of the primary sources is an unstable relationship over the life of the machine tool, and it is difficult to accurately define [24,25]. Furthermore, the relationship is generally non-linear, and is thus incompatible with linear control theory.

ii) Relating the thermal deformation to a large number of temperature measurements requires only one mathematical model, as shown in figure 4.3. The large number of inputs and the complexity of the mathematical model makes it necessary to use an expert control system [19]. An expert system does not take advantage of the direct relationship between the input and output variables, and it adds to the computational inefficiency of an already cumbersome model.

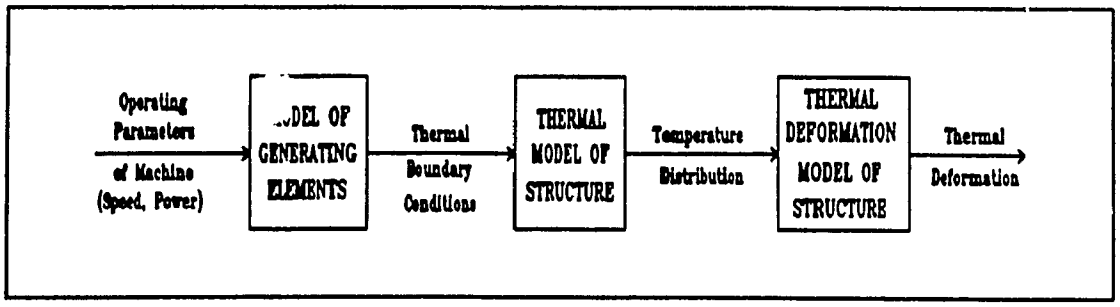

Figure 4.2: The Models Relating the Thermal Deformation to the Operating Parameters of the Machine Tool

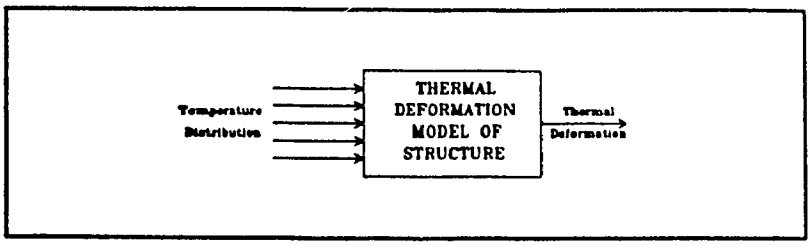

Figure 4.3: The Models Relating the Thermal Deformation to a Large Number of Temperature Measurements

iii) The thermal deformation is related to discrete temperature measurements in a structure by three mathematical models, as shown in figure 4.4. The first model represents an IHCP between discrete temperatures and the thermal boundary conditions, the second model is a direct heat conduction problem relating the thermal boundary conditions to the temperature distribution, and the third model relates the temperature distribution to the thermal deformation. A variety of researchers defined this relationship empirically, as discussed in section 2.2.3, but up until now there has been no general mathematical treatment of the problem [21,22,23]. Empirical transfer functions are generally incompatible with classical control theory, even when modified with adaptive control.

One of the objectives of this thesis is to define the mathematical relationship behind the three models shown in figure 4.4. The solution to these models will be used to define s-domain transfer functions relating discrete temperatures to the structural thermal deformation, and design a PID control system using classical control theory.

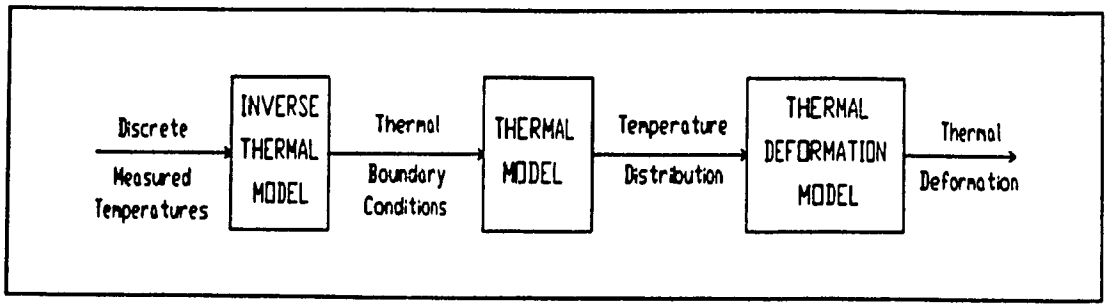

Figure 4.4: The Models Relating the Thermal Deformation to Discrete Temperature Measurements

4.4 The Compensation System

4.4.1 Types of Compensation Mechanisms

The final element to the control system in figure 4.1 is the activating mechanism to compensate for the thermal deformation. The compensating mechanism is usually a physical process or variable which is capable of making fine adjustments to the position of the tool, and is also capable of being tied in to an electronic control system. If the machine tool is numerically controlled then a numerically actuated positioning system is already available, and compensation is effected by adjusting the position of the cutting tool to neutralise the thermal deformation [20]. Most NC machines have the built in capacity to accept on-line input from a separate control system.

For NC machines, the numerical positioning system of the machine is the ideal actuating mechanism for the forward loop of the thermal deflection control system. The most important advantages are:

-The actuating mechanism is provided by the NC machine so that no additional hardware is needed [20,57],

-The execution time delay for the actuating mechanism is small, and the positioning accuracy is very high [19,20].

-The actuating system does not interfere with the normal operation of the machine tool [20].

If a machine is not already equipped with an automated position controller then the compensation is much more difficult to implement. One method of implementing the corrections for traditional non-automated machines is through the machine tool operator [20]. When used in this fashion, the electronic part of the control system performs measurement of thermal deformation only, and it is up to the operator to set the position of the cutting tool accordingly. This method is very inconvenient because it requires a high degree of human interaction and attention. The corrections can only be made intermittently, when the operator is not occupied by other tasks. Furthermore, this method cannot be implemented in a semi-automated, production type environment, where there is very little human supervision of the machine tools.

With non-automated or semi-automated machine tools, the compensation is best effected through an external actuating system. One method is to attach a piezo-electric transducer between the structure and the cutting tool [24]. This allows for fine adjustments to the position of the cutting tool when tied in to a digital control system. The problem with this method is that the transducer reduces the stiffness of the tool holder, and three-axis compensation is cumbersome.

Another way to effect compensation in non-automated machine tools is to attach artificial electric heaters onto the structure [62]. The heating is controlled by a digital

control system so that the thermal deflection that is induced is opposite to the deflection of the uncontrolled sources. The controlled sources generate an independent deflection pattern in the structure that, when superimposed onto the natural deflection field, induces zero net deflection at certain key points. This method could only work if the controlled heaters were placed at strategic locations, so that the deflection that they induce tends to nullify the deflection of the bearings, and the other natural heat sources. Therefore the artificial thermal deflection distribution has to be carefully tailored by the controller so that it stays one step ahead of the natural deflection. This is made all the more difficult by the inherent time lag between the changes in the power generation of the heaters, and the development of the resulting temperature and deflection distributions. The controller has to consider the long, as well as the short term effects of a change in the heat generation. This is in contrast to the case of a numerically controlled machine tool, where all that the controller has to do is move the cutting tool by an equal and opposite distance to the measured deflection error. There is practically no time lag between the signal from the controller and the full execution of the instruction.

Implementing a deflection control system using artificial heat sources has a number of important advantages:

-It can be applied to any machine, whether or not it is numerically controlled,

-It does not affect the structural rigidity of the frame, or interfere with the operation or performance of the machine tool.

-the method can be incorporated with existing, as well as new machine tools.

-It is simple to construct, and inexpensive to implement.

The disadvantage of using artificial heat sources is that it requires a very sophisticated controller to manage the compensation if acceptable results are to be obtained [62]. The fundamental problem, as has already been discussed, is that the relationships between the important variables in the control system are highly time dependant. For the control system to perform within acceptable bounds, a number of important pre-conditions must be met:

1) the relationships between the variables must be identified with a high degree of certainty. This is accomplished through accurate process models that can be quickly evaluated on-line, as discussed in chapter 2.

2) The action of the controller must be dynamically optimized. This process is simplified considerably if the transfer functions can be expressed in forms that are easily integrated with control theory. Thus, it would be advantageous to work with the transfer functions in the s-domain rather than in the time domain.

4.5 Conclusion

Three categories of methods to deal with the real time control of thermal deformations were discussed in section 4.1. The method of active measurement and compensation for thermal deformation is the simplest, cheapest, and most versatile method, but it has not yet gained commercial acceptance because the existing methods are not generally accurate or reliable. Methods of indirectly measuring the thermal deformation were discussed in section 4.2. The most convenient input variable is a small number of surface temperature measurements. This requires an elaborate system of

physical models, as discussed in section 4.3. The emphasis of this thesis will be on devising powerful models that accurately represent the physical processes, and eliminate the need for expert systems and adaptive control, as discussed in section 4.3. In section 4.4, a number of methods of implementing compensation were discussed. In this thesis, compensation will be effected by artificial electric heaters because of the low cost, ease of installation, and general applicability of the method.

CHAPTER 5: CONCLUSIONS OF THE LITERATURE REVIEW

5.1 The Problem of Machine Tool Error

5.1.1 Sources of Machining Error

In section 2.1.1, four primary sources of inaccuracy in machine tools were identified: *i*) structural imperfections *ii*) measurement effects, *iii*) mechanical effects, and *iv*) thermal effects. Thermal error is especially significant for large machine tools and precision parts, sometimes comprising more than 60% of the total error [7], as discussed in section 2.1.3. While the other sources of error continue to be significant, thermally induced error has traditionally received the least attention, a fact which must now change because of the widespread use of NC machines and increasing industry demands for high precision parts.

In many applications the thermal deformation of the structure is significantly greater than the thermal deformation of the cutting tool, as discussed in section 2.1.2. Structural thermal deformation is concerned with *i*) a large structure and a small temperature increase, *ii*) a convective boundary condition, and *iii*) a linear problem. The deformation of the cutting tool is concerned with *i*) a large thermal strain that is local in nature, *ii*) a radiation boundary condition, and *iii*) a non linear problem. The deformation of the cutting tool is a very different problem to that of the structural deformation, and it requires a different formulation and a different method of solution. Even though structural deformation does not account for all thermally induced errors, it is usually the dominant source when the physical dimensions of the ructure are large [65].

Section 2.1.4.1 discussed a variety of methods of reducing thermally induced error at the design stage. These methods have become indispensable to the design of precision machine tools, but they cannot eliminate all thermally induced error and they cannot be used to retrofit existing machine tools. An alternate or additional solution is to measure the thermal deformation of the structure while the machine tool is in operation and compensate for it with a real time control system. On-line compensation is an attractive solution, but it has not yet met with commercial acceptance. The most serious obstacle is that the deformation cannot be directly measured while the machine tool is in operation. Tonshoff [18] tested a variety of direct measurement methods, but he was forced to reject them because of the practical problem of implementation.

Section 2.2 discusses a variety of methods for indirectly measuring the thermal deformation of the machine tool structure. The general procedure is to devise a mathematical model or a series of models relating the thermal deformation to another variable which is more readily accessible. A variety of methods were discussed, but the models all fall into one of four categories: 1) empirical models, 2) finite-element models, 3) exact analytical models, and 4) approximate analytical models. A brief summary of the conclusions drawn from these models will now be presented.

5.1.2 Finite-Element Models

The finite-element method is a powerful tool for the solution of thermal and structural deflection problems. The method can accommodate many complex geometrical structures and boundary conditions, and the results can usually be made accurate within

any practical tolerance by increasing the fineness of the mesh. But even with a powerful computer, the finite-element algorithm is a slow solution for real time control. The solution is not in a closed form, so the entire solution procedure must be repeated for every change in the load or boundary conditions. This makes it too cumbersome to use with a control system, unless the structure is represented in a highly simplified form.

5.1.3 Analytical Models

An exact analytical solution has the advantages that it is general for any input load, and it indicates the functional relationship between the variables. It usually takes the form of a single mathematical function or equation that can be evaluated quickly for any numerical values of the input variables. But although the analytical model is computationally simple and ideal for use with an on-line control system, one must usually make unrealistic assumptions in order to get the solution. The complicated geometric characteristics of a real structure cannot be accommodated by an analytical model as well as they can by a finite-element model.

5.1.4 Empirical Models

Empirical models have no physical affinity to the mathematical form of the problem. The relationship between the input and output variables is curve-fit onto an arbitrary basis function, often a polynomial. The empirical equation statistically matches the input and output variables for a limited number of test inputs, but the models are cumbersome, especially as the order of the polynomial is increased to improve the

accuracy. The advantages of an empirical model are computational efficiency for low order polynomials, and there is no complicated modelling required, only curve fitting the empirical constants. The disadvantages are that the solution is cumbersome, not generally accurate, and unpredictable when used with untested inputs.

5.1.5 Approximate Analytical Models

Exact analytic solutions are only available for simple geometries like spheres, cylinders and slabs, and not for more complicated problems like machine tool structures. But analytical solutions are more general in the sense that the approximate structural form, or skeletal shape of the solution can be extended to a wide variety of similar problems. Hardt [32] took the analytic solution to a simple model which was solved analytically, and then calibrated the parameters until it adequately represented the solution to a complex welding process, as discussed in section 2.2.7. The solution was not exact because the functional form was not exact, but the functional form was an adequate basis on which to curve-fit a solution. This is very powerful concept that will be developed further, later on in the thesis.

5.2 The Inverse Heat Conduction Problem

When working with mathematical models where the actual boundary conditions are unknown, the first step is to determine the boundary conditions. Solving a thermal model explicitly for the boundary conditions is a special case of the heat conduction problem because it is an inverse problem, the nature of which was discussed in chapter

3. The preferred orientation of the heat transfer equation is from boundary condition to internal temperature, as discussed in section 3.1, so solving the problem in reverse poses special problems. The problems associated with inverse problems are *i*) the difficulty of expressing the solution in explicit form, *ii*) instability, *iii*) non-uniqueness of the solution.

A variety of methods of dealing with the IHCP were discussed in sections 3.3 to 3.10. These methods are primarily designed to measure the temperature or heat flux in inaccessible regions, but the temperature data is usually collected in a previous experiment so the entire temperature history is known at the outset. There are four additional problems that arise when the IHCP is used for real time control, and these are summarized here:

1) Future information is not available to stabilize the solution, because the data is collected on-line. The regularization and function specification methods can still be used, but only if a block of past data is taken to stabilize the solution at the present time. This limits the effectiveness of the methods, because the solution at the last time step is the least accurate, and that is the only one that is used. Space marching is not a viable solution when future data is not available, because the numerical extrapolation is unreliable without it [54].

2) The calculation time of the IHCP algorithm determines the cycle time of the control system, so the performance of the control system depends on the calculation time as well as the accuracy. The overall effectiveness of the method is a compromise between

speed and accuracy, making the iterative methods unattractive. Regularization and function specification methods are also too slow if a large amount of past data must be incorporated into the solution.

3) It is essential that the inherent instability of the solution be controlled, because even a small amount of instability in the IHCP can cause greater instability in the control system. This is especially true if the cycle time is small, and is frequently aggravated when accurate data is not available in the on-line environment. Unregularized methods like Stoltz' method and space marching produce large oscillations with noisy data, limiting the stable region of the controller gain, and severely affecting the performance of the control system.

4) The design and optimization of the control system is simplified if the IHCP algorithm can be characterized in terms of control theory. None of the existing algorithms can be transformed to the s-domain or z-domain, with the exception of Stoltz' method. The other methods would be seen as a 'black box' in control theory, unless the control system were designed in the time domain.

Unfortunately, most of the research into the IHCP is not relevant to the control environment, so the limitations of the methods become apparent when they are considered for that purpose. Because of the growing demand for the thermal control of machine tools, there is an urgent need for an IHCP algorithm which is specifically suited

to real time control. Such an algorithm must be computationally simple, stable for noisy data, not dependant on future data, and preferably in a form which is compatible with control theory. The major weakness of the available methods is that they stabilize the solution by controlling the form of the solution to the IHCP, and do not deal with the inherent instability of the problem itself. The only methods that are stable and accurate enough to be used for control require too much computation time to be viable.

5.3 The Control System

5.3.1 The Structure of the Control System

Three general types of control system were discussed in section 4.3, and are summarized here:

i) Classical linear control systems based on well defined mathematical transfer functions.

ii) Adaptive control systems, using approximate mathematical transfer functions and on-line parameter calibration.

iii) Expert systems which use statistical matching of the input and output variables, and do not require mathematical modelling of the physical processes.

Expert systems are a powerful control method when there is no clear relationship between the input and output variables. An expert system fills in the blanks, anticipating the response to an unpredictable input. When there is a definite relationship between the input and output variables however, the best solution is to mathematically identify the

relationship and avoid the statistical uncertainty of an expert system controller. Increasing the number of rules of an expert system increases the time factor by a power of two.

5.3.2 The Mechanism of Compensation

A number of methods of compensating for thermal deformation were considered in section 4.4. For NC machine tools the compensation is effected through the numerical positioning mechanism that is already present in the machine tool. For non-automated machine tools, compensation is a much more difficult problem because additional hardware is required. The method of compensation by artificial electric heaters was used by Sata [23] and Ichimiya [23]. The advantages of electric heaters are 1) that they do not interfere with the performance or operation of the machine tool, 2) they are inexpensive and easy to install, and 3) they can be applied to any type of machine tool. The disadvantage of compensation with artificial heaters is that it places a heavy burden on the control system to produce an acceptable response.

5.4 Objectives

The objectives of the thesis are as follows:

-Develop a multi-axis feedback control system to reduce structural thermal deflection error to a level comparable with the method of fluid showering.

-The measured variable on the structure must be readily accessible and easily measured.

-The control system must be universal and flexible to be applied to real machine tools of any type, and must be insensitive to all kinds of measurement and actuation errors.

5.5 Overview of the Thesis

5.5.1 Broad Outline of the Thesis

This objective of this thesis is to reduce the thermal deflection of key points on a large structure by means of a feedback control system. A number of researchers have previously attempted the problem, as discussed in chapter 2, but the work has not yet led to a commercial benefit. In order to be commercially viable, the method must be easy to implement on a real machine tool, it must be accurate and reliable, and it must require minimum maintenance by the user.

A broad outline of the thesis is as follows: 1) determine an accurate mathematical model that relates the thermal deflection of a machine tool structure to a small number of measured temperatures, 2) create a suitable test structure on which to evaluate the effectiveness of the mathematical models, and 3) use the models to build an operational feedback control system which measures thermal deflection on the test structure and compensates for it.

The modelling sequence which relates thermal deflection to a small number of point temperatures was given in figure 4.4, and is repeated here as figure 5.1. The sequence of the models is as follows: 1) an inverse thermal model relates discrete temperatures on the surface of the structure to the thermal boundary conditions, 2) a thermal model relates the thermal boundary conditions to the complete temperature distribution in the structure, and 3) a thermal deformation model relates the temperaturedistribution to the thermal deflection of key points, which on a machine tool structure is the relative displacement between the cutting tool and work piece. The

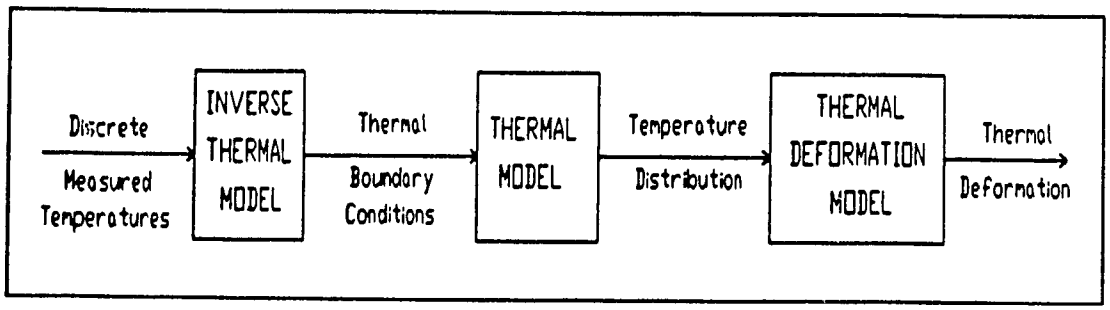

Figure 5.1: The Models Relating the Thermal Deformation to Discrete Temperature Measurements

relationship in figure 5.1 has already been defined empirically, as discussed in the literature review, by Chiappullini et al. [20] and others, but a complete mathematical treatment of the problem has never been done. Parts II and III of the thesis focus on the problem of mathematically modelling the constituent blocks of figure 5.1. Part IV of the thesis is concerned with using the models to build a control system.

5.5.2 Detailed Outline of the Thesis

In chapter 6, a systematic method for determining an approximate analytical model to simulate an actual process is developed. The method is similar to the approximate analytical method that was used by Hardt [32], but it is formalized into a general procedure called *generalized analytical modelling*. The procedure is based on the fact that physically similar problems have structurally similar solutions. If one problem can be solved analytically, then it serves as a reliable mathematical basis on which to curve-fit the solution to a more complex problem.

In chapter 7, the generalized method is used to find approximate analytical models of the thin walled shell of a machine tool structure. The mathematical form of the

generalized solution for a thin walled structure is based on the analytical solution for a thin, infinite plate with a convective boundary and a central heat source. The thermal and thermal deformation analytical solutions for the infinite plate are not available in the literature, so an original solution is derived in chapter 7 by the method of the Hankel transformation. At the end of the chapter, the generalized analytical solutions are transformed to the Laplace domain where they are turned into Laplacian transfer functions.

In chapter 8 a thermal test structure is created using the finite-element method. The test model is similar in form to the structure of a machine tool, and so it is used to evaluate the effectiveness of the generalized thermal model. A numerical method is developed for optimally curve fitting numerical data onto an analytical base function. The method is based on the least-square principle, and is used to curve-fit the generalized solutions.

Chapters 9 through 12 are concerned with the first block in figure 5.1, the inverse heat conduction problem relating point temperatures to the thermal boundary conditions of the structure. In chapter 10 a new method of solving the inverse heat conduction problem is developed, called the method of inversion by a convolution integral. The laplacian transfer function model derived in chapter 7 is algebraically inverted in the s-domain, defining a new transfer function for the thermal inverse problem. The new transfer function is numerically transformed back to the time domain, where the solution to the problem is expressed as a convolution integral in time. This method of solving the IHCP eliminates the problem of non-uniqueness, and it significantly reduces the problem

of instability by eliminating much of the inherent instability from the problem itself. Special techniques are developed to numerically transform the variables to and from the Laplace domain. A special problem arises when the transfer function is transformed to the time domain, because it contains singularity functions which cause the numerical transformation procedure to fail. None of the known methods of numerically transforming from the s-domain will work when singularity functions are present because singularities do not satisfy the existence theorem of the Laplace transform. A new method is developed which accelerates the convergence of the inverse transformation, and also filters singularities out of the solution. The new method accelerates convergence by two orders of magnitude over the numerical methods that are available in the literature. The singularity functions themselves are transformed analytically by solving the exponential integral exactly at extreme points. This solution is also not available in the literature.

The method of solving the IHCP by the convolution integral is compared to three other methods. In chapter 9 a new method of solving the problem based on a Laplacian transfer function is derived. In chapter 11 another new method called proportional inversion is derived. Finally in chapter 12, a modified version of the regularized Stoltz method that can be used in real time is tested.

In chapter 13 the thermal deflection finite-element test model is introduced, and is used to test the effectiveness of the generalized thermal deflection models.

In chapter 14 the control system is designed and optimized by methods of classical control theory. The structure of the control system is feedback PID with feedforward

loops from the disturbance inputs. The compensation mechanism employs simulated electric heaters on the surface of the finite-element model. The relationship between the generation of the heaters and the deflection of the test structure is represented by the same generalized model as the disturbance heaters. The performance of the control system is evaluated by applying simulated disturbance loads and calculating the resulting deflection with the thermal deflection finite-element algorithm. The response of the control system to simulated errors is also investigated.

PART II: THE PHYSICAL PROCESS MODELS

CHAPTER 6: THE GENERALIZED ANALYTICAL SOLUTION TO A REAL PROBLEM

6.1 The Performance Requirements for an On-Line Solution

Modelling for control systems is the most demanding modelling environment, because an on-line mathematical solution must be accurate, reliable, and computationally efficient. These requirements are best accommodated by a compact functional expression or mathematical equation, ideally defined by an exact analytic solution. Most real problems do not have a defined analytic solution but that does not necessarily mean that such a solution does not exist, it only means that it cannot be represented in mathematical form. Most control systems require an analytic expression to meet the time and accuracy demands of the controller. If the exact solution does not exist in analytical form, the next best thing is to find the closest analytical representation of the solution that does exist. In this chapter, a method of determining an approximate analytic representation of a general physical problem will be developed.

6.2 Determining the Approximate Analytic Form of a Non-Analytic Solution

As the geometry and boundary structure of a problem change, there is a gradual change in the functional relationships among the variables of the problem. The form of the solution to a complex problem that has no mathematical representation is similar to other problems that have similar geometry and boundary conditions, but where an analytical solution is available. In this way, the approximate analytical form of a complex

solution is anticipated by the analytical solution to a simpler problem with a physically similar form. An analytical solution is generalized by lumping the analytical parameters together and treating them as empirical constants. The generalized solution is adapted to another problem by adjusting the empirical constants to fit the new solution. An arbitrary functional form could also be used as a basis for the solution, but the greater the similarity between the assumed form and the actual form, the better is the agreement and reliability of the solution. It is the physical compatibility of the generalized analytic solution that makes it the ideal basis for a more complex problem.

6.3 A Comparison of The Generalized Solution with Exact Methods

6.3.1 Modelling the Thermal Boundary Conditions

The largest source of error with exact thermal modelling is identifying the boundary conditions, and accurately representing them in a mathematical model. In the case of a machine tool structure, the thermal loading comes from all of the moving parts inside of the structure, including motor, bearings, spindles, belts, and pulleys, and the way in which these sources interact with the structure is not easily established. The motor is attached to the structure through bolted brackets with an unknown thermal contact resistance. The bearings are usually supported well inside of the structural casing, and it is difficult to model the exact path that the heat flux follows as it moves through the structure. The working parts of the machine are particularly difficult to model because in some places there are physical connections, and in others there are small separations between them. This makes the mode of heat transfer a complicated combination of

conduction, convection and radiation. A generalized model is not concerned with the details of the generation process, it is only concerned with the form of the temperature response of the structure.

In the case of a machine tool structure, the simplified analytical model would contain lumped heat sources to approximate the heat generation of internal bearings and electrical components. The heat generation of the simplified sources is not intended to correspond directly to the conditions in the real structure, the simplified sources are designed so that the overall effect on the temperature distribution is similar to the effects of the actual heat sources in the real structure. It is the large scale effects of the solution that are relevant, and not the fine details of the actual generation and conduction process. In other words, it is better to lump all of the fine details into a simplified source, and find the equivalent heat magnitude that duplicates the temperature distribution in the real structure. Attempting to accurately represent the fine structure of spindles, bearing, and motor in an exact model, and duplicate the details of how they are connected to the frame would inevitably lead to gross inaccuracies in the final temperature distribution.

6.3.2 Determining the Relationship between the Input and Output Variables

An exact solution uses information at the boundary to obtain a solution at the interior of the structure. The solution is highly sensitive to flaws in the model, because the governing thermal equations are the only physical link between the boundary conditions and interior solution. With a generalized analytical solution the model only defines the basis of the solution, the complete solution is found by fitting the base to the

measured physical response of the system. Thus, the generalized solution is interpolatory, because it uses measured interior information, as well as measured boundary conditions to define the solution. This makes the solution less sensitive to weaknesses in the model.

The disadvantage of the generalized solution is that it must be possible to measure the actual response of the system in order to calibrate the analytic base equation. For a linear problem it is only necessary to measure the response to a single input to fully define the generalized solution. Nevertheless, this is sometimes difficult or even impossible to measure in a real system and furthermore, the errors in the measurement are carried into the generalized solution. The generalized solution is most powerful when the actual solution can be measured directly under certain conditions but not others, or for certain inputs and not others. For the control problem, if the response of the system can be measured under controlled conditions to calibrate the generalized equation, then the generalized solution is used on-line to estimate the response under arbitrary loading conditions. This is the situation that applies to the present problem, and that is the method that will be use in the thesis.

6.4 Determining the Generalized Analytic Model for a Machine Tool Structure

6.4.1 The Requirements for the Model

The thermal deflection of a machine tool structure cannot be measured directly during the normal operation of the machine, but it can be measured under controlled, no load conditions. It was concluded in [1] that the difference between the thermal deformation in the load and no-load conditions is not significant.

6.4.2 The Simplified Model of the Structural Frame of a Machine Tool

The approximate thermal model of a machine tool structure is a large, thin plate with a convective boundary condition on the upper and lower surfaces. The physical form of the model is similar to the form of the real structure, and the thermal solution for such a plate can be analytically derived, as shall be seen in the next chapter. Folding the plate into three dimensions does not change the model because the folds do not affect the heat flux. The wall thickness of the machine structure usually varies from one place to another, but the simplified model has a constant thickness.

6.4.3 Modelling the Heat Sources of the Machine Tool Structure

The heat sources in the real machine structure are located inside of the external shell, connecting to the shell through bolted brackets or the internal recesses of the shell's casting. The heat is generated by the machine's internal mechanisms, and is distributed internally through a complex sequence of parallel thermodynamic processes. But the mechanism through which the heat flux ultimately enters the external shell is by conduction through an internal arm or bracket. If it were possible to separate the structural shell from its internal mechanisms then, from the point of view of the structural shell, the heat is generated at localized sources on the internal surface. The shape and size of the sources is arbitrary, but they are usually small relative to the size of the frame.

In the generalized model, the heat source is represented by a thin, circular source of heat generation, located around the centre of the continuous plate at radius $r=r_0$, as

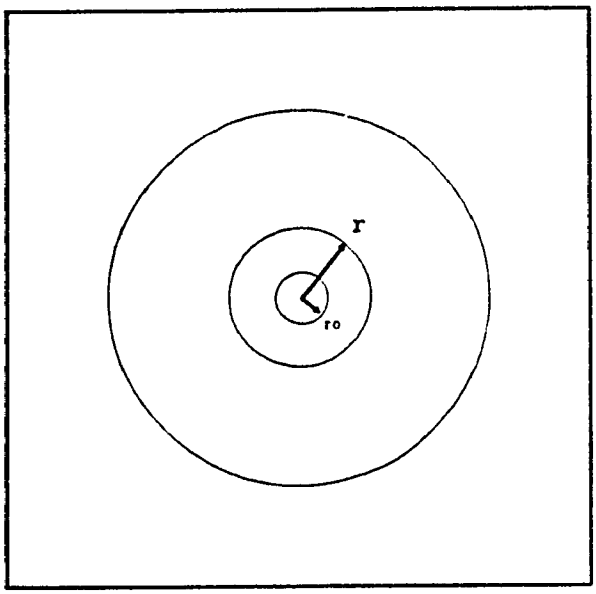

Figure 6.1: Plate Model of Structure

shown in figure 6.1. The plate continuous and all of the heat generation is assumed to occur within the infinitely thin ring of material that encircles the origin at $r=r_0$. Although the sources are not very similar at the point of heat generation, the solutions are similar in their large scale effects on the structure.

6.4.4 The Boundary Condition at the Edge of the Plate

The final element of the model to be determined is the boundary condition at the edge of the plate. In a real structure, the ends of the plate are joined, but this cannot be accommodated by the model. Insulating the edges is not the best solution because in a real structure there is no such constraint. If the external frame of the machine is large in comparison to the source, as it usually is, then the best approximate model is an

infinite plate with the heat flux approaching zero at the ends.

6.5 Accommodating Multiple Sources

If the generalized problem is linear, then it is possible to accommodate multiple sources by linearly superimposing the temperature fields of several sources. A machine tool structure behaves as a linear system because the temperature increase of the frame is not large, and radiation effects are small relative to convection. The deviation of the actual solution from the generalized one because of radiation is partially eliminated when the linear generalized solution is optimally fit to the physical response. This is the power of the generalized method.

CHAPTER 7: THE ANALYTICAL SOLUTION TO THE GENERALIZED PLATE MODEL

7.1 Deriving the Differential Equation

Figure 6.1 shows the thermal model of the machine structure. It is a thin, infinite flat plate with a circular ring heat source at its centre. Since the plate is thin and the source is radially symmetric, the heat flux is radial and one dimensional. So as to anticipate potential problems, and to aid the understanding of the problem, the governing differential equation for the temperature in the plate is derived from basic principles in appendix 1. The differential equation is:

$$T'' + \frac{1}{r}T' - aT + \frac{g(r,t)}{k} = \frac{1}{\alpha}\dot{T} \qquad (7.1)$$

where:

$$a = \frac{h}{kw}, \qquad \frac{1}{\alpha} = \frac{\rho C_p}{k} \qquad (7.2)$$

and g(r,t) is the internal heat generation per unit volume. The internal generation is zero everywhere in the plate except for the thin ring at $r=r_0$. If the thickness of the heat generating ring is Δr, then the internal heat generation per unit volume is expressed as:

$$g(r,t) = \frac{q(t)}{2\pi r_0 w}\delta(r-r_0) \qquad (7.3)$$

Where $\delta(r-r_0)$ is the space impulse function, derived in appendix 1. If the plate is at

ambient temperature at t=0, then the boundary and initial conditions are:

$$\begin{aligned} T &= 0 , \qquad \text{when} \quad t=0 \\ T &= 0 , \qquad \text{when} \quad r=\infty \end{aligned} \tag{7.4}$$

Equation (7.1) expresses the internal heat generation as a part of the governing equation. An alternate method is to make the heat generation term zero in the governing equation:

$$T'' + \frac{1}{r}T' - aT = \frac{1}{\alpha}\dot{T} \tag{7.5}$$

and specify the heat generation as one of the boundary conditions:

$$\begin{aligned} \frac{dT}{dr} &= -\bar{q}(t) \qquad \text{when} \quad r=r_o \\ T &= 0 \qquad \text{when} \quad t=0 \\ T &= 0 \qquad \text{when} \quad r=\infty \end{aligned} \tag{7.6}$$

where q(t) is the normalized boundary heat generation.

7.2 Literature Survey of the Plate Model Solution

Equations (7.1) and (7.5) are alternate forms of the same problem, representing a thin, infinite plate with a central ring heat source, and a convection boundary on its face. The available texts on heat transfer, such as *Heat Conduction in Solids* by Carslaw and Jaeger [65] and *Analytical Heat Diffusion Theory* by Likov [66], deal extensively with spheres, cylinders, and slabs, but they do not deal with the geometry of a convecting plate. Michalopoulos et al. [67] solve the problem of a thin plate with a transverse circular hole, but the face of the plate is constrained to have zero temperature, not a convective boundary.

The only difference in the problem formulation between an infinitely long cylinder and a convective plate is the aT term in equations (7.1) and (7.5). The standard methods developed in the texts on heat transfer cannot accommodate the extra term. A thorough search of the literature was unable to turn up any solutions to this problem. An original analytical solution has been derived, and will be presented shortly.

7.3 Attempting the Separation of Variables Method to Solve the Problem

If the heat generation is included in the boundary conditions of the problem, then the governing differential equation is equation (7.5). Equation (7.5) is a linear partial differential equation with constant co-efficients. As a first attempt at a solution, the method of separation of variables will be tried. Assuming that the temperature is a product of two functions, one in time and one in space, then:

$$T = f(r)g(t) \tag{7.7}$$

Substituting equation (7.7) into equation (7.5) yields:

$$f''g + \frac{1}{r}f'g - afg - \frac{1}{\alpha}f\dot{g} = 0 \tag{7.8}$$

This is rearranged to:

$$\frac{f''}{f} + \frac{1}{r}\frac{f'}{f} - a = \frac{1}{\alpha}\frac{\dot{g}}{g} \tag{7.9}$$

The left hand side of equation (7.9) is a function of r alone, and the right hand side is

a function of t alone, so both must equal to a constant value:

$$\frac{f''}{f} + \frac{1}{r}\frac{f'}{f} - a = -\gamma \qquad (7.10a)$$

$$\frac{1}{\alpha}\frac{\dot{g}}{g} = -\gamma \qquad (7.10b)$$

The constant parameter γ is determined from the boundary conditions of equation (7.10a) and so, in general, it is a function of the boundary heat generation q(t). But by definition γ cannot be a function of either r or t. Thus, the method of separation of variables cannot be used to solve this problem. Nevertheless, obtaining the general solution to equation (7.10a) will be a useful tool in developing a new strategy to solve the problem.

Equation (7.10a) is a second order differential equation with non-constant coefficients, but if one makes the substitution:

$$u = \sqrt{\gamma - a}\, r \qquad (7.11)$$

then it becomes the Bessel equation of order zero:

$$u^2 f'' + u f' + u^2 f = 0 \qquad (7.12)$$

The general solution to equation (7.12) is:

$$f = C_1 J_0(\sqrt{\gamma - a}\, r) + C_2 Y_0(\sqrt{\gamma - a}\, r) \qquad (7.13)$$

where J_0 is the Bessel function of the first kind of order zero.
Y_0 is the Bessel function of the second kind of order zero.

The first boundary condition is that $T(t,\infty)=0$, which means that $f(\infty)=0$. This condition is implicitly satisfied, because both $J_0(s)$ and $Y_0(s)$ equal zero as $s\rightarrow\infty$. There is another condition that $T(r,t)$ remain finite over the entire plate, including at $r=0$. This implies that C_2 in equation (7.13) is zero since $Y_0(s)$ becomes infinite at $s=0$. Since the second term in equation (7.13) vanishes, C_1 is arbitrarily set to one, so that:

$$f = J_0(\sqrt{\gamma-a}\,r) \tag{7.14}$$

The next step is to determine the parameter γ. There are a finite number of discrete γ_i, corresponding to the solutions for the second boundary condition. The heat generation boundary, corresponding to the third condition in equation (7.6), requires that:

$$\frac{\partial T}{\partial r}\Big|_{r_0} = \frac{\partial f}{\partial r}\Big|_{r_0} g(t) = \sqrt{\gamma-a}\,J_1(\sqrt{\gamma-a}\,r_0)\,g(t) = -\bar{q}(t) \tag{7.15}$$

where g(t) is the solution to equation (7.10b):

$$g_i(t) = C_i e^{-a\gamma_i t} \tag{7.16}$$

Because of the time dependant boundary condition, the values of γ_i which satisfy equation (7.15) are functions of the variable t, which is an impossible conclusion because of equation (7.10). The method of separation of variables cannot solve the problem, as predicted. But since the form of the solution in the space dimension is now known, it follows that equation (7.1) can be transformed by a suitable Hankel transformation.

7.4 The Solution to the Thermal Model by the Method of the Hankel Transformation

The Hankel Transform is the polar equivalent to the Fourier transform in rectilinear co-ordinates. In practice, the method is similar to the method of Laplace transformation because, as with Laplace, a differential equation is transformed to a new domain where it is more easily solved, and then transformed back by an inverse transform.

In order to apply the Hankel transformation, the boundary conditions should be incorporated into the governing equation through a heat generation term, as in equation (7.1):

$$T'' + \frac{1}{r}T' - aT + \frac{g(r,t)}{k} = \frac{1}{\alpha}\dot{T} \qquad (7.17)$$

where,

$$T = 0 \ , \quad when \quad t=0$$
$$T = 0 \ , \quad when \quad r=\infty \qquad (7.18)$$

The aT term in equation (7.1) complicates the governing equation. The first step in the solution is to apply the transformation:

$$T = \Theta e^{-a\alpha t} \qquad (7.19)$$

which eliminates the aT term in the transformed equation. The next step is to transform the differential equation with the following Hankel transformation:

$$\overline{\Theta}(B,t) = \int_0^\infty r J_0(Br)\Theta(r,t)\,dr \qquad (7.20)$$

where B is a new parameter. The inverse transformation corresponding to equation (7.20)

is:

$$\Theta(r,t) = \int_0^\infty B\,J_0(Br)\,\bar{\Theta}(B,t)\,dB \qquad (7.21)$$

Taking the Hankel transformation of equation (7.1), and replacing the heat generation term by the expression in equation (7.3), results in the transformed equation:

$$\int_0^\infty (\bar{\Theta}'' + \tfrac{1}{r}\bar{\Theta})\,r J_0(Br)\,dr + \tfrac{1}{k}\int_0^\infty e^{-\alpha\alpha t}\frac{q(t)}{2\pi r w}\,\delta(r-r_0)\,r J_0(BR)\,dr = \tfrac{1}{\alpha}\bar{\Theta}$$

It may be shown [68] that:

$$\int_0^\infty (\bar{\Theta}'' + \tfrac{1}{r}\bar{\Theta}')\,r J_0(Br)\,dr = -B^2\bar{\Theta} \qquad (7.23)$$

and the second integral can be evaluated because of the npulse function:

$$\tfrac{1}{k}\int_0^\infty e^{\alpha\alpha t}\frac{q(t)}{2\pi w}\,\delta(r-r_0)\,J_0(Br)\,dr = \frac{q(t)}{2\pi k w}\,e^{\alpha\alpha t}J_0(Br_0) \qquad (7.24)$$

Substituting expressions (7.23) and (7.24) into equation (7.22) results in the following first order equation in the time domain:

$$\bar{\Theta} + \alpha B^2\bar{\Theta} = \frac{\alpha q(t)}{2\pi k w}\,e^{\alpha\alpha t}J_0(Br_0) \qquad (7.25)$$

The partial differential equation (7.1) has been reduced to an ordinary linear differential equation in time. The homogeneous solution is:

$$\bar{\Theta} = \bar{C}e^{-\alpha B^2 t} \qquad (7.26)$$

where C is a constant of integration. The next step is to solve the differential equation for an arbitrary forcing function q(t), and then transform the result back to the time

domain with equation (7.21). Finally, the expression is substituted into equation (7.19) to yield:

$$T(r,t) = \frac{1}{2\pi kw}\int_0^{\infty} BJ_0(Br)\,J_0(Br_0)\,e^{-(a+B^2)\alpha t}\int_0^{t} q(\tau)\,e^{(B^2+a)\alpha\tau}\,d\tau\,dB$$

Equation (7.27) is the analytical temperature distribution for a thin infinite plate with a convective boundary condition on the face, and a central, circular ring heat source. The input is an arbitrary boundary generation function q(t). All of the mathematical details that were left out of the derivation are included in appendix 2.

7.5 The Step Solution

For a linear problem it is not necessary to have a general expression for the temperature distribution, because the general solution to an arbitrary input can be derived from the step solution. This is explained by considering the Laplacian representation of the problem, where the general transfer function H(s) can be derived from:

$$H(s) = \frac{T(s)}{q(s)} \qquad (7.28)$$

Where T(s) is the temperature solution corresponding to input q(s). When q(t) in equation

(7.27) is replaced by the step function $qU_s(t)$, then the step solution is:

$$T = \frac{q}{2\pi kw}\left[F_1(r) - e^{-a\alpha t}F_2(r,t)\right] \qquad (7.29)$$

where,

$$F_1(r) = \int_0^\infty \frac{B}{B^2+a} J_0(Br_1)\, J_0(Br)\, dB \qquad (7.29a)$$

$$F_2(r,t) = \int_0^\infty \frac{B}{B^2+a} J_0(Br_1)\, J_0(Br)\, e^{-\alpha t B^2} dB \qquad (7.29b)$$

The details of the derivation are given in appendix 2.

Equation (7.29) is the theoretical temperature distribution for a central heat source in an infinite plate, with a step heat input applied at t=0. The expression cannot be simplified any further because the improper integrals in (7.29a) and (7.29b) have no closed form solution. The integral in (7.29a) is a function of position but is independent of time, so if the temperature is required at a constant value of r, then equation (7.29a) need only be evaluated once. The integral in (7.29b) is a function of time as well as geometry, so it has to be numerically re-integrated at every time step. Numerical integration of the expression is not always convenient in practice, especially because of the improper limits for β. An approximate expression for temperature at a constant value of r is obtained in the next section by replacing the improper integrals in (7.29a) and (7.29b) by approximate analytical expressions.

7.6 Simplifying the Form of the Thermal Solution

7.6.1 The Physical Form of the Solution

The mathematical form of the expressions for F_1 and F_2 in equation (7.29) are important because they determine the physical nature of the solution. If not for the exponential term inside the integral F_2, then F_2 would equal F_1 and equation (7.29) would be the first-order time response to a step input, with time constant $1/(a\alpha)$. It is tempting to simplify the solution by neglecting the exponential term inside of F_2 but this would not be a realistic assumption, as is evident when the integrals in F_1 and F_2 are numerically evaluated. Figure 7.1 shows a plot of F_2 versus time, integrated numerically by Gaussian quadrature for different values of r, with r_0 (the outer radius of the source) fixed at 2.5 cm. For the purpose of the illustration, the material properties for cast iron were used to define the numerical parameters of F_2. Term F_1 is not a function of time, and is equal to $F_2(t=0)$, as is seen from equation (7.29). $F_2(t)$ is not constant over a reasonable time

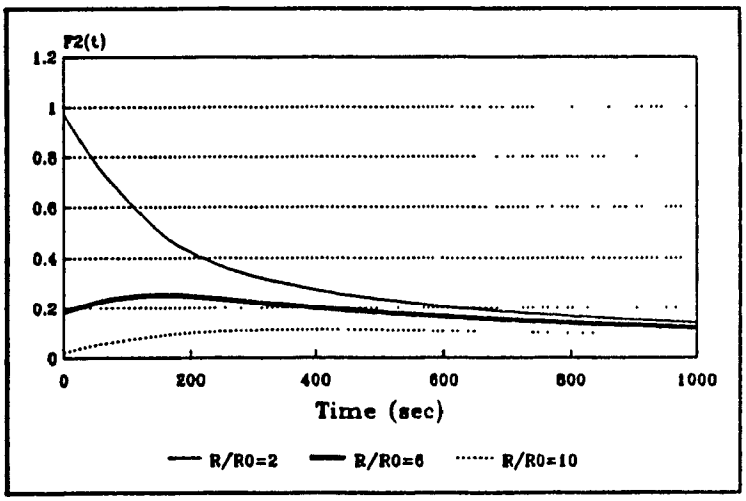

Figure 7.1: Plot of F_2 versus Time

period, and so the response cannot be considered first order.

A further examination of figure 7.1 reveals that the mathematical form of $F_2(t)$ depends on the value of r. For large r, the response goes through a local maximum before decaying to zero, but for small values of r it does not. The behaviour of $F_2(t)$ for small values of time reflects the damped and delayed nature of the temperature solution. For small values of time, $F_2(r,t)$ is approximately equal to:

$$F_2(r,t) \approx e^{\alpha\alpha t} F_1(r) \qquad (7.30)$$

Thus, the temperature remains close to zero for a considerable time period after the application of the heat step at t=0. This is illustrated in figure 7.2, where the analytical temperature profile from equation (7.29) at $r/r_0=6$ is plotted as a function of time. The temperature at profile $r/r_0=6$ hardly responds at all until nearly one minute after the

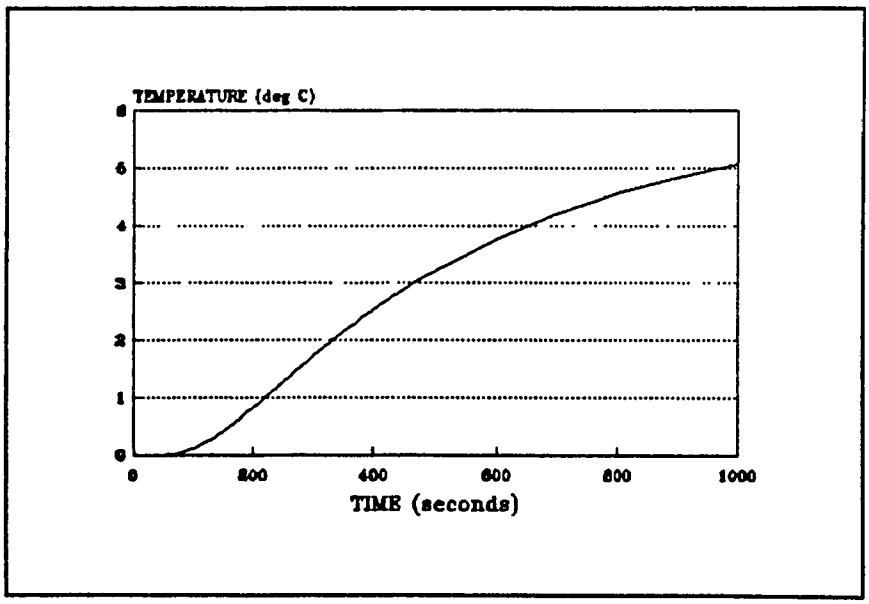

Figure 7.2: Temperature Solution Corresponding to Equation (7.29) for $r/r_0=6$

change in q(t). The larger the r/r_0 ratio, the greater the time lag between changes in the heat input and the temperature response.

Returning to figure 7.1, the reason for the positive initial slope of F_2 for larger r/r_0 ratios is to offset the decaying exponential component in equation (41), and introduce the time delay shown in the solution in figure 7.2. F_2 does not have a positive initial slope for small r/r_0 ratios because the time lag of the solution is small, and no compensation for the exponential component is required. Figure 7.3 shows the solution to equation (7.29) at $r/r_0=2$. The time delay is so small that it is not a factor in the form of the solution.

The initial time delay in the step solution to the direct problem is responsible for the instability of the corresponding IHCP, as discussed in chapter 3. If the general

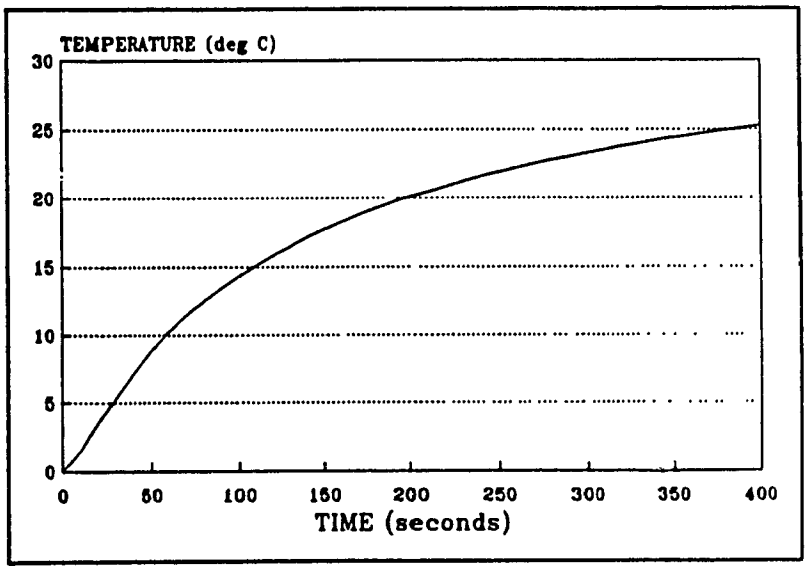

Figure 7.3: Temperature Solution Corresponding to Equation (7.29) for $r/r_0=2$.

solution in equation (7.29) is restricted to its stable form shown in figure 7.3, then the inherent instability of the IHCP is eliminated. The stable form of equation (7.29) corresponds to the mathematical form of $F_2(t)$ with a small r/r_o ratio, shown in figure 7.1. Since the stable form of equation (7.29) is of particular interest, a stable form of the equation will be derived in the next section.

7.6.2 The Stable Temperature Solution for Small Radii

Presuming that r is small, and that the shape of the curve for $r/r_0=2$ is the characteristic form of the response, then the integrals in F_1 and F_2 can be replaced by approximate functional expressions. Figure 7.4 compares the time response of $F_2(t)$ with $r/r_0=2$ to e^{-bt}, again using the material properties of cast iron for the numerical parameters. Although the $F_2(t)$ term and the exponential term behave quite differently, their time constants are similar, so the approximation has to be accurate over the entire useful domain of the solution. It does not be acceptable to approximate $F_2(t)$ as a simple constant or linear function, because it would not fit $F_2(t)$ over the whole domain.

$F_2(t)$ starts from a constant value at t=0, and decays to zero as time approaches infinity. The decay is not exponential, but roughly a first power inverse, closely approximated by the function:

$$F_2(t) = \frac{A}{1+bt} \qquad (7.31)$$

where the parameters A and b are determined individually for each value of r. Figure 7.5 compares $F_2(t)$ with $r/r_0=2$, to equation (7.31) with A=0.952 and b=0.00603. Equation (7.31) is a good representation to $F_2(t)$, provided that r/r_0 does not exceed about 4.

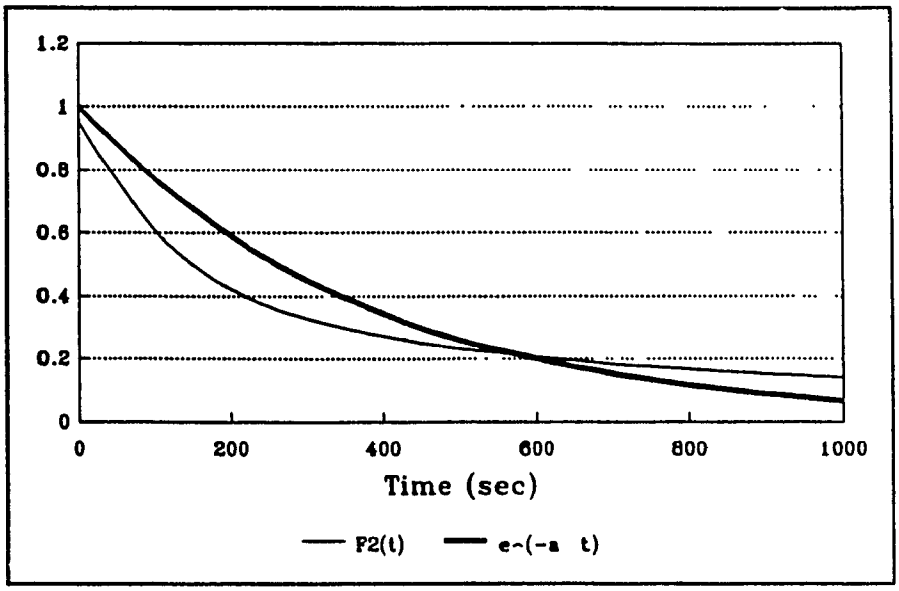

Figure 7.4: Comparison of $F_2(t)$ and e^{-act}

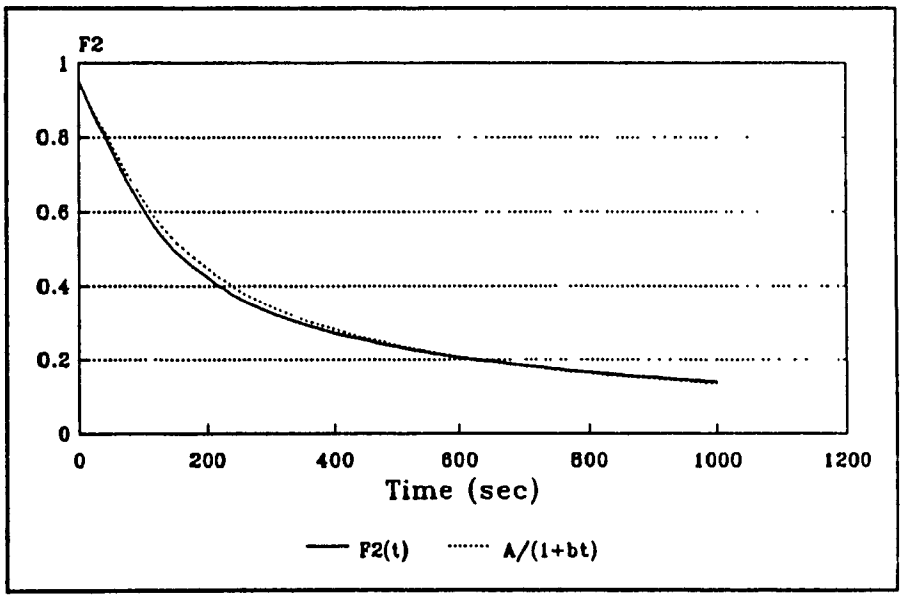

Figure 7.5: $F_2(t)$ and Functional Approximation

Replacing $F_2(t)$ by equation (7.31) and $F_1(t)$ by $F_2(0)$ in equation (7.29), and lumping the analytical parameters into three empirical parameters K, a, and b, then the following approximate expression is obtained:

$$T = qK\left(1 + \frac{e^{-at}}{1 + bt}\right) \qquad (7.32)$$

7.7 The Deflection Solution for an Infinite Plate

7.7.1 The Relationship Between the Temperature Distribution and the Thermal Deflection

If there are no external mechanical constraints, then the thermal deflection is related to the temperature distribution by the well-known relation:

$$\epsilon = \alpha_c (T^{\bullet} - T_0^{\bullet}) \qquad (7.33)$$

where, ϵ is the strain
α_c is the co-efficient of thermal expansion
$(T^{\bullet}-T_0^{\bullet})$ is the change in temperature from the stress free reference temperature.

The differential expression for the strain is given by $\epsilon = d\delta/dr$, where $d\delta$ is the differential thermal deflection, and dr is the differential radius of the plate. If the atmospheric temperature $T_a^{\bullet}$ is also the unstressed reference temperature $T_0^{\bullet}$, then $T^{\bullet}-T_0^{\bullet}$ is equal to $T=T^{\bullet}-T_a^{\bullet}$, and equation (7.33) may be expressed as:

$$\delta = \alpha_c \int_0^r T(r, t)\, dr \qquad (7.34)$$

where T(r,t) is the theoretical temperature distribution in the plate, derived earlier in the section.

7.7.2 The Analytical Deflection Solution

The temperature distribution in an infinite plate, with a central heat source subjected to a step input at t=0 seconds, was already derived in section 3.5.5. Substituting the temperature distribution from equation (7.29) into equation (7.34) yields:

$$\delta = \alpha_c \int_0^r \frac{q}{2\pi k w} \left[F_1(r) - e^{-a\alpha t} F_2(r,t) \right] dr \qquad (7.35)$$

Substituting for F_1 and F_2, and reversing the order of integration, the solution becomes:

$$\delta = \frac{q\alpha_c}{2\pi k w} \left[G_1(r) - e^{-a\alpha t} G_2(r) \right] \qquad (7.36)$$

where,

$$G_1 = \int_0^\infty \frac{B}{B^2+a} J_0(Br_1) \int_0^r J_0(Br)\, dr\, dB \qquad (7.36a)$$

$$G_2 = \int_0^\infty \frac{B}{B^2+a} J_0(Br_1)\, e^{-\alpha t B^2} \int_0^r J_0(Br)\, dr\, dB \qquad (7.36b)$$

The integral:

$$I = \int_0^r J_0(Br)\, dr \qquad (7.37)$$

appears in the expressions for G_1 and G_2. The integral can be evaluated if the bessel function inside the integration is replaced by its power series expansion. The

mathematical details are given in appendix 3. The end result is:

$$G_1 = \int_0^{\infty} \frac{B}{B^2+a} J_0(Br_1) \sum_{m=0}^{\infty} T_m(Br) \frac{r}{2m+1} dB \qquad (7.38a)$$

$$G_2 = \int_0^{\infty} \frac{B}{B^2+a} J_0(Br_0)\, e^{-a\alpha t} \sum_{m=0}^{\infty} T_m(Br) \frac{r}{2m+1} dB \qquad (7.38b)$$

where Tm is the m^{th} term of the Bessel series.

7.8 The Simplified Form of the Deflection Solution

7.8.1 The Functional Form of the Solution

As was the case with F_1 and F_2, there is no closed form solution for the improper integrals in G_1 and G_2. The expression G_2 is integrated for different r/r_0 ratios, and the results are shown in figure 7.6. The function has a finite, non-zero value when t=0, and decays to zero as time approaches infinity, just like $F_2(t)$ from the thermal problem. As before, the analytical form that best describes the functional decay is a first-power inverse, that is $f(t)=1/t$.

7.8.2 The Approximate Solution for Large Radii

The purpose of the deflection solution is to determine the thermal deflection at discrete points in a machine structure, the points corresponding to the positions of the table and the cutting tool. These points are always separated by a considerable distance, so it is only the large scale solution of equation (7.36) that is significant. A simplified expression for the deflection is derived by replacing the complicated expressions G_1 and

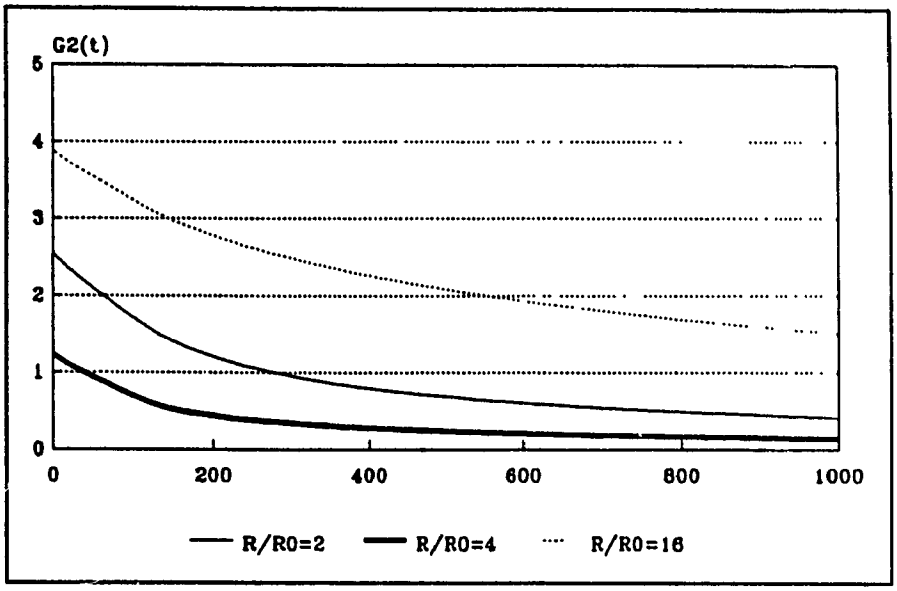

Figure 7.6: Plot of $G_2(t)$

G_2 by functional approximations that are valid at a large radius from the source.

Focusing on the functional form of the $r/r_0=16$ solution, figure 7.7 shows a comparison between G_2 and $e^{-\alpha ct}$. The most significant feature of figure 7.7 is that the time constant of the exponential term is much smaller that the time constant of the G_2 term. As time becomes large, the exponential term approaches zero very quickly, and so the product $G_2(t)e^{-\alpha ct}$ tends to zero quickly also. Thus, unlike the situation with $F_2(t)$, it is only the first part of $G_2(t)$ that is significant, between about $t=0$ and $t=1000$. It does not matter how G_2 behaves after that, because the exponential term makes it zero anyway.

In the interval $0<t<1000$, $G_2(t)$ can be approximated by a straight line:

$$G_2(t) = A - bt \qquad (7.39)$$

as shown in figure 7.8.

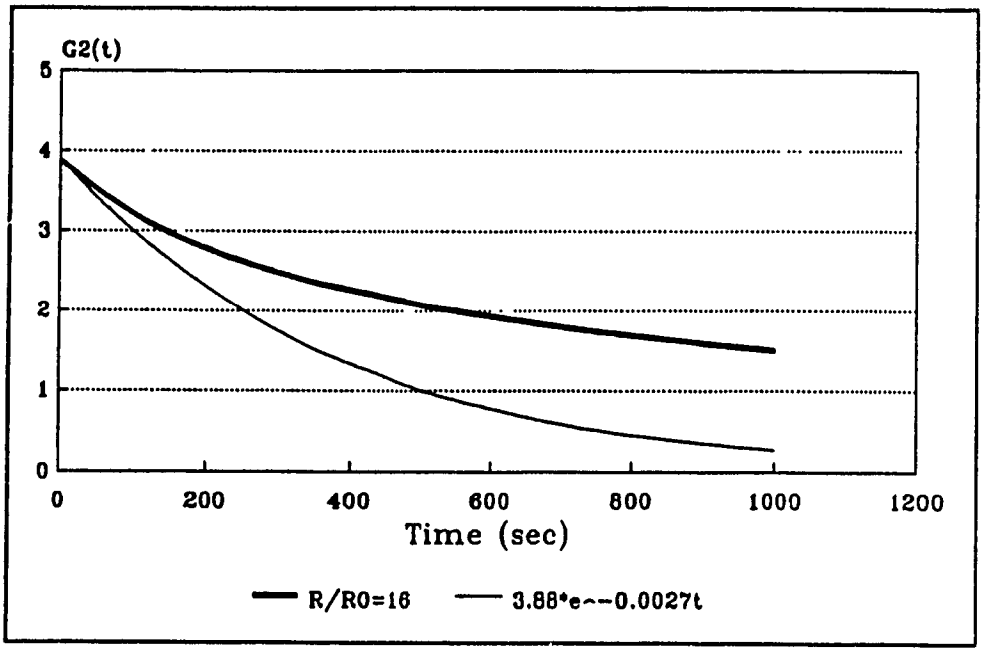

Figure 7.7: Comparison of $G_2(t)$ and $e^{-\alpha t}$

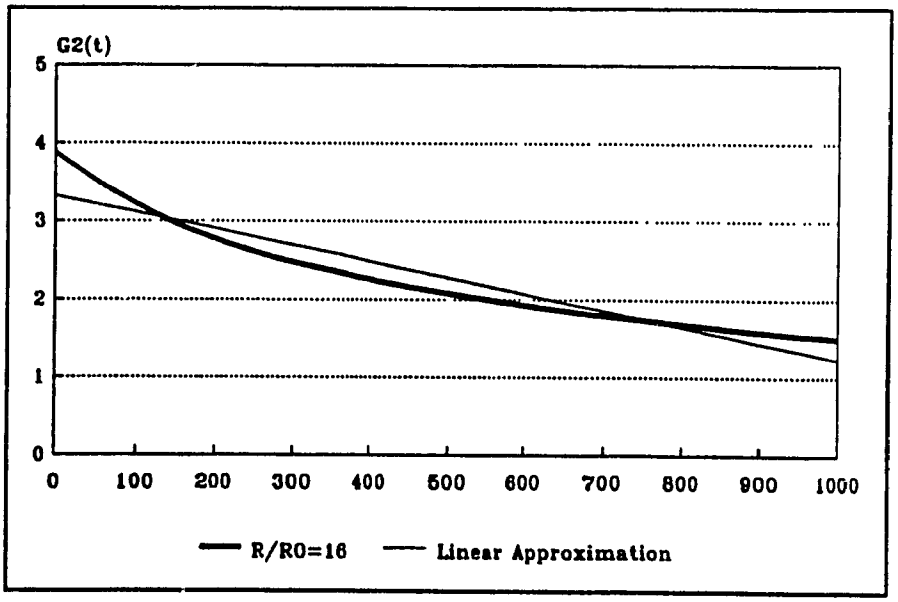

Figure 7.8: $G_2(t)$ and Functional Approximation

Since G_2 is equal to G2(t=0), G1 and G2(t) in equation (7.38) can be replaced by the functional approximation in equation (7.39) to give:

$$\delta = \frac{q\alpha_c}{2\pi kw}(A - (A-bt)\, e^{-a\alpha t}) \qquad (7.40)$$

This represents the large r deflection response in an infinite plate with a central heat source, subject to a step input in heat generation. The solution is generalized by lumping the analytical parameters into three empirical parameters A, B, and a:

$$\delta = q\,(A - [A - Bt]\, e^{-at}) \qquad (7.41)$$

7.9 Converting the Infinite Plate Step Solutions to the Laplace Domain

7.9.1 The Laplace Transformation Equation

The transformation equation from the time domain to the s-domain is given by the integral:

$$F(s) = \int_0^{\infty} e^{-st} f(t)\, dt \qquad (7.42)$$

where s is the complex Laplacian variable.

Three step solutions for the infinite plate have already been derived in the time domain: 1) the general step solution for the temperature distribution in the plate, as given by equation (7.29), 2) the stable step solution for the temperature profile at discrete points, derived on the assumption that the distance between the point and the generating source is small, given by equation (7.32), 3) The approximate step solution for the thermal deflection at discrete points, derived on the assumption that the distance between

the point and the generating source is large, given by equation (7.41), Each of these solutions will be transformed to the Laplace domain by equation (7.42) in the following subsections.

7.9.2 Converting the General Thermal Step Solution to the Laplace Domain

The general thermal solution is transformed to the s-domain by directly substituting equation (7.29) into the transformation equation (7.42):

$$T(s) = \frac{q}{2\pi kw}\int_0^{\infty} F_1(r) - e^{-a\alpha t}F_2(r,t)\,e^{-st}\,dt \qquad (7.43)$$

where F_1 and F_2 are defined by equations (7.29a) and (7.29b). The first term, $F_1(r)$, is not a function of time so it can be brought outside of the integration. The second term in equation (7.43) is the product of two time functions, $F_2(r,t)$ and the exponential $e^{-a\alpha t}$. The solution is obtained by reversing the order of the integration and applying the shifting theorem. The mathematical details of the integration are given in appendix 4. The final result is:

$$T(r,s) = \frac{q}{2\pi kw}\left[\frac{F_1(r)}{s} - \int_0^{\infty}\frac{B}{B^2+a}J_0(Br_1)J_0(Br)\frac{1}{s+\alpha(a+B^2)}\,dB\right]$$

where $F_1(r)$ is given in equation (7.29a). The result is not fully analytical because the improper integral has no closed form solution. Obtaining the solution in the s-domain is a powerful tool however, because it can now be used to define a general solution to the infinite plate problem. Furthermore, inverting the equation in the s-domain is as simple as algebraically inverting the transfer function.

7.9.3 Converting the Stable Temperature Solution for Small Radii to the Laplace Domain

The temperature solution for small radii that is given in equation (7.32) has two terms. The term on the left is a simple constant that transforms to a multiple of 1/s. The right hand term is more difficult, so it will be handled separately. Neglecting the constant multiplier, the right hand term is:

$$f(t) = \frac{e^{-at}}{1+bt} \tag{7.45}$$

The s-domain is a complex plane and s is, in general, a complex variable. Substituting u=(1+bt)(s+a)/b, into equation (7.45) results in the complex line integral:

$$\frac{e^{\frac{a\cdot s}{b}}}{b} \int_{\frac{a\cdot s}{b}}^{\infty} \frac{e^{-u}}{u}\, du \tag{7.46}$$

The complex integration goes from the point s=(R+a)/b + I/bj to s=∞ + ∞ j, as shown in figure 7.9. Since the complex plane is a conservative vector field, the solution is independent of the path of integration. The integration will be performed in two parts, along path 1 from the starting point to s=∞ + I/bj, and then along path 2 from s=∞+I/bj to s=∞+∞j. It can be shown that the integration over the second path is zero, so the transformation is given by the integration of the function over path one only. The details of the complex integration are given in appendix 5, and the end result is:

$$\frac{qA}{2\pi r w}\left(\frac{R-Ij}{R^2+I^2} + \frac{1}{b}\int_0^{\infty} \frac{\left([u+z]-\frac{I}{b}j\right)e^{-u}}{(u+z)^2+\left(\frac{I}{b}\right)^2}\, du\right) \tag{7.47}$$

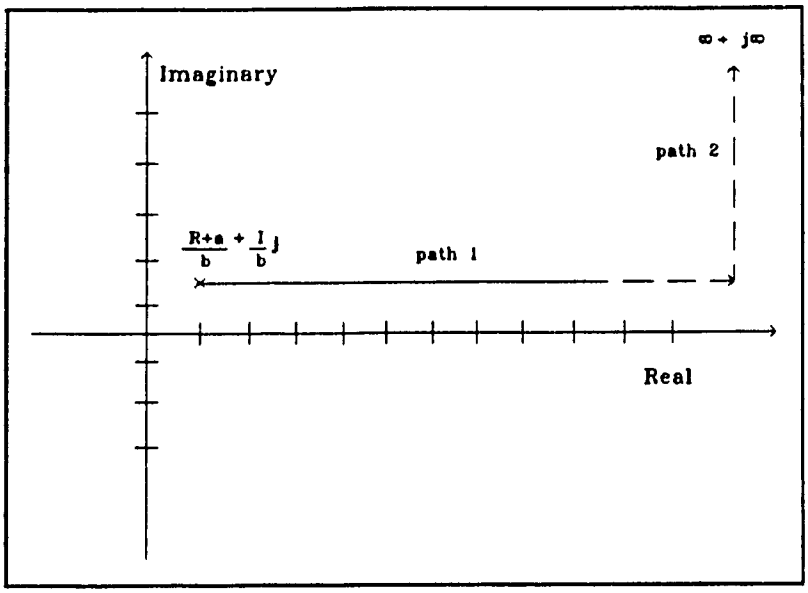

Figure 7.9: Path of Integration for Equation (7.46)

which is the s-domain representation of equation (7.32), where R and I are the real and imaginary components of s, and z is defined by:

$$z = \frac{R+a}{b} \qquad (7.48)$$

7.9.4 Converting the Deformation Solution for Large Radii to the Laplace Domain

The deformation solution for small radii is given by equation (7.41). The equation is composed of simple expressions, and the Laplace transforms are readily available in standard tables. The Laplace transformation of equation (7.41) is given by:

$$\delta(s) = q\left(\frac{A}{s} - \frac{A}{s+a} + \frac{B}{(s+a)^2}\right) \qquad (7.49)$$

7.10 Expressing the Solutions in Transfer Function Form

For a linear problem, the solution to an arbitrary input is completely defined by the step solution in the s-domain. If $T_s(s)$ is the step solution in the s-domain, then the transfer function H(s) is found by dividing the step solution by the step input. Thus,

$$H(s) = sT_s(s) \tag{7.50}$$

The solution to an arbitrary input q(s) is found in the s-domain by multiplying the input by the transfer function:

$$T(s) = H(s)\,q(s) \tag{7.51}$$

CHAPTER 8: THE FINITE-ELEMENT THERMAL TEST MODEL

8.1 The Need for a Finite-Element Thermal Model

The purpose of a finite element thermal model is to provide a standard test model, through which the performance of the various IHCP algorithms can be evaluated. A finite element model is a better test model than a physical model for three reasons:

1) There is no physical limitation in applying the heat inputs or accurately measuring the data.

2) The environment is controlled, so that specific problems can be investigated independently, giving better insight into the methods, and making it easier to identify the sources of the problems.

3) The model is easily modified so that a simple model can be used at first, and then later it can be expanded to accommodate a more complicated structure.

8.2 The Configuration of the Finite-Element Model

Figure 8.1 shows the thermal finite element model of the test structure, constructed with 1249 three dimensional brick elements. The shape is a hollow rectangular column, representing part of a machine tool structure. The column has two small transverse holes cut into it, and there is a source of heat generation on the inside surface of each hole, labelled Q_d in figure 8.1. Q_d represents the heat generation of the main spindle bearings of a milling machine. The two horizontal projections are roughly equivalent to the arm and table, and the vertical column represents the main column of a milling machine. There are three additional sources of heat generation on the surface

of the structure, labelled Q_{C1}, Q_{C2}, and Q_{C3}. These sources represent artificial heating elements, used for control purposes. Q_{C3} consists of two sources symmetrically located on the upper and lower surfaces of the arm of the structure.

All of the sliding contacts and internal mechanisms which would be present in a real machine tool structure have been neglected in the finite element model, as a preliminary step before applying the method to an actual machine tool. The model is designed in such a way that the geometry could be easily duplicated by a physical model. The external faces of the model are exposed to a convective environment, and the internal faces are insulated. In practice the inside faces would also be exposed to convection, but since the thickness of the wall is thin in comparison to the dimensions

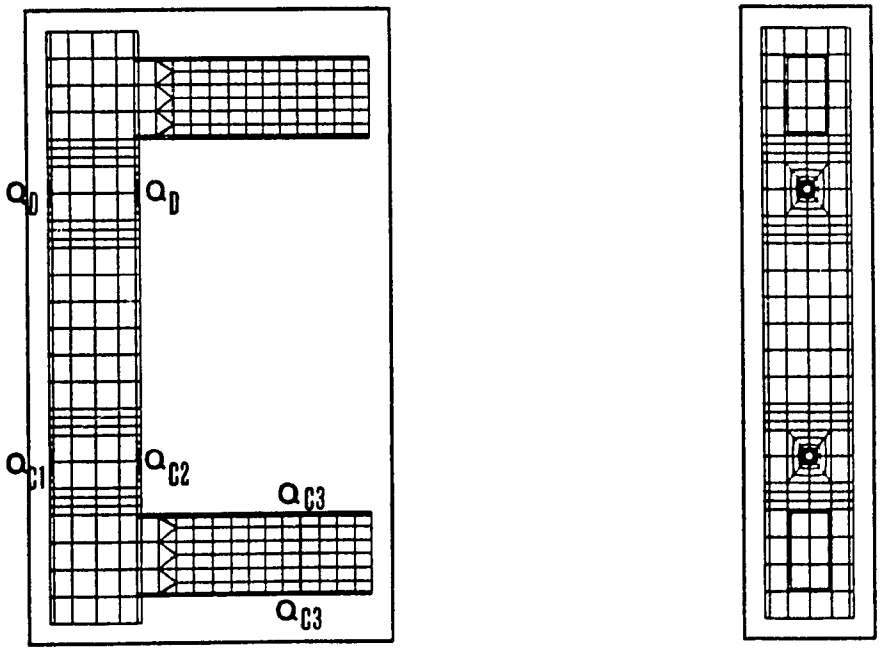

Figure 8.1: Finite-Element Model of Test Structure

of the column, it is reasonable to assume that there is no temperature variation across the thickness of the wall. Thus, doubling the co-efficient of convective heat transfer on the outer surface is sufficient to account for the internal and external convection. The ambient and initial temperatures are taken to be zero, so that the temperature solution represents the increase above the ambient conditions.

8.3 The Solution Algorithm

The thermal finite-element model is solved by the super SAP finite element algorithm, as part of the ALGOR finite element modelling and solver package. The basic principle of the method is based on:

-dividing the structure (continuum) into a number of finite elements which are assumed to be interconnected at a discrete number of nodes situated on their boundaries

-within each finite element a function (called the weight function) is chosen to uniquely define the temperature solution within the finite element in terms of the nodal values.

Algor has a choice between first, second and third order weight functions for its three-dimensional brick elements. The models are created in three dimensional wire frame by a CAD system, and decoded by a mesh generating software package. Boundary conditions are added prior to decoding, or by editing the solution matrix. The solution matrix is solved by a block solver, and the output can be sent to a viewing file, or redirected to a data file. The nodal positions of the thermal model must be identical to the nodal positions of the thermal deformation model, so that the temperature solution

can be used in the thermal deformation solution. For a more detailed description of the finite-element method and how it is implemented, the reader may refer to the references [69-71].

8.4 The Temperature Solution for the Thermal Model

Figure 8.2 shows the isothermal lines representing the steady state temperature distribution in the test model, when the heat generation of source Q_d is increased from zero to 164 W at time equal to zero. Figure 8.3 shows an expanded view of Q_d, indicating six points where the temperature is measured, and figure 8.4 shows the transient temperature profiles at these points as functions of time. The further the position of the measured point from the source, the lower the maximum temperature rise, and the greater the time lag between the application of the input and the beginning of the temperature rise, as expected from the analytical solution in an infinite plate, considered previously.

8.5 Defining the Input and Output Variables

The temperature profile at each position in figure 8.3 is completely defined by the model of the structure and the thermal boundary conditions, including the heat generation. Therefore, it is possible to apply the IHCP to any one of the nodes in figure 8.3 to determine the heat generation of the source, as discussed in section 3.2.4. But a problem arises when more than one source is independently active at the same time, because with only one measured point it is impossible to determine how much of the

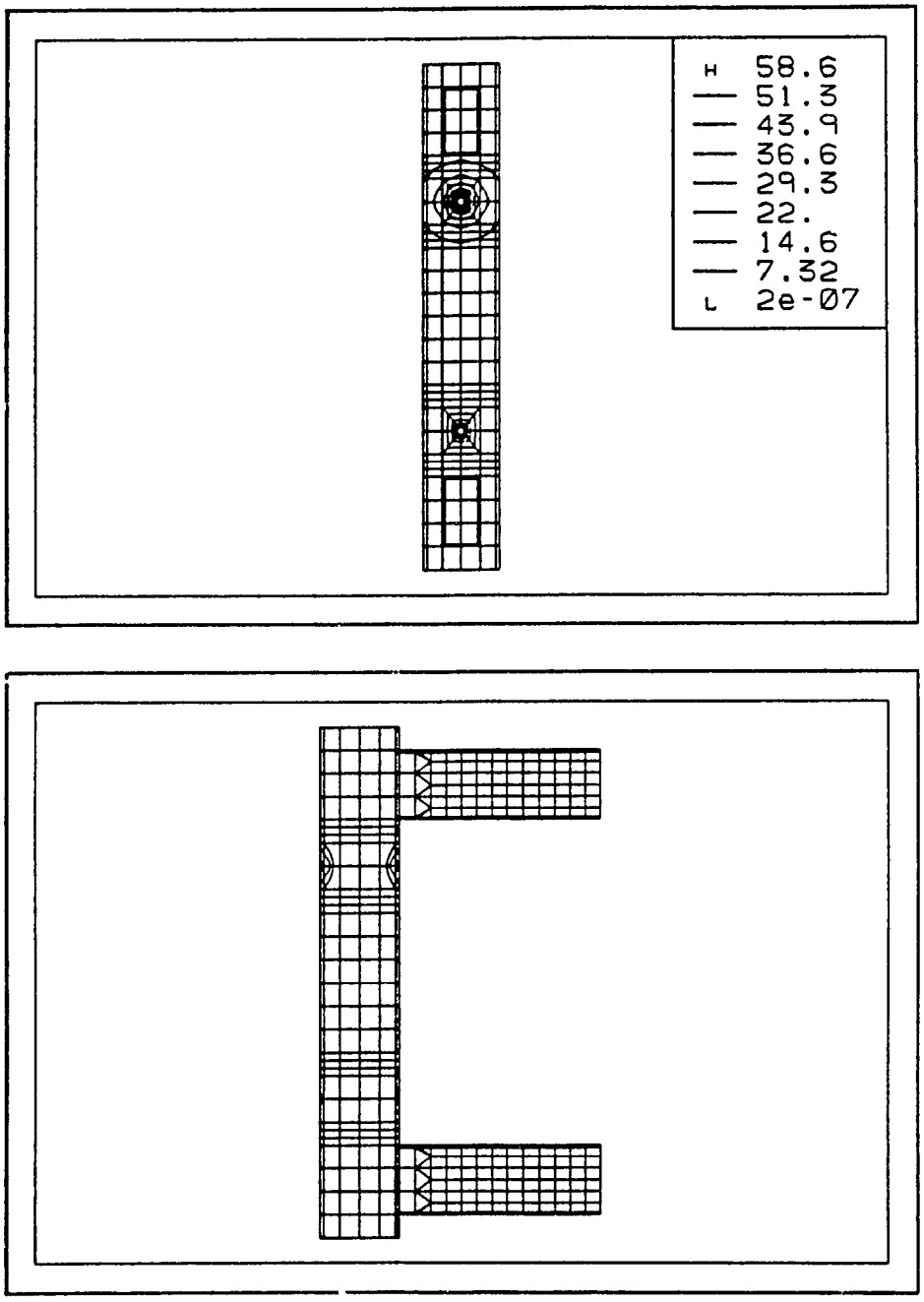

Figure 8.2: Steady-State Isothermal Lines in Test Model for Unit Heat Generation

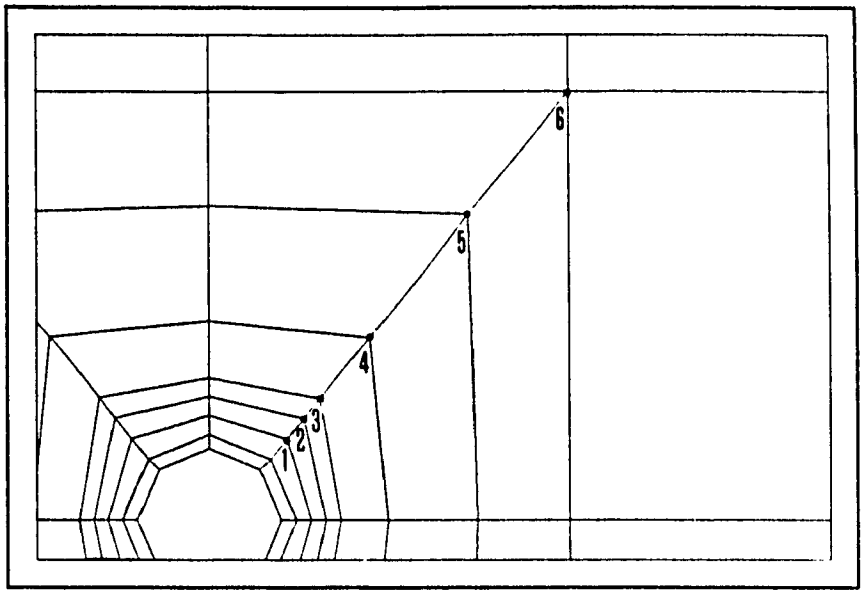

Figure 8.3: The Six Measured Nodes

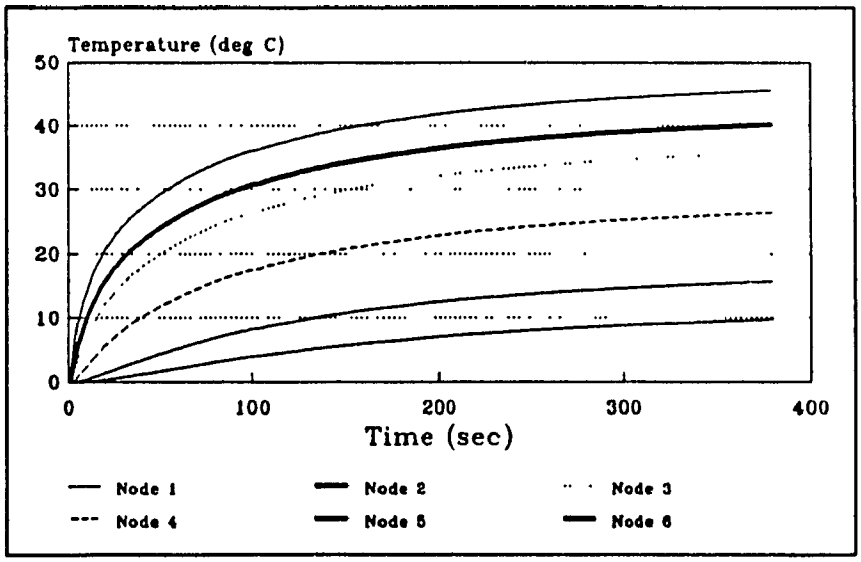

Figure 8.4: Temperature Profiles of Nodes 1 through 6

temperature increase is due to each source. There have to be as many measured temperatures as there are independent sources in order to uniquely define the generation of multiple sources. Furthermore, solving for the heat generation of multiple sources is very difficult unless the IHCP can be decoupled, so that the temperature history of each input corresponds to the heat generation of a single source. Table 8.1 gives the steady state temperatures of the nodes in figure 8.3, for a 164 W step in the heat generation of Q_2. The temperatures are not zero, indicating that there is a coupling between the sources in the IHCP if one of those temperatures is used to define the input.

It is possible to reduce the coupling of the heat sources by defining a temperature difference as the input to the IHCP, instead of a single temperature. Table 8.1 indicates that while the point temperatures in the vicinity of Q_1 do respond to the generation of source Q_2, temperature differences in the vicinity of Q_1 do not.

Figure 8.5 shows the temperature difference between nodes 3 and 4 in figure 8.3. Node 3 is 1.4cm from the source, and the distance between the two nodes is 1.4cm. The position of the measured nodes and the spacing between them is reasonable for an experimental apparatus.

Table 8.1: Steady-State Temperatures of Key Nodes in the Vicinity of Q_{c1} and Q_{c2} for $Q_{c1}=2$

Temp	Node 1	Node 2	Node 3	Node 4	Node 5	Node 6
Q_{c1}	0.7	0.7	0.6	0.6	0.6	0.6
Q_{c2}	45.8	40.3	35.9	26.6	15.8	9.7

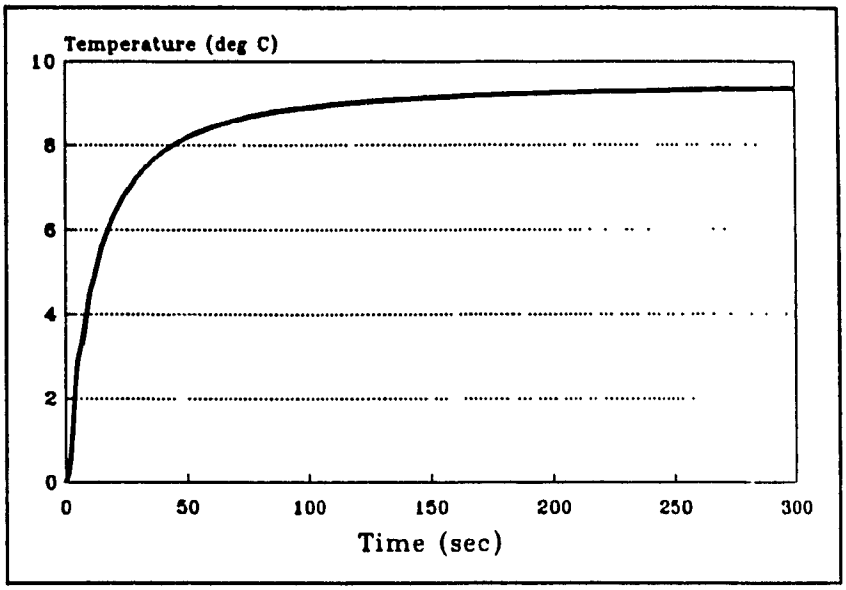

Figure 8.5: The Temperature Difference Profile between Nodes 3 and 4

The temperature difference between nodes 3 and 4 will be used as the standard temperature input for estimating the thermal boundary conditions of the test structure. The temperature profile in figure 8.4 is thus the step solution, which will be used to used to define the Laplace transfer function in the next part of the thesis.

8.6 Curve-Fitting the Generalized Thermal Transfer Function

8.6.1 The Curve-Fitting Algorithm

The generalized thermal transfer function given by equation (7.47) is adapted to a particular problem by curve fitting the empirical parameters of equation (7.32) to the step solution of the direct problem. There are a number of ways to curve-fit the parameters, but the best method is to minimize the sum of the square of the error between the measured data and the analytical basis. If the error residual is defined by the

equation:

$$S = \sum_{i=1}^{n} (Y(t_i) - T(t_i, a_1, a_2, .. a_m))^2 \qquad (8.1)$$

Where $Y(t_i)$ is the measured data and $T(t_i)$ is the analytical base, and a_1, a_2,...a_m are the empirical parameters of the analytical base. The least square solution is found by solving the following system of equations:

$$\sum_{i=1}^{n} \frac{\partial T(t_i, a_1, a_2, .. a_m)}{\partial a_2} T(t_i, a_1, a_2, .. a_m) - \sum_{i=1}^{n} \frac{\partial T(t_i, a_1, a_2, .. a_m)}{\partial a_2} Y(t_i$$

$$\sum_{i=1}^{n} \frac{\partial T(t_i, a_1, a_2, .. a_m)}{\partial a_1} T(t_i, a_1, a_2, .. a_m) - \sum_{i=1}^{n} \frac{\partial T(t_i, a_1, a_2, .. a_m)}{\partial a_1} Y(t_i$$

.... (8.2)

$$\sum_{i=1}^{n} \frac{\partial T(t_i, a_1, a_2, .. a_m)}{\partial a_m} T(t_i, a_1, a_2, .. a_m) - \sum_{i=1}^{n} \frac{\partial T(t_i, a_1, a_2, .. a_m)}{\partial a_m} Y(t_i$$

The function $T(t_i, a_1, a_2, .. a_n)$ is the analytical base that is to be optimally fit to the measured data. There are m empirical parameters to be determined, yielding m simultaneous equations in the form of equation (8.2). In general the equations are non-linear, so the solution requires a method of solving a system of m non-linear equations for m unknown parameters. Such a program has been written in Fortran code, and this will be used in all subsequent situations where curve-fitting is required. The major difficulty that had to be overcome was the problem of false convergence to inflexion points, especially for the thermal base function.

8.6.2 Curve-Fitting the Temperature Difference

The generalized solution for a temperature profile is given by equation (7.32):

$$T(t) = K\left(\frac{1-e^{-at}}{1+bt}\right) \qquad (8.3)$$

The analytical expression for a temperature difference is found by taking the difference $T_1(t)$-$T_2(t)$, where $T_1(t)$ and $T_2(t)$ are the temperature profiles at two distinct nodes. Thus,

$$\Delta T(t) = K_1+K_2+\frac{K_2(1+b_1t)\,e^{-a_2t}-K_1(1+b_2t)\,e^{-a_1t}}{(1+b_1t)\,(1+b_2t)} \qquad (8.4)$$

There are 6 parameters to be determined in equation 8.4. These are found by curve fitting each of the temperature profiles to equation (8.3) separately, thereby determining the parameters three at a time. The problem with this method is that it is the temperature profiles that are optimally matched, not the temperature difference. Furthermore, six empirical parameters is very cumbersome, and unnecessary in practice. If the parameters in equation (8.4) are arbitrarily constrained such that K_1=K2, $a_1=a_2$, and $b_1=b_2$, then equation (8.4) reduces to equation (8.3). The analytical form of the temperature difference is similar to the analytical form of the temperature profile, so equation (8.3) can serve as the generalized solution to the temperature difference, as well as the temperature profile.

Figure 8.6 shows the finite-element temperature difference between nodes 3 and 4 previously given in figure 8.5, compared to the approximation based on equation (8.3). The optimal parameters were found by the least square method to be K=17.0, b=0.07, and a=0.01. Figure 8.6 shows that equation (8.3) is the ideal basis function for

representing the temperature difference profile. Very little accuracy was lost by accepting the simpler temperature difference relation in equation (8.3) instead of the more complicated relation in equation (8.4).

The importance of an analytical derivation is illustrated by the graphs in figure 8.7, in which a number of other analytical functions are curve-fit to the temperature difference profile. None of the functions simulates the temperature response as well as equation (8.2). The analytic functions in figure 8.7 cannot be made to exactly fit the temperature difference profile, because the temperature difference does not physically resemble any of these standard functions. Even the functions in graphs E and F, although they appear to be reasonable approximations, do not match the mathematical behaviour of the temperature difference curve in its first and second derivatives at critical points

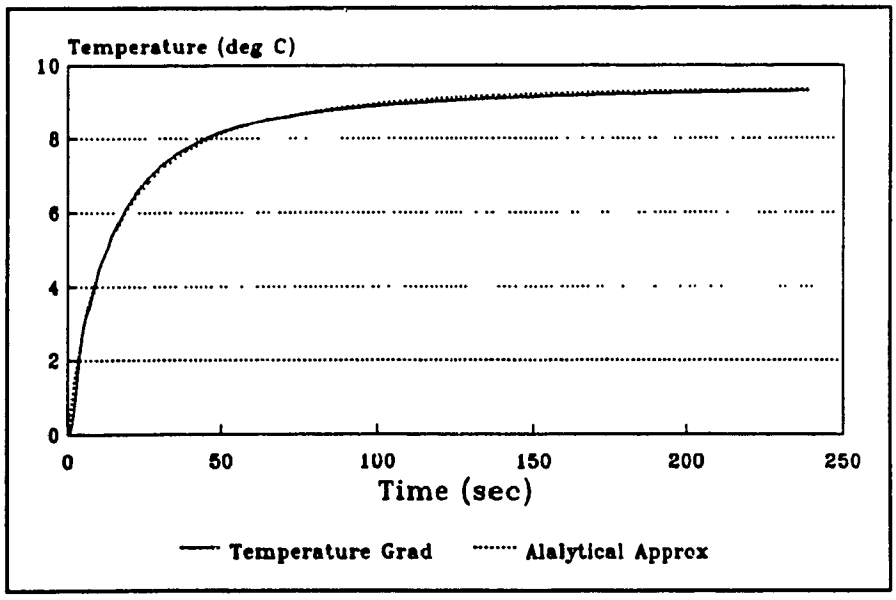

Figure 8.6: Finite-Element Temperature Difference and Analytical Approximation

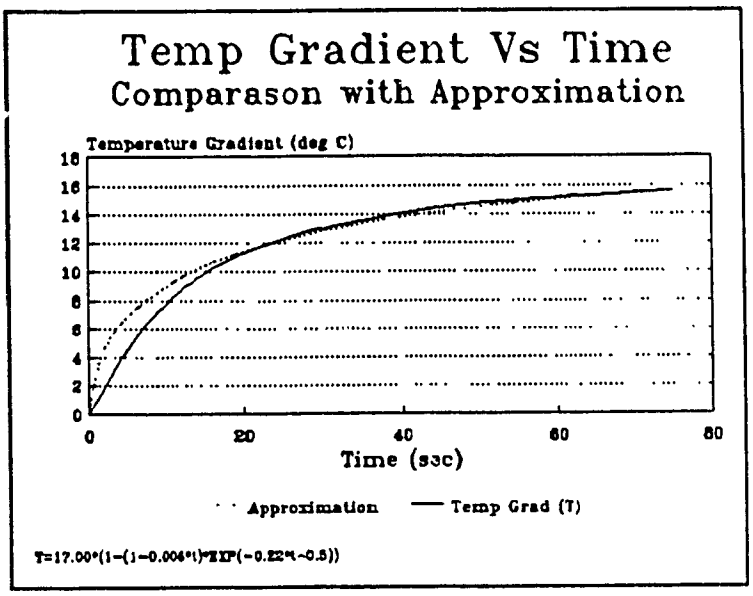

Graph A: Functional Curve-Fit to Temperature Difference Based on

$$T = K(1 - e^{-at})$$

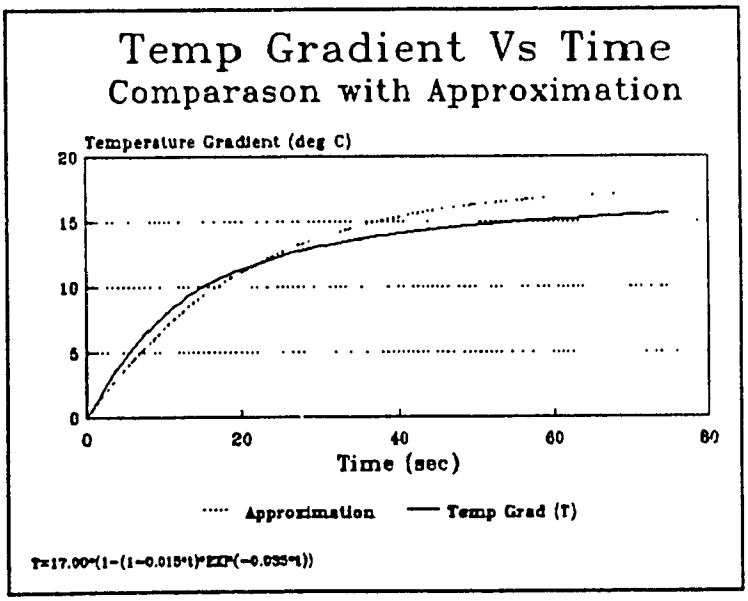

Graph B: Functional Curve-Fit to Temperature Difference Based on

$$T = K(1 - (1 + bt)\, e^{-a\sqrt{t}})$$

Figure 11: Various Functional Approximations to the Temperature Difference

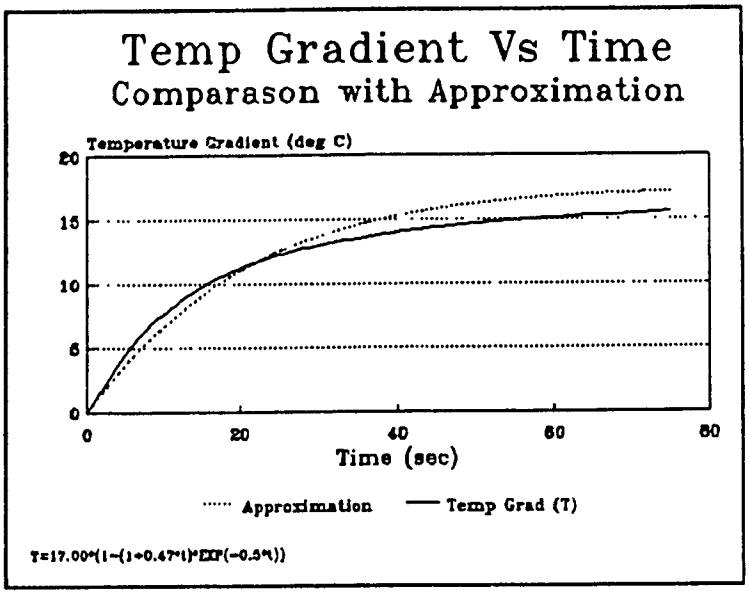

Graph C: Functional Curve-Fit to Temperature Difference Based on

$$T = K(1 - (1 + bt)e^{-at})$$

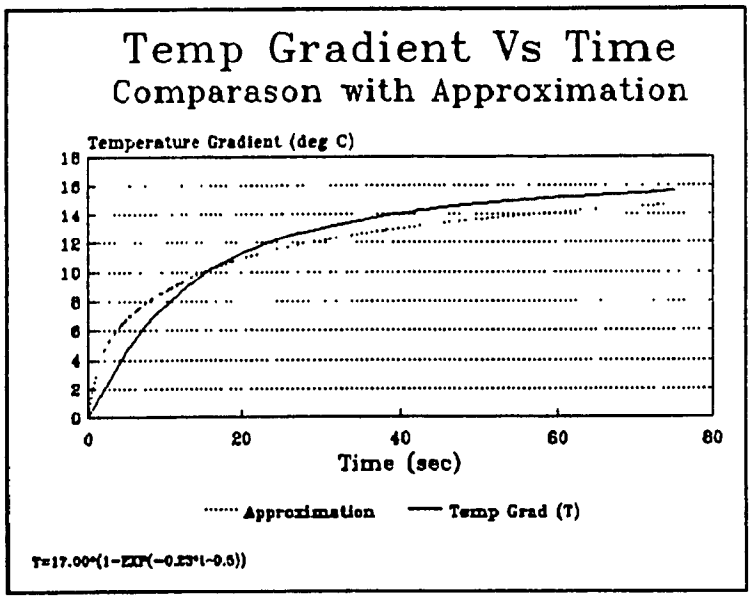

Graph D: Functional Curve-Fit to Temperature Difference Based on

$$T = K(1 - e^{-a\sqrt{t}})$$

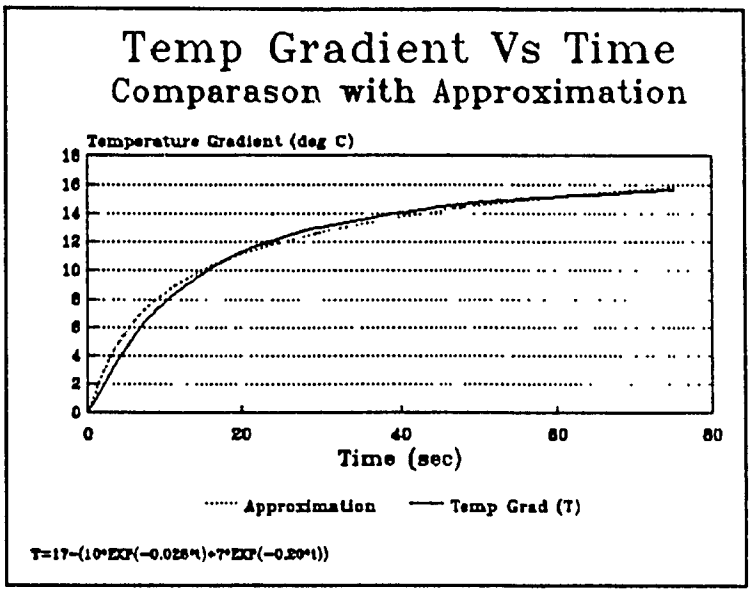

Graph E: Functional Curve-Fit to Temperature Difference Based on

$$T=(A_1+A_2)\ -\ \left(A_1 e^{-a_1 t}\ +\ A_2 e^{-a_2 t}\right)$$

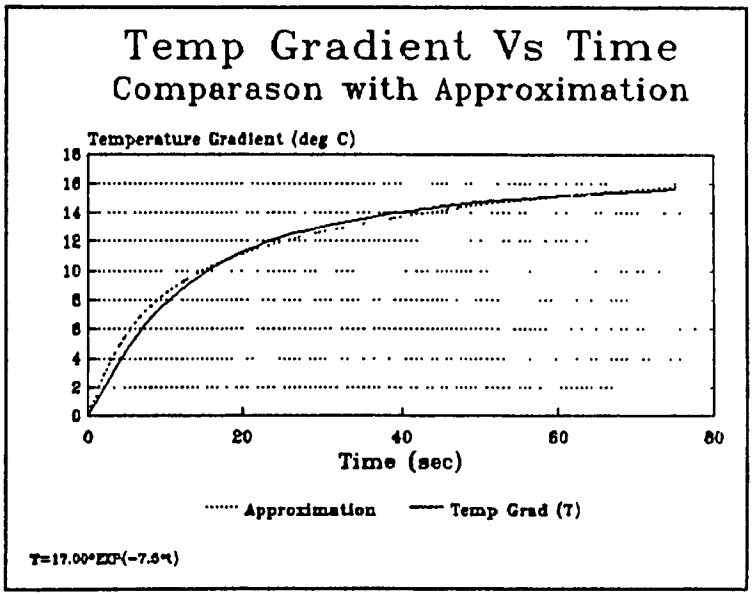

Graph F: Functional Curve-Fit to Temperature Difference Based on:

$$T\ =\ Ke^{-a/t}$$

in the temperature profile. It is important that the mathematical form of the analytical step solution be as similar as possible to the actual solution, because it will be used later to derive a transfer function that extrapolates beyond the step solution.

In contrast to the functions in figure 8.7, Equation (8.3) plotted in figure 8.6 fits the form of the temperature difference perfectly. This is the advantage of knowing the analytical form of the solution in advance. It might have taken hundreds of trials before the form of equation (8.3) were guessed by trial and error, if at all. The analytical step is essential for a thorough understanding of the physical process, and allows for an efficient utilization of the empirical data in a simple and accurate expression. The extra time and effort required to formulate the analytical expression will be justified later on by the improved accuracy of the transfer function.

PART III: THE INVERSE HEAT CONDUCTION PROBLEM

Introduction

This part of the thesis is concerned with the first part of the model in figure 5.1, the transfer function relating discrete temperature measurements to the thermal boundary conditions of a machine tool structure. This part of the model represents a special problem because it is formulated as an IHCP, and the solution requires special attention, as discussed in chapter 3. Three new methods of solving the IHCP will be introduced in this part of the thesis. These methods are:

1) The method of inversion by a Laplace domain transfer function

2) The method inversion of by a convolution integral.

3) The method of proportional inversion.

These new methods will be compared with one of the well known literature methods:

4) The Stoltz method with first order regularization

The three new methods will be tested, and their performance evaluated, using four performance criteria: accuracy, computational speed, stability, and compatibility with control theory. The performance of the methods will be investigated by testing them on a finite-element model of a machine tool structure.

CHAPTER 9: METHOD 1; SOLUTION TO THE IHCP BY DERIVING A LAPLACIAN TRANSFER FUNCTION

9.1 The Mathematical Basis of the Method

The Laplace transformation is a powerful method for solving linear differential equations and corresponding initial and boundary value problems. The transformation reduces a differential equation to an algebraic expression, which can then be solved explicitly for the output variable, and transformed back to the time domain. The method is ideally suited to the IHCP, because the most difficult part of the problem, inverting the direct problem, is as simple as algebraically inverting the transfer function in the Laplace domain (s-domain). In this chapter, the Laplacian transfer function relating the heat generation of a source to the temperature difference in the vicinity of the source will be derived from the step solution to the direct problem. If $\Delta T(t)$ is the measured temperature difference, $Q(t)$ is the heat generation of the source, and $\Delta T_s(t)$ is the step solution for the temperature difference, then the procedure is as follows:

1) Transform the step solution from the t-domain to the s-domain, and define the transfer function corresponding to the direct problem by dividing the step solution by the input:

$$H(s) = \frac{\Delta T(s)}{Q(s)} = \frac{\Delta T_s(s)}{1/s} \qquad (9.1)$$

2) Inverse the problem by algebraically inverting the transfer function in the s-domain:

$$G(s) = \frac{1}{H(s)} = \frac{Q(s)}{\Delta T(s)} = \frac{1}{s\Delta T_s(s)} \qquad (9.2)$$

3) The solution to the IHCP for an arbitrary input is obtained by transforming the input $\Delta T(t) \rightarrow \Delta T(s)$, evaluating Q(s) from equation (9.2), and then transforming the solution back to the time domain $Q(s) \rightarrow Q(t)$.

The method is conceptually simple, but there are a number of special problems which must be dealt with in this thesis:

i) The temperature difference and the step solution are measured on the model at discrete intervals, so they are numerically defined, and cannot be represented as analytical functions. A numerical scheme is therefore required to convert the input from the time domain to the s-domain.

ii) Because the input is defined numerically, the solution in the s-domain is also defined numerically, and a numerical scheme is required to convert the solution from the s-domain to the time domain.

iii) The Laplace transformation maps the entire space of the time domain into the s-domain, which means that the entire time history of the input, from $t=0$ to $t=\infty$, is required for the transformation. This poses a problem in real time because the input is

only defined between t=0 and t=τ, where τ is the present time.

Figure 9.1 shows a schematic illustration of the proposed method. The step solution is transformed to the s-domain, where it defines the s-domain transfer function. There are two transformation algorithms from t→s and from s→t. The problem is solved in the s-domain by multiplying the input by the s-domain transfer function. The process of implementing the method is divided into three steps:

1) Devising a numerical procedure to transform the temperature inputs to the s-domain, as in the t→s transformation boxes.

2) devising a numerical procedure to transform the solution from the s-domain to the time domain, as in the s→t transformation boxes.

3) Mathematically defining the solution to the IHCP in the s-domain.

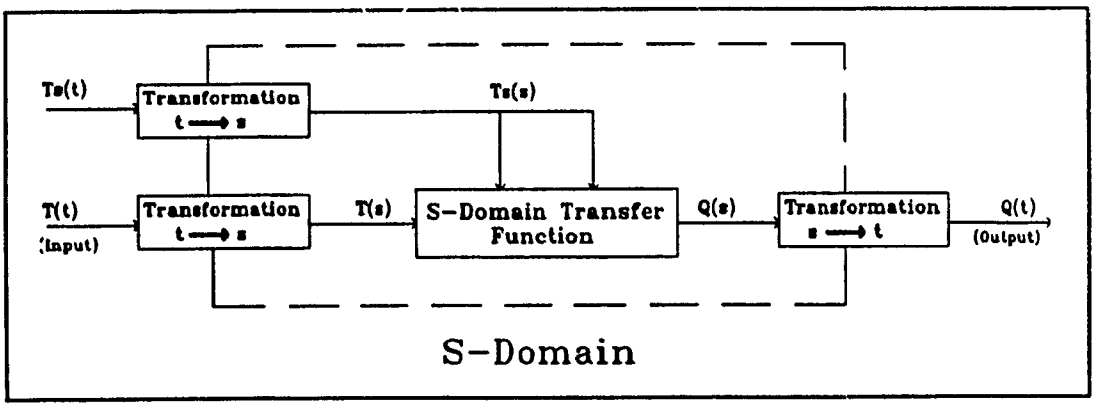

Figure 9.1: Schematic Drawing of the Laplacian Transfer Function Method

9.2 Numerical Transformation from Time Domain to Laplace Domain

The Laplace transformation of a function from the time domain to the s-domain is defined by the equation:

$$F(s) = \int_0^{\infty} e^{-st} f(t)\, dt \qquad (9.3)$$

The transformations corresponding to a number of analytic functions are available in tables, but if f(t) is not analytically defined, then numerical integration is the only way to evaluate F(s). Since the Laplacian variable s cannot be separated from the time integral in equation (9.3), the integral must be numerically evaluated for every discrete value of s. Furthermore, for the Laplacian expression to be complete, it must include the complex behaviour of F(s) as well as its real valued behaviour. Integrating equation (9.3) with only the real values of s would not provide enough information to fully define F(s) in the Laplacian domain, so no re-conversion back to the time domain would be possible. Therefore, s has to be treated as the general complex variable s=R+Ij, where R and I are the real and imaginary components.

The variable s in equation (9.3) is expanded into its complex representation s=R+Ij, to yield the expanded equation:

$$F(s) = \int_0^{\infty} e^{-Rt} e^{-Itj} f(t)\, dt \qquad (9.4)$$

Equation (9.4) is simplified by means of the Euler relation,

$$e^{\omega j} = \cos(\omega) + j \sin(\omega) \qquad (9.5)$$

to yield:

$$F(s) = \int_0^{\infty} e^{-Rt}(\cos(It) + j\sin(It))\, f(t)\, dt \qquad (9.6)$$

F(s) is a complex function with real and imaginary components. For the complex input s=R+Ij, the components of F(s) are defined by:

$$\begin{aligned} \Re\{F(s)\} &= \int_0^{\infty} e^{-Rt} \cos(-It)\ f(t)\, dt \\ \Im\{F(s)\} &= \int_0^{\infty} e^{-Rt} \sin(-It)\ f(t)\, dt \end{aligned} \qquad (9.7)$$

The transformation of equation (9.3) into equation (9.7) has yielded a form which can be numerically evaluated. Both the measured temperature input and the step solution have to be transformed by equation (9.7) in order to obtain a solution to the IHCP in the s-domain. This conversion is a time consuming process, especially since the integrals in equation (9.7) must be re-evaluated for every discrete value of s.

9.3 Numerical Transformation from the Laplace Domain to the Time Domain

The inverse transformation from the s-domain to the time domain is defined by the complex line integral:

$$Q(t) = \int_{\sigma-j\infty}^{\sigma+j\infty} e^{st} Q(s)\, ds \qquad (9.8)$$

From the nature of the inversion formula, it is clear that Q(s) cannot be converted to the time domain unless its complex behaviour is known. The integral is especially difficult

because Q(s) is defined numerically and not as an analytic function, as discussed above.

The numerical evaluation of the inverse transform is based on a paper by K.S. Crump [72], which uses the trapezoidal rule to numerically evaluate the complex integral in equation (9.8). Given a complex valued function Q(s), an approximation $g(t)$ to $Q(t)$ is obtained by computing the partial sums of:

$$g(t) = \frac{e^{at}}{T}\left[\frac{1}{2}Q(a) + \sum_{k=1}^{\infty}\left\{\Re Q\left(a+\frac{k\pi j}{T}\right)\cos\left(\frac{k\pi t}{T}\right) - \Im Q\left(a+\frac{k\pi j}{T}\right)\sin\left(\frac{k\pi t}{T}\right)\right\}\right]$$

where the parameters a and T satisfy the conditions $T > t$ and $a > \alpha$, such that:

$$|q(t)| \leq Me^{\alpha t} \qquad (9.10)$$

The computational efficiency of the algorithm is improved if T is taken to be 2t. In this case, equation (9.9) becomes:

$$g(t) = \frac{e^{at}}{2t}\left[\frac{1}{2}Q(a) + \sum_{k=1}^{\infty}\left\{\Re Q\left(a+\frac{\pi j}{t}\right)(-1)^k - \Im Q\left(a+\frac{(2k-1)\pi j}{2t}\right)(-1)^{k-1}\right\}\right]$$

The parameter a is approximated by:

$$a = \frac{3}{t} \qquad (9.12)$$

The choice of the parameter a is critical to the convergence of equation (9.11). Increasing a improves the accuracy of the solution but it also slows convergence by increasing the required number of iterations. Equation (9.11) is the product of two functions, one that includes the term e^{at} and the other that includes the infinite series. If the product {at} becomes large then the first term becomes very large, and the infinite series becomes very small. Figure 9.2 shows the results of the numerical transformation for different values of the product {at}. As the product {at} increases, the accuracy of the solution improves until numerical round-off errors in the summation algorithm cause

instability in the solution. When {at} is equal to 3.0 in figure 9.2, the accuracy and reliability of the solution are optimal. Equation (9.12) ensures that the product {at} will equal 3.0, for any value of the time parameter t.

The process of converting Q(s) to the time domain requires the computation of enough partial sums in equation (9.11) so that g(t) approximates Q(t) with a sufficient degree of accuracy. Since Q(s) is defined by $\Delta T(s)$ and $\Delta T_a(s)$, and there is a different value of s for each partial sum, the latter two expressions must be evaluated from equation (9.7) for every iteration. This is time consuming because each iteration requires that four numerical integrations with indefinite limits be performed. Figure 9.3 shows the numerical approximation of g(t) to Q(t), based on equation (9.11), where Q(t) is the

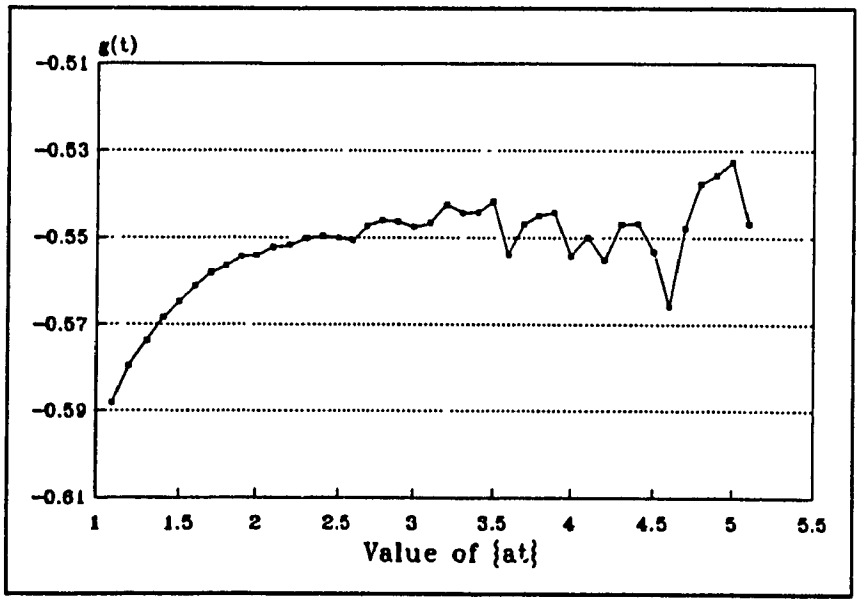

Figure 9.2: Plot of the Solution to Equation (9.11) as a Function of Parameter a

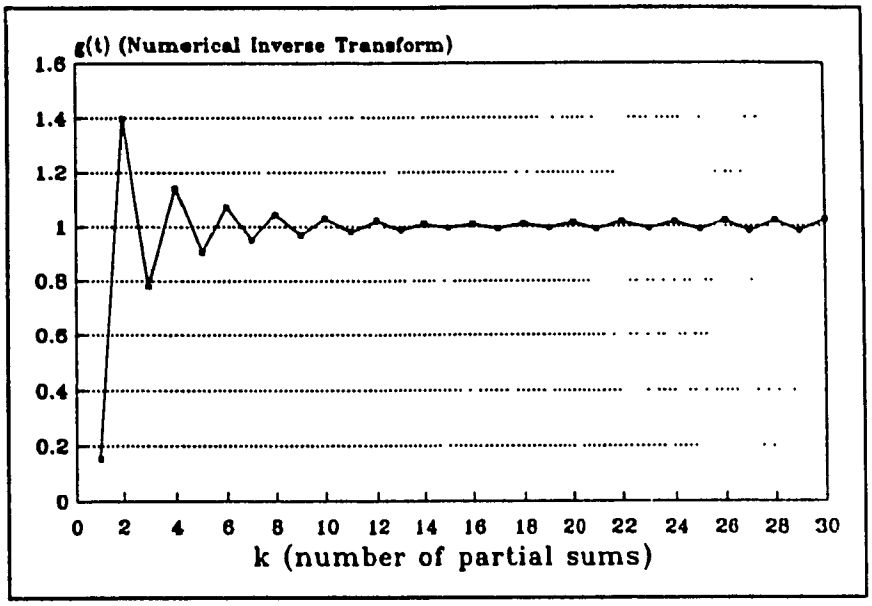

Figure 9.3: Plot of g(t) versus k for Step Input

step input $U_s(t)$. The approximation is at t=2, and is plotted as a function of k, the number of partial sums. g(t) converges to the proper value of 1, but it does so in an oscillatory manner. It is critical that the number of iterations be kept at a minimum, both for time considerations and because the solution becomes unstable as the number of iterations increases.

9.4 Obtaining the Solution in the Laplace Domain

9.4.1 Inverting the Transfer Function in the Laplace Domain

The transfer function relating Q(s) to the temperature input $\Delta T(s)$ is defined by

the step solution $\Delta T_s(s)$, as in equation (9.2):

If the real part of the step solution is $\Re$, and the imaginary part of the step solution is

$$G(s) = \frac{1}{s\,\Delta T_s(s)} \qquad (9.13)$$

$\Im$, and s is represented by R+Ij, then equation (9.13) becomes:

$$G(s) = \frac{\Re R - \Im I}{(\Re R-\Im I)^2 + (\Im R+\Re I)^2} - \frac{\Im R + \Re I}{(\Re R-\Im I)^2 + (\Im R+\Re I)^2}\, j$$

With $\Re$ and $\Im$ defined by equation (9.7), equation (9.14) defines the transfer function of the IHCP for any s=R+Ij. The IHCP solution to an arbitrary input is found by multiplying the transfer function by the transformed temperature input $\Delta T(s)$ in the s-domain. The solution to the problem in the s-domain is simple compared to the problem of transforming the variables from the time domain to the s-domain and then back again.

The transfer function for the IHCP is defined in the s-domain by equations (9.14) and (9.7), but the transfer function must be incorporated into an real time process, and there two ways to do that:

1) The first is to tabulate values of the function G(s) for different values of variable s while the system is off-line. G(s) is stored as a table of data, and when G(s) is needed for a particular value of s, a subroutine interpolates the tabular data. The advantage of this procedure is that the time-consuming work is done before the system is put on line, and only an interpolation routine is needed to call up the values of G(s). The disadvantage of this procedure is that a very large table of data is required. The data table is two-dimensional because for each value of the real component R, the imaginary component I must be tabulated through the entire usable range. This is cumbersome and

requires a lot of memory, especially because the data intervals must be small to give good accuracy.

2) An alternate procedure is to plug the appropriate value of $s=R+Ij$ into equation (9.7) and integrate it on-line. This is a simpler process, but it is more time consuming for the controller. Since the input must be transformed on-line anyway, and since the memory requirements of storing a table of data is considerable, this is the procedure that will be adopted for this method.

9.4.2 Transforming the Measured Temperature Data

$\Delta T(t)$ is measured on-line and stored as a table of temperature differences. There is a problem with using equation (9.7) to transform $\Delta T(t)$ because equation (9.7) requires a function that is defined between $t=0$ and $t=\infty$, but the entire range of $\Delta T(t)$ is not available to an on-line controller. At any real time τ, only the behaviour of $\Delta T(t)$ between $t=0$ and $t=\tau$ is known. The future behaviour of $\Delta T(t)$, between $t=\tau$ and $t=\infty$, is not defined. The only way to deal with this problem is to assign values to $\Delta T(t)$ in the undefined region. Since it is only the value of $Q(t)$ at $t=\tau$ that is of interest, it does not matter what happens to $\Delta T(t)$ and $Q(t)$ when t is greater than τ. Theoretically, the controller could assume any values for $\Delta T(t)$ for $t>\tau$, and it would not affect the solution for $Q(t)$ where $t\leq\tau$. In practice however, any abrupt changes in $\Delta T(\tau+)$ would alter the numerical solution for $Q(\tau)$. In order to smooth the transition, it will be assumed that $\Delta T(t)$ is constant between $t=\tau$ and $t=\infty$, and that the constant is equal to $\Delta T(\tau)$. Figure 9.4 shows how the controller would represent the temperature difference profile

that was given in figure 8.5 at $\tau = 10$ seconds. All of the temperature differences for $t \geq 10$ seconds are equal to $\Delta T(10)$.

There is another difficulty that arises when $\Delta T(t)$ is transformed into the s-domain by equation (7). Since the transformation integral is evaluated from $t=0$ to $t=\infty$, the entire time history of the temperature difference $\Delta T(t)$ must be included in the integration. If the machine were in operation for several hours, then τ would become exceedingly large, and the computation of the integrals in equation (9.7) would require more and more time. But it is not necessary to store the entire temperature time history of $\Delta T(t)$ in order to get an accurate solution for $Q(\tau)$. The convolution integral illustrates

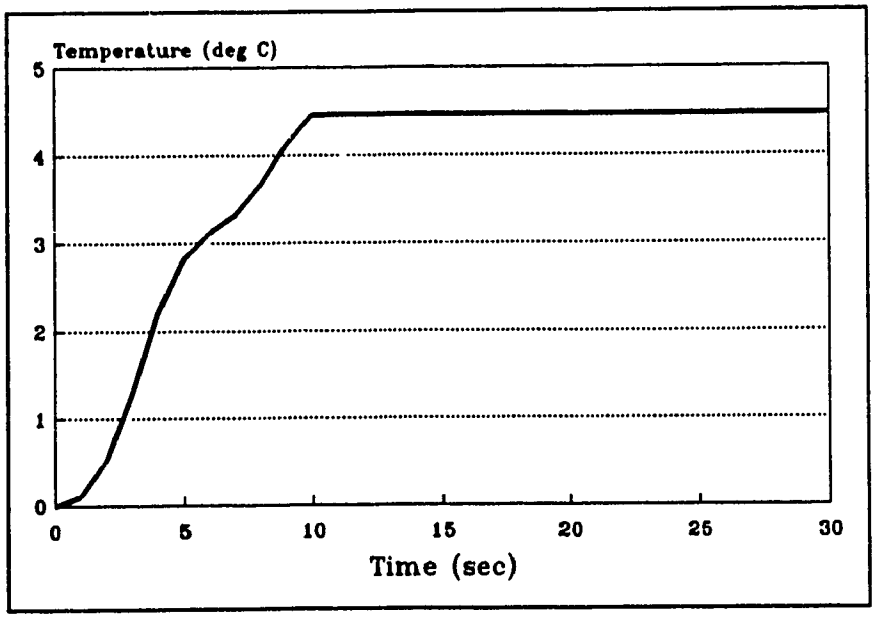

Figure 9.4: Temperature Difference Stored by The Controller at t=10 seconds

the mathematical reason behind this fact. The relationship between Q(s) and $\Delta T(s)$ is as follows:

$$Q(s) = G(s)\,\Delta T(s) \qquad (9.15)$$

where H(s) is the transfer function. The convolution integral of equation (9.15) is then:

$$Q(\tau) = \int_0^{\tau} G(\tau - t)\,\Delta T(t)\,dt \qquad (9.16)$$

where t is a dummy variable.

Since the convolution integral is evaluated from t=0 to $t=\tau$, the entire time history of the temperature difference $\Delta T(t)$ is included in the solution. But not all of the $\Delta T(t)$ temperatures make an equal contribution to the solution, because of the presence of the $G(\tau-t)$ term in the convolution integral. As t becomes smaller, $G(\tau-t)$ tends toward zero, and so the values of $\Delta T(t)$ with small t make a small contribution to the integral. Thus, it is thus the most recent temperatures that make the largest contribution to the integral and the earlier ones that make the smallest. It is only necessary to store the most recent part of the temperature time history, without any significant loss in accuracy. This also makes sense physically. Disturbances that have occurred several hours in the past have very little bearing on the present temperature field.

The period of the temperature time history that must be stored by the controller depends on the time constant of the system. In these experiments, the time history that is retained by the controller is $T_p=100$ seconds. Initially, $\Delta T(t)$ is equal to zero for all t, but after each control cycle of Tc seconds, the most recent temperature readings are

added to T(t) and the earlier ones are discarded. Thus, the controller maintains a constant 'window' of the previous 100 seconds of $\Delta T(t)$, and equation (9.7) is always evaluated over a constant period T_p.

9.5 Generating a Solution in the Time Domain

9.5.1 Stabilizing the Transfer Function

The initial time lag in the step solution to the direct problem is the source of instability in the IHCP, as discussed in the literature review. The time lag can be eliminated by approximating the step solution with an inherently stable analytic function. Figure 9.5 shows the step solution to the direct problem and the stable analytic approximation defined by equation 7.32 zooming in on the initial behaviour. Using the stable analytical function to define the transfer function, instead of the numerically defined step solution, considerably reduces the inherent instability of the IHCP. In all of the methods discussed in the literature review, the stability of the problem was controlled at the level of the input or output. In the present method, the stability is controlled by redefining the problem in such a way that the stability is increased at the structural level of the problem. Therefore, the problem of a non-unique solution does not apply to this method, and the input can be defined continuously in the time domain. None of the literature methods have those properties.

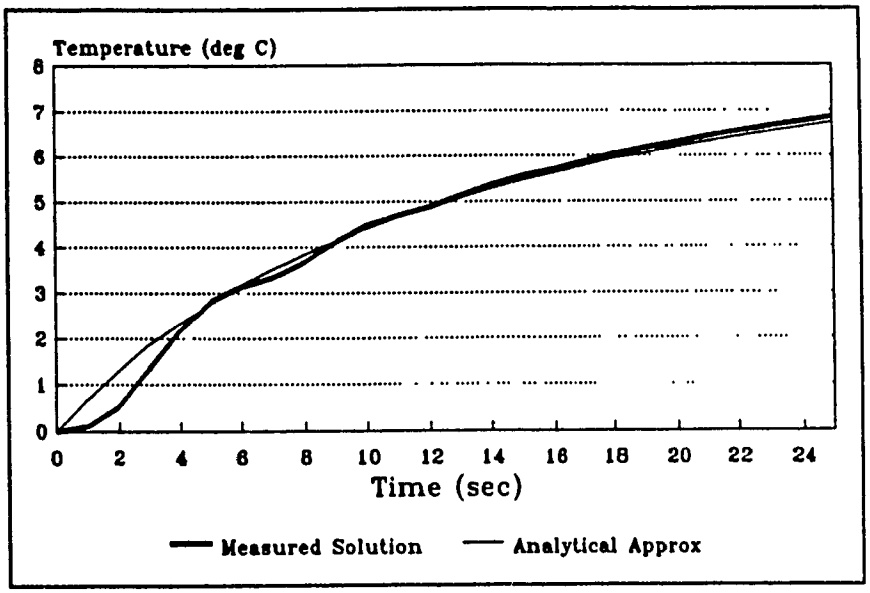

Figure 9.5 Measured Step Solution and Analytical Approximation

9.5.2 Stabilizing the Transformation from t to s

When Q(s) is transformed to the time domain at $t=\tau$, the solution tends to be unstable because of the way in which $\Delta T(s)$ is determined. As explained in section 9.3, $\Delta T(t)$ abruptly becomes constant for $t \geq \tau$, and that interferes with the numerical inversion at $t=\tau$. The interference can be eliminated if the controller calculates the heat generation at 1 second in the past, at $Q(\tau\text{-}1)$, instead of when t is exactly equal to τ. This does not present a practical problem because the deformation time constant of the structure is considerably larger than one second.

9.6 Implementing the Procedure in a Computer Program

A computer program implementing the procedure has been written in Fortran code to run on an IBM 486 PC. A brief summary of the method and the details of the

numerical procedure will now be discussed in point form:

1) The transformation from t→s must performed twice, as shown in figure 9.1. The transformation equation (9.7) is evaluated by Simpson's rule with N=80 iterations. The right hand limit is improper, but it is approximated by the expression 323/(R+1) where R is the real part of s, because the magnitude of the integrand becomes small enough to be neglected after that point. Both the analytical step solution and the measured input are transformed by equation (9.7) on line.

2) The transfer function in the s-domain is defined by equation (9.14). The solution in the s-domain is obtained by multiplying equation (9.14) by T(s).

3) The transformation from s→t is evaluated by equation (9.11). Each of the iterations requires four numerical integrations to transform the real and imaginary components of the input and step solution by equation (9.7). So as to compromise between speed and accuracy, the solution is truncated at 16 iterations. Figure 9.3 shows that for a step input, 16 iterations is where the accuracy of the solution is optimal. For other inputs 16 iterations is not necessarily an optimal value, but the number is an acceptable approximation in practice, as will be seen in the next section.

3) The window of previous temperature data that is stored by the controller has a duration of 100 seconds. While the time step is variable in the algorithm, it is fixed at 1 second for the tests in the next section.

9.7 Testing the Solver

9.7.1 The Test Input

In order to evaluate the effectiveness of this method, a simple heat generation duty cycle was applied to the finite element test structure, and the temperature difference between nodes 3 and 4 in figure 8.5 was determined. This temperature difference is used to test the algorithm by comparing the solution to the actual input. The duty cycle is shown in figure 9.6, along with the temperature difference profile. The magnitude of the heat generation is non-dimensionalized for convenience, so that an input of 164 watts corresponds to a heat generation of 1.0. The time interval between the measured data points is one second, and that is the step size for the numerical integration. The total duration of the triangular input is two minutes, representing a rather high frequency input

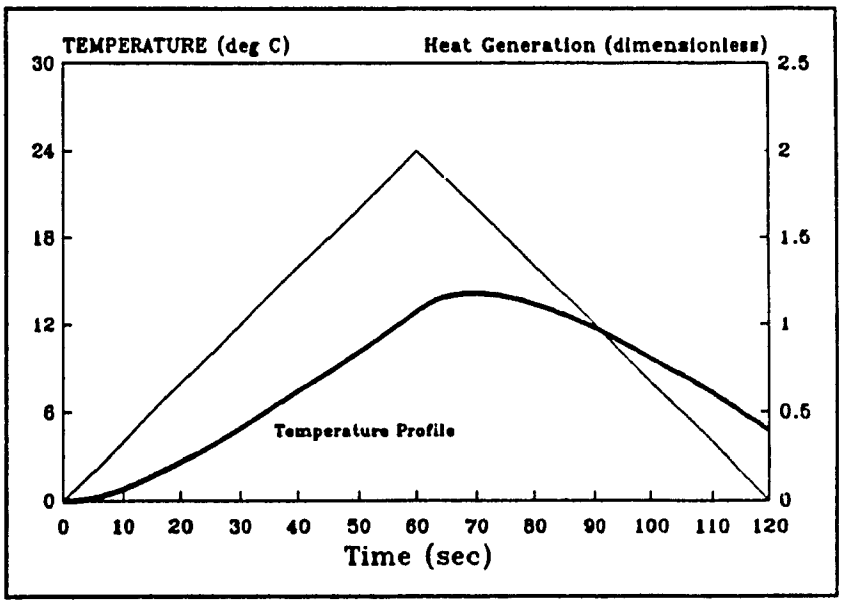

Figure 9.6: Temperature Difference Profile for a Ramp Input

for a machine tool, and provides a difficult test for the algorithm. The algorithm will be tested with exact input data, and with simulated temperature errors superimposed on the data. The simulated errors have two components: a constant component, and a component that is proportional to the measured temperature. The sign of the error oscillates between positive and negative with each time step, representing a worst case scenario for a given error resolution.

In the test results that follow, the solution at each time step is determined from a window of 100 seconds of previous temperature data. No future information is used in the calculation of the heat generation at each time step, so as to simulate the actual operation of the algorithm on-line. Thus, at τ=50 seconds, figure 9.7 shows the temperature window that is used by the algorithm to obtain the solution for $Q(\tau)$. The

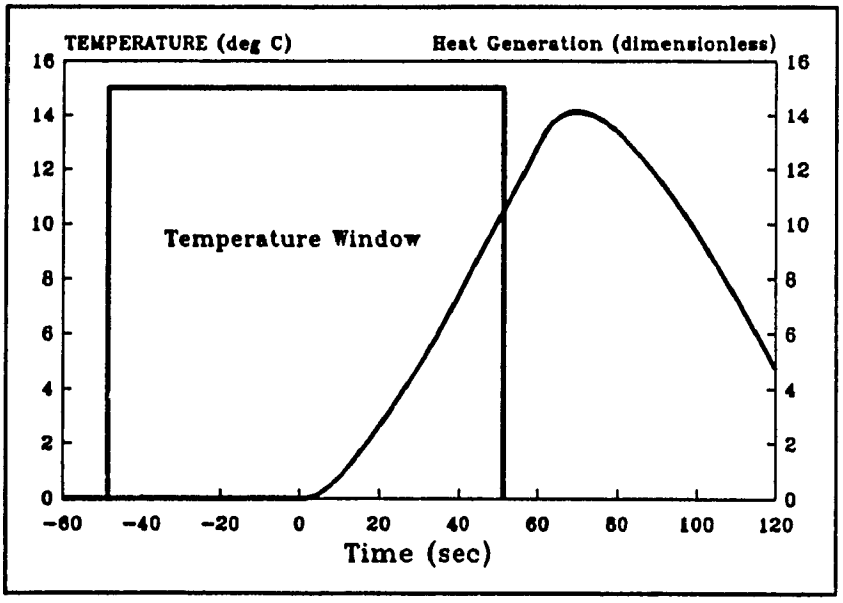

Figure 9.7: Temperature Window for τ=50 seconds (Ramp Input)

temperature difference before t=0 is assumed to be constant at zero. 120 separate evaluations of the algorithm will be used to generate a curve similar to figure 9.6.

9.7.2 The Test Results

9.7.2.1 The Solution for Exact Data

Figure 9.8 shows the approximation to the ramp input in heat generation for exact measured data. The numerical solution lags behind the exact solution by about 5 seconds for most of the interval. Part of this lag is due to the fact that the algorithm determines the heat generation at 1 second in the past, as discussed in section 9.4.2, but most of the deviation is due to an accumulation of errors in the numerical transformations:

1) The step size of the numerical integration of equation (9.7).

2) The choice of the right hand limit of equation (9.7) to approximate infinity.

2) The finite number of iterations that were used to evaluate equation (9.11).

These limitations are necessary so that the time required for the solution is acceptable for an on-line controller. Even so, the average running time for the algorithm was 64.4 seconds, a rather large time value for an on-line process.

9.7.2.2 The Solution when the Data Contains Errors

Figure 9.9 shows the solution for the same ramp input as in the previous test, but with simulated temperature measurement errors superimposed on the data. The

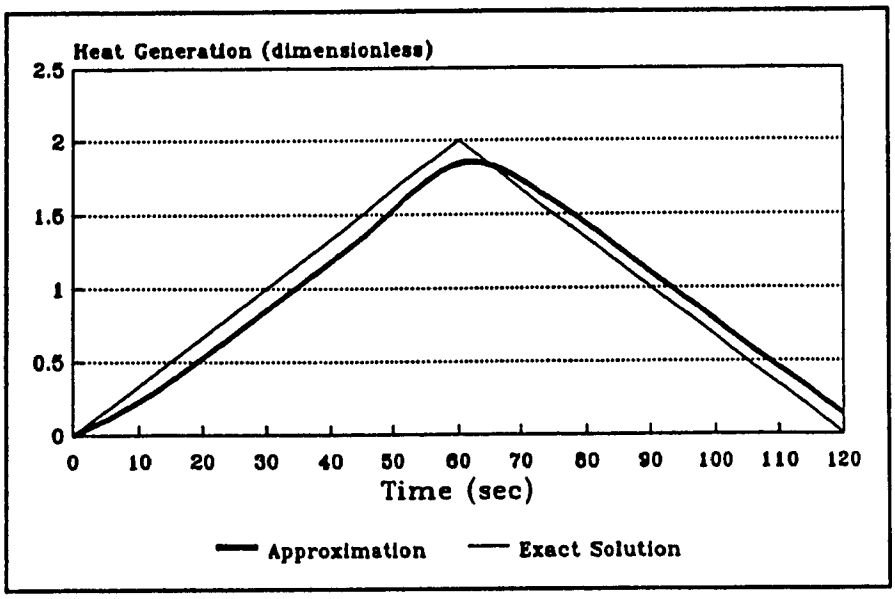

Figure 9.8: Solution for a Ramp Input with Exact Data

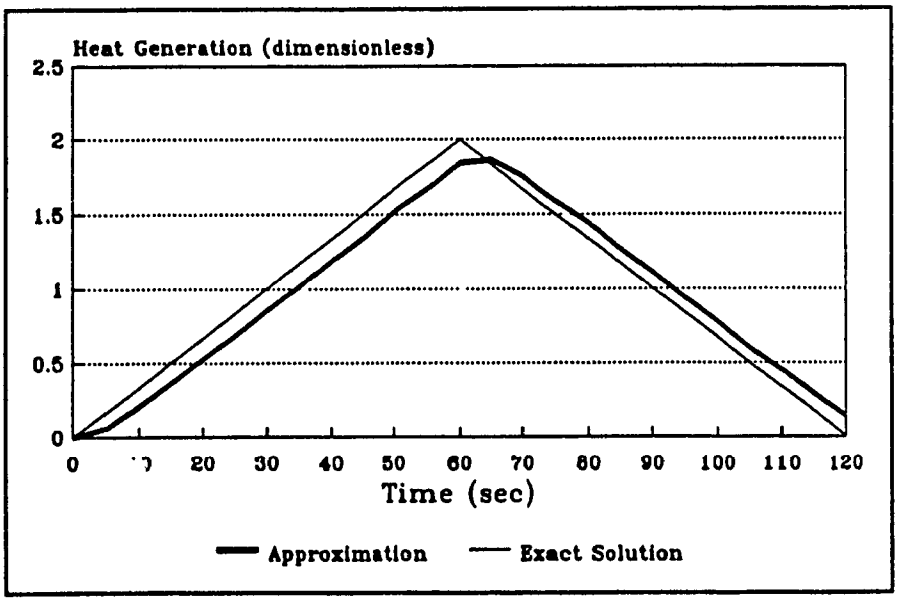

Figure 9.9: Solution for a Ramp Input with 0.5% Simulated Measurement Errors

measurement error in figure 9.9 is defined by:

$$e = 0.1 + 0.005T_i \qquad (9.17)$$

The error has a constant component of 0.1 degrees Celsius, and a variable component equal to 0.5% of the measured temperature. The error oscillates between positive and negative with each time step, representing a worse case. Figure 9.9 shows that the response of the algorithm is highly stable for relatively small errors. There are two reasons for this:

1) Much of the inherent instability of the problem was eliminated by defining the transfer function with an approximate analytical step solution, as discussed in section 9.5.1.

2) The numerical inefficiency of the algorithm helps to filter out high frequency input components in the same way that it produces a lag in the exact solution. Since the solution is not 'crisp', the high frequency oscillations become jumbled together and averaged, reducing the propensity for instability.

Figure 9.10 shows the solution to the test case when the simulated error is 0.1 degrees plus 5% of the measured temperature. Even for very significant measurement errors, the solution is highly stable, and reasonably accurate. The most significant weakness is the long computation time.

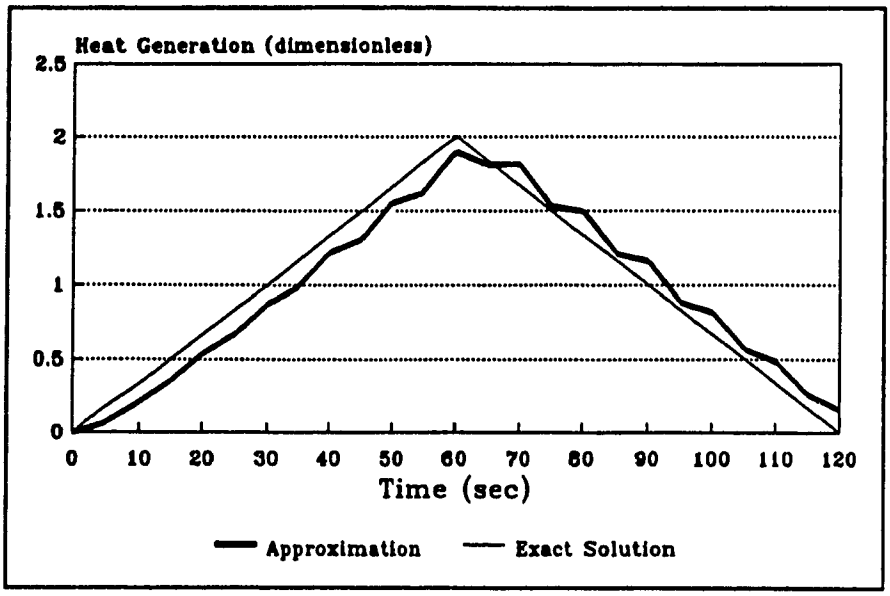

Figure 9.10: Solution for a Ramp Input with 5% Simulated Measurement Errors

9.8 Summary and Conclusions of the Method

This method solves the IHCP by defining a Laplacian transfer function G(s) from the step solution to the direct problem as follows:

$$H(s) = \frac{T(s)}{Q(s)} = \frac{T_s(s)}{1/s} \qquad (9.18)$$

where $T_s(s)$ is the step solution to the direct problem. The solution to the IHCP is then found by algebraically inverting H(s) in the s-domain, to yield the solution in the form of an s-domain transfer function:

$$Q(s) = G(s)\,T(s) \qquad (9.19)$$

where $G(s) = 1/H(s)$. The Laplace method of solving time variable problems is commonly used when all of the variables can be analytically defined and their Laplace transforms

are available in tables. This new procedure extends the method to include problems where the variables are not defined analytically, such as real time control problems where the variables are defined by a table of numerical data. The method uses numerical transformation schemes from t→s and from s→t to replace the tables of analytical transforms, and uses a complex variable representation to manipulate the numerically defined variables in the s-domain. The end result is a fully general numerical program for solving the IHCP, which requires only one step solution to the direct problem. The step solution can be defined analytically or numerically. The only limitation is that the problem must be linear.

The method lends itself well to the real time control problem because the solution is available in the s-domain as well as in the t-domain to aid in control system design. The stability of the solution is very good for noisy input data, partly because it was possible to reformulate the problem when the transfer function was defined so as to increase the inherent stability. The accuracy of the solution is also quite good, but there is a 5 second lag in the solution for the test input that was considered. The major flaw in the method from the point of view of real time control is the long processing time, 64.4 seconds on a 486-PC.

CHAPTER 10: METHOD 2; THE METHOD OF INVERSION BY A CONVOLUTION INTEGRAL

10.1 Introduction

10.1.1 The Advantages of Solving the Problem in the Time Domain

The procedure that will be developed in this chapter is similar to the method of the previous chapter in that the step solution to the IHCP will be transformed to the s-domain, and a general solution will be expressed as a Laplacian transfer function. The difference is that in this method the transfer function is transformed to the time domain while the system is off-line. Thus, there are two representations of the solution, one in the s-domain to be used for control system design and optimization, and one in the t-domain to be used for real time solution of the problem. This eliminates the time consuming processes of transforming the input temperatures and the step solution to the s-domain, and transforming the solution back to the time domain on-line, as in the previous method.

10.1.2 The Problems Associated with Transforming a Transfer Function From the Laplace Domain to the Time Domain

Figure 10.1 shows a schematic representation of this method. Instead of transforming the input to the s-domain so that it can be multiplied by the s-domain transfer function, the transfer function is transformed to the t-domain where it operates on the input in real time. The transformation of the transfer function to the t-domain is done before the system goes on-line. Since time is not a factor, the transformation process can be performed with much greater accuracy.

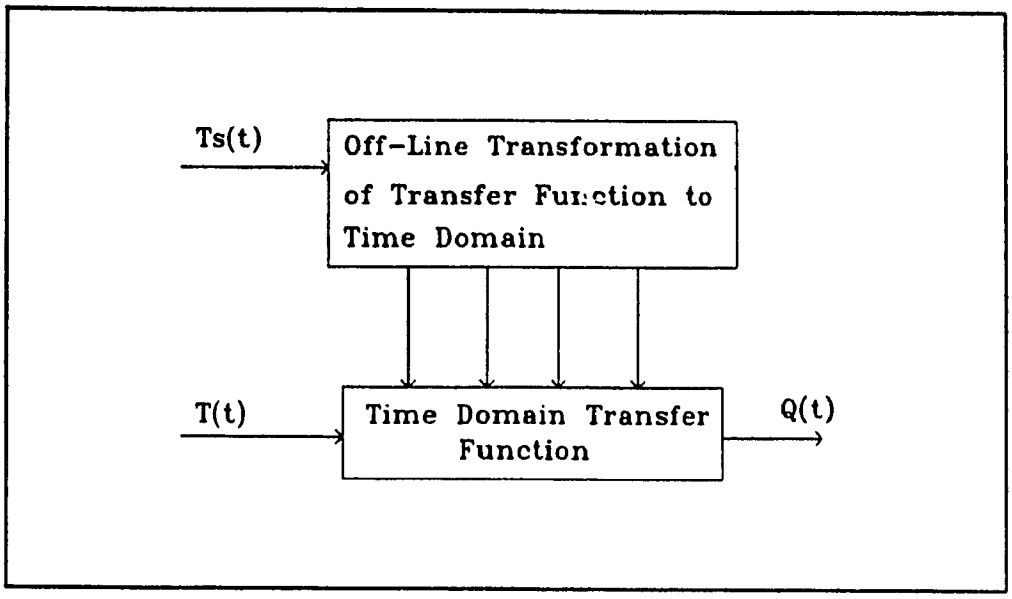

Figure 10.1: Schematic Representation of Convolution Integral Solution to the IHCP

The solution is represented in the time domain by a convolution integral of the time domain transfer function with the temperature input data, as already discussed in section 9.4.2. In the sections that follow it will be seen that the transformation of the transfer function from the s-domain to the t-domain is a far more complicated problem than was the transformation of the solution in chapter 9. The reason is that the solution to a forcing function is usually well defined in the time domain, but the transfer function is not. In fact, it is not even required that an s-domain transfer function exist in the time domain.

The s-domain transfer function is defined by the step solution to the direct problem, as seen in figure 10.1, and as was the case in the previous method. For the present method it is essential that the analytical step solution be used to define the transfer function. In order to transform the transfer function its mathematical behaviour

must be known precisely, and that can only be provided by an analytical solution.

There were two thermal solutions derived in chapter 6, one general solution and one approximate solution for small radii from the source. The general solution accommodates the temperature lag that was discussed in chapter 3, but the approximate solution does not. Since the form of the approximate solution is not lagged, the corresponding IHCP has an inherent stability built into it. Thus, using the inherently stable form of the thermal solution to define the transfer function forces an inherent stability onto the IHCP, as was seen in the method in chapter 9. For the same reason, the approximate analytic solution will be used to represent the step solution in this method.

10.2 Deriving the Laplace Domain Transfer Function of the IHCP from the Generalized Analytical Solution to the Direct Problem

The Transfer function in the s-domain is derived in the same way as in chapter 9, the only difference is that it is then transformed to the time domain. The procedure is shown schematically in figure 10.1, and is outlined here as follows:

1) Transform the analytical step solution to the s-domain. This has already been done in chapter 7, where the s-domain representation of the step solution is given by equation (7.47).

2) Define the transfer function of the IHCP, as in section 9.4.1, as the reciprocal

of the transfer function of the direct problem:

$$G(s) = \frac{1}{s\Delta T_s(s)} \qquad (10.1)$$

where,

$$Q(s) = H(s)\,T(s) \qquad (10.2)$$

3) Transform the transfer function G(s) to the time domain, where equation (10.2) is expressed as a convolution integral:

$$T(t) = \int_0^{\tau} G(\tau - t)\,Q(t)\,dt \qquad (10.3)$$

Equation (10.3) is the time domain transfer function shown in figure 10.1. The expression for G(s) has already been defined by equation (9.14), and is repeated here:

$$G(s) = \frac{\Re R - \Im I}{(\Re R - \Im I)^2 + (\Im R + \Re I)^2} - \frac{\Im R + \Re I}{(\Re R - \Im I)^2 + (\Im R + \Re I)^2}\, j$$

where, $\Re$ and $\Im$ are defined by the real and imaginary components of equation (7.47):

$$Kq\left\{\frac{R}{R^2+I^2} - \frac{1}{b}\int_0^{\infty} \frac{(u+z)\,e^{-u}}{(u+z)^2+\left(\frac{I}{b}\right)^2} - \left(\frac{I}{R^2+I^2} + \frac{I}{b^2}\int_0^{\infty} \frac{e^{-u}}{(u+z)^2+\left(\frac{I}{b}\right)^2}\right) j\right\}$$

The integrals in equation (10.5) do not have a closed form solution, so equation (4) is too complicated to be analytically transformed to the t-domain. The only alternative is to use a numerical transformation scheme, and to define the G(t) as a table of discrete data points. No accuracy is lost by using this approach, since the measured temperature data T(t) is also represented as a tabular function. The integral in equation (10.3) can only be evaluated by Gaussian quadrature or Simpson's rule at discrete points in time,

defined by the sampling period of the temperature measurement system. The time interval of the tabular values of G(t) should correspond to the time interval between the measured temperatures T(t).

10.3 Transforming the IHCP Transfer Function from the s-Domain to the Time Domain

10.3.1 Difficulties Associated with Transforming the Transfer Function

The numerical transformation equation proposed by Crump [72], given by equation (9.11), was applied to equation (10.4), but the solution did not converge to a finite value for any value of t. The transformation of an s-domain transfer function to the t-domain poses a special problem because of the presence of singularities in the solution. While singularities (impulse functions, doublet functions, etc.) can also be present in the response to a forcing input, they are nearly always present in transfer functions, and they cannot be handled by conventional numerical transformation schemes. The problem of singularities will now be considered in detail, in the following section.

10.3.2 Transforming the Singularity Functions of the Laplacian Transfer Function

When singularity functions are present in the Laplacian expression, the transformation formula in equation (9.11) does not converge to a unique or finite value. To understand the reason for this, it is necessary to derive the Crump equation (9.11) from basic principles.

The transformation equation from the s-domain to the t-domain is given, as

previously discussed, by the complex line integral:

$$f(t) = \frac{1}{2\pi j}\int_{R-j\infty}^{R+j\infty} e^{st}F(s)\,ds \qquad (10.6)$$

where R is an arbitrary value on the real axis in figure 10.1 Integrating along the path shown in figure 10.2, the parametrized variable s is given by:

$$s = R+uj \qquad (10.7)$$

and,

$$\frac{ds}{du} = j \qquad (10.8)$$

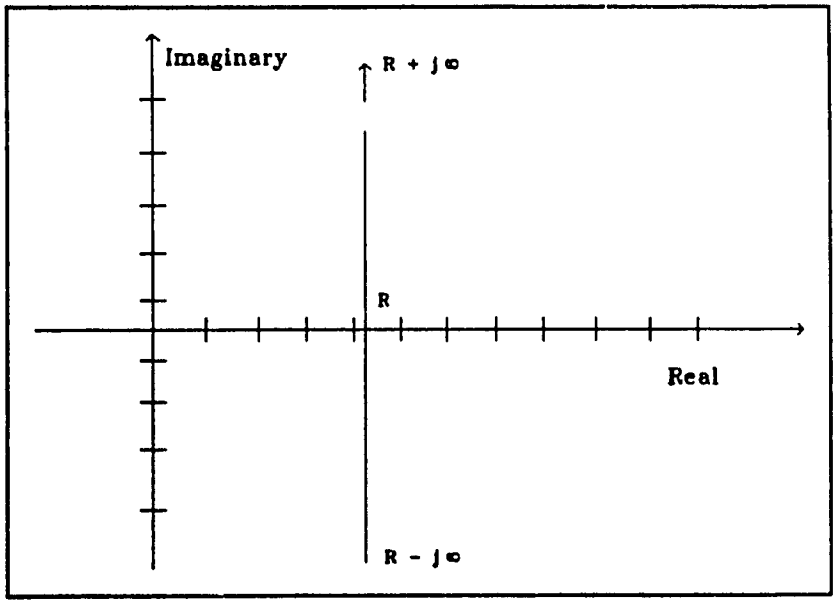

Figure 10.2: Path of Integration of Equation (10.6) in the Complex s-Domain

Thus, the parametrized form of equation (10.6) is:

$$\frac{1}{2\pi}\int_{-\infty}^{+\infty} e^{(R+uj)t} F(R+uj)\, du \qquad (10.9)$$

Equation (10.9) is expanded with the Euler equation, to yield:

$$\frac{e^{Rt}}{2\pi}\int_{-\infty}^{+\infty} F(R+uj)\, Cos(tu) + F(R+uj)\, Sin(tu)\, j\, du \qquad (10.10)$$

The real part of a complex function is always even, and the imaginary part is always odd. Therefore, equation (10.10) can be simplified by dividing the complex function F(R+uj) into its real and imaginary components, and recognizing that the product of even and odd functions is zero when integrated from $-\infty$ to $+\infty$. Thus,

$$f(c) = \frac{e^{Rt}}{\pi}\int_{0}^{\infty} \Re\{F(R+uj)\} Cos(tu) - \Im\{F(R+uj)\} Sin(tu)\, du$$

Crump's formula, given by equation (9.11), is derived by applying the trapezoidal rule to evaluate the integrals in equation (10.11). In order for those integrals to be finite, the real and imaginary components of the function F(R+uj) in equation (10.11) must tend toward zero as $u \to \infty$. The transfer function G(R+uj), as defined by equations (10.4) and (10.5), becomes infinite as $u \to \infty$, so the indefinite integrals in equation (10.11) are unbounded. The reason why the transfer function diverges is because it contains singularity functions.

10.3.2.1 The Laplace Transformation of an Impulse

The impulse function $\delta(t)$ has an infinite magnitude at t=0 and it is zero

elsewhere. Furthermore, the integral of the impulse over any domain encompassing the origin is equal to 1. An impulse function is present in many transfer functions because it specifies an initial value for the solution at t=0. The Laplace transformation of $f(t)=\delta(t)$ is well known from tables of Laplace transforms to be $F(s)=1$. The practical difficulty with the impulse function is that is does not satisfy the existence theorem of the Laplace transformation [73]. The expression $F(R+uj)=1$ does not tend toward zero as $u\rightarrow\infty$ (it remains constant at 1), so the integrals in equation (10.11) do not converge to a unique value as $u\rightarrow\infty$. Figure 10.3 shows the integrand of equation (10.11) for an impulse function at t=1 second. The integrand does not decay to zero, so the integral never converges to a unique value.

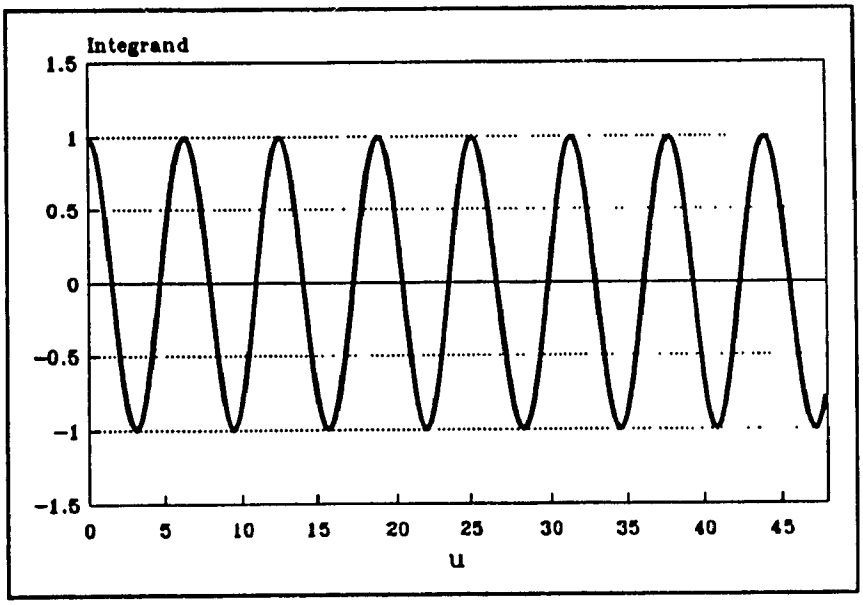

Figure 10.3: Integrand of Equation (10.11) for an Impulse

10.3.2.2 Laplace Transformation of a Doublet

The doublet function is the derivative of the impulse function, so logically it is represented in the s-domain by the expression F(s)=s. The doublet function does not satisfy the existence theorem of the Laplace transformation either. For a doublet, $F(R+uj) = R + uj$ tends toward the value $R + \infty j$ as $u \to \infty$. Figure 10.4 shows the integrand of equation (10.11) for a doublet at t=1 second. Figure 10.4 explains why the transformation of the transfer function defined by equations (10.4) and (10.5) does not converge to a finite value: there is one doublet and one impulse present in the transfer function, as will be shown in section 10.3.2.4. There could also be higher order singularities present in G(s), but it will be shown that this is not the case. It could also be possible to have singularities at a point other than t=0, but this is not the case in the present problem, as shall be seen soon.

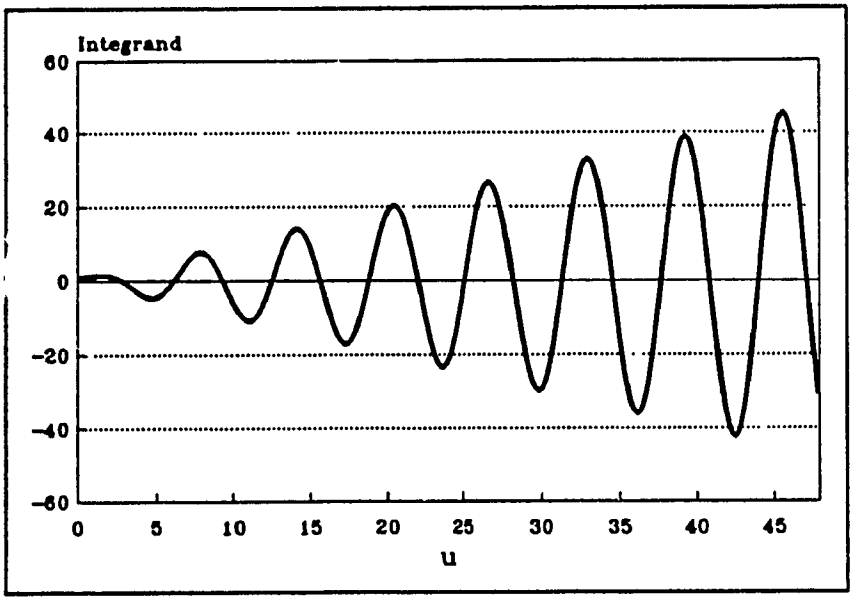

Figure 10.4: Integrand of Equation (10.11) for a Doublet

10.3.2.3 Dealing with Singularities

When a singularity is transformed by equation (10.11), the solution diverges for all values of t, even though the singularities should be zero in the time domain at all values of t other than t=0. The reason is that the Laplace transformation is a space mapping equation, so there is no direct correspondence from a point in one space to a point in the other.

There are two ways to deal with the singularity functions:

1) Identify all of the singularities first, and then remove them from the transfer function. The balance of the transfer function can be transformed by equation (10.11).

2) Identify the singularities first, and then transform the entire transfer function, while filtering out the singularities.

Both of the above methods will be investigated in this chapter. For the second method, a special technique will be used to filter singularities out of a Laplacian function while it is being transformed to the t-domain.

The magnitudes of the singularities are found by replacing s in G(s) by the complex variable R+Ij, and allowing $I \to \infty$. If no singularities were present, G(R+Ij) would tend toward zero as $I \to \infty$. If $G(R+\infty j)$ is not equal to zero but is equal to a complex expression, then that expression is the representation of the singularities in the s-domain. This point will be clarified in the next section.

10.3.2.4 Transforming the Singularities

The complete transfer function for the direct problem was derived previously, and is given by equations (10.4) and (10.5). As discussed above, equation (10.4) has no closed form solution. However, it is possible to obtain a closed form solution for the particular value of s=R+Ij, when I→∞. This particular expression is useful because it identifies the singularity functions that are present at t=0.

The analytical representation of the step solution to the direct problem in the s-domain is given by equation (10.4). Although the I→∞ solution of IHCP transfer function could be obtained directly from equation (10.5), it is more convenient to obtain the transfer function for the direct problem first, and then take its reciprocal. The transfer function for the direct problem is given by:

$$H(s) = sT_s(s) \tag{10.12}$$

Replacing s in equation (10.12) by R+Ij, and $T_s(s)$ by the analytical expression in equation (10.14) yields the analytical expression for the transfer function to the direct problem:

$$H(R+Ij) = Kq((1+I\Im-R\Re) - (R\Im+I\Re)j) \tag{10.13}$$

where $\Re$ and $\Im$ are defined by:

$$\Re = \frac{1}{b}\int_0^\infty \frac{(u+z)e^{-u}}{(u+z)^2+\left(\frac{I}{b}\right)^2} \tag{10.14}$$

and,

$$\Im = \frac{I}{b^2}\int_0^{\infty} \frac{e^{-u}}{(u+z)^2+\left(\frac{I}{b}\right)^2} \qquad (10.15)$$

There are four elements to equation (10.13) that have to be evaluated. These are, from left to right, $(1+I\Im)$, $R\Re$, $R\Im$, and $I\Re$. The last three elements will be found from the solutions to $\Re$ and $\Im$ as $I\to\infty$. The first element poses a special problem that must be dealt with separately.

As $I\to\infty$:

$$\Re = \frac{b}{I^2}(1+z) \qquad (10.16)$$

and,

$$\Im = -\frac{1}{I} \qquad (10.17)$$

The mathematical derivation of these equations is given in appendix 1.

The first term in equation (10.13) is $1+I\Im$. As $I\to\infty$, $I\Im\to 1$, so the term $1+I\Im\to 0$. The problem is that $1+I\Im\to 0$ at the same order as $R\Re\to 0$, so the term cannot be neglected. Furthermore, even though the term is approaching zero, it does not disappear when the reciprocal of equation (10.13) is taken, because it becomes multiplied by a term that is approaching infinity. A closed form of the solution for $1+I\Im$ as $I\to\infty$ can be obtained, but the mathematical derivation is highly complex. The solution is obtained by differentiating the whole expression with respect to a parameter, rearranging its structure, and then reintegrating it with respect to the same parameter, by methods of variational calculus. The details of the derivation are given in appendix 5, and the

solution is:

$$1 + I\mathfrak{S} = \frac{b^2}{I^2}(Z^2+2z+2) \qquad (10.18)$$

Substituting equations (10.16), (10.17), and (10.18) into equation (10.13) yields the equation:

$$G(R+\infty j) = \frac{b}{I^2}(bz^2+(2b-R)z+(2b-R)) - \frac{1}{I}(bz+(b-R))j$$

Taking the reciprocal of equation (10.19), and replacing z=(R+a)/b yields the equation:

$$Kq\left(\frac{(a+b)R+a^2+2ab+2b^2}{(a+b)^2} + \frac{I}{a+b}j\right) \qquad (10.20)$$

Substituting R+Ij=s into equation (10.20) yields:

$$G(s) = \frac{s}{a+b} - \frac{a^2+2ab+2b^2}{(a+b)^2} \qquad (10.21)$$

as s→R+∞j, equation (10.21) shows that there are two singularities at t=0 in the time domain: one impulse and one doublet. The magnitude of the impulse is:

$$\frac{Kq}{a+b} \qquad (10.22)$$

and the magnitude of the doublet is:

$$-\frac{Kq(a^2+2ab+2b^2)}{(a+b)^2} \qquad (10.23)$$

The parameters in equations (10.22) and (10.23) are the empirical parameters of the generalized step solution, given in equation (7.32).

10.3.3 Transforming the Laplace Domain Transfer Function to the Time Domain

10.3.3.1 The Method of Extracting the Singularities

Now that the singularities in the transfer function have been identified, it is possible to extract them, and then transform the balance of the expression. The singularities are extracted by subtracting equation (10.21) from the transfer function in equation (10.5). Thus, the new transfer function, with the singularities removed is given by:

$$G^*(s) = \left(\frac{\Re R - \Im I}{(\Re R - \Im I)^2 + (\Im R + \Re I)^2} - \frac{(a+b)R + a^2 + 2ab + 2b^2}{(a+b)^2} \right)$$

$$- \left(\frac{\Im R + \Re I}{(\Re R - \Im I)^2 + (\Im R + \Re I)^2} + \frac{I}{a+b} \right) j$$

where $\Re$ and $\Im$ are given by equation (10.5), as before. Since equation (10.21) represents the residue of G(s) as $s \to R + \infty j$, then $G^*(R + \infty j) \to 0$, and the transformation of $G^*(s)$ to the time domain by equation (10.11) converges to a finite value for any value of t.

Equation (10.11) was used to transform $G^*(s)$ in equation (10.14) to $G^*(t)$ for different values of t, using gaussian quadrature to perform the integration. The result is shown in figure 10.5. The evaluation of $G^*(t)$ by gaussian quadrature took more than two weeks to run on a VAX mainframe computer. The solution required so much time because the step size of the integration cannot be larger than the period of the sine and cosine functions in equation (10.11). Furthermore, $G^*(s)$ decays to zero very slowly as $I \to \infty$. Since the right hand limit of the integration is improper, the right hand limit must be extended until the contribution of the integrand is negligible. This requires hundreds

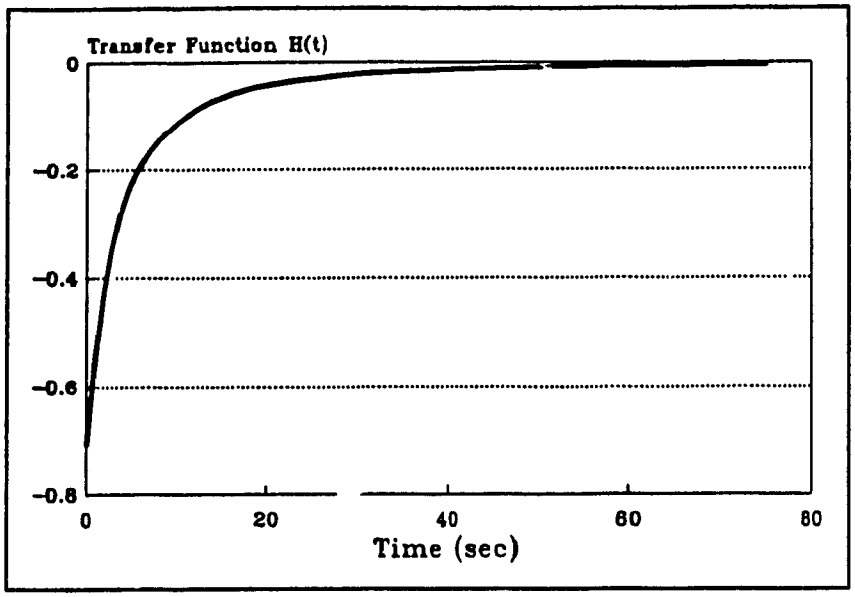

Figure 10.5: Time Domain Transfer Function Determined by Gaussian Integration

of cycles of the sine and cosine functions for most values of t. Finally, because the integrand in equation (10.11) oscillates about zero for hundreds of cycles before becoming negligible, the solution is highly susceptible to round off error. This requires a very fine interval size for the numerical integration, and that increases the computation time.

There is another problem associated with direct integration of equation (10.11). The doublet that is subtracted from the transfer function in equation (10.24) is proportional to I. As $I \rightarrow \infty$ when equation (10.11) is integrated, the computer must take the difference between two large r mbers. Thus, the right hand limit of the integration in equation (10.11) cannot exceed the number of significant digits carried by the computer. The integration had to be performed in quadruple precision in order to eliminate the round off error for all values of t.

10.3.3.2 The Method of Filtering the Singularities

10.3.3.2.a The Crump Method of Inverting from the s-Domain

In the previous section, the singularities were removed by subtracting them from the transfer function and then numerically transforming the balance of the expression. In this section, a method will be devised whereby the entire transfer function is transformed, but the singularity functions are filtered out in the process.

The method of numerical transformation from the s-domain to the t-domain that was devised by Crump [72] is based on the numerical integration of equation (10.11) by the trapezoidal rule. It is a simple matter to derive equation (9.9) from equation (10.11) by replacing the integrals in equation (10.11) by the trapezoidal integration formula. The assumption that T=2t that was used to derive equation (9.11) is equivalent to defining the step size of the numerical integration to be one quarter of the period of the sine and cosine functions. Since one iteration of equation (9.11) integrates one half of the period of the integrand, the solution oscillates between positive and negative with each iteration. Figure 10.6 shows the numerical approximation to the modified transfer function $G^*(t)$ at t=1 second, determined by the Crump method, and plotted as a function of the number of partial sums k. The algorithm converges to the correct solution in an oscillatory manner, until the accumulation of round off errors causes the solution to begin diverging at about k=12. The highest accuracy that can be obtained by the Crump method is 2 significant digits at k=12. Thi level of accuracy is insufficient for the purpose of a convolution integral, so the Crump method by itself cannot be used.

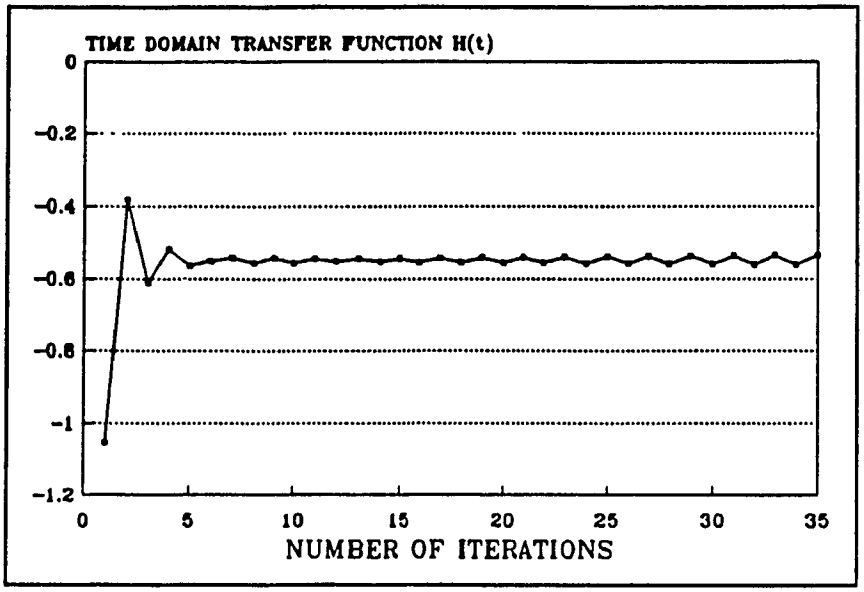

Figure 10.6: Transformation of G*(s) by Crump Method without Acceleration

10.3.3.2.b Accelerating the Crump Method

Figure 10.6 shows that the Crump algorithm does not converge to a definite value before an accumulation of round off errors causes the solution to begin diverging. Defining the accuracy by the range of the oscillations in figure 10.6 gives a misleading picture, however. By drawing an imaginary line through the centre of the oscillations, it is possible to anticipate what value the algorithm was converging to before it began diverging at k=12. In fact, one could even trace a line backwards from beyond k=12, and still estimate the final value quite well. In this section, a method of anticipating the final value from a limited number of iterations will be developed.

Figure 10.7 shows the first 8 iterations of H(t=1). Figure 10.7 shows that is possible to decrease the range of the oscillations by calculating the average of $G(t_k)$, the present estimate, and $G(t_{k-1})$, the previous estimate. A plot of the average values gives

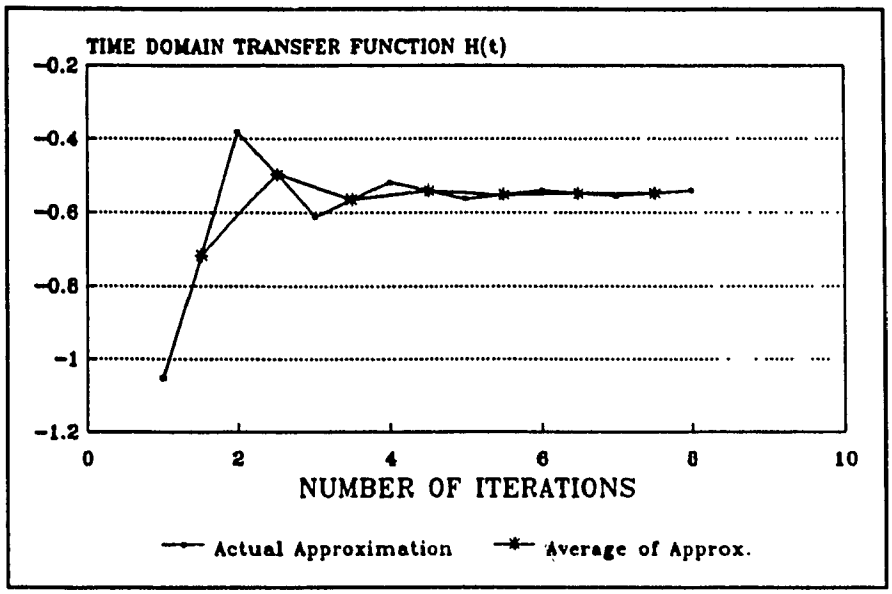

Figure 10.7: First Eight Iterations of G*(t) from Crump Method and Plot of Average Values

a more reliable estimate to G(t) for the same reason that an imaginary line through the centre of the oscillations anticipates the ultimate value. This idea is taken further in figure 10.8, where 3 'nested averages' are taken for the 4 data points. The fourth average is simply a point (marked by a *) which represents the accelerated solution at N=4. The more averages that are taken, the smaller the range of the oscillations, and the faster is the convergence of the algorithm.

The number of nested averages that is possible depends on the number of successive approximations that are available. At k=2, only one nested average is possible:

$$f=\frac{a_1+a_2}{2} \qquad (10.25)$$

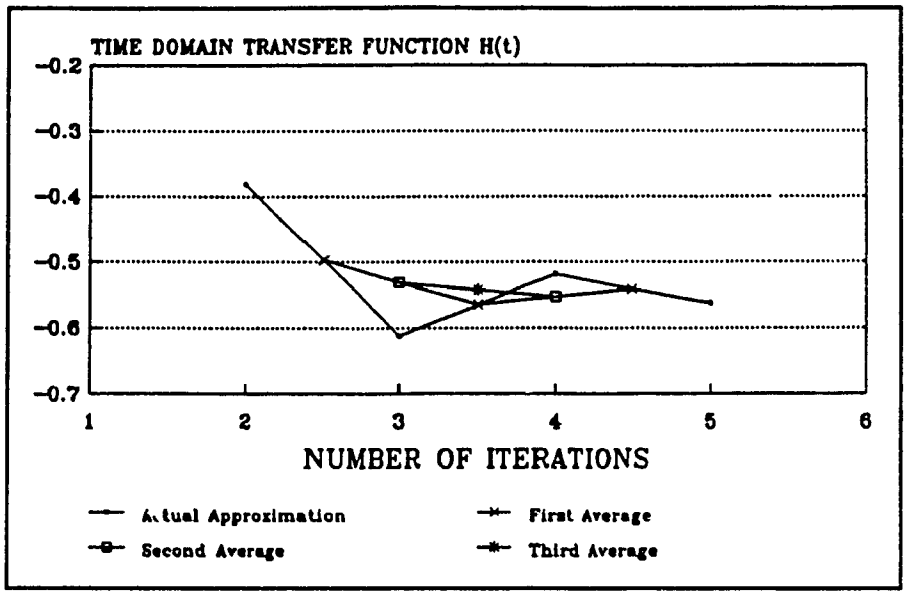

Figure 10.8: Plot of Crump Approximation without Acceleration and Nested Averages

At k=3, the average of the averages is:

$$f=\frac{\frac{a_1+a_2}{2}+\frac{a_2+a_3}{2}}{2}=\frac{2a_1}{4}+\frac{a_2}{4}+\frac{2a_3}{4} \qquad (10.26)$$

Similarly for k=n, the $(n-1)^{th}$ nested average is given by:

$$f_n=\frac{a_1T_1+a_2T_2+a_3T_3+.....a_nT_n}{b} \qquad (10.27)$$

where the co-efficients a_i are given in table 1. The co-efficients in table 2 can be derived by a recursive formula for any k. Thus, if a_{ij} is the co-efficient in column i and row j, then:

$$a_{i,j}=a_{i-1,j-1}+a_{i,j-1} \qquad (10.28)$$

Table 10.1: Coefficients for the Accelerating Algorithm

a1	a2	a3	a4	a5	a6	a7	a8	b
1	1							2
1	2	1						4
1	3	3	1					8
1	4	6	4	1				16
1	5	10	10	5	1			32
1	6	15	20	15	6	1		64
1	7	21	35	35	21	7	1	128

For any iteration number n, the $(n-1)^{th}$ nested average of the preceding values is given by equation (10.28), with the a_{in} given by table 1. This shall be called the accelerating algorithm,in this case applied to the Crump algorithm. Figure 10.9 shows how the accelerating algorithm speeds the convergence of $G^{*}(t)$ at $t=1$ second, compared to figure 10.6 without acceleration. The accelerated algorithm converges to the correct value 0.5467206 after 11 iterations. Thus, the Crump method with acceleration is as accurate as Gaussian quadrature, but many times faster. The accelerated Crump method required 44 seconds to obtain $H(t=1)$ with an accuracy of 6 significant digits on an IBM 486. The unaccelerated Gaussian quadrature method required more than 4 hours on a VAX2 mainframe computer to give the same accuracy.

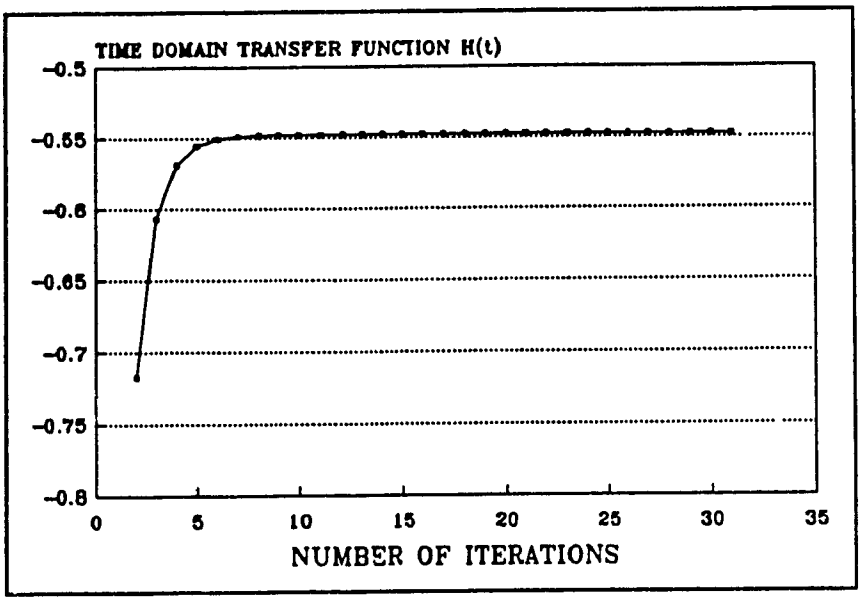

Figure 10.9: The Convergence of the Crump Method with Acceleration for G(t=1)

One interpretation of table 1 is that the accelerating algorithm takes a weighted average of the data points that is heavily weighted on the centre of the data. This leads one to wonder whether another average would also accelerate convergence. If a simple average of all the data is taken then:

$$f = \frac{1}{N} \sum_{i=1}^{N} a_i \qquad (10.29)$$

This average does not accelerate convergence, in fact it does not even converge to the correct value.

10.3.3.2.c The Effect on Singularities

There is another important advantage to the accelerating algorithm: it filters out

singularity functions. To understand why this is so, consider the transformation of the impulse function F(R+uj)=1 by equation (11). Substituting F(R+uj)=1 into equation (10.11) yields the following expression in the time domain, which should be equivalent to the impulse function:

$$f(t) = \frac{e^{Rt}}{\pi}\int_0^{\infty} Cos(tu)\,du \qquad (10.30)$$

When t=0, equation (10.30) is infinite, as expected. When $t \neq 0$ equation (10.30) should be zero but it is not, as was shown in figure 10.3. Evaluating the integral in equation (10.30) when $t \neq 0$ yields:

$$f(t) = \frac{e^{Rt}}{\pi t} Sin\infty \qquad (10.31)$$

which does not equal zero unless ∞ is a multiple of π. The problem arises because the impulse function does not satisfy the existence theorem of the Laplace transform, as previously discussed.

Figure 10.10 shows the Crump transformation of the impulse function at t=1 second. The solution would oscillate about zero forever without converging, except that numerical round off error eventually results in divergence. The centre of the oscillations is zero, however, so the solution that would be anticipated by the accelerating algorithm is zero. Figure 10.10 also shows the Crump transformation of the impulse function with acceleration at t=1 second. As expected, the accelerated algorithm converges to zero Hence, the accelerating algorithm filters out impulse functions that would otherwise prevent convergence of the algorithm. The successive approximations to higher order

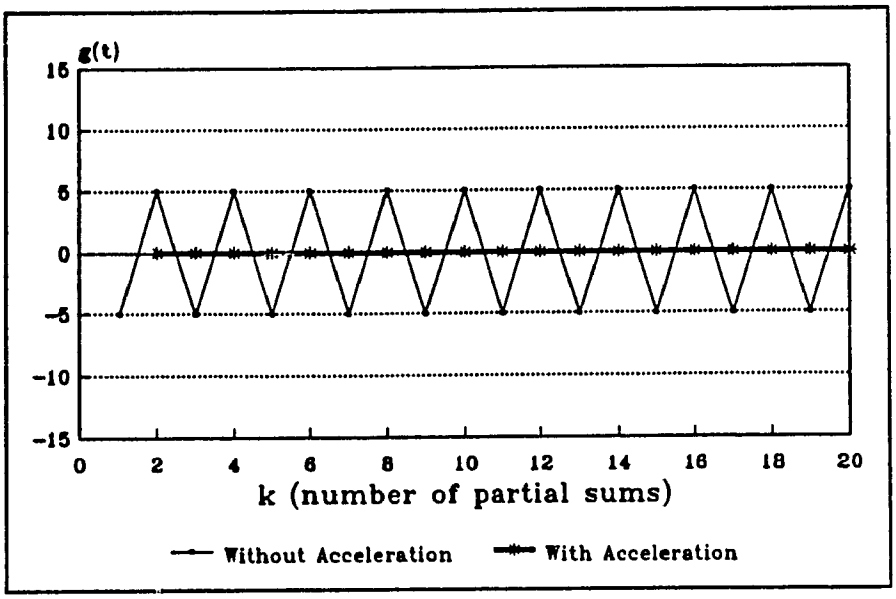

Figure 10.10: The Crump Transformation of an Impulse with and without Acceleration

singularities also centre on zero, so they disappear when the accelerating algorithm is used.

10.4 The Convolution Integral

Figure 10.11 shows the complete time domain transfer function H(t), as determined by the Crump algorithm with acceleration, with a time interval of one second between data points. The singularity functions were determined analytically in equation (10.21), and are included in the figure. The singularities specify initial values for the convolution integral in equation (10.3). When the impulse function is integrated it adds a multiple of $T(\tau)$, and when the doublet is integrated it adds a multiple of $dT(t=\tau)/dt$. It is therefore the last temperature value (at $t=\tau$) that has the largest influence on the solution. The rest of the temperature history is integrated in convolution with G(t), and

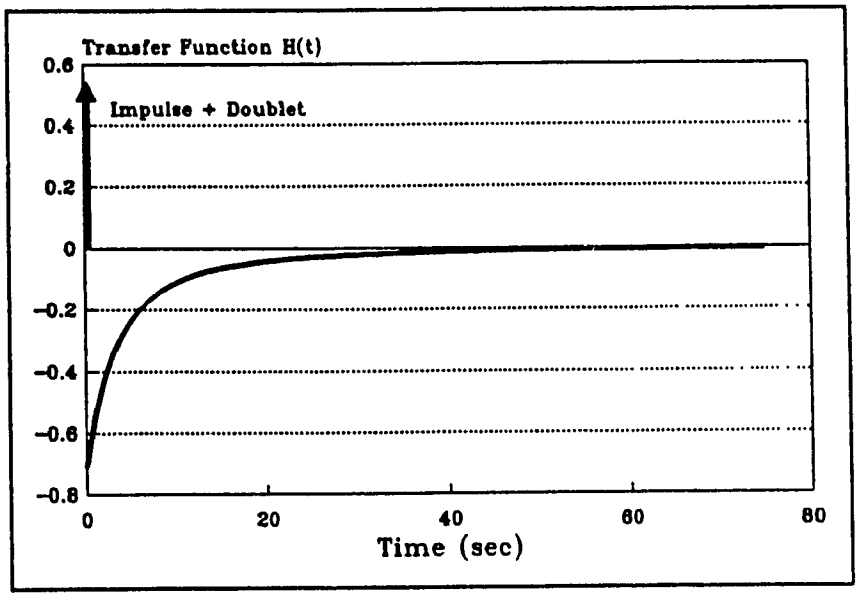

Figure 10.11: Time Domain Transfer Function Determined by Accelerated Crump Method including Singularities

becomes subtracted from the initial values.

With G(t) now defined, the convolution integral in equation (10.3) is the solution to the IHCP for a measured temperature history T(t). The convolution integral is evaluated by Simpson's rule to give the solution for q(t) at $t=\tau$. Simpson's rule is used for the integration because it accommodates equally spaced data points. The time interval between the measured temperature data points must be a multiple of one second because that is the interval of the transfer function G(t). It is possible to accommodate any other sampling interval by recalculating G(t) with the appropriate time interval between data points.

The limits of the convolution integral in equation (10.3) are from zero to τ. If the boundary of the integration were allowed to expand as τ increases with time, the

numerical evaluation of equation (10.3) would require more time with each cycle. In order to maintain a constant processing time, a constant 'window' of 100 seconds of past data is included in the integration. As τ increases, the new temperatures are added and the oldest ones are discarded, moving the temperature window one time interval to the right with each cycle. Truncating T(t) does not seriously affect the solution because for $q(\tau)$ because G(t) decays to zero well before t=100 seconds. The same procedure was used in chapter 9 to define a constant window of input data.

10.5 Testing the Solver

The convolution integral was tested using the same standard inputs as the Laplace transfer function method in chapter 9. The solution at each time step τ is determined independently from a 100 second window of previous data. The solution for the triangular test case shown in figure 9.6, with errorless data is given in figure 10.12. The accuracy of the solution is considerably better than the previous method because the transformation of the transfer function was done off-line, and with greater precision. Furthermore the average processing time was only 0.14 seconds, or 140 milli seconds.

Figure 10.13 shows the solution for the triangular input with simulated measurement errors of 0.1 degree plus 0.5% of the measured temperature. The solution oscillates noticeably with measurement errors because of the precision with which heat generation is estimated. Figure 10.14 shows the solution for a constant error of 0.1 degrees plus 5% of the measured temperature. The magnitude of the oscillations indicates excellent stability for a solution that has such high accuracy. The stability is due to the

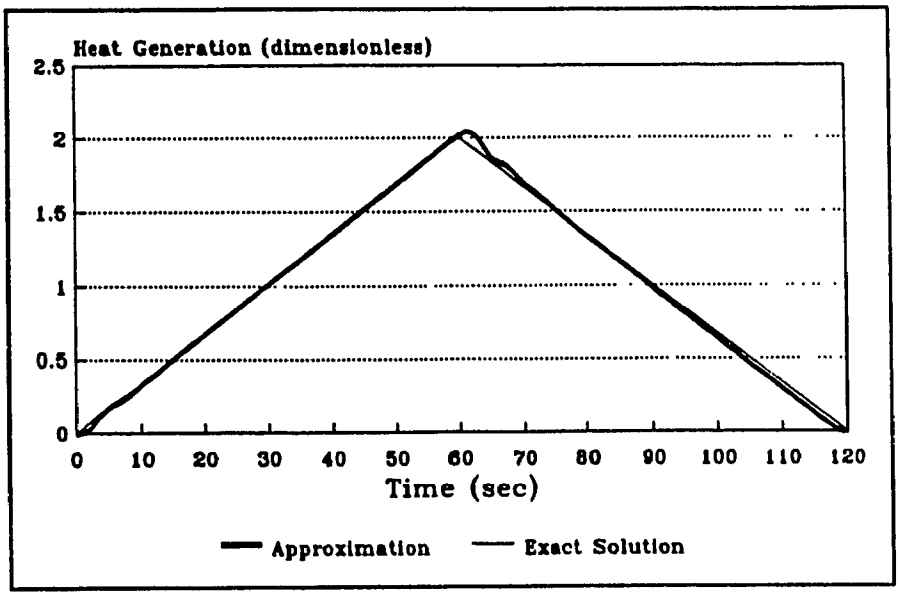

Figure 10.12: Solution for Triangular Test Input (Exact Matching Data)

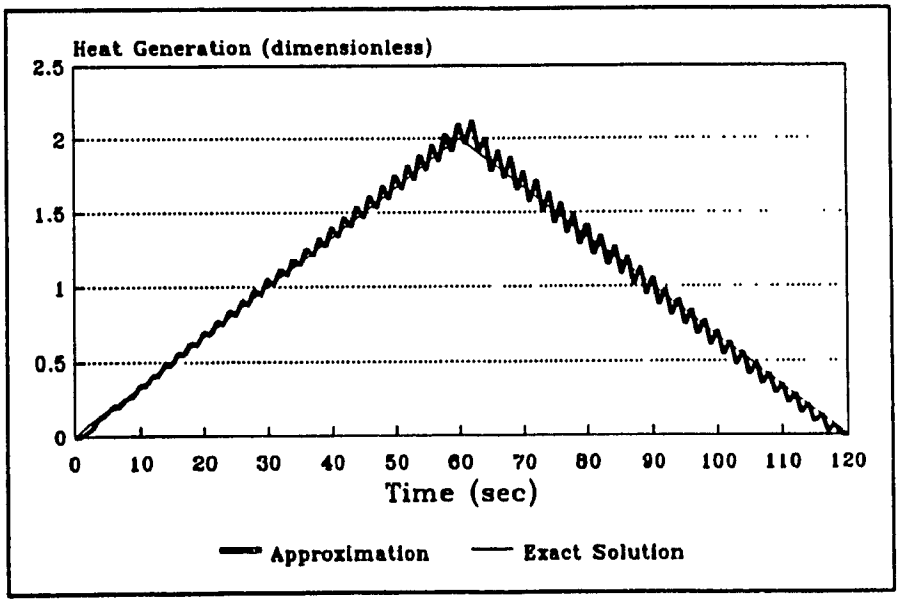

Figure 10.13 Solution for Triangular Input with 0.5% Measurement Error

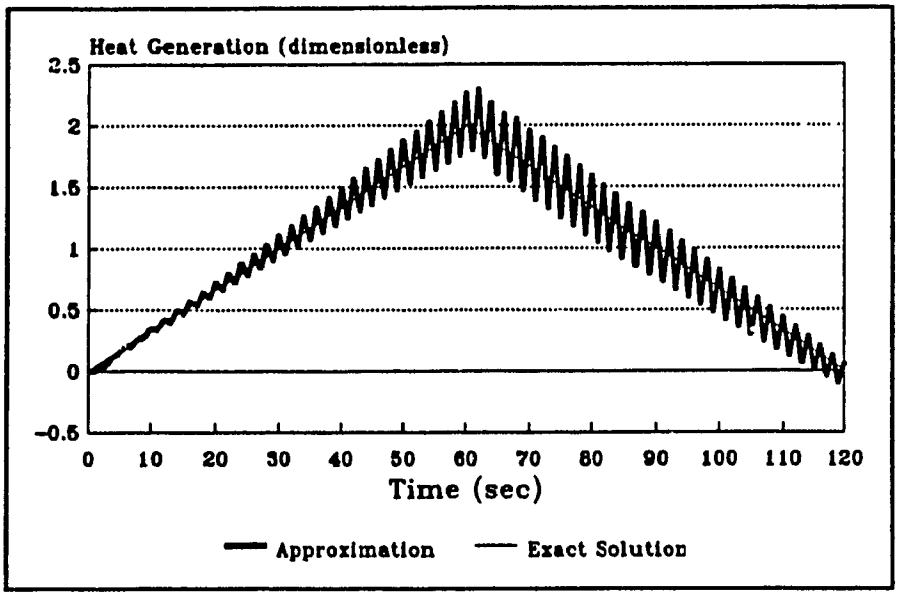

Figure 10.14: Solution for a Triangular Input with Measurement Error of 5%

stable form of the analytical step solution that was used to derive the transfer function. Even when the measurement errors were increased to 25% of the measured value, the oscillations of the solution did not cause divergence of the algorithm. Because the solution is unique and the input is continuously defined, there is no tendency for the algorithm to mistakenly converge to the wrong solution.

10.6 Summary and Conclusions of the Method

This method of solving the IHCP is similar to the previous method in that it uses a Laplacian transfer function to express the solution to the problem. The difference is that the Laplacian transfer function is transformed to the time domain so that there are two representations of the solution, one in the s-domain and one in the t-domain. The s-

domain transfer function is represented as follows:

$$Q(s) = G(s)\,T(s) \qquad (10.32)$$

When equation (10.32) is transformed to the time domain it takes the form of a convolution integral:

$$Q(\tau) = \int_0^{\tau} G(\tau - t)\,T(t)\,dt \qquad (10.33)$$

where the time domain transfer function is defined by:

$$G(t) = \mathcal{L}^{-1}\{G(s)\} \qquad (10.34)$$

G(s) has no analytical representation in the s-domain and G(t) has no analytical representation in the t-domain, so the transformation from s→t in equation (10.34) must be performed numerically. A further complication is that the only available numerical inverse Laplace transformation procedure, the Crump method, cannot transform a function when singularities are present. The problem is solved by breaking the s-domain transfer function into two parts: 1) the singularity functions are transformed analytically by solving equation (10.34) for the special case when I→∞ by methods of variational calculus, and 2) the rest of the transfer function is transformed by a newly developed method which accelerates the convergence of the Crump algorithm and filters the singularity functions out of the solution. The end result is simple convolution integral with a transfer function G(t) defined partly numerically and partly analytically.

The speed and accuracy of the time domain transfer function method is superior to the s-domain transfer function method given previously, because the time consuming

work of transforming from one space to another is done while the system is off-line. Only one numerical integration is required to obtain the solution in the time domain. Because the transfer function is defined by an approximate functional expression, the inherent instability of the problem has been eliminated, as with the previous method. The transfer function can also be analyzed by classical control theory because it has a second representation in the s-domain. The disadvantage of this method compared to the previous s-domain transfer function method is that the solution is specific to the particular geometry of a large, thin walled structure. For a different geometry, the transfer function would have to be completely re-formulated.

CHAPTER 11: METHOD3; PROPORTIONAL HEAT INVERSION

11.1 The Method of Proportional Heat Inversion

The method of proportional heat inversion is the simplest of the three methods of solving the IHCP that will be investigated in this thesis. The solution is based on a linear relationship between the input and output variables:

$$Q(t) = k\,T(t) \tag{11.1}$$

where, K is a constant. The constant K is chosen such that the solution will be correct when the steady-state condition is reached. Therefore,

$$Q = \left(\frac{q_i}{T_{ss}}\right) \Delta T \tag{11.2}$$

where, T_{ss} is the steady-state temperature difference corresponding to the constant input q_i.

The temperature difference profile for a unit step in heat generation at t=0 was given in figure 8.5. Figure 11.1 shows the temperature difference that results from step inputs of various magnitudes, from Q=0.1 to Q=1.0. Because of the linearity of the problem, the values of the temperature profiles at any fixed value of t are proportional to the magnitude of the input. Since the steady-state temperature is proportional to the magnitude of the input, equation (11.2) represents an exact solution when the input is constant and steady-state conditions have been established.

The proportional inverse method is simple, but it is a surprisingly reliable estimate for the heat generation for the purpose of real time control. It is only strictly correct in the steady-state condition with a constant input, but in an on-line environment

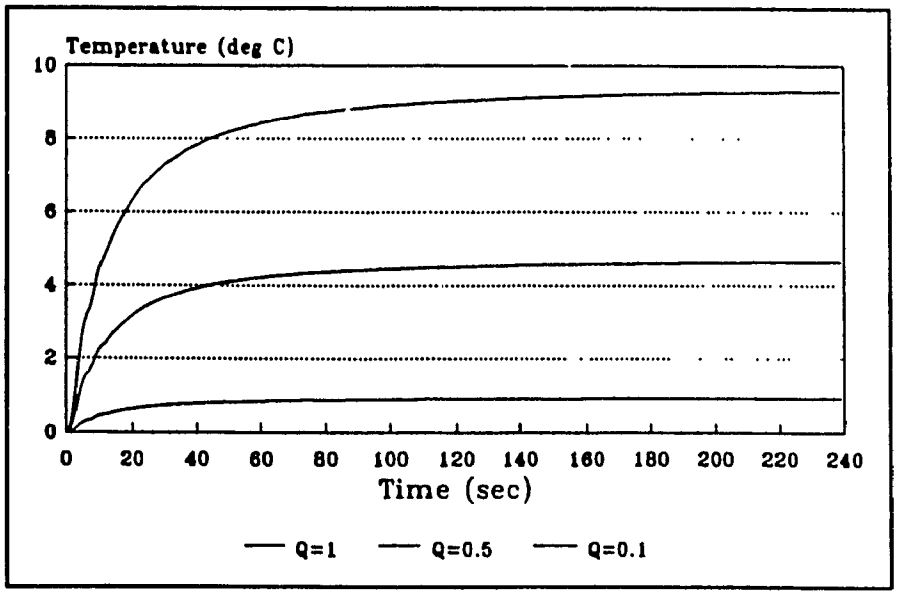

Figure 11.1: Temperature Difference Profiles for Step Inputs of Different Magnitudes

it is often close to correct most of the time. For a step input, such as the centre curve in figure 11.1, equation (11.2) simply scales the temperature profile so that the steady state value equals 0.5, as shown in figure 11.2. Thirty six seconds after the change in the input, the error in the approximation has dropped to 10%, as shown in figure 11.2. The significance of those 36 seconds depends on the period of the control cycle. Suppose that an alternate method could recognize the change in the input much faster, say instantaneously at $t=0^+$. If the period of the control cycle is much less than 36 seconds, then a control system based on the alternate method would respond faster and perform better than a control system based on proportional inversion. On the other hand, if the period of the control cycle is much greater than 36 seconds then the advantage is lost. By the time the controller is ready to estimate Q, both methods are equally reliable, and there is no advantage to be gained from the more advanced method. This example

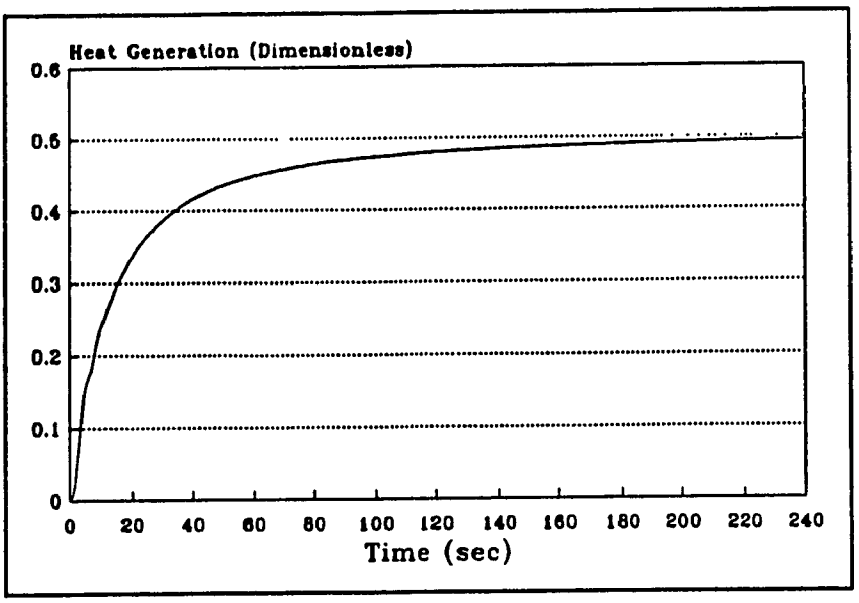

Figure 11.2: Solution of IHCP by Proportional Inversion (Step Input of Magnitude 0.5)

illustrates the special requirements of a solution when it is to be used with real time control. An algorithm which approaches the accuracy of figure 11.3 twenty seconds faster, but increases the control cycle by 30 seconds, would actually produce a deterioration in the performance of the control system.

11.2 The Test Results

Figure 11.3 shows the solution of the IHCP by the proportional method to the standard input given in figure 9.6. The accuracy is not as impressive as the other two methods, but the computation time is less than 1 millisecond. Furthermore, the solution is exact when steady state conditions at the measured node have been reached, which takes about 3 minutes following a step change. For many applications in the thermal

control of machine tools, proportional inversion is all that is required. The structural deformation of a machine tool requires in the range of 30 minutes to reach steady state, so it may not be critical to recognize high frequency components in the input.

Figure 11.4 shows the results of the proportional algorithm for the standard input given in figure 9.6, with a simulated error of 0.1 degrees plus 5% of the measured temperature. The solution is highly stable, even for excessively bad measurement problems.

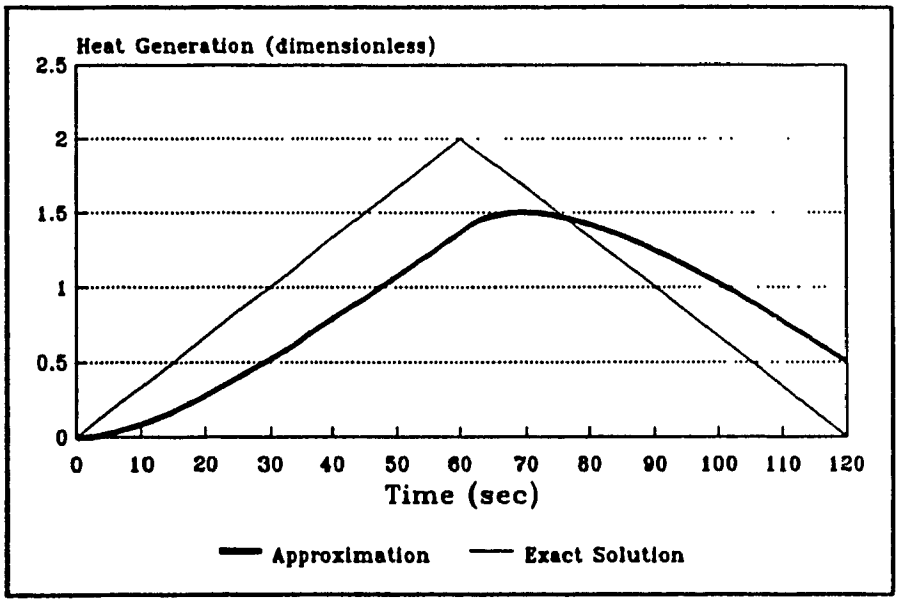

Figure 11.3: Proportional Inversion of the Standard Test Input with Errorless Data

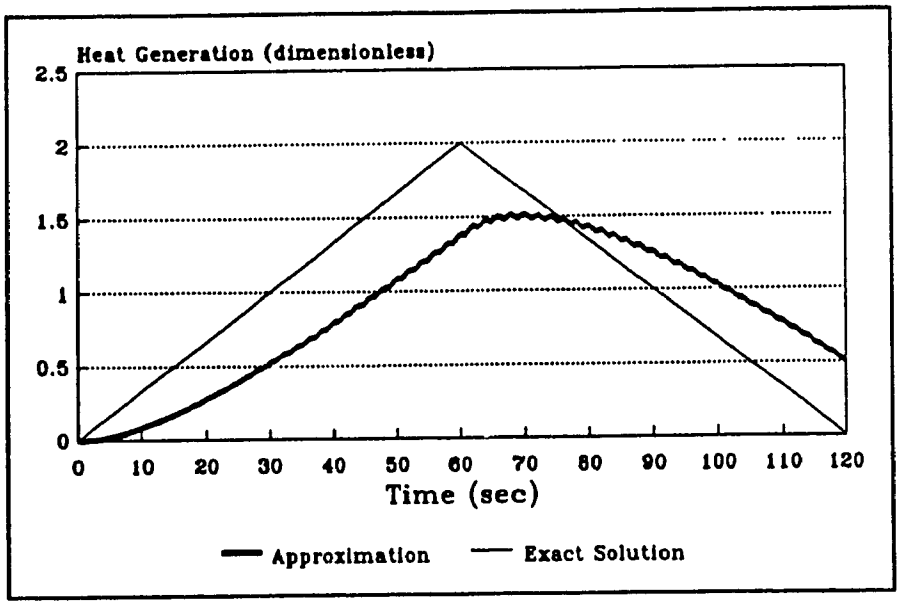

Figure 11.4: Proportional Inversion of Standard Test Input with Simulated Measurement Error of 5%

11.3 Summary and Conclusions of the Method

The Proportional Inversion method is the simplest of the four methods tested in this thesis. The heat generation of the source is estimated by determining the heating value that would produce a given temperature difference if the thermal system were in steady-state. While the accuracy of the solution is not very good, especially for high frequency inputs, the stability and computation time are excellent. Furthermore, the solution is compatible with classical control system theory. It is an attractive solution for control systems with a large time period between cycles because of the simplicity and reliability of the method.

CHAPTER 12: METHOD 4; THE REGULARIZED STOLTZ METHOD

12.1 The Basis for the Method

The Stoltz method is applicable to linear problems and is based on the Duhammel integral, as discussed in the literature review. The Stoltz method by itself is not a practical solution to the IHCP because there is no mechanism to control the inherent instability of the problem. A functional form of the Stoltz solution is the Stoltz method with first order regularization. The Stoltz method is regularized by replacing the temperatures in equation (3.9) by the Duhammel solution to the direct problem, and minimizing the error residual with respect to each of the discrete heat magnitudes q_i. The derivation of the solution matrix is given in appendix 6. The solution is obtained by solving the matrix by the Gauss-Jordan method. For N data points, the solution matrix is constructed from:

$$[\Phi]\,[q] = [B] \qquad (12.1)$$

where [Φ] is given by,

$$\begin{bmatrix} \sum_{i=1}^{N} \Delta\Phi_i\Delta\Phi_i+\alpha & \sum_{i=2}^{n} \Delta\Phi_i\Delta\Phi_{i-1}-\alpha & \sum_{i=3}^{n} \Delta\Phi_i\Delta\Phi_{i-2} & .. & \sum_{i=n}^{n} \Delta\Phi_i\Delta\Phi_{i-n-1} \\ & \sum_{i=1}^{n-1} \Delta\Phi_i\Delta\Phi_i+\alpha & \sum_{i=2}^{n-1} \Delta\Phi_i\Delta\Phi_{i-1}-\alpha & .. & \sum_{i=n-1}^{n-1} \Delta\Phi_i\Delta\Phi_{i-n+1} \\ & & \sum_{i=1}^{n-2} \Delta\Phi_i\Delta\Phi_{i-1}+\alpha & .. & \sum_{i=1}^{n-2} \Delta\Phi_i\Delta\Phi_{i-n+2} \\ & & & .. & ..... \\ \textit{Symmetric} & & & & \\ & & & & \sum_{i=1}^{1} \Delta\Phi_i\Delta\Phi_i+\alpha \end{bmatrix}$$

and [B] is given by,

$$[B] = \begin{bmatrix} \sum_{i=1}^{n} (Y_i-T_0)\Delta\Phi_i \\ \sum_{i=1}^{n-1} (Y_{i+1}-T_0)\Delta\Phi_i \\ \sum_{i=1}^{n-2} (Y_{i+2}-T_0)\Delta\Phi_i \\ ..... \\ \sum_{i=1}^{1} (Y_{i+n-1}-T_0)\Delta\Phi_i \end{bmatrix} \qquad (12.3)$$

The parameter α in equation (12.2) is the regularization factor. Increasing the regularization factor increases the stability of the problem, but at the expense of non-

exact matching of the solution.

The Stoltz method and the regularized Stoltz method solve the IHCP for an entire interval, not just at one point. The interval usually represents the entire temperature history of the input, and the solution is found simultaneously for the entire interval. But in real time control, only a partial interval is available. There are two ways to incorporate the regularized Stoltz method into a real time control process:

1) Collect the temperature data at a faster rate than the period of the controller cycle, and then process the data one interval at a time. This method requires an auxiliary mechanism to sample and store temperature data independently of the controller. Furthermore, a high sampling frequency makes the regularized Stoltz method unstable, as will be seen in the next section.

2) Another procedure is to use the regularized Stoltz method to solve for a block of past temperature data, and then use only the solution for the last time step to represent the heat generation at the present time. The purpose of the previous data is only to stabilize the solution at the present time. The problem with this procedure is that the solution is least accurate at the last time interval.

The objective of this thesis is to use a controller with a high cycle frequency so that it can deal effectively with high frequency thermal inputs. Thus, the first procedure is not practical because dividing a small interval still further would not yield a stable solution

to the regularized Stoltz method. Therefore, the second procedure is the only viable alternative.

The idea of using a block of data to stabilize the solution at one time is not new, it is the basis of the Beck method, discussed in section 3.6. The Beck method uses future data so it is not applicable to real time control, but an analogous method is to use a small interval of past data to determine the regularized solution in the interval, and then discard all but the last value. The problem with this method is that the solution at each time interval carries over into the next time step. Thus, if q_i is the solution for the heat generation at time t_i, then $q_{i+1}=q_i + \delta q_i$, where δq_i is the change in the heat generation from t_i to t_{i+1}. Errors accumulate with each time step because there is no fixed reference frame other than the initial heat generation value. The solution algorithm is not stable in real time because the error will eventually propagate out of control.

The solution can be 'grounded' in real time by defining the regularized interval large enough so that all relevant data is included into the solution with each time step. This is the same idea as the temperature window that was used in methods one and two, where it was found that disturbances that occur a long time in the past have a negligible influence on the present temperature distribution. If all of the relevant temperature data is processed with each iteration of the method, there is no need to rely on the solution at the previous time steps and errors do not propagate down the line.

In methods one and two, a temperature window of 100 seconds was used. For the present method, the longer processing time of the algorithm requires that a compromise be made between the size of the interval and the processing time per cycle. Thus, a

temperature window of 50 seconds will be used in the following experiments.

12.2 Testing the Regularized Stoltz Solution

It was stated in the last section that the temperature window for the data is 50 seconds. This generates a 50x50 solution matrix which is solved by Gauss-Jordan elimination.

Figure 12.1 shows one iteration of the regularized Stoltz method for the standard test input from figure 9.6 with errorless data and a 100 second interval. The interval starts arbitrarily at t=20 seconds. the regularization factor α is 1.2, which was chosen by trial and error to optimally regulate the interval. There is considerable instability at the beginning of the interval, and a smaller deviation at the end of the interval. The initial instability is not a concern because it is only the final value that is of interest for

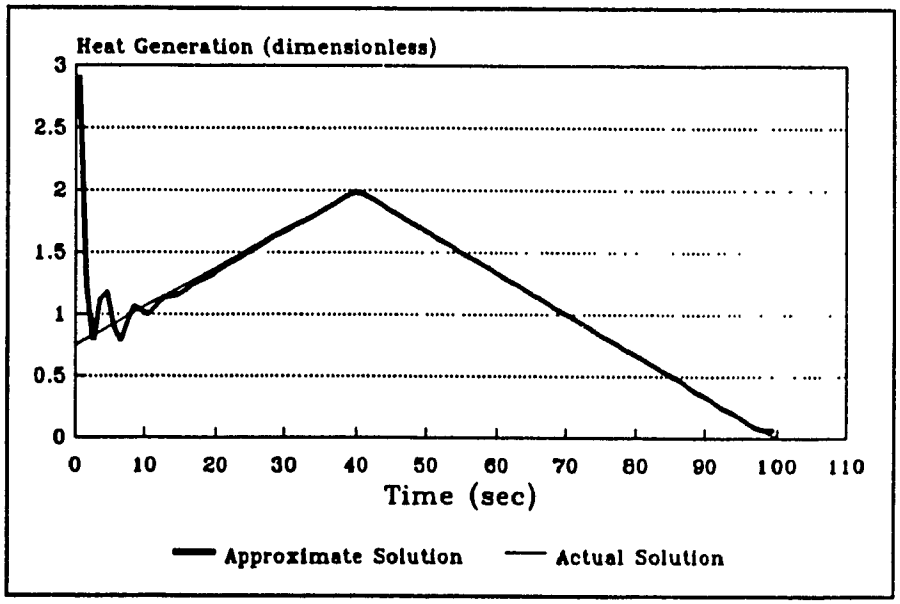

Figure 12.1: One Iteration of Regularized Stoltz Method (T_p = 100 seconds)

the real time algorithm. The solution deviates from the exact curve at the end of the interval because at that point it is only regularized from one side, while in the rest of the interval the solution is regularized on both sides.

Figure 12.2 shows the results of method four for a temperature window of 50 seconds and a regularization factor of 1.2. The solution at each time step was determined independently by determining a regularized Stoltz solution similar to figure 12.1 at each time step, and then discarding all but the last value. The accuracy of the solution to the standard test input is good, but the process time of the algorithm is an average of 97.4 seconds per iteration.

Figure 12.3 shows the solution of method four with an input error of 5% of the measured value.

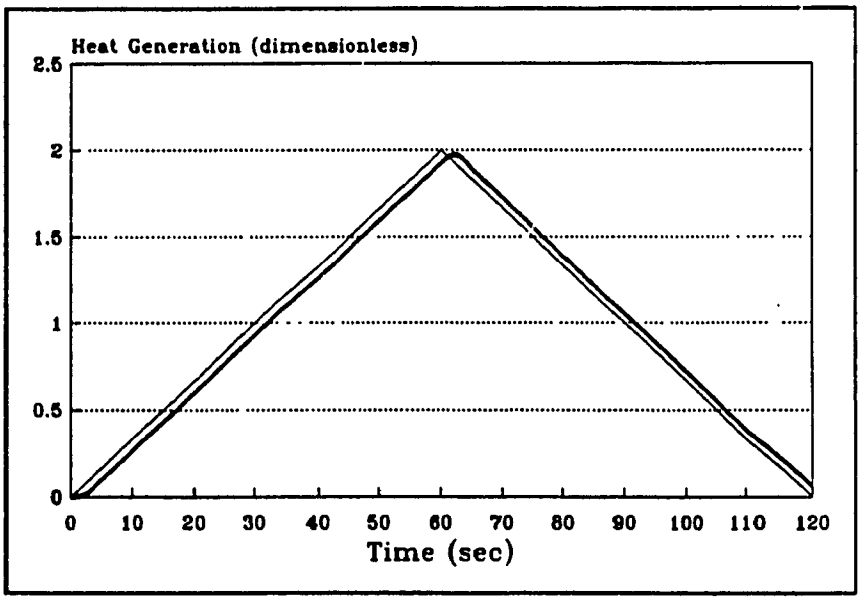

Figure 12.2: Solution of Method Four with Errorless Data

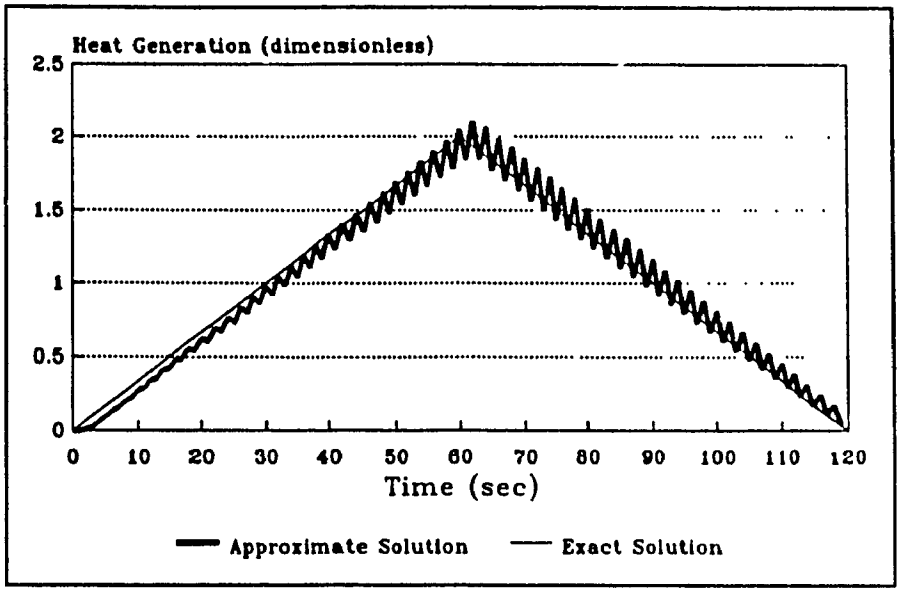

Figure 12.3: Solution of Method Four with 5% Simulated error

12.3 Summary and Conclusions of the Method

Regularization is the most commonly used method of stabilizing the IHCP, and The regularized Stoltz method is the most common method for linear problems. However, the method was not designed for a real time environment because it relies on future data to stabilize the solution, and the calculation time is large. In this chapter the regularized Stoltz method was adapted to real time by defining a temperature window of past data to stabilize and ground the solution at a particular value of time. The accuracy of the solution is good, and the stability is very good, but the processing time is prohibitively large for real time control, 97.4 seconds on a 486-PC. Also, the solution is not available in the s-domain and the method cannot be analyzed by classical methods.

Table 12.1: Performance Criteria for the Four Methods

	Absolute Error	Absolute Differences	Computation time (sec)	Compatibility with Control Theory
Method 1	15.3	1.37	4.4	yes
Method 2	0.81	6.52	0.14	yes
Method 3	51.3	0.526	$< 1 \times 10^{-3}$	yes
Method 4	9.21	5.04	97.4	no

12.4 Conclusion of Part III

In order to compare the performance of the four methods, there are four performance criteria that are used:

1) The cumulative absolute value of the error is defined by:

$$E = \sum_{i=0}^{n} |Q_a(t_i) - Q_m(t_i)| \qquad (12.4)$$

where Q_a is the actual heat generation, and Q_m is the calculated heat generation without measurement error.

2) The stability is measured by the sum of the absolute value of the differences between successive time steps for a solution with a 5% simulated measurement error. That is:

$$D = \sum_{i=0}^{n} |Q_m(t_{i+1}) - Q_m(t_i)| \qquad (12.5)$$

3) The calculation time is the time required to evaluate the solution at one time step on a 486-PC.

4) The final measure is the compatibility of the solution with control theory which

is a qualitative judgement.

For the four methods, the performance criteria are tabulated in table 12.1. The best overall performance is given by the Convolution integral method. This is the method that be used to estimate the heat generation of the uncontrolled source in this thesis.

PART IV: THERMAL DEFLECTION AND CONTROL

CHAPTER 13: THE MODEL FOR THERMAL DEFORMATION

13.1 Compensating for Thermal Deformation

13.1.1 The Displacement Variables

The goal of this thesis is to design a control system to reduce the thermal displacement error of key points on the test structure. The compensation is provided by artificial heat sources placed on the structure, with the magnitude of the heat generation regulated by the system controller. There are a total of six displacement variables which define the relative position and orientation between points on the structure: the three linear displacement variables dx, dy, and dz, and the three rotational variables $d\Theta$, $d\phi$, and $d\psi$.

13.1.2 The Artificial Heat Sources

It is possible to control all six displacement variables, but that would require elements that are capable removing heat as well as generating heat. Cooling is more expensive and more difficult to implement than heating, because it requires an external source of cooling fluid. The heat transfer rate is a function of the temperature of the fluid and the temperature of the structure, so there is a dynamic relationship between the variables, and it is difficult to control the temperature of the fluid precisely. Electrically activated cooling pads are available but they are large, expensive, have a low power removal capacity, and there is a non-linear relationship between the input and output.

Resistance coil heating elements are more convenient because they are compact, inexpensive, and the heat generation can be exactly controlled by regulating the voltage input. The problem with resistance coil elements is that only heating is possible, and so it is not possible to control the position and orientation variables simultaneously. Any positive heat generation makes the structure deform in the vertical (z-axis) direction, so the only way to compensate for z-deflection with positive heating elements is to strategically rotate the structure so that the vertical elevation of one key point is reduced. There is no way to eliminate the rotation of the points with heating elements alone because that would reintroduce the problem of vertical deflection. Rotation of the cutting tool is not a significant problem in most cutting operations because it normally never exceeds 10^{-4} radians. Rotations this small do not change the profile of the cutting tool that makes contact with the workpiece, so there is no problem with inaccuracy or increased tool wear. On the other hand, the corresponding linear deformation of 10^{-4} meters significantly affects the accuracy of the machine.

In this thesis, resistance coil heaters will be used to control the linear deformation of key points on the test structure. The corresponding rotations of the points will not be considered because it is not an important consideration in most machining operations.

13.1.3 Three-Axis Control

Thermal disturbances generally produce deformation along all three co-ordinate axes. This requires three independent control systems to handle the deformation in each direction, and each of these requires at least one controlled heat source. A controlled

source must be located so that a positive generation tends to reduce the net deflection of the key points along the direction that is being controlled. It is usually not possible to position the controlled sources so that they induce a deflection only along one axis, so the three control systems are linked together by the controlled sources. This is shown schematically in figure 13.1 where the controlled heat generation for axes x and y are treated as disturbance inputs by the controller for axis z, and so on. The other disturbance inputs come from the uncontrolled heat sources, which must be estimated from temperature measurements.

The controlled heat sources are placed so that they induce defection predominantly along one of the three co-ordinate axes. The larger the secondary deflection along the other axes, the larger the thermal disturbance to those axes, and the greater the coupling

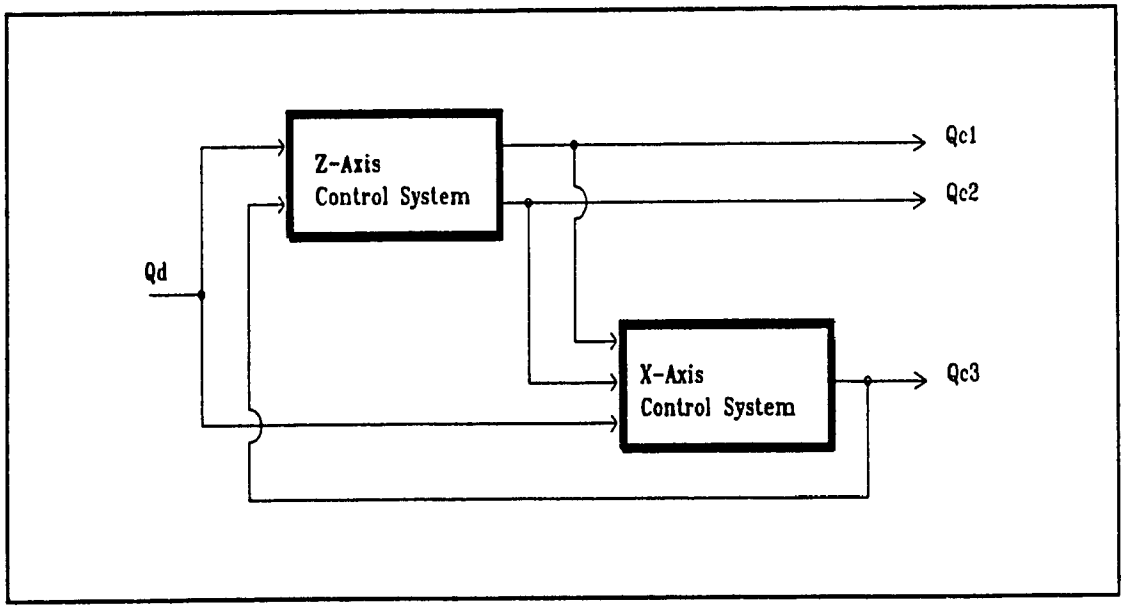

Figure 13.1: Schematic Representation of Two-Axis Control System

of the control systems. A high degree of coupling means that the steady-state generation of the artificial sources is large, and the dynamic performance of the control systems is reduced.

Optimal positioning of the artificial heat sources is another form of the inverse problem that was discussed in chapter 3 [50]. Neto et al. used the conjugate gradient method to estimate the strength and location of a plane heat source inside a plate [52]. Finding the location of a source must be formulated as an inverse problem because the position of the source is one of the boundary conditions of the problem, just like the heat generation. While this could be the subject of several chapters in the thesis, it is not necessary to consider the problem at this point because of the simplicity of the test structure. The optimal locations of the controlled sources can easily be determined by an investigation of the thermal deformation behaviour of the structure, without a formal mathematical treatment. If the optimal location of the sources were to be treated as an inverse problem for a real machine tool structure, additional difficulties would arise because there are physical constraints on where the heating elements can be located. This would have to be taken into consideration by the solution algorithm. The best method for solving the inverse problem for the optimal location of the sources is by iterative regularization, as discussed in chapter 3.

13.2 The Finite-Element Test Model

13.2.1 The Configuration of the Model

Figure 13.2 shows the finite-element test model for thermal deformation. The geometry of the model is identical to the thermal model discussed in chapter 8. The finite-element thermal deformation algorithm determines the deformation of the structure that is induced by the temperature distributions determined in chapter 8.

Figure 13.3 shows a schematic drawing of the model setup. The controlled position r=xi+yj+zk is shown in the figure. The positional displacement vector dr is measured from the nodal deflections at d_1, and d_2. If the box model represents part of a machine tool structure, then dr represents the relative displacement error between the cutting tool and the workpiece.

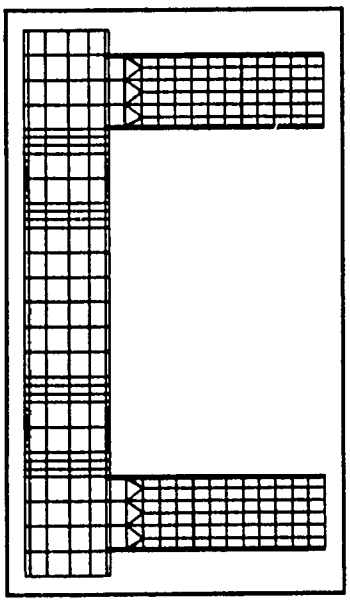

Figure 13.2: Finite-Element Model Drawing of for Thermal Deformation

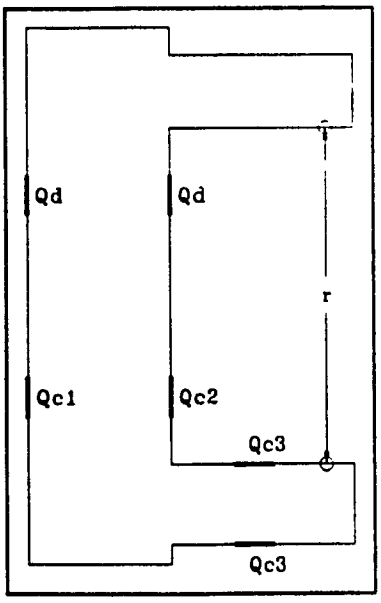

Figure 13.3: Schematic Model Setup

As stated previously, there are four independent heat sources in the finite-element model: Q_{C1}, Q_{C2}, Q_{C3} and Q_i. The only uncontrolled source is Q_i, the disturbance to the system. The controlled sources are Q_{C1}, Q_{C2} and Q_{C3}, which represent artificial heating pads applied to the outer surface of the structure. Each of the four independent sources creates part of the deflection of d_1 and d_2. Because of the linearity of deformation problem, the deflection from each source can be treated independently from the others. The total deflection at d_1 and d_2 is the sum of the deflection contributions from each source acting independently. Figure 13.4 shows a comparison between the deflection d_1 produced by Q_{C1} and Q_{C2} acting simultaneously, to d_1 determined by applying each source independently and then adding the deflections together. The two curves are so similar that they are indistinguishable from one another, confirming that the sources are truly independent and superimposable.

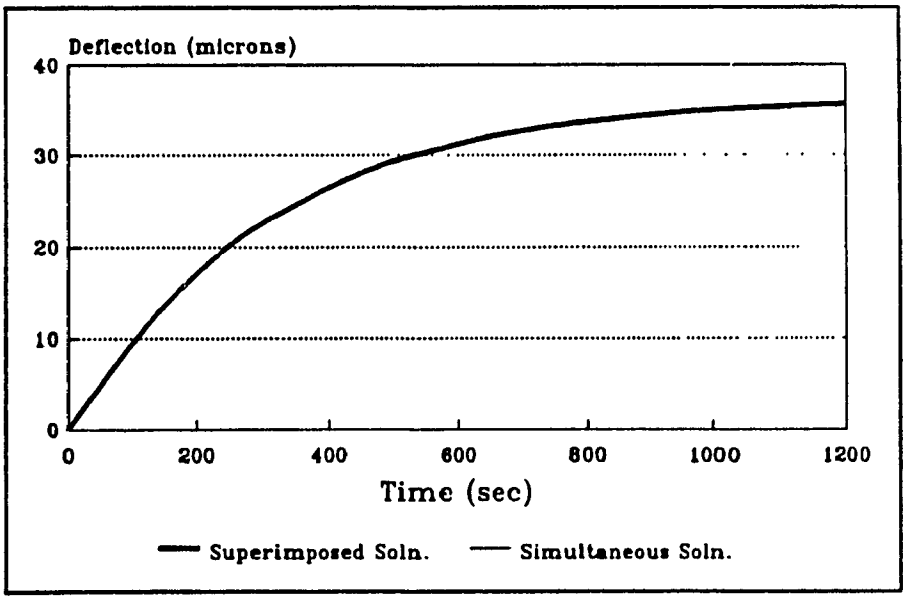

Figure 13.4: Comparison of Theoretical and Superimposed Deflection Solutions

13.2.2 Results of the Finite-Element Test Model

13.2.2.1 The Disturbance Input

Figure 13.5 shows the steady-state thermal deformation of the test structure for a non-dimensionalized heat input $Q_d=1$, and a scale factor of 1:10000 for the deformation. The deflection of the measured points d_1 and d_2 are given in figures 13.6 and 13.7. From figure 13.7, the z-deflection of d_2 is larger than the deflection in the x-direction, and the y-deflection is zero. The y-deflection is always zero because of the symmetry of the structure, so it is not included in any of the figures. Although the disturbance deflects primarily in the z-direction, that does not mean that the x-deflection is a less serious problem. The controlled heaters for the z-axis control system produce significant deflection in the x-direction, as shall be seen shortly, so two-axis control is required.

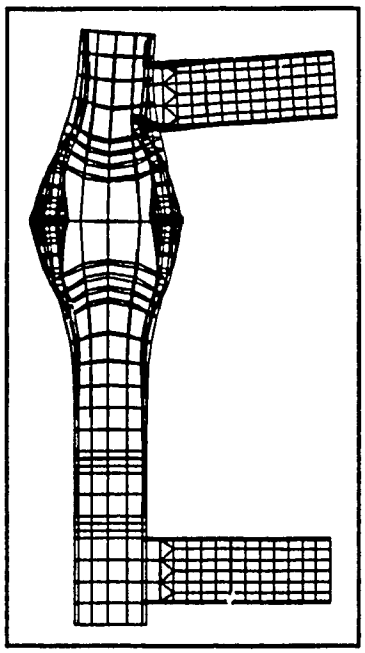

Figure 13.5: Steady-State Thermal Deformation of the Test Structure for a Disturbance Heat Generation $Q_d=1$

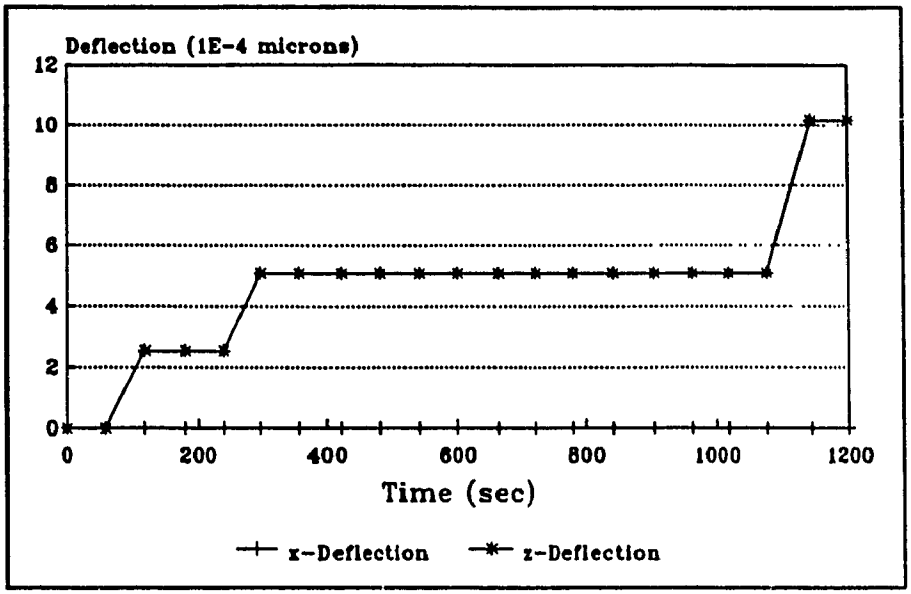

Figure 13.6: Deflection of d_1 for Q_d=1

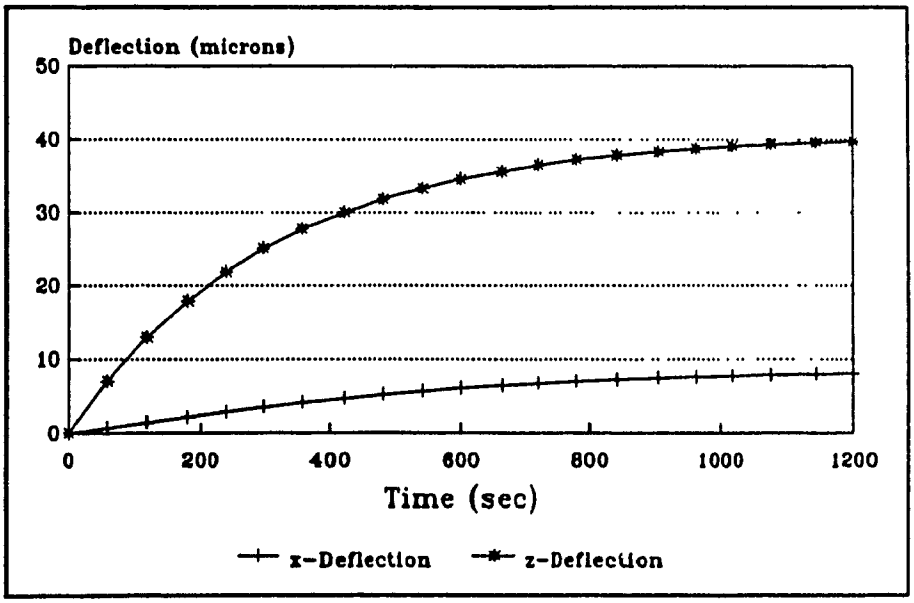

Figure 13.7: Deflection of d_2 for Q_d=1

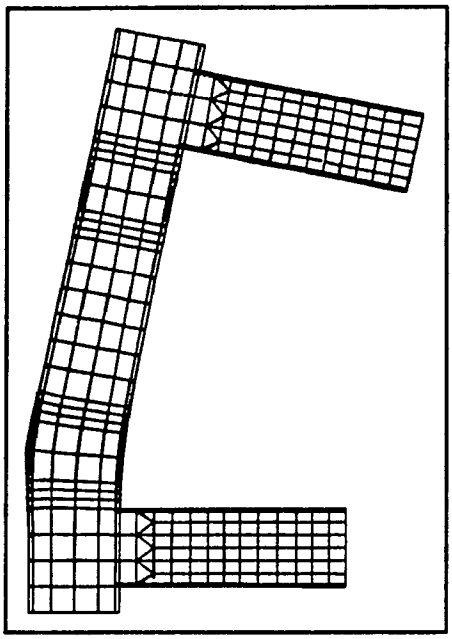

Figure 13.8: Steady-State Thermal Deformation of Test Structure for $Q_{c1}=1$

A comparison of figures 13.6 and 13.7 shows that d_2 dominates the displacement error d_2-d_1 in both the x and z directions. The deflection d_1 is so small that it is below the numerical resolution of the solution algorithm. The dominance of d_2 means that it is not necessary to determine separate transfer functions for each of the deflections d_1 and d_2, instead d_2-d_1 is curve-fit directly onto the generalized transfer function.

13.2.2.2 The z-Axis Control Heaters

Figure 13.8 shows the thermal deformation of the test structure for $Q_{C1}=1$, and a scale factor of 1:1000. The controlled heat source produces a negative z-deflection by bending the upper arm with respect to the lower arm. The controlled source Q_{C1} also introduces a displacement of d_2 in the x-direction, as shown in the figure. Figure 13.9

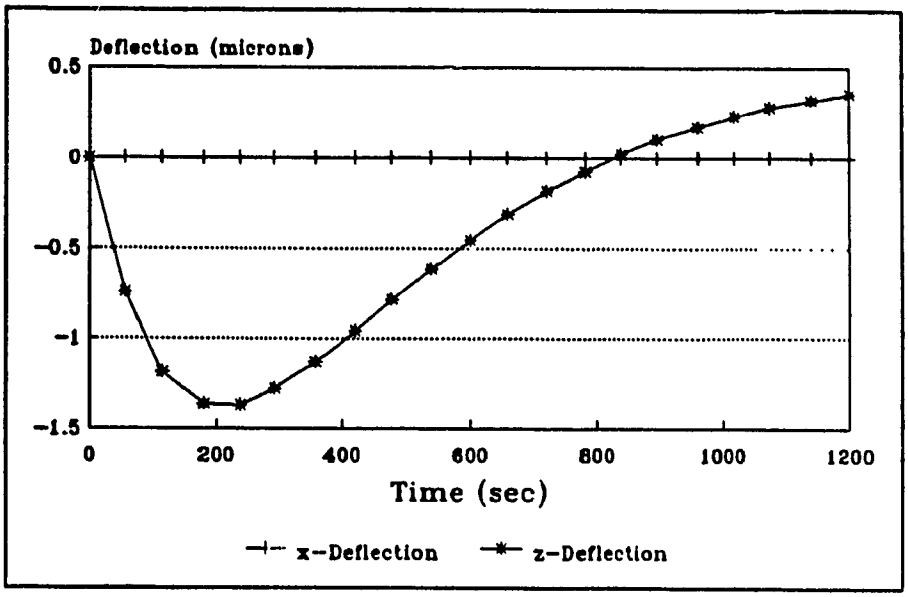

Figure 13.9: Deflection of d_1 for Q_{C1}=1

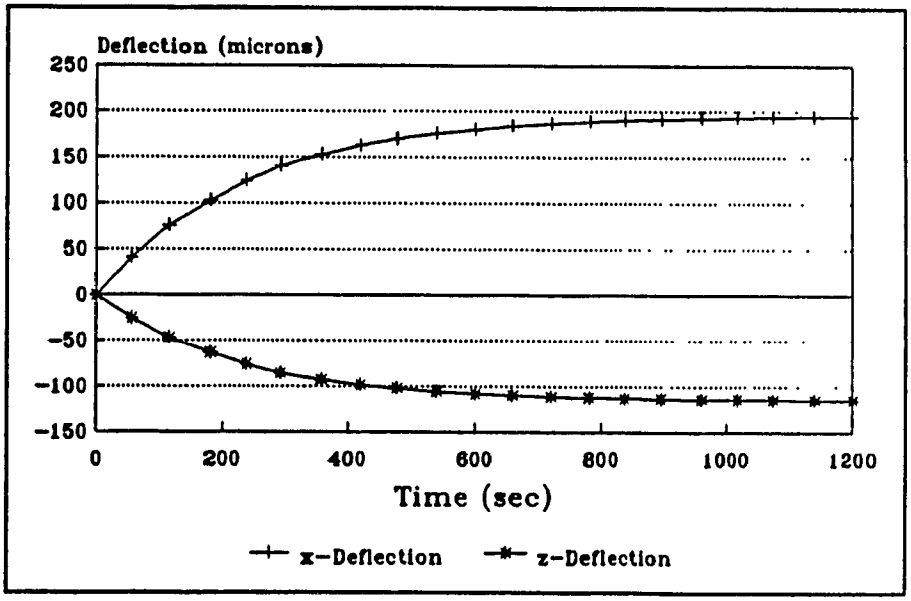

Figure 13.10: Deflection of d_2 for Q_{C1}=1

shows the displacement d_1 and figure 13.10 shows the displacement d_2 for the same thermal input $Q_{C1}=1$. The z-component of d_1 in figure 13.9 goes through a local minimum before settling on a final positive value. This behaviour is due to the fact that the heat originates on one side of the structure, and then slowly propagates to the other side. The initial effect is to bend the lower arm downward, but as the temperature rises on the other side of the column the arm deflects upward. As with the disturbance input, the deflection in the y-direction is zero because of the symmetry of the model, and d_2 dominates the displacement error.

The position of Q_{C1} was chosen so that a positive heat input would produce a negative displacement error in the z-direction. However, Q_{C1} also produces secondary deflection in the x-direction that is larger than the corresponding z-deflection, as shown in figure 13.10. Thus, while Q_{C1} corrects the disturbance in the z-direction it actually creates a greater deflection problem in x. The greater the coupling between the x and z axes, the worse is the performance of the control system, as discussed in section 13.1.3. If the control heater for the x-axis also produces a significant secondary z-deflection then the steady-state values of the controlled heaters will be very large, even for relatively small disturbance inputs, and the dynamic performance of the control system will be poor. Fortunately, the x-control heater does not produce significant deflection in the z-direction, as will be seen shortly. The heater Q_{C1} is really the critical control element because of the problem of producing a negative displacement error with a positive heat source. It is a much easier to induce a positive x-displacement, as shall be seen when the response of Q_{C3} is considered.

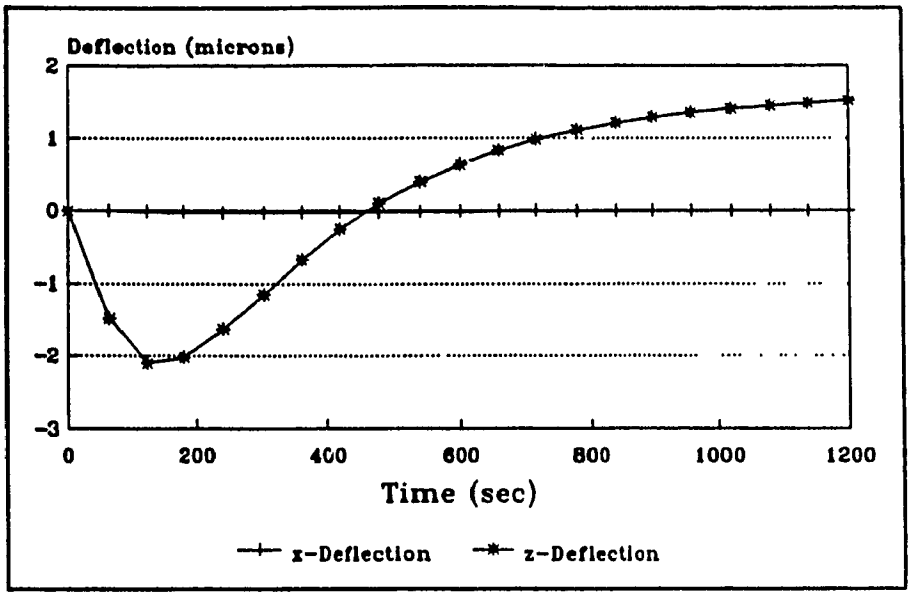

Figure 13.11: Deflection of d_1 for $Q_{C2}=1$

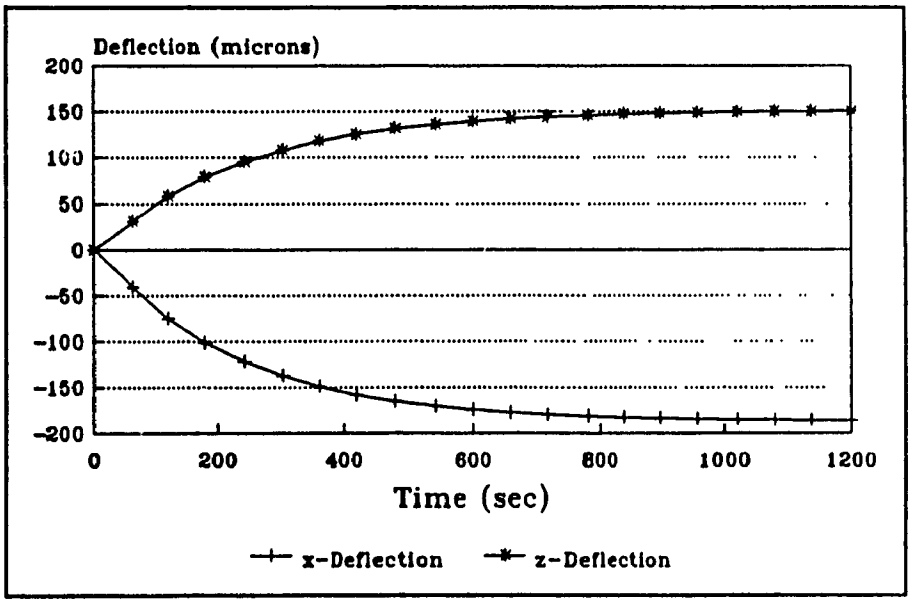

Figure 13.12: Deflection of d_2 for $Q_{C2}=1$

Figures 13.11 and 13.12 show the deflections d_1 and d_2 respectively for the unit input $Q_{C2}=1$. The controlled sources Q_{C1} and Q_{C2} produce deflections that are almost mirror images because the structure has a certain degree of symmetry in the xz plane. The purpose of Q_{C2} in a control system is to induce a positive z-deflection to complement Q_{C1}.

13.2.2.3 The x-Axis Control Heater

Figure 13.13 shows the deflection d_1 and figure 13.14 shows the deflection d_2 for $Q_{C3}=1$. The predominant deflection is along the x-axis, with a small secondary z-deflection. The coupling with the z-axis control system is not very great because most of the deformation is along the lower arm, as shown in figure 13.13. Q_{C3} was strategically placed near the centre of the lower arm so as to maximize the elongation of the arm, while minimizing the coupling with the z-axis deflection, just as the positions of Q_{C1} and Q_{C2} were chosen to maximize the bending of the column.

13.3 Curve-Fitting the Generalized Deflection Transfer Functions

In the previous section, the solutions for the deflections d_1 and d_2 were determined for various step inputs, by direct measurement of the test model. In this section, the step solutions will be used to obtain approximate analytical transfer functions relating the deflections d_1 and d_2 to the four thermal inputs Q_{C1}, Q_{C2}, Q_{C3}, and Q_d by means of the stable analytical solution that was derived in chapter 7. The Generalized analytical step

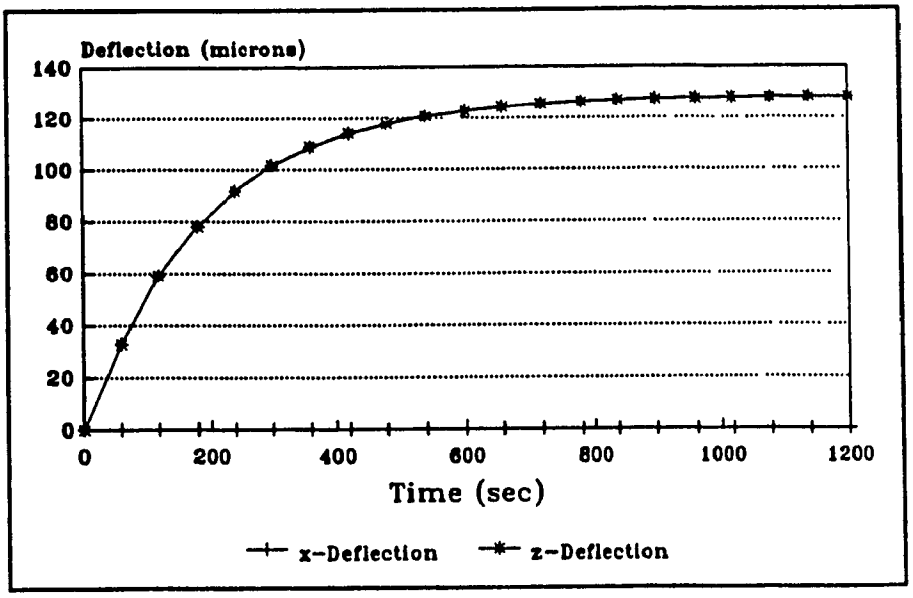

Figure 13.13: Deflection of d_1 for $Q_{C3}=1$

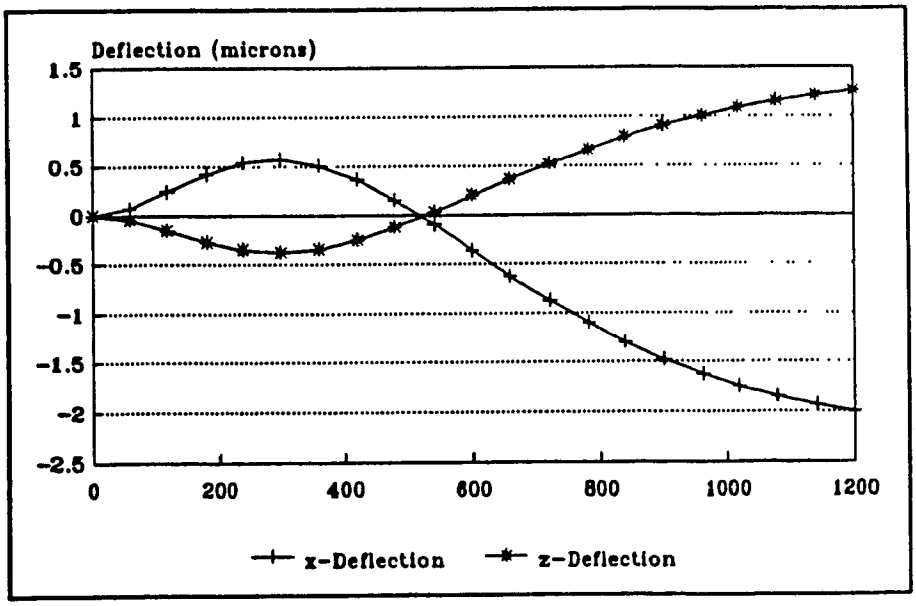

Figure 13.14: Deflection of d_2 for $Q_{C3}=1$

solution was given in equation (7.41) and is repeated here:

$$\delta = Q(A - [A - Bt]\, e^{-at}) \qquad (13.1)$$

The Laplace transformation of equation (13.1) was given in equation (7.49), which is repeated here:

$$\frac{\delta(s)}{Q(s)} = \frac{(Aa+B)\,s + Aa^2}{(s+a)^2} \qquad (13.2)$$

Equation (13.2) is the generalized analytical deflection transfer function, containing three adjustable parameters, A, B, and a. The generalized solution is adopted to a particular process by curve fitting the adjustable parameters to the step solution by means of equation (13.1). There are a total of 16 deflection transfer functions, relating Q_{C1}, Q_{C2}, Q_{C3}, and Q_d to d_{1x} d_{1z}, d_{2x} and d_{2z}. It is possible to reduce the number of equations, however, because one of the two nodal displacements always dominates the displacement error, as discussed in the last section. The relevant variable for control is the displacement error $\delta = d_2 - d_1$, which will be curve-fit directly onto the generalized transfer function. The displacement error δ is not strictly a nodal defection because it is defined by the difference between two deflections, but it does not introduce much error to treat it like a nodal deflection if $d_2 >> d_1$.

The generalized deflection step solution in equation (13.1) was curve-fit to the actual step solutions for δ using the least square method, discussed in section 8.6, and the results are given in table 13.1. There are a total of 8 transfer functions, relating the four independent heat sources to the two components of the displacement error δ_x and δ_z. Figures 13.15 to 13.18 show the actual step solutions for δ_x and δ_z, along with the curve-

Table 13.1: Table of Constants for the Thermal Deflection Transfer Functions

Transfer Function	A	B	a
δ_x/Q_d	8.5	-0.0197	0.00352
δ_z/Q_d	40.5	+0.00731	0.00303
δ_x/Q_{C1}	197.	-8.66×10^{-6}	0.00411
δ_z/Q_{C1}	-116.	-0.0758	0.00356
δ_x/Q_{C2}	-187.	-0.116	0.00368
δ_z/Q_{C2}	152.	-1.30×10^{-6}	0.00416
δ_x/Q_{C3}	-127.	-0.109	0.00437
δ_z/Q_{C3}	-2.8	+0.0148	0.00270

fit approximations based on equation (13.1). The generalized solution provides an excellent base for curve-fitting, as seen in the figures. The approximations are so good that they are difficult to discern from the actual deflection curves. This might be somewhat surprising since the analytical solution is only valid for a flat plate, and cannot anticipate the corners of the structure. But the generalized solution only represents the basic form of the solution, and the actual solution is transposed onto it. Even though the geometry of the infinite plate is different, the form of the solution is not radically different in its analytical structure. This is an indication of the power and versatility of the generalized solution method.

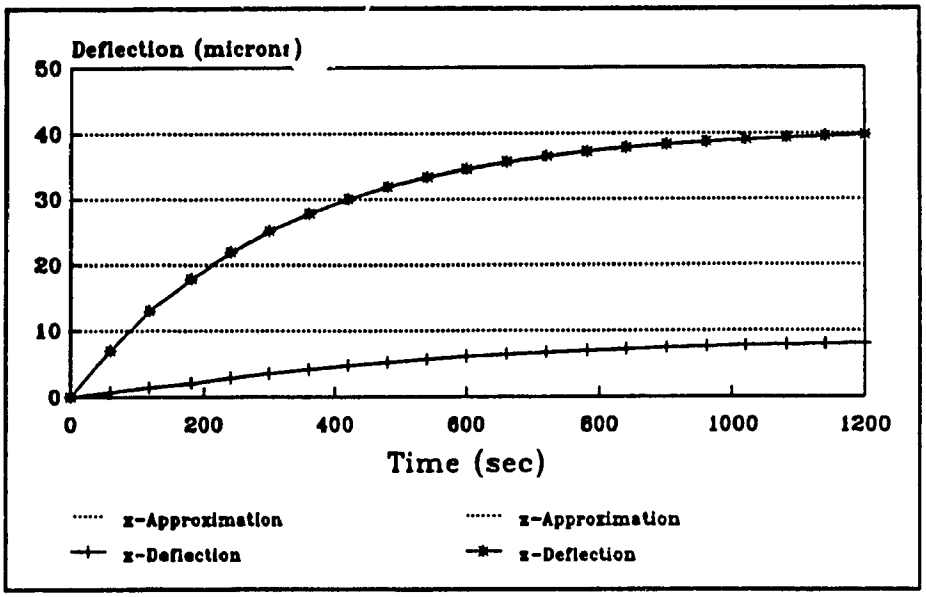

Figure 13.15: Thermal Deflection Error for a Unit Step to Q_d

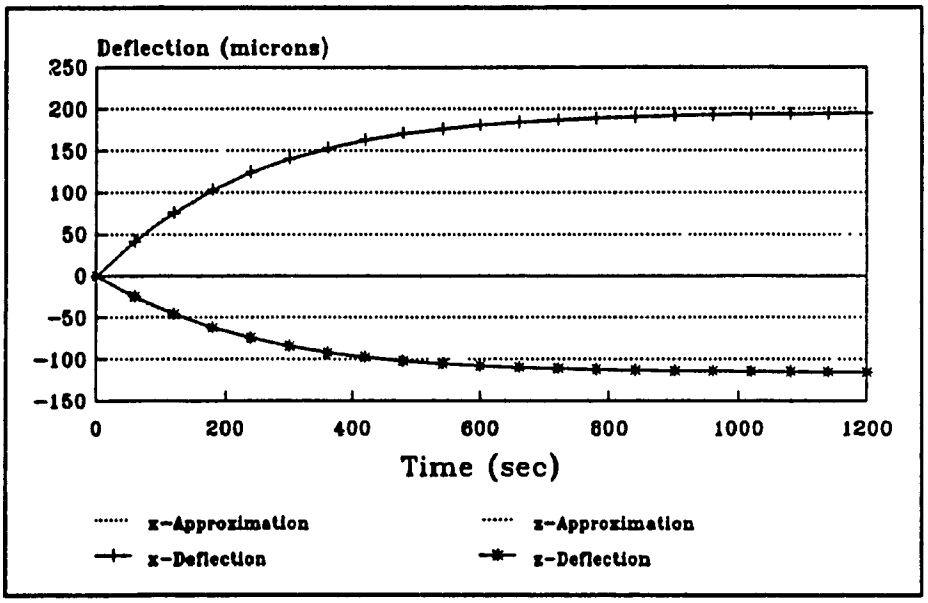

Figure 13.16: Thermal Deflection Error for a Unit Step to Q_{cl}

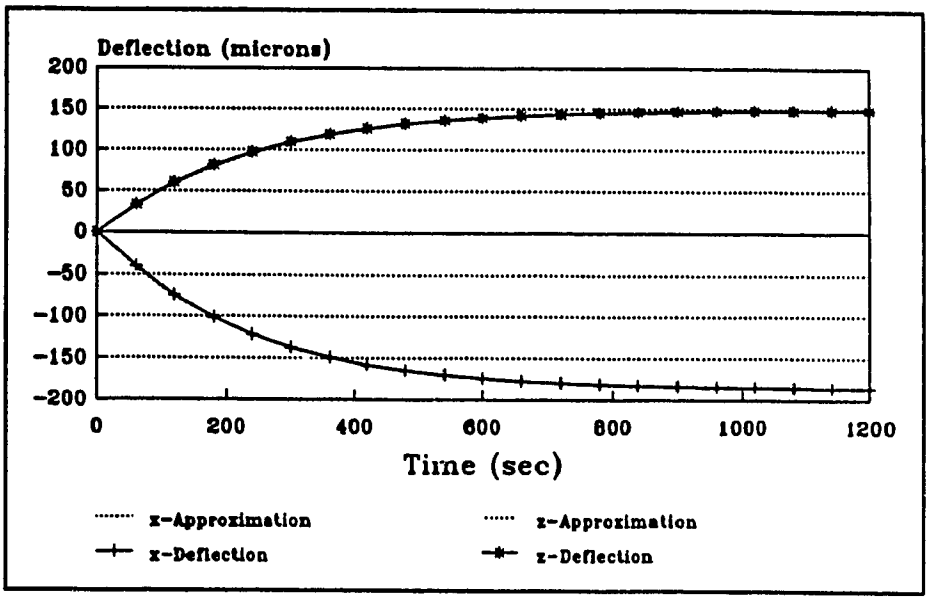

Figure 13.17: Thermal Deflection Error for a Unit Step to Q_{c2}

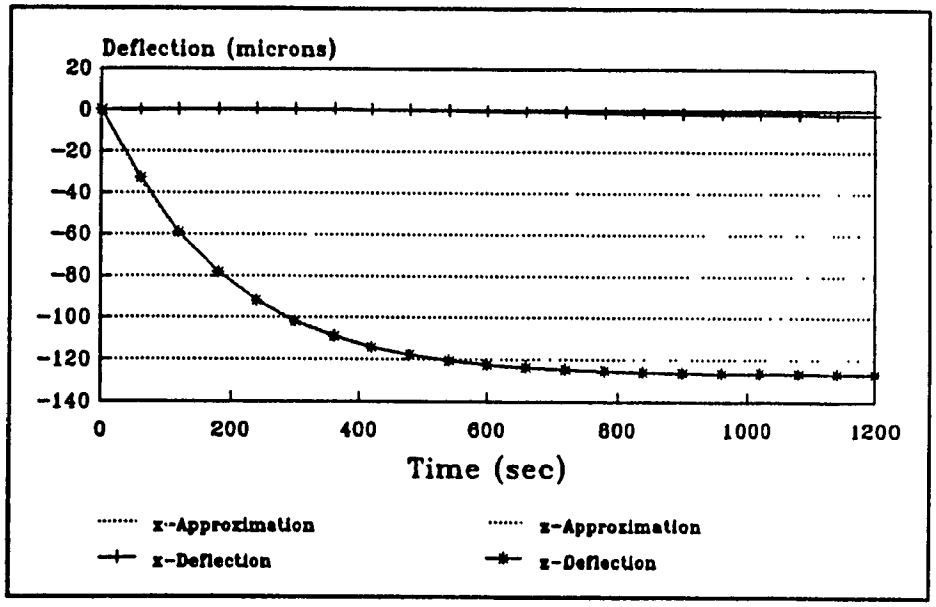

Figure 13.18: Thermal Deflection Error for a Unit Step to Q_{c3}

CHAPTER 14: THE CONTROL SYSTEM

14.1 Block Diagram Representation of the Control System

Figure 14.1 shows the complete block diagram representation of the z-axis control system, where δ_z is the controlled variable, Q_{C1} and Q_{C2} are the manipulated variables, Q_d is the external disturbance input, and Q_{C3} is the disturbance input from the x-axis control system. T_d is a temperature gradient input that is measured on the test model in the vicinity of the disturbance heat source, which defines Q_d through the IHCP transfer function G(s), which has already been developed and tested in part III of the thesis. Q_d, determined from T_d, is the only external input to the control system. Q_{C3} is the heat generation of the x-axis controlled source, which introduces a secondary disturbance in z. Since the generation of Q_{C3} is controlled by the x-axis controller, its magnitude is known precisely, but Q_d is related to the measured input T_d through a transfer function.

The transfer functions T1(s), T2(s), T3(s), and T4(s) are all defined by equation (13.2) and the parameters given in table 13.1. In order to be consistent with the terminology of figure 13.1, the deflection transfer functions are defined as follows:

$$T1(s) = \frac{\delta_z}{Q_{C3}} \qquad T2(s) = \frac{\delta_z}{Q_d}$$
$$T3(s) = \frac{\delta_z}{Q_{C1}} \qquad T4(s) = \frac{\delta_z}{Q_{C2}} \qquad (14.1)$$

Figure 14.2 shows the block diagram representation of the x-axis control system. Unlike the z-axis control system, the x-axis control system has only one forward loop because

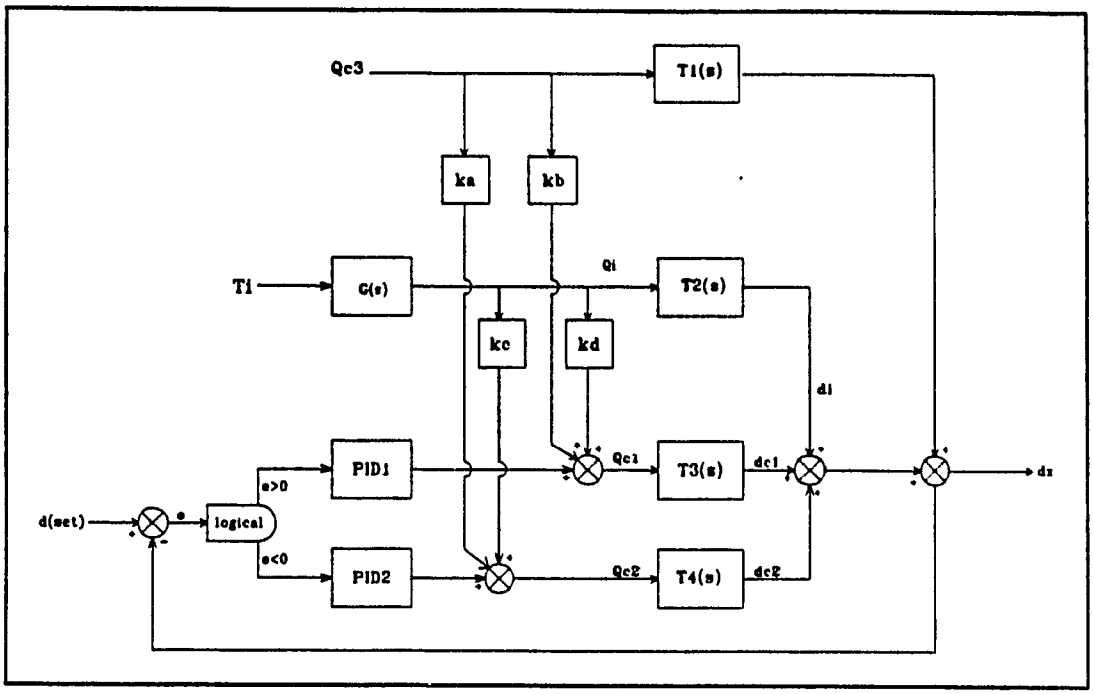

Figure 14.1: z-Axis Control System

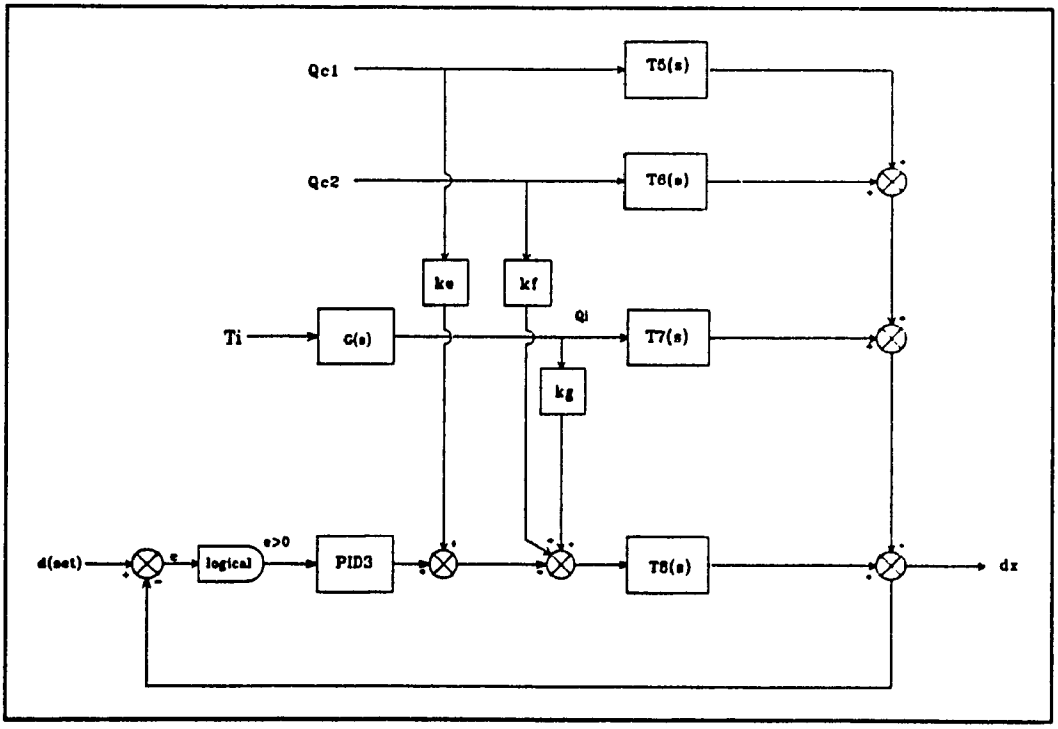

Figure 14.2: x-Axis Control System

there is only one manipulated variable Q_{C3}. Thus, the control system has no capacity to force a negative x-deflection, except by bringing Q_{C3} to zero. There are two internal disturbances to the x-control system, Q_{C1} and Q_{C2}. The external disturbance is Q_d, as with the z-control system. The control systems are linked together by the controlled heaters Q_{C1}, Q_{C2}, and Q_{C3}. Figure 11.1 shows one disturbance input Q_{C3} which originates from the x-axis control system. Similarly, the x-axis control system in figure 11.2 has the disturbance inputs Q_{C1} and Q_{C2} which are controlled by the z-axis control system. The disruption created by these disturbances is less severe than the external disturbance Q_d because the controlled heating magnitudes are known precisely from elsewhere in the control system. Q_d is potentially more disruptive because it is estimated through G(s) from external temperature measurements.

The block diagrams in figures 14.1 and 14.2 determine the deflections δ_x and δ_z by the linear addition of the stress fields due to each source acting independently. This is justified by the linearity of the governing equation, as discussed in chapter 13.2. The control system uses a PID controller with feedforward loops from the disturbance variables. There is a logical element in the z-axis controller which distinguishes between positive and negative deflection errors. A positive error activates the Q_{C1} loop because a positive Q_{C1} produces a negative deflection. Similarly, a negative deflection error activates the Q_{C2} loop because a positive Q_{C2} produces a positive deflection. The logical element in the x-axis control system only allows positive control signals to pass, while negative signals are increased to zero. The purpose of the logical branches is to prevent negative heating values in the controlled heaters.

The control systems include feedforward branches from all of the disturbance inputs. Feedforward branches significantly improve the performance of the control system because they allow the control system to anticipate deflection errors before they actually occur. It is possible to take advantage of feedforward loops in this control system because the intermediate variables are so well defined. The constant gains of the feedforward branches are chosen so that the deflections due to the control heaters exactly balances the deflection due to the disturbances in the steady state condition. Thus k_a is defined by the ratio:

$$k_a = \frac{\delta C2_{ss}}{\delta C3_{ss}} \qquad (14.2)$$

where $\delta C2x_{ss}$ is the steady-state deflection in x due to Q_{C2}, and $\delta C3x_{ss}$ is the steady-state deflection in x due to Q_{C3}. The other feedforward constants are defined in a similar way. The steady-state deflections for each variable are given by the parameter A in table 13.1.

The forward loops of the control systems contain a PID controller which either increases or decreases the controlled heating values to compensate for the deflection error. Hence, the feedforward loops estimate the required values of the controlled heat sources, and the PID controller fine tunes the response depending on the magnitude of the deflection error.

14.2 Frequency Response of the IHCP Transfer Function

The transfer function G(s) in figures 14.1 and 14.2 relates the temperature difference measured on the surface of the test structure to the heat generation of the

disturbance source Q_d. The transfer function was derived in chapter 7 and is given in the time domain by equation (7.32) and in the Laplace domain by equation (7.47). The transfer function is defined numerically in the s-domain because the integral in equation (7.47) has no closed form solution, as previously discussed. Figure 14.3 shows a graphical representation of the real and imaginary components of G(s) in the complex plane. A static analysis of the transfer function reveals that there are no real poles on the positive side of the real axis so it is inherently stable for DC inputs. The dynamic performance of the transfer function is illustrated by cutting a slice along the imaginary axis and plotting the magnitude and complex frequency of the transfer function in a Bode diagram, as shown in figure 14.4. The magnitude plot of the Bode diagram shows the amplitude gain of the transfer function as a function of the frequency of the input. The magnitude plot shows that the gain of the transfer function is constant and relatively small for low frequency changes in the input. However, at input frequencies higher than 1.59 cycles/sec (10 radians/sec), the gain increases linearly on a log scale. At an input cycling frequencies of 159 cycles/sec (1000 radians/sec) the gain of the transfer function is almost 10. This effectively establishes an upper limit on the cycling frequency of the control system, and places an upper limit on the proportional gain of the controller.

14.3 Determining the PID Constants

A PID controller generates an actuating signal that is proportional to a constant plus integral plus derivative of the displacement error. The purpose of adding the PID controller to the forward loops in figures 14.1 and 14.2 is to alter the frequency

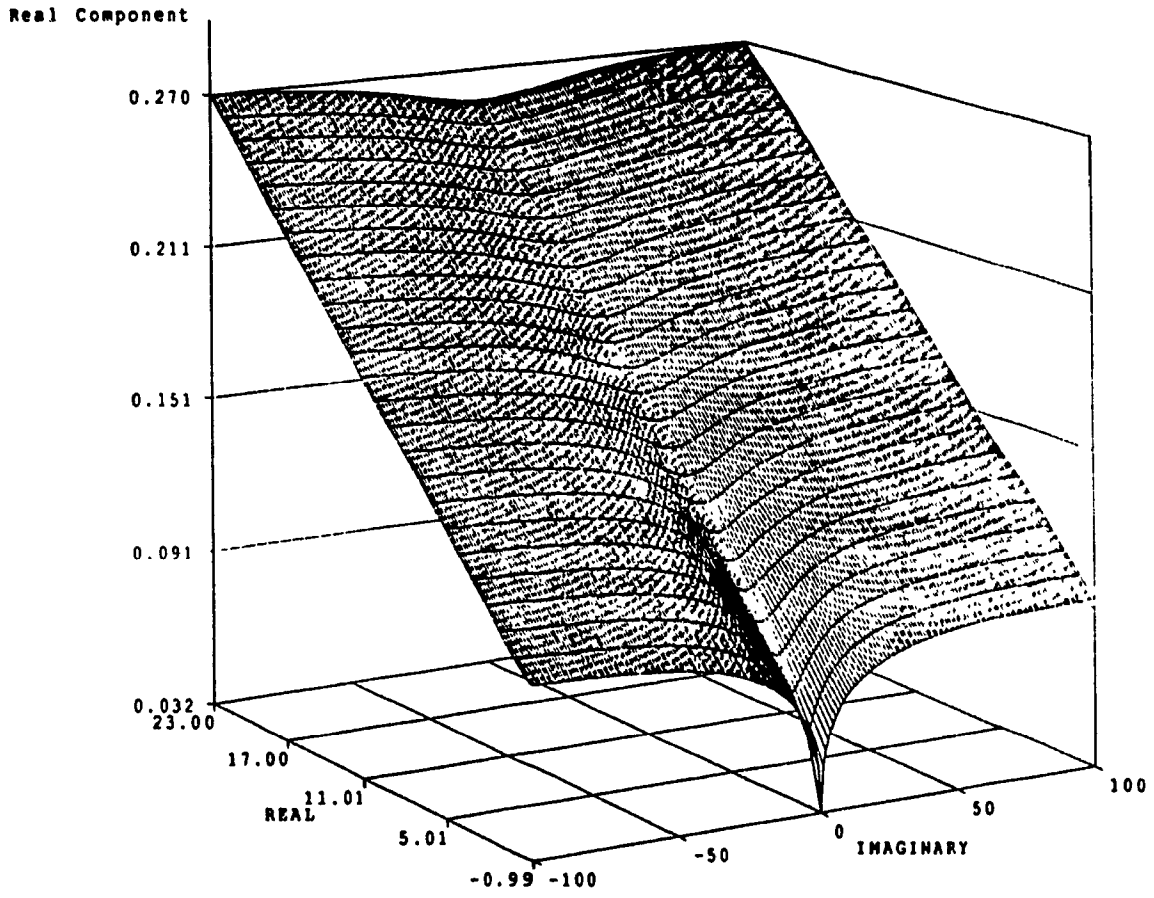

Figure: 14.3a: s-Domain Plot of Complex Function G(s) (Real Component)

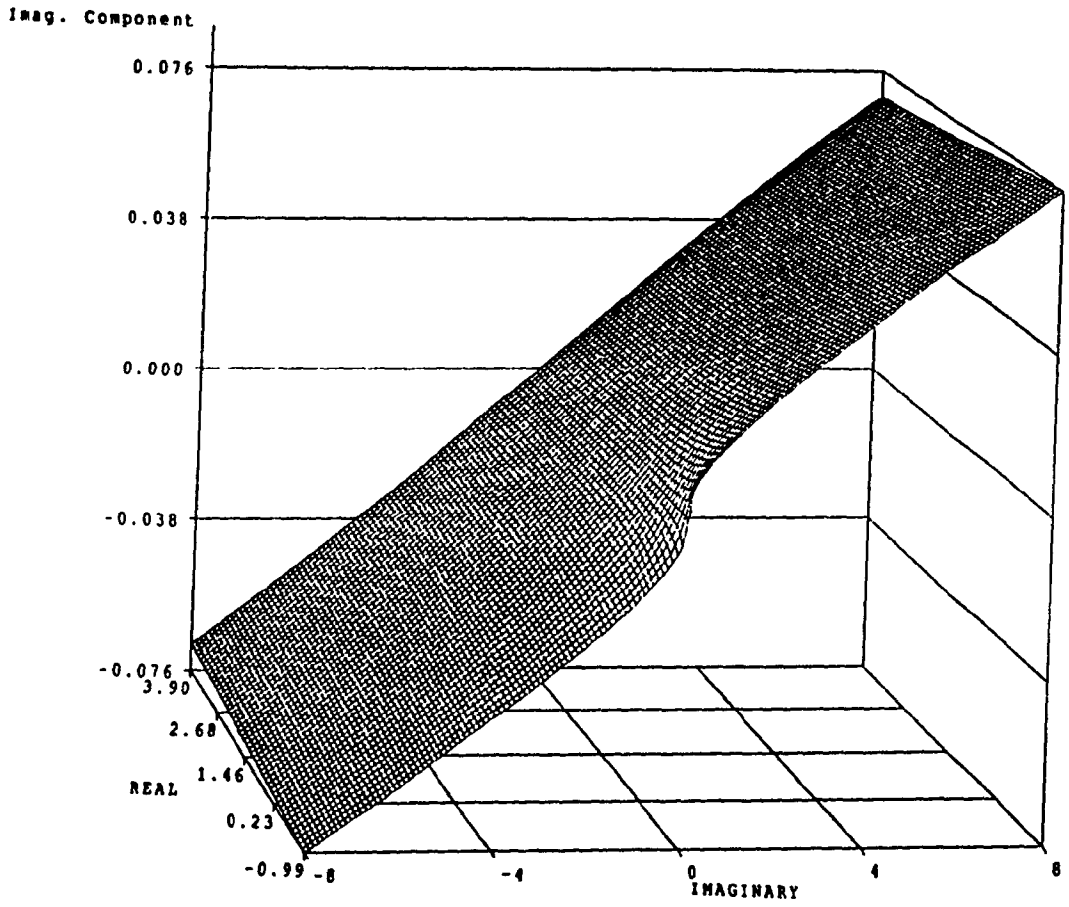

Figure 14.3b: s-Domain Plot of Complex Function G(s) (Imaginary Component)

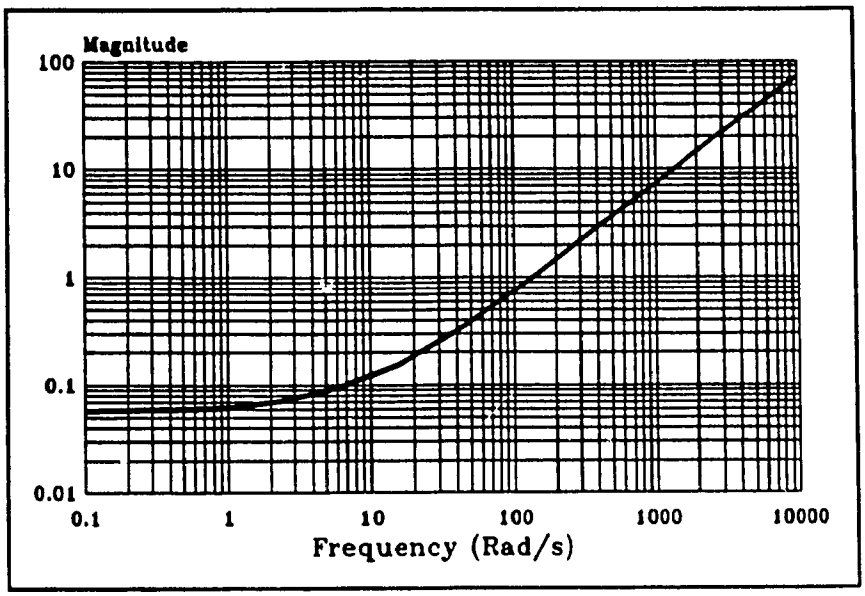

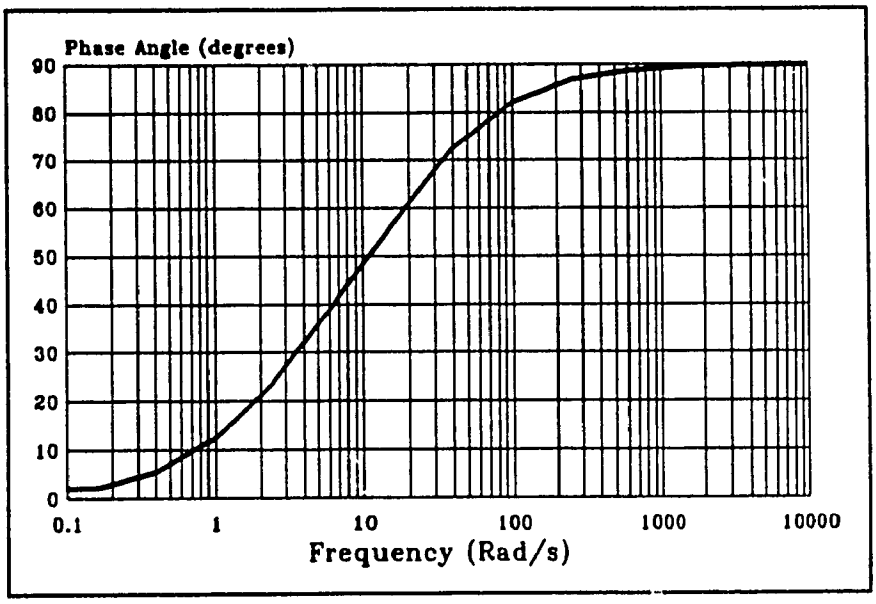

Figure: 14.4 Bode Diagram of IHCP Transfer Function G(s)

behaviour of the control systems to meet required performance specifications. The time domain representation of a PID controller is as follows:

$$P = K_c\left(e + \frac{1}{T_R}\int e\,dt + T_D\frac{de}{dt}\right) \qquad (14.3)$$

The representation of a PID controller in the s-domain is:

$$P = K_c\left(1 + \frac{1}{T_R s} + T_D s\right) \qquad (14.4)$$

The PID controller shapes the frequency response of the control system by adding poles and zeros to the appropriate locations in the complex s-plane.

Figure 14.5 shows Bode diagrams of the three forward transfer functions of the control system. The magnitude plot shows that the gains decreases linearly on a log scale as the frequency increases, indicating that the control system is inherently stable at any cycling frequency. This is not the case when the disturbance inputs are considered however, because of the behaviour of G(s) in figure 14.4. If the cycle frequency of the control system is too large then the amplitude gain of the disturbance input will produces large oscillations and instability.

There are two common methods for tuning the PID parameters, the reaction curve method and the continuous cycling method. The continuous cycling method is based on frequency response theory, whereas the reaction curve method is based on transient response theory. The continuous cycling method requires finding the *critical frequency* at which the phase angle of the response is shifted by 180 degrees with respect to the input. The forward loops of the control system approach a phase shift of 180 degrees asymptotically, as shown in figure 14.5, so the continuous cycling method is not

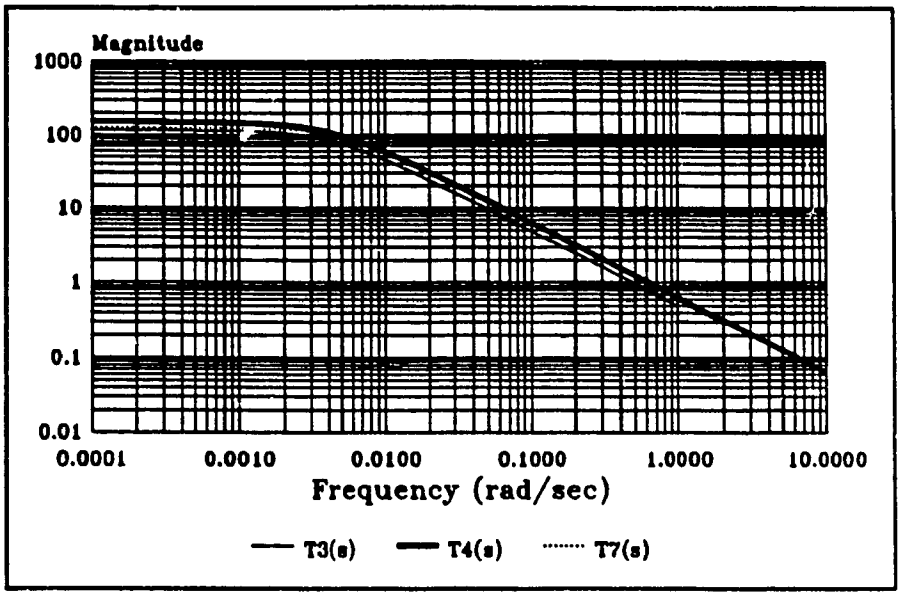

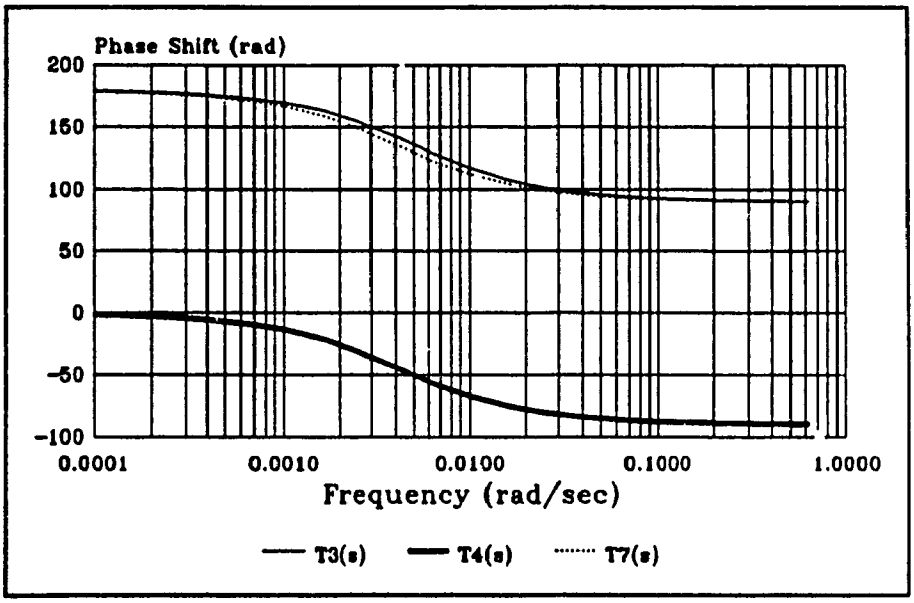

Figure 14.5: Bode Diagrams for the Forward Loop Transfer Functions

appropriate for the present problem. The reaction curve method tunes the co-efficients of the PID controller based on the transient step response of the forward loop transfer function. The suggested settings of Ziegler and Nichols are:

$$K = \frac{1.2}{SL} \qquad T_R = \frac{L}{0.5} \qquad T_D = 0.5L \tag{14.5}$$

where S is the maximum slope of the step response of the forward loop of the control system,and L is the effective delay. The maximum slope of the transfer functions T3(s), T4(s), and T7(s) are found from the step response curves given in figures 13.15 to 13.18. The figures show that the effective delay of the deflection transfer functions is zero for a continuous process. However, the controller processes the input at a finite cycling frequency, so the real effective delay of the discrete process is equal to the period of the control cycle. This is the average delay between the time that the input changes and the time that it is sensed by the control system. The period of the control cycle depends of the processing time of the numerical controller, and on the maximum allowable cycling frequency, determined from figure 14.4. A realistic period for the control cycle is one second. This includes time to evaluate G(s) by the convolution integral in equation (10.3), and time to evaluate the deflection transfer functions in figures 14.1 and 14.2 by the method that will be presented in section 14.4.

Figure 14.6 shows the step response for $T3(s)=\delta(s)/Q_{C1}(s)$, along with a line showing the maximum slope S. For this transfer function S=0.412. The effective delay L is equal to the period of the control cycle, one second in this case, as discussed above.

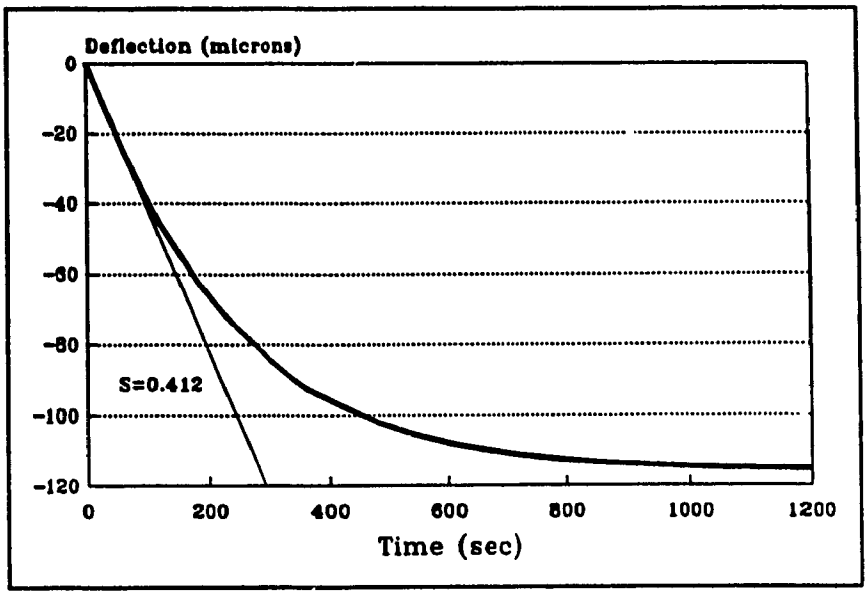

Figure 14.6: Maximum Slope of Step Response of T3(s)

Thus, the Zeigler Nicholls recommended PID constants are:

$$K = -2.91 \qquad T_R = 2.0 \qquad T_D = 0.5 \tag{14.6}$$

The PID constants for the two other forward branches are based on T4(s) and T8(s), and the constants are given as follows:

$$\begin{array}{lll} K = 2.18 & T_R = 2.0 & T_D = 0.5 \\ K = -2.20 & T_R = 2.0 & T_D = 0.5 \end{array} \tag{14.7}$$

Figure 14.7 shows the Bode diagrams of the three forward loops including the PID elements. The PID quickens the response of the control system for all input frequencies by increasing the gain of the forward transfer functions. The price, however, is that the gain increases linearly on a log scale as the frequency of the input approaches zero. This means that DC disturbances in the forward loop generate an unbounded response from

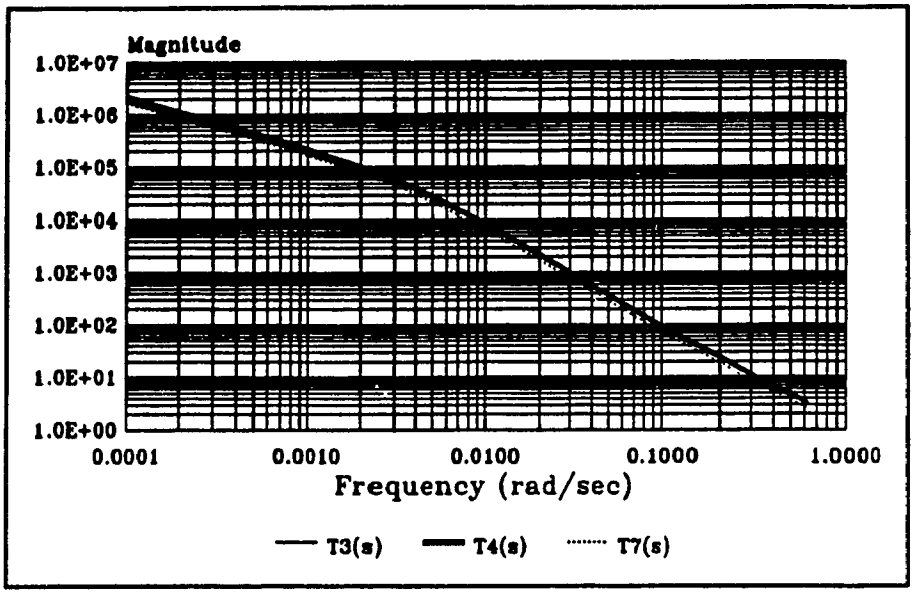

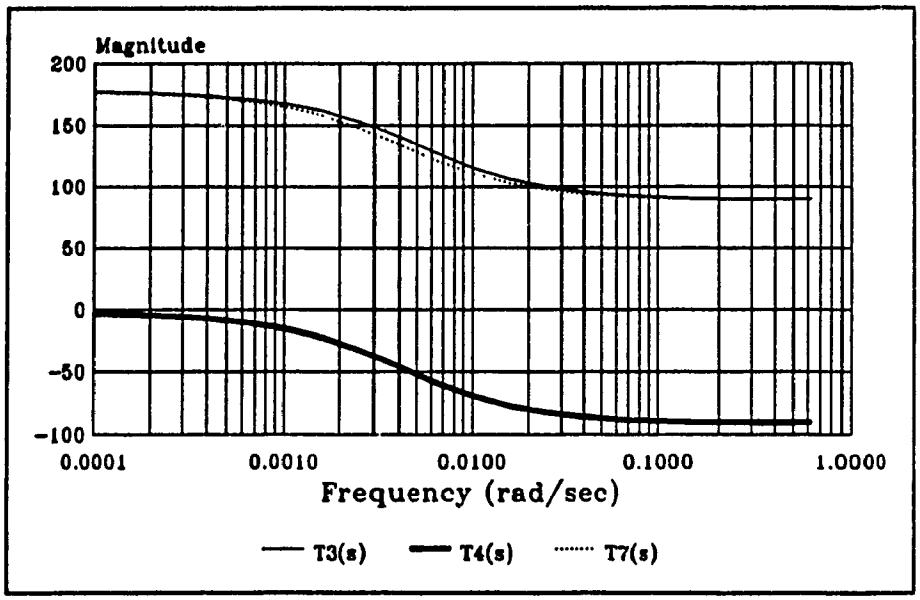

Figure 14.7: Bode Diagram of Three Forward Loops Including the PID elements

the controller. Disturbances in the forward loop includes actuation errors in the controlled heat generation.

The closed loop transfer function relating the disturbance Q_d to the z-deflection error can be derived from figure 11.1 for the positive loop including Q_{C1}. The transfer function is given by:

$$\frac{\delta_z}{Q_d} = \frac{G(s)\,(T3(s)+T2(s))}{1+T3(s)\,P(s)}$$

where P(s) in the Laplace transform of the PID element. The Bode diagram of equation (14.8) is plotted in figure 17.7a. The ideal system gain for a disturbance input is zero. The gain does decrease linearly toward zero as the frequency approaches zero, but it increases linearly as the frequency of the input increases. This is the opposite situation to the forward transfer function which decreases toward zero as the frequency increases, and increases linearly as the frequency approaches zero. Therefore, there is a band of stable cycling frequencies for the controller which is bounded by instability on either side. The stable band corresponds roughly to the flat plateau in figure 14.7b.

14.4 Implementing the Control System

Each cycle of the control system in figures 14.1 and 14.2 requires the evaluation of eight deflection transfer functions in the form of equation (7.49), one convolution integral in the form of (10.3), and three PID blocks. The PID blocks are an assembly of three processes: multiplication, differentiation, and integration. The numerical differentiation process requires that at least one previous value of the deflection error be

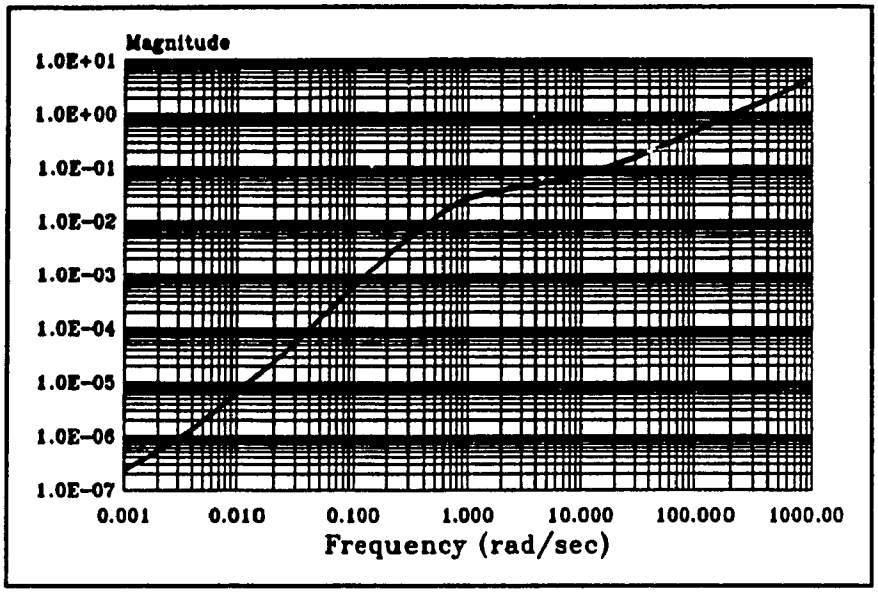

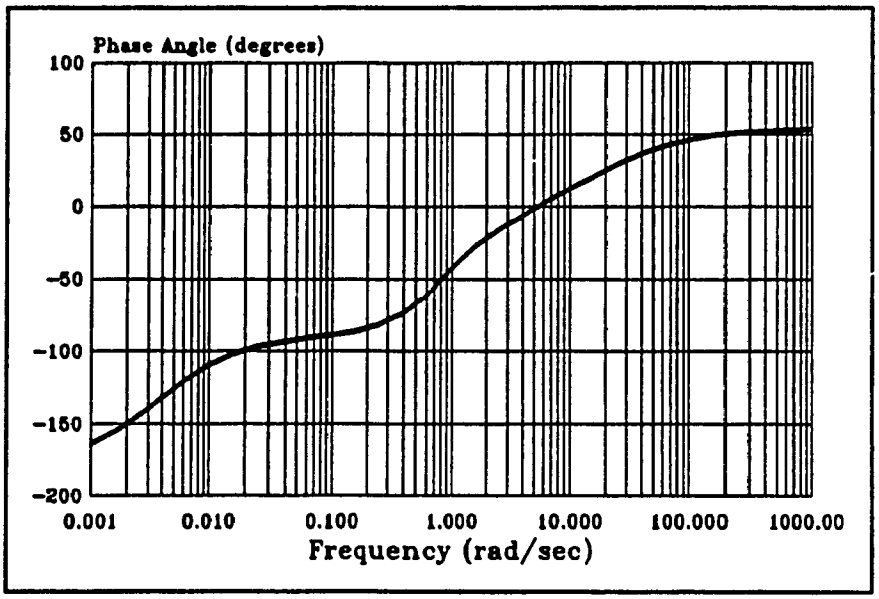

Figure 14.7a: Bode Diagram of Disturbance Forward Loop

stored by the PC controller. The integration process requires storage of the cumulative integration of the deflection error. The convolution integral relating the measured temperature difference to the disturbance heat generation in evaluated by Simpson's rule, as discussed in chapter 9.

The deflection transfer functions are given in equation (7.49) in the form of a Laplacian expression, but in order to evaluate them in real time a numerical solution algorithm is required. The convolution integral method developed in chapter 9 could be extended to the deflection transfer functions also, but since the transfer functions are available in a well defined analytical form it is easier to reformulate the problem in the time domain. Equation (7.49) is in a form of one linear polynomial is s divided by another linear polynomial in s. Thus, it can be converted to a linear differential equation and solved by ordinary numerical methods. By cross-multiplication, Equation (7.49) takes the form:

$$(Aa+B)\,sQ(s) + Aa^2Q(s) = s^2\delta(s) + 2as\delta(s) + a^2\delta(s)$$

Then the governing differential equation is given by:

$$(Aa+B)\,\dot{Q} + Aa^2Q = \ddot{\delta} + 2a\dot{\delta} + a^2\delta \qquad (14.10)$$

Equation (14.10) is solved numerically by the Runge-Kutta method on-line for the numerical values of the input.

The control system in figures 14.1 and 14.2 is formulated as a Fortran program called Control.For with one external input T_d and three outputs Q_{C1}, Q_{C2}, and Q_{C3}. These variables correspond to the temperature difference and artificial sources of the finite-

element test model in figure 13.2.

14.5 Testing the Control System

14.5.1 Introduction

The effectiveness of the thermal deflection control system is investigated by applying simulated disturbance inputs to the finite-element test model. The deflection response of the test structure is determined with control and without control, and the performance of the control system is evaluated by comparing the results. For each simulated thermal disturbance, the input temperature difference profile T_d is determined by the finite-element thermal algorithm, and then the program Control.For is used to determine the appropriate magnitudes of Q_{C1}, Q_{C2}, and Q_{C3} to minimize the deflection error. The initial tests are done with errorless temperature data and precise regulation of the controlled heating magnitudes. The consequence of errors in the measurement and data acquisition system, and in the regulation of the controlled heaters are investigated in subsequent tests.

14.5.2 Triangular Test Disturbance

Figure 14.8 shows the thermal deflection error of the test structure without control for the triangular disturbance shown in the figure. The duration of the disturbance is 1200 seconds or 20 minutes, and the amplitude is 2 dimensionless units. The maximum deflection error approaches 60 microns in the z-direction and exceeds 10 microns in the x-direction. If left uncontrolled, this deflection represents a serious accuracy problem

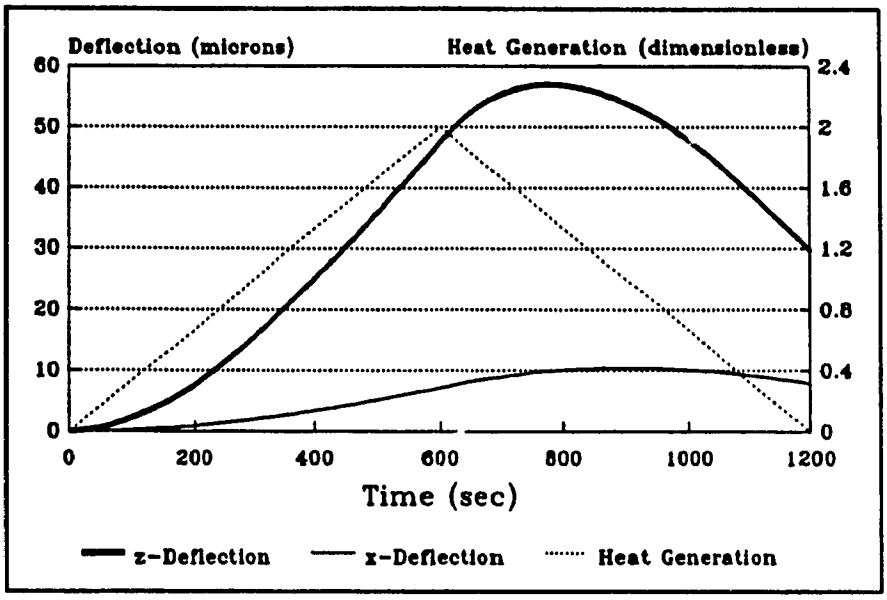

Figure 14.8: Thermal Deflection Error without Control Heating with Exact Data

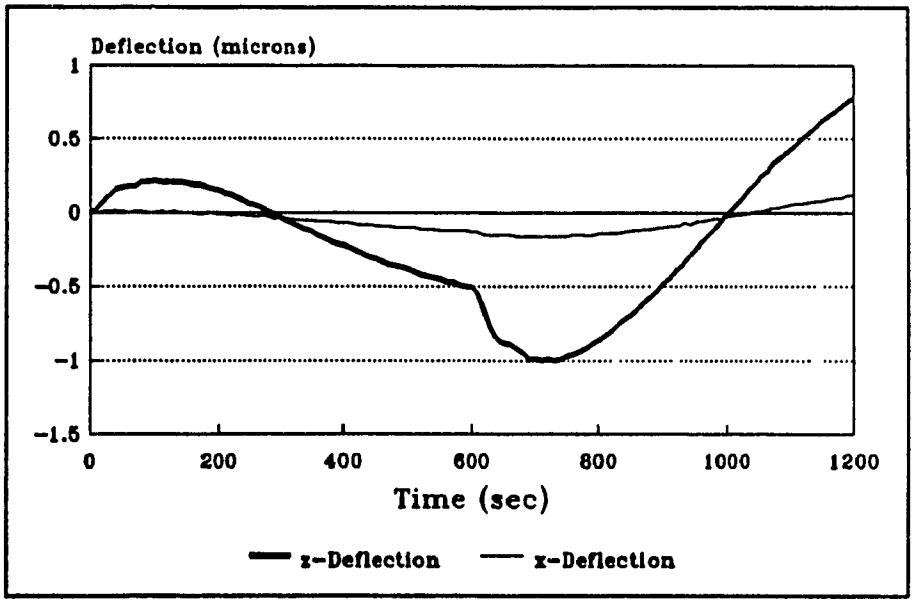

Figure 14.9: Thermal Deflection Error with Control Heating with Errorless Data

when precision tolerencing is required.

Figure 14.9 shows the net thermal deflection error of the test structure for the same input, but with the deflection control system active. The maximum deflection error is reduced to less than one micron in both the x and z directions by the control system. The maximum deflection error now occurs following an abrupt change in the input, rather than at the maximum value of the disturbance generation, as was the case with the uncontrolled deflection error. Figure 14.10 shows how the three controlled heaters responded to the triangular disturbance input. The heating magnitudes of Q_{C1} and $_{C3}$ rise and fall gradually, following the shape of the triangular disturbance, but the positive deflection z-control heater Q_{C2} never becomes active at all. Q_{C2} introduces a deflection along the positive z-axis, so it is only needed when there is a negative z-deflection error, which arises when Q_{C1} overshoots the zero deflection point or when there is an abrupt

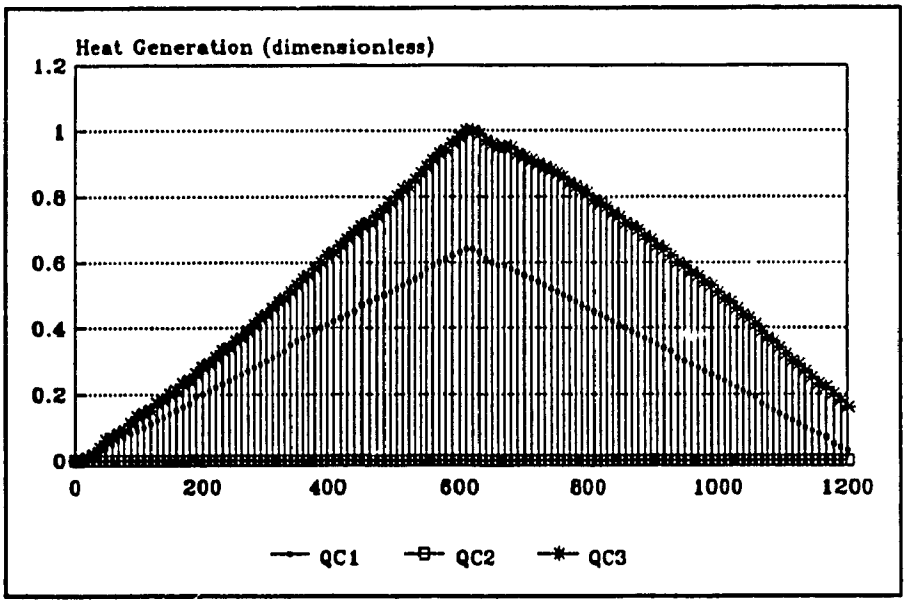

Figure 14.10: Heat Generation of Control Heaters for Ramp Input with Errorless Data

decrease in the disturbance generation.

Figures 14.8 and 14.9 show that the control system is highly stable and accurate when there are no errors in the measurement and actuation processes. The triangular disturbance input is not a difficult test however, because there are no abrupt changes in the magnitude of the disturbance and the period is somewhat large, giving the control system a lot of time to anticipate the changes. A more demanding test occurs when the disturbance changes abruptly and frequently, and the magnitude of the disturbance is large.

14.5.3 Three-Step Test Disturbance

Figure 14.11 shows another disturbance input consisting of three step changes in the disturbance heat generation from zero to two, from two to four, and then from four

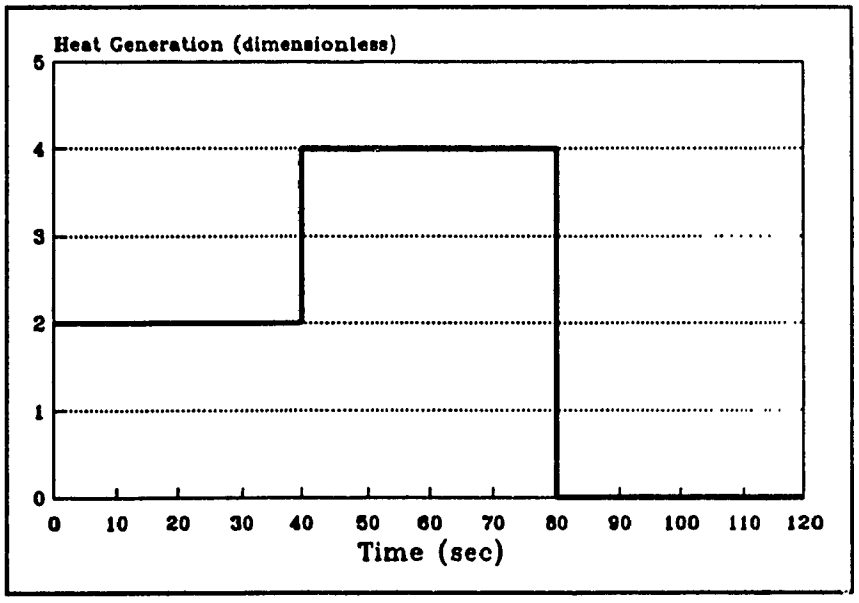

Figure 14.11: Three Step Heat Generation of Disturbance Input

to two dimensionless units. The time period between changes is 40 seconds and the total period of the input is 120 seconds. This disturbance will be used as the standard test input for the control system because it represents the most difficult test case that would be experienced by a machine tool in practice. Figure 14.12 shows how the convolution transfer function G(s) estimates the heat generation of the disturbance for the three step input. At the points of the discontinuity, there is a lag of approximately three seconds before the transfer function responds, and then there is an overshoot of the correct value. Figure 14.13 shows the deflection error of the test structure for the three step disturbance without control. The maximum deflection error is over 30 microns in z and less than 5 microns in x. The deflection increases almost linearly between step changes because the period of the input is short and the deflection response is still in its initial linear mode.

Figure 14.14 shows the deflection error of the structure with the control system

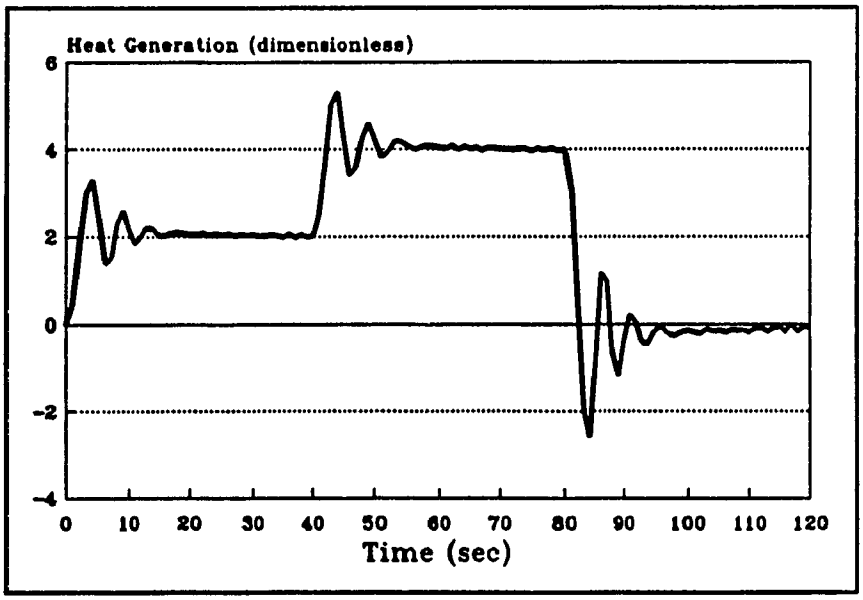

Figure 14.12: Estimate of Three Step Input by Convolution Integral Transfer Function with Errorless Data

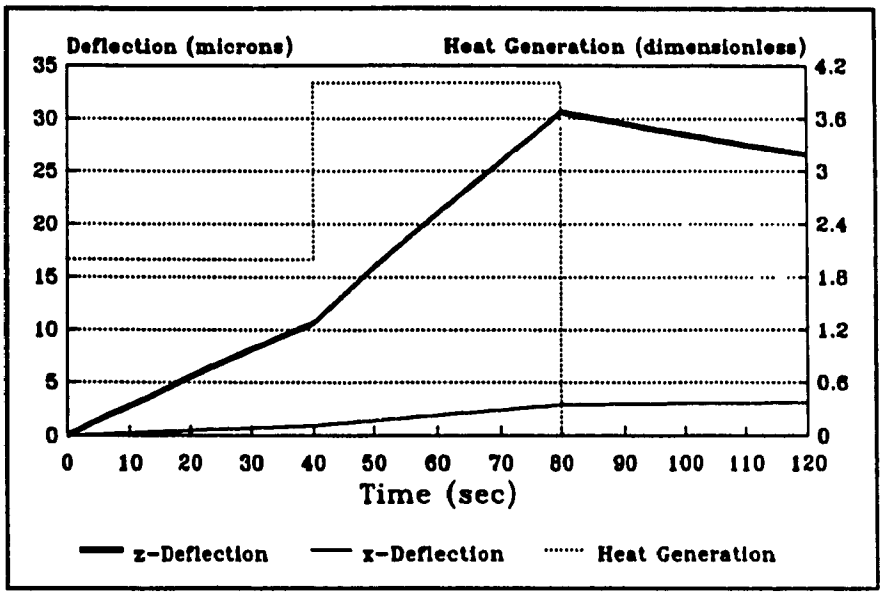

Figure 14.13: Thermal Deflection Error for Three Step Input without Control with Exact Data

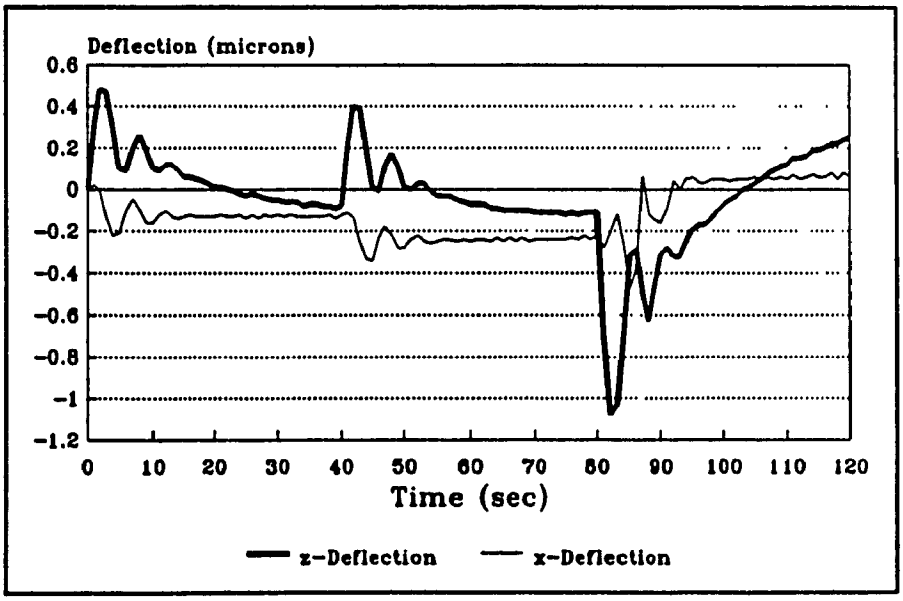

Figure 14.14: Thermal Deflection Error for Three Step Disturbance with Control with Errorless Data

active. The deflection error is significantly reduced, having a maximum amplitude of just over one micron following the step change in the disturbance heat generation from four to zero dimensionless units. Figure 14.15 shows the heat generation of the controlled sources for the three step input. In this case there is much more oscillation of the controlled heat sources than for the triangular test input, but the oscillations are not so large as to initiate instability. This example illustrates the predominance of the IHCP transfer function G(s) in controlling the performance and stability of the control system.

From the test results so far, it has been proven that the control system is highly effective at eliminating thermal deflection errors, even in the most extreme load cases. However, the tests have excluded measurement and actuation errors that would be present in a real machine tool control system. These errors shall now be simulated, and their influence on the performance of the control system will be evaluated.

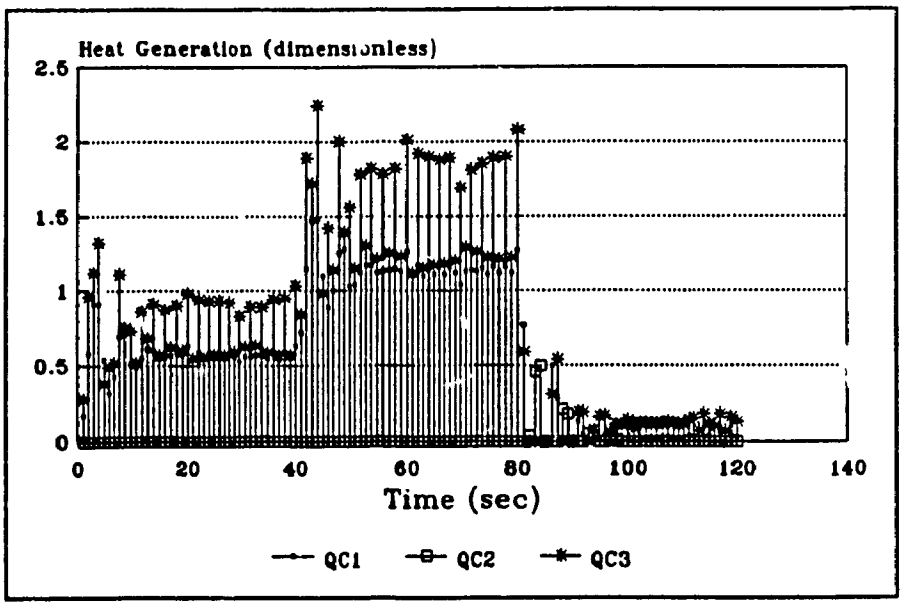

Figure 14.15: Heat Generation of Control Heaters for Three Step Disturbance with Errorless Data

14.5.4 Three-Step Disturbance with Temperature Measurement Error

Figure 14.16 shows how the IHCP transfer function H(s) inverts the three step disturbance input when simulated errors representing 5% of the measured temperature difference are included in the input. The simulated error oscillates between positive and negative with each control cycle, similar to the simulated errors that were used to test the IHCP methods in chapter 12. The simulated errors produce oscillations in the estimated disturbance, and increase the oscillations that already existed at the transition points. The oscillations demonstrate why there is a lower limit on the cycle period of the controller. Figure 14.7b shows that such oscillations would produce instability if the frequency were above 1.59 oscillations per second. Since it is unlikely that the actual error of a thermocouple would oscillate between full scale positive and negative with each reading, the simulated error represents a worst case situation for a thermocouple

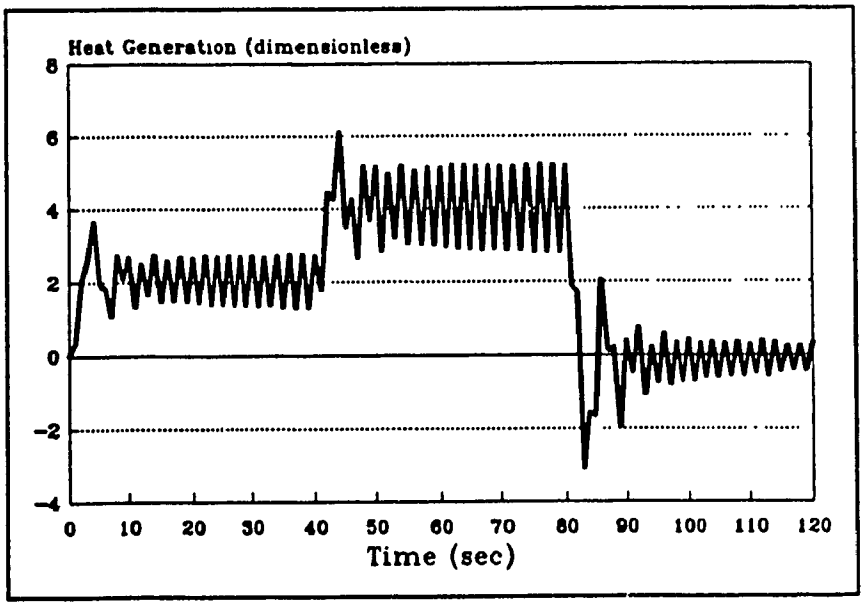

Figure 14.16: Estimate of Three Step Disturbance by Convolution Integral Transfer Function with 2% Measurement Error

with a 5% accuracy.

Figure 14.17 shows the deflection error of the test structure for the three step input with 5% measurement error, and figure 14.18 shows the corresponding magnitudes of the heat generation of the controlled sources. The oscillations of the input are not amplified by the forward transfer function, as expected from figure 14.7. Although the deflection error is more oscillatory, the maximum amplitude has not increased very much, remaining within 1.5 microns. The conclusion from figures 14.17 and 14.18 is that oscillating temperature measurement errors do not significantly reduce the accuracy of the control system, in this case from 1 micron to 1.5 microns. The figures also show that oscillating errors require a greater utilization of positive z-deflection from Q_{c3} during the cooling off phase. Positive z-deflection was hardly needed for errorless data, but is becomes more essential when only imperfect data is available. Since thermocouples with better than 5% accuracy are readily available, there is no need to consider the effect of larger errors.

14.5.5 Three-Step Disturbance with Temperature Measurement Error and Power Actuation Error

Another potential source of error in an actual control system is the uncertainty in the power generation of the controlled sources. That uncertainty arises from the dynamics of the resistance elements themselves, and from inaccuracies in the signal amplification and actuation mechanisms. The effect of errors in the power actuation mechanism shall be investigated by applying a simulated error into the heat generation of the controlled sources. One way to do this is to apply an oscillating error into the controlled heat

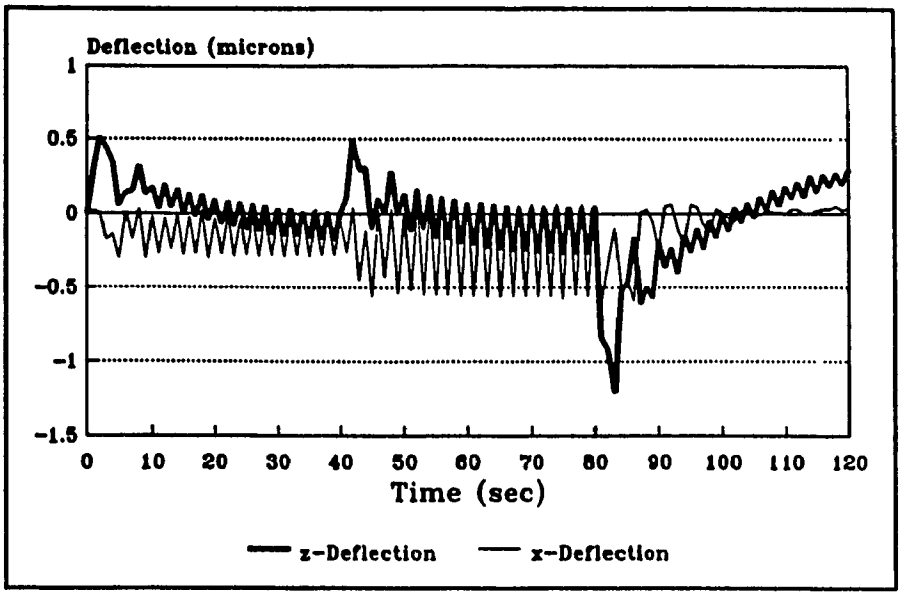

Figure 14.17: Thermal Deflection Error for Three Step Input with Control with 5% Measurement Error

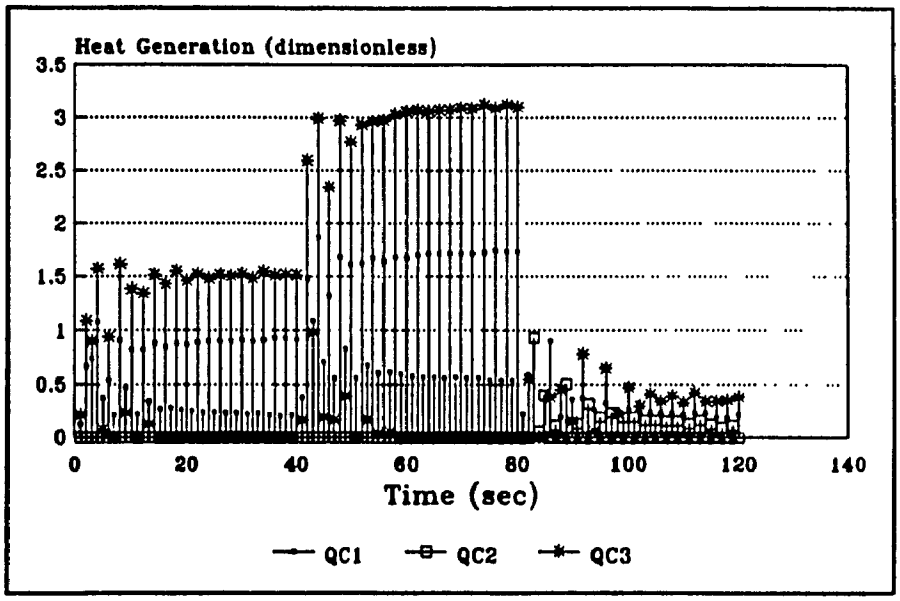

Figure 14.18: Heat Generation of Controlled Sources for Three Step Input With 5% Measurement Error

magnitudes, similar to the temperature measurement error. This tends to underestimate the problem because the forward gains of the control system are relatively small for high frequency inputs, as shown in figure 14.7. Furthermore, errors in the power actuation mechanism tend to be low frequency in practice. It is unlikely for the generation of a source to change abruptly by itself unless there is a physical defect in the equipment. The power actuation error is simulated for the purpose of illustration by adding a factor of 5% to the intended controlled heat magnitudes, with the sign of the error oscillating between positive and negative every 10 seconds. Thus, for the first 10 seconds the magnitudes of Q_{C1}, Q_{C2}, and Q_{C3} are increased by 5% above their intended values, and for the second 10 seconds they are reduced by 5% from their intended values. The deflection error is shown in figure 14.19 for the same three-step input with 5% temperature measurement error, and 5% power actuation error with an oscillation period of 20 seconds. The generation of the controlled sources for this test case is shown in figure 14.20. Figure 14.20 shows a slight deterioration in the x-deflection error, but a negligible change in the z-deflection error. The frequency of the error is still too high to be amplified by the control system.

Figure 14.21 shows the deflection error of the test structure for the three-step disturbance with a 5% temperature measurement error, and a constant positive 5% power actuation error. The power actuation error does not change sign, so its frequency is zero. The maximum x-deflection error has now increased considerably to just under 2.5 microns, exceeding the z-deflection error which has remained relatively constant. Nevertheless, the deflection error is considerably reduced compared to the uncontrolled

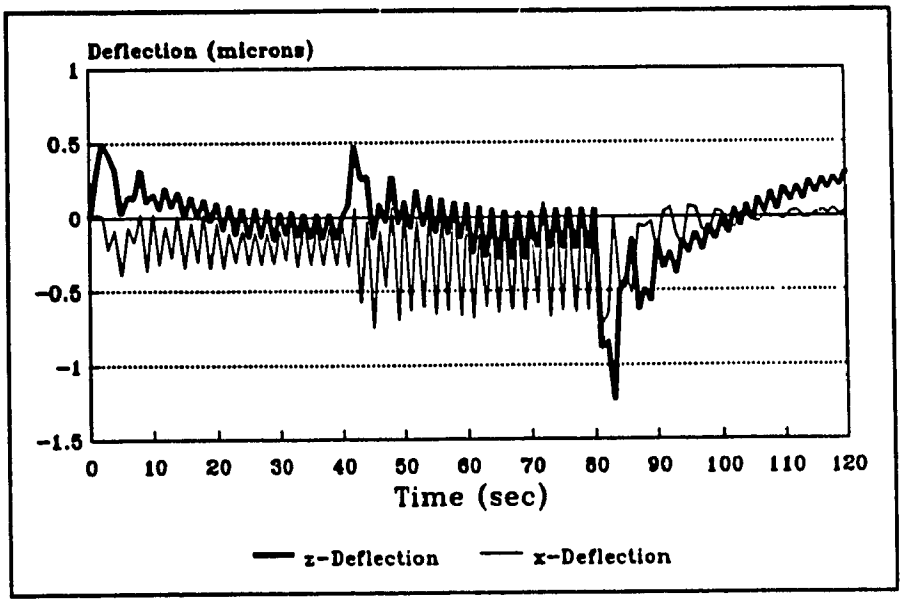

Figure 14.19: Thermal Deflection Error for Three Step Input with 5% Temperature Measurement Error and 5% Heat Generation Error with period of 20 seconds

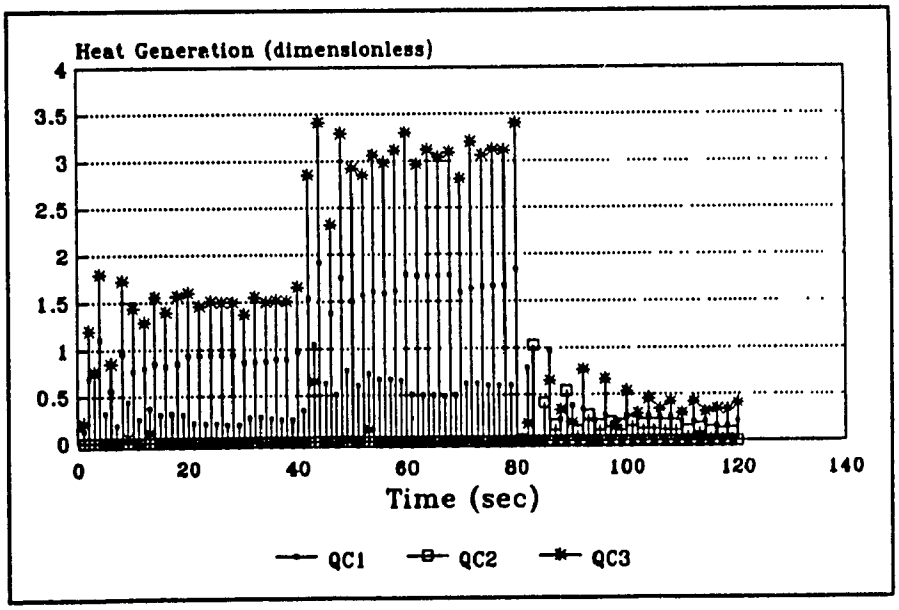

Figure 14.20: Heat Generation of Controlled Sources for Three Step Disturbance with 5% Temperature Measurement Error and 5% Heat Generation Error with Period of 20 seconds

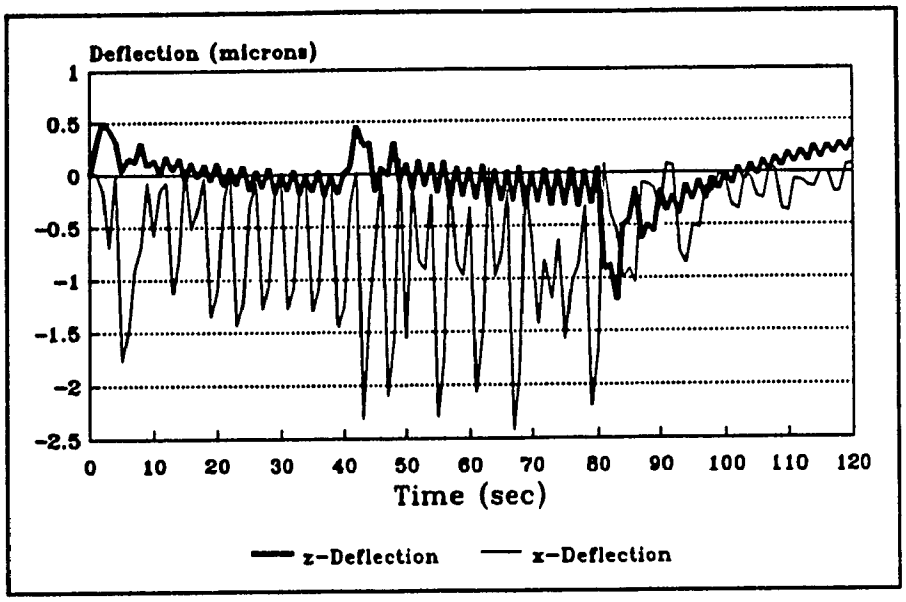

Figure 14.21: Thermal Deflection Error for Three Step Disturbance with 5% Temperature Measurement Error and 5% Constant Source Generation Error

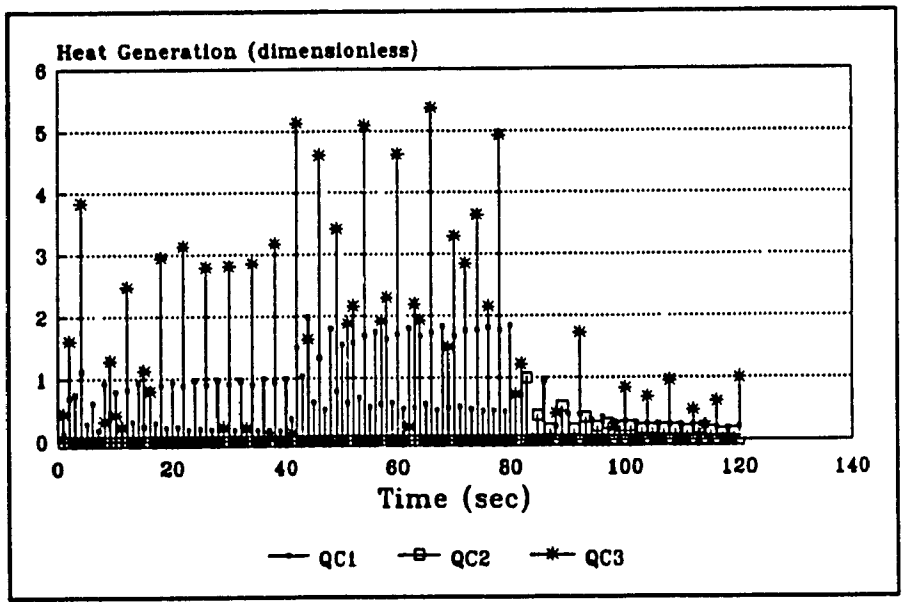

Figure 14.22: Heat Generation of Controlled Sources for Three Step Input with 5% Temperature Measurement Error and 5% Constant Source Generation Error

deflection for the same input in figure 14.13. Furthermore, figure 14.21 represents the worst possible case for both the temperature measurement error and the power actuation error. Since the frequency of the power actuation error is zero, the forward gain of the control system on the error is maximum, as shown in figure 10.5. Also, since the frequency of the temperature measurement error is equal to the cycle frequency of the control system, its gain is maximum, as shown in figure 10.4. Also, an accuracy of 5% for the temperature measurement error and 5% for the power actuation error are conservative values which would not be so severe in practice. An accuracy greater than 5% of the maximum temperature rise (10 degrees C) can be obtained by calibration, or by using thermistors. This control system could reasonably be expected to reduce the thermal deflection error to less than 2 microns for a structure similar to the test model if the data acquisition and power actuation mechanisms are calibrated correctly.

CHAPTER 15: CONCLUSIONS AND RECOMMENDATIONS FOR FUTURE WORK

15.1 Conclusions

The trend in recent years has been to devote less time to modelling for control system design because of the availability of statistical matching software, such as expert systems, and because of the ever increasing complexity of the control problems. The control systems that do not use statistical matching usually use process models that are only partially reliable, and use adaptive control to compensate for the weakness of the models. The goal of this thesis was to develop the closest possible analytical simulations of the physical processes, so that no statistical matching and no external calibration of the models by adaptive control is required. This goal was achieved by the development of the "generalized analytical solution method", and the derivation of analytical solutions for modelling the temperature and thermal deformation fields in a machine tool structure. The analytical temperature and thermal deformation solutions for an infinite plate in convection were derived for that purpose.

The Laplace transformation was used to derive transfer functions for each of the process models. These Laplace transfer functions were used in two ways: 1) to obtain a solution for the process to an arbitrary input, and 2) to allow the control system to be designed and analyzed in the s-domain. The Laplace method is an underdeveloped technique for numerical problems because of the obstacles that were encountered in chapters 9 and 10, including: 1) the transformation requires knowledge of the entire time domain, 2) the transformation requires s to be treated as a complex variable, 3) the

inverse transformation is difficult to evaluate numerically and the procedure fails when singularity functions are present. Very little work has been done in this area, besides a few software applications of the Crump method [ref] for inverse transforming analytical s-domain functions. In order to overcome these problems, a new method of accelerating the Crump inverse transformation by two orders of magnitude was developed. The accelerating algorithm makes the Crump solution more reliable because it filters out singularity functions which would otherwise cause complete divergence of the algorithm. An alternative to the Crump method based on Gaussian quadrature instead of the trapezoidal rule was also developed. The new method is slower than the Crump method, but it is more accurate when greater precision is required, and it can also be accelerated by the accelerating algorithm.

The power of using the numerical Laplace transformation to solve control problems was demonstrated in this thesis, especially for solving the inverse heat conduction problem (IHCP). Transforming the IHCP to the s-domain makes it possible to obtain an explicit solution, eliminating the need for an iterative solution and eliminating the problems of existence and stability that were of such great concern to the researchers in the literature review. Furthermore, s-domain plots and Bode diagrams of the transfer functions are available to show the static and dynamic characteristics of the process models, allowing for better design and understanding of the control system. The general numerical version of the Laplace transformation that was developed in this thesis allows the basic methods of s-domain modelling and control to be extended to complex real problems, just as the numerical finite-difference and finite-element methods allowed

the Navier Stokes equation, the dynamic equation, and the heat conduction equation to be extended to complex geometrical problems.

Two versions of the numerical Laplace transformation method were developed in this thesis. The convolution integral method uses the generalized analytical process models to derive a time domain transfer function in the form of a convolution integral. The method is extremely fast, and it effectively deals with the problem of instability by defining a stable analytical form for the step solution. The second method is called the Laplace transfer function Method, which uses direct numerical methods on-line to transform the measured input to the s-domain, solve the problem, and then transform the solution back the time domain. This method does not require an analytical solution, only a numerically defined step solution to the direct problem, which could be measured experimentally. The method is completely general, requiring only a step solution to fully define any linear system. Furthermore, the chirality of the solution in the s-domain makes it possible to solve the corresponding IHCP by algebraically inverting the transfer function.

The performance of the mathematical models and the Laplace transformation solution method were tested by designing a control system to control the thermal deflection for a finite-element test model. In order to make the method applicable to manual and semi-automated machine tools as well as NC machines, the compensation was effected through artificial electric heaters on the surface of the test structure. The control system was found to reduce the deflection error from the order of 150-200 microns, to below 2.5 microns for the worst case combination of temperature

measurement errors and power actuation errors. The control system is somewhat more sensitive to errors in power actuation than in temperature measurement at the operating cycling rate of the control system. Power actuation errors are also easier to eliminate by proper selection of power generating equipment. The method of controlling thermal deflection that was developed in this thesis effectively eliminates structural thermal deflection error for the tolerance requirements of most machining processes. Even greater accuracy could be obtained for specialty operations by increasing the cycling time of the control system on a faster computer, and increasing the complexity of the feedforward branches of the control system. For such an operation, the accuracy of the temperature measurements could be improved by using calibrated thermistors with an accuracy of 0.05°C.

15.2 Recommendations for Future Work

The next step in the development of the method is to get experimental verification from a single-component test model. The method should first be tested on a simplified, single-component structure, similar in form to the finite-element test structure that was tested in this thesis. The next step after that is to extend the method to a actual multi-component machine tool structure. A single-component model should be tested first so as to isolate the effect of the non-linear joint interactions in a real machine tool structure [1]. Non-linear effects are partially compensated by the generalized analytical method, but if the non-linearity is too severe in practice, then some form of adaptive control will be necessary to calibrate the process models.

Many of the procedures that have been developed in this thesis could be extended to encompass the thermal deflection of the whole machine tool structure-cutting tool-workpiece system. The generalized analytical model of a cutting tool would be based on the solution for a basic shape model such as a hollow cylinder, a solid block, or a combination of both, depending on which parts of the tool post assembly contribute to the thermal deflection of the cutting edge. The cutting tool deformation is a non-linear problem, so the Laplace solution method would not be effective without adaptive control.

It would be interesting to study the feasibility of using heat sinks as well as heat sources to increase the flexibility of the control system to compensate for bending as well as linear deflection. Heat sinks could be provided by miniature heat pipes or thermo-electric cooling units, as discussed in the literature review. Mechanical actuators such as piezoelectric transducers could also be incorporated into such a multi-mode control system.

A thermal deflection compensation system based on heating and cooling elements is versatile because it can be used to retrofit any existing machine tool. It would be useful to study the feasibility of adapting the method with an intelligent controller, so that the control system can be installed and calibrated on a machine tool with the minimum user interaction.

REFERENCES

1. Attia, H., "Thermal Deformation of Machine Tools and its Effect on Machining Accuracy", Lecture Notes, Mechanical Engineering Department, Concordia University.

2. Moriwaki, T., Horiuchi, A., and Okuda, K., "Effect of Cutting Heat on Machining Accuracy in Ultra Precision Diamond Turning", Annals of the CIRP Vol 39, Jan 1990.

3. Spur, G., and Fischer, H., "Thermal Behaviour of Machine Tools", Proc. of 10th Int. MTDR Conf., pp.147-152, MacMillan Press, 1969.

4. Lowen, E., "Air Shower Thermal Stability", proc. SME Prec. Machining Workshop, Williamsburg, Va., (1978).

5. Hemingray, C.P., "Some Aspects of the Accuracy Evaluation of Machine Tools", Proc. 14th Int. MTDR Conference, MacMillan Press, 1973, pp.281-284.

6. Bryan, J., "International Status of Thermal Error Research (1990)", Annals of the CIRP vol. 39 Feb 1990.

7. Mottu, A., Guidages et paliers de machinesoutils. Industrielle Org. 29 (1960).

8. Mc Clure, E.R. and Thal-Larsen, H., "Thermal Effects in Precision Machining". ASME, 70-WA/Prod - 25, 1970.

9. Spur, G., Konstruktive Gestaltung und Automatisierung der Werkzeugmaschine", Industrie - Anzeiger, 90 Jg, Nr. 67 v.20, 1968.

10. Okushima, K., Kakino, Y., Kondo, K., and Kikuchi, T., "An Optimum Design of Machine Tools for Thermal Deformations". Bull. Japan Soc. of Prec. Engg., Vol. 7, No. 2, 1973.

11. Bryan, J.B. and Mc Clure, E.R., "Thermal Stability-Key to NC Accuracy". Proc. 7th Annual Meeting, Numerical Control Society, pp.119-126.

12. Spur, G., Hoffman, E., Paluncic, Z., Benzinger, and K., Nymoen., H., "Thermal Behaviour Optimization of Machine Tools", Annals of the CIRP, 37 (1988) 1, pp.401-405.

13. Yoshida, Y., and Honda, F., "Thermal Deformation of a Vertical Milling Machine, Part II", Proc. 8th Int. MTDR Conference, MacMillan Press, 1967, pp.83-96.

14. Trapet, E., and Walede, F., "Co ordinate Measuring Machines in the Production Line: Influence of Temperature and Measuring Uncertainties", IV Congress Intl. Metrologia Industrial, Zaragosa, Nov 1989.

15. Bryan, J., Donaldson, R., McLure, E., and Clouser, R., "A Practical Solution to the Thermal Stability Problem in Machine Tools", S.M.E. MR72-138 UCRL 73577 (1972).

16. Donaldson, R., and Patterson, S., "Design and Construction of a Large Vertical Axis Diamond Turning Machine", SPIE 27th ann. Tech. Symp. (1983).

17. Jedrzejewski, J., "kompensation Thermischer Verlagerungen einer Drehmaschinen", Werkstatt und Betrieb, Vol. 118, No.2: 85-87.

18. Tonshoff, H.K., and Wulfsburg, J.P., "Developments in Diagnosis of Thermally Induced Displacements in Machine Tools", Symposium on Grinding Fundamentals and Applications, edited by S. Malkin and J.A. Kovach, ASME Winter Annual Meeting, San Francisco, Calif., Dec., 1989, pp.281-295.

19. Balsamo, A., Marques, D., and Satori, S., "A Method for Thermal Deformation Corrections of CMM's, CIRP Annals (1990).

20. Chiappulini, L., Gianotti, L., and Galbersanini, A., "On-Line Correction Via Software of Thermal Errors in Numerically Controlled Machine Tools", Paper Presented at the Scientific Technical Committee "M", on August 22, 1991, 41st CIRP General Assembly - Stanford, California, USA.

21. Jedrzejewski, J. and Modrzycki, W., "Determination of Conditions for Compensating Thermal Displacements of Drilling Machine Spindle", Reports Techn. University of Wroclaw, I24/34, 1987.

22. Ichimiya, R., Yokoyama, K., and Watanabe, Y., "Experimental Study on Thermal Deformation of Machine Tool", Research Report No. 25, Faculty of Engineering, Niigata University, 1976.

23. Sata, T., Takeuchi, Y., Sato, N., and Okubo, N., "Analysis of Thermal Deformation of Machine Tool Structure and its Application". Proc. 14th Int. MTDR Conference, MacMillan Press, 1973, pp.275-280.

24. Moriwaki, T., "Thermal Deformation and its On-Line Compensation of Hydrostatically Supported Spindle", Annals of the CIRP Vol 37 Jan 1988.

25. Jedrzejewski, J., Kwasny, W., and Strauchold, S., "Numerical Modelling of the Thermal Behaviour of Spindle Bearing Assemblies for Precision Machine tools", Proceedings of CIRP

Conference on PE and MS, Sept., 1991, pp. 525-536.

26. Weck, M. and Zangs, L., "Computing Thermal Behaviour of Machine Tools Using the Finite-Element Method - Possibilities and Limitations". Proc. 16th MTDR Conference, MacMillan Press, 1975, pp.185-194.

27. Camera, A., Favareto, M., Militano, L., and D'Aprile, F., "Analysis of the Thermal Behaviour of a Machine Tool Table Using the Finite Element Method". Annals of C.I.R.P. Vol. 25, 1976, pp.297-300.

28. Sata, T., Yasui, T., Okabo, N., Suzuki, H., Naritani, T., and Yamoda, T., "Development of Machine Tool Structure Analysis Program", Annals of the CIRP, col. 25, 1976, pp.287-290.

29. Hardt, D.E., Garlow, D.A., and Weinart, J.B., "A Model of Full Penetration Arc Welding for Control System design", Transactions of the ASME, Vol 107, 40-46, Mar 1985.

30. Holman, J.P., "Heat Transfer". 4th ed., McGraw-Hill Book Co. Inc., 1976.

31. Zienkiewicz, O.C., "The Finite Element Method". McGraw-Hill Book Co. (UK) Limited, 3rd Ed., 1977.

32. Hardt, D.E., Garlow, D.A., and Weinart, J.B., "A Model of Full Penetration Arc-Welding for Control System Design", Transactions of the ASME Vol. 107, March 1985.

33. Torteili, D.A., and Wang, Z., "A Systematic Approach to Shape Sensitivity Analysis", Proceedings of the Fifth Annual Inverse Problems in Engineering, Lansing, Michigan, June 11-12, 1992.

34. Stoltz, G., Jr., Numerical solutions to an Inverse Problem of Heat Conduction for Simple Shapes", J.Heat Transfer 82, 20-26 (1960).

35. Burggraf, O.R., "An Exact Solution of the Inverse Problem in Heat Conduction Theory and Applications", Transactions ASME, J.Heat Transfer, August 1964. pp.373-382.

36. Artyukhin, E.A., "Applications of Inverse Methods in Identification of Thermal Processes in Materials and Structures", Presented at the Fifth Annual Inverse Problems in Engineering Seminar, Lansing Michigan, June 11-12, 1992.

37. M.H. Attia, S.Fraser, and M.O.M. Osman, "Computer Simulation of Machine Tools - Part II: Issues Related to the Inverse Heat Conduction Problem", Proceedings of the Fifth International Conference on Production Engineering, Design and Control", Alexandria, Egypt, Dec. 1992.

38. Murio, D.A., and Hinestroza, D., "On the Space Marching Solution of the Inverse Heat Conduction Problem and the Identification of the Initial Temperature Distribution", Presented at the Fifth Annual Inverse Problems in Engineering Seminar, Lansing Michigan, June 11-12, 1992.

39. Alifanov, O.M., and Artyukhin, F.A., "Regularized Numerical Solution of Non-Linear Inverse Heat Conduction Problem", J.Eng Phy 29, 934-938, 1975.

40. Tikhonov, A.N., and Arsenin, V.Y., "Solutions of Ill-Posed Problems", V.H. Winston & Sons, Washington DC (1977).

41. Beck, J.V., Blackwell, B., and St.Clair, C., Jr., "Inverse Heat Conduction: Ill-posed Problems", Wiley-Interscience, New York, 1985.

42. Alifanov, O.M., "Inverse Problems in Investigation of Heat Transfer Processes", Presented at the Fifth Annual Inverse Problems in Engineering Seminar, Lansing Michigan, June 11-12, 1992.

43. Frank, I., "An Application of Least Square Methods to the Solution of the Inverse Problem of Heat Conduction", J.Heat Transfer 85, 378-379, (1963).

44. Thatcher, E.F., and Craparo, J.C., "Deconvolution of Radiometer Signals Using the Whole Domain Function Specification Method", Presented at the Fifth Annual Inverse Problems in Engineering Seminar, Lansing Michigan, June 11-12, 1992.

45. Rauensky, M., and Horsky, J., "Experimental Study of Water Jet Cooling of Hot Steel Surfaces", Presented at the Fifth Annual Inverse Problems in Engineering Seminar, Lansing Michigan, June 11-12, 1992.

46. Beck, V., and Osman, A.M., "Analysis of Quenching and Heat Transfer Processes Using Inverse Heat Transfer Method", Presented at the Fifth Annual Inverse Problems in Engineering Seminar, Lansing Michigan, June 11-12, 1992.

47. Beck, J.V., "Surface Heat Flux Determination Using an Integral Method", Nucl.Eng.Des.7, 170-178 (1968).

48. Twomey, S., "On the Numerical Solution of the Fredhold Integral Equations of the First Kind by the Inversion of the Linear Systems Produced by Quadrature", J.Assoc.Comp.Mach. 10, 97-101, (1963).

49. McCormick, N.J., "A Review of Inverse Radiative Transfer Problems: 1986-1992", Presented at the Fifth Annual Inverse Problems in Engineering Seminar, Lansing Michigan, June 11-12, 1992.

50. LeBrizaut, J.S., Jarny, Y., and Delaunay, D., "Inverse Methods for the Optimal Cure of Elastomers", Presented at the Fifth Annual Inverse Problems in Engineering Seminar, Lansing Michigan, June 11-12, 1992.

51. Kang, S., and Zabaras, N., "Control of Interface Heat Flux and Front Velocity in a Solidification Process Using Minimization Techniques in Finite and Infinite Dimensional Space", Presented at the Fifth Annual Inverse Problems in Engineering Seminar, Lansing Michigan, June 11-12, 1992.

52. Neto, S.A.J., and Ozisk, M.N., "Simultaneous Estimation of Location and Timewise Varying Strength of a Plane Heat Source", Presented at the Fifth Annual Inverse Problems in Engineering Seminar, Lansing Michigan, June 11-12, 1992.

53. Osman, M.O., Beck, V.B., and John, T., "Improvement of the Direct Problem Solver TOPAZ3D by Using the Conjugate Gradient Method", Presented at the Fifth Annual Inverse Problems in Engineering Seminar, Lansing Michigan, June 11-12, 1992.

54. Raynaud, M., "A Quick and Easy Method for the Design of 1-D Solidification Processes". Presented at the Fifth Annual Inverse Problems in Engineering Seminar, Lansing Michigan, June 11-12, 1992.

55. Attia, M.H., "Modelling of Thermal Deformation of Machine Tool Structures: Design and Control Issues", A keynote paper presented at and published in the Proceedings of the International Symposium on Manufacturing and Materials Processing, organized by the International Center of Heat and Mass Transfer, Dubrovnik, Yugoslavia, August, 1990.

56. Bifano, T., and Hosler, J., "Precision Grinding of Ultra-Thin Quartz Wafers", Symposium on Precision Machining, ASME Winter Annual Meeting, Anaheim, Calif., November 8-13, 1992.

57. Sata, T., Takeuchi, Y., Sakamoto, and M., Weck, M., "Improvement of Working Accuracy on NC Lathe by Compensation for the Thermal Expansion of the Tool", Annals of the CIRP Vol. 30, Jan, 1981.

58. Kurtoglu, A., and Sohlenius, G., "The Accuracy Improvement of Machine Tools", Annals of the CIRP Vol. 39, Jan, 1990.

59. Dorf, R.C., "Modern Control Systems", 4th ed. Addison Wesley, Reading Mass., 1986.

60. Bryson, A.E., "Applied Optmal Control, Optimization, Estimation and Control", Blaisdell Publishing Co., Waltham Mass., 1969.

61. Gervarter, W.B., "Artificial Intelligence and Robotics: Five Overviews", Business/Technology Books, Orinda, Ca., 1984.

62. Sata, T., Takeuchi, Y., and Okubo, N., "Control of the Thermal Deformation of a Machine Tool", Proceedings of the 16th International Machine Tool Design and Research Conference, Edited by F. Koenigsberger and S.A. Tobias, MacMillan Press, Manchester, U.K., 1975, pp.203-208.

63. Bates, B.E., and Hardt, D.E., "A Real Time Calibrated Thermal Model for Closed Loop Weld Bead Geometry Control", Journal of Dynamic Systems, Measurement, and Control, Vol. 107, March 1985.

64. Ichimiya, R., Yokoyama, K., and Watanabe, Y., "Experimental Study on Thermal Deformation of Machine Tool", Research Report No. 25, Faculty of Engineering, Niigata University, 1976.

65. Carslaw, H.S., and Jeagar, J.C., "Conduction of Heat in Solids", 2nd ed., Oxford University Press, London, 1959.

66. Luikov, A.V., "Analytical Heat Diffusion Theory", Academic Press, New York, 1968.

67. Michalopoulous, C.D., and Seco, J.J., "Transient Heat Conduction in an Infinite Plate with a Transverse, Circular, Cylindrical Hole", Transactions of the ASME, August 1973, pp 414-416.

68. Sneddon, I.N., "The Use of Integral Transforms", McGraw-Hill, New York, 1972.

69. Segerlind, L.J., "Applied Finite-Element Analysis", 2nd ed., Wiley & Sons, New York, 1984.

70. Sabonnadiere, J.C., "Fi-ite-Element Methods in CAD", North Oxford Academic, London, 1987.

71. Bernadow, M., The Finite-Element Method in Thin Shell Theory: Application to Arch Dam Simulations", Birkhauser, Boston, 1982.

72. Crump, K.S., "Numerical Inversion of Laplace Transforms Using a Fourrier Series Approximation", Journal of the Association for Computing Machinery, vol. 23, No. 1, Jan. 1976, pp 89-96.

73. Kreysig, E., "Advanced Engineering Mathematics", 5th ed., John Wiley & Sons, Toronto, 1986.

APPENDIX 1: DERIVING THE GOVERNING DIFFERENTIAL EQUATION FOR THE TEMPERATURE DISTRIBUTION IN A THIN PLATE

Because of the radial symmetry of the problem, a thin ring of radius r is considered, as shown in figure 7.1. A heat balance on the ring gives:

$$q_i = -k(2\pi rw)\frac{dT^*}{dr}\Big|_i + g(r,t)\,(2\pi rw)\,dr$$

$$q_0 = -k(2\pi rw)\frac{dT^*}{dr}\Big|_0 + h(T^*-T^*_a)\,(2\pi r)\,dr$$

$$= -k(2\pi rw)\frac{dT^*}{dr}\Big|_i - k(2\pi w)\left(r\frac{d^2T^*}{dr^2} + \frac{dT^*}{dr}\right)dr + h(2\pi r)\,(T^*-T^*_a)\,d$$

Where, g(r,t) is the internal heat generation per unit volume
h is the co-efficient of thermal convection on the surface
k is the thermal conductivity
w is the thickness of the plate
T^* is the absolute temperature of the plate

If the net heat into the element is equated to the change in enthalpy then q_i-q_0 is equal to:

$$(2\pi wk)\left(r\frac{d^2T^*}{dr^2}+\frac{dT^*}{dr}\right)dr - 2\pi hr\,(T^*-T^*_a)\,dr + 2\pi rwg(r,t)\,dr = (2\pi rw)\,\rho C$$

This is rearranged to give:

$$T^{*\prime\prime} + \frac{1}{r}T^{*\prime} - \left(\frac{h}{kw}\right)(T^*-T^*_a) + \frac{g(r,t)}{k} - \left(\frac{\rho C}{k}\right)\dot{T}^* = 0 \qquad \text{(A1.1)}$$

Equation (A1.1) can be made homogeneous by defining a new variable $T=T^*-T^*_a$. It can

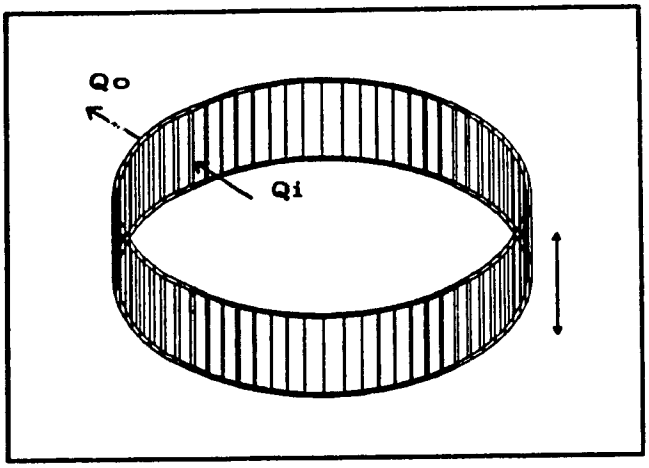

Figure A1.1: Heat Balance on a Differential Element

also be simplified by defining the new parameters:

$$a = \frac{h}{kw} , \qquad \frac{1}{\alpha} = \frac{\rho C_p}{k} \tag{A1.2}$$

Thus, equation (A1.1) becomes:

$$T'' + \frac{1}{r}T' - aT + \frac{g(r,t)}{k} = \frac{1}{\alpha}\dot{T} \tag{A1.3}$$

The internal heat generation term is zero everywhere in the plate, except for the thin ring at $r=r_0$. Thus, if the thickness of the heat generating ring is Δr, then the internal heat generation per unit volume is defined by:

$$\begin{aligned} g(r,t) &= \frac{q(t)}{2\pi r_0 w \Delta r} , \qquad \text{when } r=r_0 \\ &= 0 , \qquad \text{when } r \neq r_0 \end{aligned} \tag{A1.4}$$

Where q(t) is the magnitude of the heat generation.

As $\Delta r \to dr$, it is required that:

$$\int_0^{\infty} g(r,t)\,dr = \int_{r_0^-}^{r_0^+} \frac{q(t)}{2\pi r_0 w dr}\,dr = \frac{q(t)}{2\pi r_1 w} \qquad \text{(A1.5)}$$

Thus, as $\Delta r \to dr$, equation (A1.4) can be expressed as follows:

$$g(r,t) = \frac{q(t)}{2\pi r_0 w}\,\delta(r-r_0) \qquad \text{(A1.6)}$$

Where $\delta(r-r_0)$ is the space impulse function.

The internal heat generation per unit volume is expressed as a heat impulse in the plate at the radius of the generating ring. There is no generation anywhere else in the plate. Assuming that the plate is at ambient temperature at t=0, then the boundary and initial conditions are:

$$\begin{aligned} T &= 0\,, \quad \text{when} \quad t=0 \\ T &= 0\,, \quad \text{when} \quad r=\infty \end{aligned} \qquad \text{(A1.7)}$$

Equation (A1.3) expresses the internal heat generation as a part of the governing equation. An alternate method is to make the heat generation term zero in the governing equation:

$$T'' + \frac{1}{r}T' - aT = \frac{1}{\alpha}\dot{T} \qquad \text{(A1.8)}$$

and specify the heat generation as one of the boundary conditions:

$$\begin{aligned} \frac{dT}{dr} &= -\bar{q}(t) \quad \text{when} \quad r=r_o \\ T &= 0 \quad \text{when} \quad t=0 \\ T &= 0 \quad \text{when} \quad r=\infty \end{aligned} \qquad \text{(A1.9)}$$

where q(t) is the normalized boundary heat generation.

APPENDIX 2: DERIVATION OF THE TRANSIENT TEMPERATURE DISTRIBUTION IN AN INFINITE PLATE WITH A CONVECTIVE BOUNDARY ON THE FACE AND CENTRAL CIRCULAR HEAT SOURCE

Part A: The General Solution

In order to apply the Hankel transformation, the boundary conditions should be incorporated into the governing equation through a heat generation term, as in equation (A2.1):

$$T'' + \frac{1}{r}T' - aT + \frac{g(r,t)}{k} = \frac{1}{\alpha}\dot{T} \qquad \text{(A2.1)}$$

where,

$$T = 0 \quad , \quad \text{when} \quad t=0$$
$$T = 0 \quad , \quad \text{when} \quad r=\infty \qquad \text{(A2.2)}$$

The aT term in equation (A2.1) complicates the governing equation. The first step in the solution is to apply the transformation:

$$T = \Theta e^{-a\alpha t} \qquad \text{(A2.3)}$$

Substituting (A2.3) into equation (A2.1) yields:

$$e^{-a\alpha t}\Theta'' + \frac{1}{r}e^{-a\alpha t}\Theta' - ae^{-a\alpha t}\Theta + \frac{g(r,t)}{k} = \frac{1}{\alpha}(e^{-a\alpha t}\dot{\Theta} - a\alpha e^{-a\alpha t}\Theta)$$

After collecting terms and simplifying, this results in the somewhat simpler equation:

$$\Theta'' + \frac{1}{r}\Theta' + \frac{e^{a\alpha t}}{k}g(r,t) = \frac{1}{\alpha}\dot{\Theta} \qquad \text{(A2.5)}$$

The transformation has eliminated the aT term that was present in equation (A2.1).

It was shown in appendix 1 that the heat generation per unit volume can be

expressed as a space impulse as in equation (A1.6):

$$g(r,t) = \frac{q(t)}{2\pi r_0 w}\,\delta(r-r_0) \qquad \text{(A2.6)}$$

It was also shown previously that the homogeneous solution is reducible to the Bessel equation of order zero in the space co-ordinate. Thus, anticipating the form of the solution, the following integral Hankel transformation is used:

$$\bar{\Theta}(B,t) = \int_0^\infty r\,J_0(Br)\,\Theta(r,t)\,dr \qquad \text{(A2.7)}$$

where B is a new parameter.

The objective of taking the Hankel transformation of the governing partial differential equation is to obtain a solution in the B-domain, and then inverse transform the solution back to the space domain. Unlike the Laplace transformation, the form of the Hankel transformation is variable, so a form must be found which corresponds to a particular problem.

The inverse transformation corresponding to equation (A2.7) is:

$$\Theta(r,t) = \int_0^\infty B\,J_0(Br)\,\bar{\Theta}(B,t)\,dB \qquad \text{(A2.8)}$$

Taking the Hankel transformation of equation (A2.1), and replacing the heat generation term by the expression in equation (A2.6), results in the transformed equation:

$$\int_0^\infty (\bar{\Theta}'' + \tfrac{1}{r}\bar{\Theta}')\,r\,J_0(Br)\,dr + \tfrac{1}{k}\int_0^\infty e^{-a\alpha t}\frac{q(t)}{2\pi r w}\,\delta(r-r_0)\,r\,J_0(BR)\,dr = \tfrac{1}{\alpha}\bar{\Theta}$$

It may be shown [68] that:

$$\int_0^{\infty} (\bar{\theta}'' + \tfrac{1}{r}\bar{\theta}')\, r J_0(Br)\, dr = -B^2\bar{\theta} \qquad \text{(A2.10)}$$

The second integral can be evaluated because of the impulse function:

$$\tfrac{1}{k}\int_0^{\infty} e^{\alpha\alpha t}\frac{q(t)}{2\pi w}\,\delta(r-r_0)\,J_0(Br)\,dr = \frac{q(t)}{2\pi k w}e^{\alpha\alpha t}J_0(Br_0) \qquad \text{(A2.11)}$$

Substituting expressions (A2.10) and (A2.11) into equation (A2.9) results in the following first order equation in the time domain:

$$\dot{\bar{\theta}} + \alpha B^2\bar{\theta} = \frac{\alpha q(t)}{2\pi k w}e^{\alpha\alpha t}J_0(Br_0) \qquad \text{(A2.12)}$$

The Hankel Transformation has reduced the partial differential equation (A2.1) to an ordinary linear differential equation in time. The homogeneous solution is:

$$\bar{\theta} = \bar{C}e^{-\alpha B^2 t} \qquad \text{(A2.13)}$$

where C is a constant of integration. The initial condition T(r,0)=0, is transformed by equations (22) and (25) to $\Theta(B,0)=0$.

The differential equation (A2.12) is in the form:

$$\dot{y} + ay = r(t) \qquad \text{(A2.14)}$$

An expression for the complete solution to equation (A2.14), including the forcing function and the zero initial condition, can be determined by a number of elementary

techniques, including the method of variation of parameters [70]. The expression for the complete solution is given by:

$$y(t) = e^{-at}\int_0^t r(\tau)\, e^{a\tau} d\tau \qquad \text{(A2.15)}$$

Thus, the complete solution to equation (A2.12) is given by:

$$\bar{\Theta} = \frac{e^{-\alpha B^2 t}}{2\pi k w} J_0(Br_0)\int_0^t q(\tau)\, e^{(a+B^2)\alpha\tau} d\tau \qquad \text{(A2.16)}$$

The transformed variable Θ is returned to the space domain by the inverse Hankel transformation from equation (A2.8):

$$\Theta = \frac{1}{2\pi k w}\int_0^\infty B J_0(Br)\, J_0(Br_0)\, e^{-\alpha B^2 t}\int_0^t q(\tau)\, e^{(B^2+a)\alpha\tau} d\tau\, dB \qquad \text{(A2.17)}$$

Finally, replacing Θ by the expression in equation (A2.3) and rearranging yields the expression for the temperature distribution in the plate:

$$T(r,t) = \frac{1}{2\pi k w}\int_0^\infty B J_0(Br)\, J_0(Br_0)\, e^{-(a+B^2)\alpha t}\int_0^t q(\tau)\, e^{(B^2+a)\alpha\tau} d\tau\, dB$$

This is the analytical temperature distribution for a thin infinite plate with a convective boundary condition on the face, and a central, circular ring heat source. The input is an arbitrary boundary generation function q(t).

Part B: The Step Solution

With $q(\tau)$ in equation (34) replaced by $q(\tau)=qU_s(\tau)$, the transformed solution becomes:

$$\bar{\Theta} = \frac{q\,J_0(Br_0)}{2\pi kw\,(B^2+a)}\left[e^{a\alpha t} - e^{-\alpha B^2 t}\right] \qquad \text{(A2.19)}$$

As before, the transformed variable Θ is returned to the space domain by the inverse Hankel transformation from equation (A2.8):

$$\Theta(r,t) = \frac{q}{2\pi kw}\int_0^\infty \frac{B}{B^2+a} J_0(Br_0)\,J_0(Br)\,\left[e^{a\alpha t}-e^{-\alpha B^2 t}\right]\,dB$$

Finally, Θ is replaced by the expression in equation (A2.3) to yield the step solution:

$$T = \frac{q}{2\pi kw}\left[\int_0^\infty \frac{B}{B^2+a} J_0(Br_0)\,J_0(Br)\,dB - e^{-a\alpha t}\int_0^\infty \frac{B}{B^2+a} J_0(Br_0)\,J_0(Br)\,e^{-\alpha B^2 t}dB\right]$$

This is expressed more conveniently in the form:

$$T = \frac{q}{2\pi kw}\left[F_1(r) - e^{-a\alpha t}F_2(r,t)\right] \qquad \text{(A2.21)}$$

where,

$$F_1(r) = \int_0^\infty \frac{B}{B^2+a} J_0(Br_1)\,J_0(Br)\,dB \qquad \text{(A2.21a)}$$

$$F_2(r,t) = \int_0^\infty \frac{B}{B^2+a} J_0(Br_1)\,J_0(Br)\,e^{-\alpha t B^2}dB \qquad \text{(A2.21b)}$$

APPENDIX 3: DERIVATION OF THE TRANSIENT THERMAL DEFLECTION DISTRIBUTION IN AN INFINITE PLATE WITH A CONVECTIVE BOUNDARY ON THE FACE AND CENTRAL CIRCULAR HEAT SOURCE

If there are no external mechanical constraints, then the thermal deflection is related to the temperature distribution by the well-known relation:

$$\epsilon = \alpha_c (T^* - T_0^*) \qquad \text{(A3.1)}$$

where, ϵ is the strain
α_c is the co-efficient of thermal expansion
$(T^*-T_0^*)$ is the change in temperature from the stress free reference temperature.

The differential expression for the strain is given by $\epsilon = d\delta/dr$, where $d\delta$ is the differential thermal deflection, and dr is the differential radius of the plate. If the atmospheric temperature T_a^* is also the unstressed reference temperature T_0^*, then $T^*-T_0^*$ is equal to $T=T^*-T_a^*$, and equation (A3.1) may be expressed as:

$$\delta = \alpha_c \int_0^r T(r, t)\, dr \qquad \text{(A3.2)}$$

where T(r,t) is the theoretical temperature distribution in the plate, derived earlier in the section.

The temperature distribution in an infinite plate, with a central heat source subject to a step input at t=0 seconds, was derived in appendix 2. Substituting the temperature distribution from equation (A2.21) into equation (A3.2):

$$\delta = \alpha_c \int_0^r \frac{q}{2\pi k w} \left[F_1(r) - e^{-a\alpha t} F_2(r, t)\right] dr \qquad \text{(A3.3)}$$

Substituting for F_1 and F_2, and reversing the order of integration, the solution becomes:

$$\delta = \frac{q\alpha_c}{2\pi kw}\left[G_1(r) - e^{-a\alpha t}G_2(r)\right] \qquad \text{(A3.4)}$$

where,

$$G_1 = \int_0^{\infty} \frac{B}{B^2+a} J_0(Br_1) \int_0^{r} J_0(Br)\, dr\, dB \qquad \text{(A3.4a)}$$

$$G_2 = \int_0^{\infty} \frac{B}{B^2+a} J_0(Br_1)\, e^{-\alpha t B^2} \int_0^{r} J_0(Br)\, dr\, dB \qquad \text{(A3.4b)}$$

The integral:

$$I = \int_0^{r} J_0(Br)\, dr \qquad \text{(A3.5)}$$

appears in the expressions for G_1 and G_2. The integral can be evaluated if the bessel function is replaced by its power series expansion:

$$I = \int_0^{r} \sum_{m=0}^{\infty} \left(\frac{Br}{2}\right)^{2m} \frac{(-1)^m}{m!^2}\, dr = \int_0^{r} \sum_{m=0}^{\infty} \frac{(-1)^m}{2^{2m} m!^2} (Br)^{2m}\, dr \qquad \text{(A3.6)}$$

The terms of the Bessel series can be expressed more conveniently in the form:

$$T_m = A(m)\,(Br)^{2m} \qquad \text{(A3.7)}$$

where,

$$A(m) = \frac{(-1)^m}{2^{2m} m!^2}$$

Evaluating the integral in equation (A3.6) yields:

$$I = \int_0^r \sum_{m=0}^{\infty} A(m)\ (\mathbf{B}r)^{2m} dr = \sum_{m=0}^{\infty} A(m)\ \frac{(\mathbf{B}r)^{2m+1}}{2m+1}\ \frac{1}{\mathbf{B}} \Big|_0^r = \sum_{m=0}^{\infty} A(m)\ \frac{(\mathbf{B}r)^{2m+1}}{2m+1} \cdot \frac{1}{\mathbf{B}} - 0$$

This can be rewritten in the form:

$$I = \sum_{m=0}^{\infty} A(m)\ (\mathbf{B}r)^{2m}\ \frac{\mathbf{B}r}{\mathbf{B}(2m+1)} \qquad \text{(A3.9)}$$

Substituting from equation (A3.8), the summation becomes:

$$I = \sum_{m=0}^{\infty} T_m(\mathbf{B}r)\ \frac{r}{2m+1} \qquad \text{(A3.10)}$$

where T_m is the m^{th} term of the Bessel series, from equation (51).

Substituting equation (A3.10) into equations (A3.4a) and (A3.4b), simplifies the expressions for G_1 and G_2:

$$G_1 \quad \int_0^{\infty} \frac{\mathbf{B}}{\mathbf{B}^2+a} J_0(\mathbf{B}r_1)\ \sum_{m=0}^{\infty} T_m(\mathbf{B}r)\ \frac{r}{2m+1}\ d\mathbf{B} \qquad \text{(A3.11a)}$$

$$G_2 = \int_0^{\infty} \frac{\mathbf{B}}{\mathbf{B}^2+a} J_0(\mathbf{B}r_0)\ e^{-\alpha\alpha t}\ \sum_{m=0}^{\infty} T_m(\mathbf{B}r)\ \frac{r}{2m+1}\ d\mathbf{B} \qquad \text{(A3.11b)}$$

where Tm is the m^{th} term of the Bessel series.

APPENDIX 4: CONVERTING THE INFINITE PLATE STEP SOLUTIONS TO THE LAPLACE DOMAIN

The transformation equation from the time domain to the s-domain is given by the integral:

$$F(s) = \int_0^\infty e^{-st} f(t)\, dt \qquad \text{(A4.1)}$$

where s is the complex Laplacian variable.

Part A: Converting the General Thermal Solution to the Laplace Domain

The general thermal solution is transformed to the s-domain by substituting equation (41) into the transformation equation (A4.1):

$$T(s) = \frac{q}{2\pi kw} \int_0^\infty F_1(r) - e^{-a\alpha t} F_2(r,t)\, e^{-st}\, dt \qquad \text{(A4.2)}$$

where F_1 and F_2 are defined by equations (A2.21a) and (A2.21b). The first term, $F_1(r)$, is not a function of time so it can be brought outside of the integration. The second term in equation (A4.2) is the product of two time functions, $F_2(r,t)$ and the exponential $e^{-a\alpha t}$. It is evaluated with the help of the shifting theorem:

$$\int_0^\infty e^{-at} f(t)\, e^{-st} dt = F(s+a) \qquad \text{(A4.3)}$$

where F(s) is the transformation of f(t). The transformation of $F_2(r,t)$ is given by the equation:

$$\int_0^\infty F_2(r,s)\, e^{-st}\, dt = \int_0^\infty\int_0^\infty \frac{B}{B^2+a} J_0(Br_1)\, J_0(Br)\, e^{-\alpha t B^2} e^{-st}\, dB\, dt$$

The integration with respect to time is performed first to yield:

$$\int_0^\infty F_2(r,t)\, e^{-st}\, dt = \int_0^\infty \frac{B}{B^2+a} J_0(Br_1)\, J_0(Br)\, \frac{1}{s+\alpha B^2}\, dB \qquad (A4.5)$$

Applying the shifting theorem to equation (A4.5) yields the transformation of the second term in equation (A4.2):

$$\int_0^\infty e^{-a\alpha t} F_2(r,t)\, e^{-st}\, dt = \int_0^\infty \frac{B}{B^2+a} J_0(Br_1)\, J_0(Br)\, \frac{1}{s+\alpha(a+B^2)}\, dB$$

Thus, the general thermal solution is represented in the s-domain by the equation:

$$T(r,s) = \frac{q}{2\pi kw}\left[\frac{F_1(r)}{s} - \int_0^\infty \frac{B}{B^2+a} J_0(Br_1)\, J_0(Br)\, \frac{1}{s+\alpha(a+B^2)}\, dB\right]$$

where $F_1(r)$ is given in equation (A2.21a).

Part B: Converting the Approximate Temperature Solution for Small Radii to the Laplace Domain

The temperature solution for small radii that is given in equation (44) has two terms. The term on the left is a simple constant that transforms to a multiple of 1/s. The right hand term is more difficult, so it will be handled separately. Neglecting the constant

multiplier, the right hand term is:

$$f(t) = \frac{e^{-at}}{1+bt} \qquad \text{(A4.8)}$$

Equation (A4.8) is transformed to the Laplace domain by substituting in equation (A4.1):

$$F(s) = \int_0^\infty e^{-st} \frac{e^{-at}}{1+bt}\, dt \qquad \text{(A4.9)}$$

Making the substitution u=(1+bt)(s+a)/b, equation (A4.9) becomes:

$$\frac{e^{\frac{s+a}{b}}}{b} \int_{\frac{s+a}{b}}^{\infty} \frac{e^{-u}}{u}\, du \qquad \text{(A4.10)}$$

The s-domain is a complex plane and s is, in general, a complex variable. Substituting s=R+Ij into equation (A4.9) results in the complex line integral:

$$\frac{e^{\frac{R+a}{b}+\frac{I}{b}j}}{b} \int_{\frac{R+a}{b}+\frac{I}{b}j}^{\infty+\infty j} \frac{e^{-u}}{u}\, du \qquad \text{(A4.11)}$$

The complex integration goes from the point s=(R+a)/b + I/bj to s=∞ + ∞ j, as shown in figure 7.10. Since the complex plane is a conservative vector field, the solution is independent of the path of integration. The integration will be performed in two parts, along path one from the starting point to s=∞ + I/bj, and then along path two from s=∞ + I/bj to s=∞ +∞ j. It can be shown that the integration over the second path is zero, so the transformation is given by the integration of the function over path one

only. The parametric representation for the variable u over path one is given by:

$$u(\zeta) = \frac{R+a}{b}\zeta + \frac{I}{b}j \qquad \text{(A4.12)}$$

where zeta goes from $1 \rightarrow \infty$.

The parametrized form of equation (A4.11) is then:

$$\frac{e^{\frac{R+a}{b}}}{b}\int_1^{\infty} \frac{e^{-\left[\frac{R+a}{b}\zeta+\frac{I}{b}j\right]}}{\frac{R+a}{b}\zeta+\frac{I}{b}j}\,\frac{R+a}{b}\,d\zeta \qquad \text{(A4.13)}$$

When equation (A4.13) is simplified, and the substitution $v=\zeta-1$ is made, the expression simplifies to:

$$\frac{R+a}{b^2}\int_0^{\infty} \frac{\left[\frac{R+a}{b}[v+1]-\frac{I}{b}j\right]e^{-\frac{R+a}{b}v}}{\left(\frac{R+a}{b}[v+1]\right)^2+\left(\frac{I}{b}\right)^2}\,dv \qquad \text{(A4.14)}$$

The expression can be further simplified for computational efficiency by defining the parameter:

$$z = \frac{R+a}{b} \qquad \text{(A4.15)}$$

and making the substitution $u=zv$, to yield the expression:

$$\frac{1}{b}\int_0^{\infty} \frac{\left([u+z]-\frac{I}{b}j\right)e^{-u}}{(u+z)^2+\left(\frac{I}{b}\right)^2}\,du \qquad \text{(A4.16)}$$

With the transformation of the right hand term in equation (44) now defined, the

complete transformation of equation (44) can now be expressed as:

$$\frac{qA}{2\pi rw}\left(\frac{R-Ij}{R^2+I^2} + \frac{1}{b}\int_0^{\infty}\frac{\left([u+z]-\frac{I}{b}j\right)e^{-u}}{(u+z)^2+\left(\frac{I}{b}\right)^2}\,du\right) \qquad \text{(A4.17)}$$

APPENDIX 5: INTEGRATION OF THE EXPONENTIAL INTEGRAL AT EXTREME POINTS

The equation that is to be evaluated as I→∞ is given as follows:

$$(1 + I\Im - R\Re) - (R\Im + I\Re)j \qquad \text{(A5.1)}$$

where,

$$\Re = \frac{z^2}{b}\int_0^{\infty} \frac{(u+1)\,e^{-zu}}{(z[u+1])^2+\left(\frac{I}{b}\right)^2}\,du \qquad \text{(A5.2)}$$

and,

$$\Im = \frac{zI}{b^2}\int_0^{\infty} \frac{e^{-zu}}{(z[u+1])^2+\left(\frac{I}{b}\right)^2}\,du \qquad \text{(A5.3)}$$

The first term in equation (A5.1) is F1=1+I$\Im$. This term tends toward zero as I→∞, the task in section *i* is to determine the rate of convergence. In sections *ii* and *iii*, the solutions for $\Re$ and $\Im$ respectively, will be found as I→∞.

Section *i*

It is convenient to simplify the form of F1 in equation (A5.1) so that the derivation is clearer. The simplifications will be removed at the end of the derivation. The simplified form of F1 is:

$$1 - zI^2\int_0^{\infty} \frac{e^{-zu}}{(au)^2+I^2}\,du \qquad \text{(A5.4)}$$

Integrate term 2 with respect to the parameter I, and then differentiate with respect to the same parameter:

$$\frac{d}{dI}\left(\int 1 - zI^2\int_0^{\infty}\frac{e^{-zu}}{(au)^2+I^2}\,du\,dI\right) \qquad (A5.5)$$

This is rearranged to:

$$\frac{d}{dI}\left(I - \int_0^{\infty} ze^{-zu}\left[\int\frac{I^2}{(au)^2+I^2}\,dI\right]du\right) \qquad (A5.6)$$

The term inside the square brackets will be integrated seperately from equation (A5.6). The integral is:

$$\int\frac{I^2}{(au)^2+I^2}\,dI \qquad (A5.7)$$

Make the substitution:

$$\begin{aligned} V^2 &= (au)^2+I^2 \\ V &= \pm\sqrt{(au)^2+I^2} \end{aligned} \qquad (A5.8)$$

and the following equations can be derived:

$$\begin{aligned} I &= \pm\sqrt{v^2-(au)^2} \\ dI &= \frac{\pm V}{\sqrt{v^2-(au)^2}}\,dv \end{aligned} \qquad (A5.9)$$

Substituting equations (A5.8) and (A5.9) into equation (A5.7) yields the integral:

$$\int \frac{\pm\sqrt{v^2-(au)^2}}{v}\,dv \qquad \text{(A5.10)}$$

Equation (A5.10) can be integrated. The solution is:

$$\sqrt{v^2-(au)^2} - au\ Sec^{-1}\left|\frac{v}{au}\right| + C \qquad \text{(A5.11)}$$

Substituting for v yields:

$$I - au\ Sec^{-1}\left|\frac{\sqrt{(au)^2+I^2}}{au}\right| + C \qquad \text{(A5.12)}$$

Now substitute the integrated expression for equation (A5.12) back into equation (A5.6):

$$\frac{d}{dI}\left(I - \int_0^{\infty} ze^{-zu}\left[I - au\ Sec^{-1}\left|\frac{\sqrt{(au)^2+I^2}}{au}\right|\right] + C\,du\right)$$

The integral is divided into two parts:

$$\frac{d}{dI}\left(I - I\int_0^{\infty} ze^{-zu}du + \int_0^{\infty} ze^{-zu}(au)\ Sec^{-1}\left|\frac{\sqrt{(au)^2+I^2}}{au}\right| + C\,du\right)$$

The first integral on the left can be integrated by parts:

$$\int_0^{\infty} ze^{-zu}du = \frac{1}{z} \qquad \text{(A5.15)}$$

When equation (A5.15) is substituted into equation (A5.14), the first two terms on the

left side of equation (A5.14) cancel, resulting in the equation:

$$\frac{d}{dI}\left(\int_0^{\infty}(au)\,ze^{-zu}\,Sec^{-1}\left|\frac{\sqrt{(au)^2+I^2}}{au}\right|+C\,du\right) \qquad (A5.16)$$

Rearranging the variables, and bringing the differentiation into the equation:

$$az\int_0^{\infty}ue^{-zu}\,\frac{d}{dI}\left\{Sec^{-1}\left|\frac{\sqrt{(au)^2+I^2}}{au}\right|+C\right\}du \qquad (A5.17)$$

The differentiation in equation (A5.17) will now be performed, seperately from the main equation. The derivitive is:

$$\frac{d}{dI}\left\{Sec^{-1}\left|\frac{\sqrt{(au)^2+I^2}}{au}\right|+C\right\} \qquad (A5.18)$$

Making the substitution:

$$X=\frac{\sqrt{(au)^2+I^2}}{au} \qquad (A5.19)$$

the solution to equation (A5.18) is:

$$\frac{1}{X\sqrt{X^2-1}}\,\frac{dX}{dI} \qquad (A5.20)$$

Evaluating the derivitive:

$$\frac{dX}{dI}=\frac{I}{au\sqrt{(au)^2+I^2}} \qquad (A5.21)$$

and substituting equations (A5.20) and (A5.21) into equation (A5.18) yields the final

result:

$$\frac{d}{dI}\left\{Sec^{-1}\left|\frac{\sqrt{(au)^2+I^2}}{au}\right| + C\right\} = \frac{au}{(au)^2+I^2} \qquad (A5.22)$$

Equation (A5.22) is substituted back into equation (A5.17) to yield:

$$z\int_0^{\infty}\frac{(au)^2e^{-zu}}{(au)^2+I^2}du$$

The final result is given as follows:

$$1 - zI^2\int_0^{\infty}\frac{e^{-zu}}{(au)^2+I^2}du = z\int_0^{\infty}\frac{(au)^2e^{-zu}}{(au)^2+I^2}du \qquad (A5.23)$$

The proper form of equation (A5.23) is obtained by making the following substitutions:

$$\begin{aligned} u &\rightarrow [u+1] \\ I &\rightarrow \frac{I}{b} \end{aligned} \qquad (A5.24)$$

Which results in:

$$1 - \frac{zI^2}{b^2}\int_0^{\infty}\frac{e^{-zu}}{(a[u+1])^2+\left(\frac{I}{b}\right)^2}du = z\int_0^{\infty}\frac{(a[u+1])^2e^{-zu}}{(a[u+1])^2+\left(\frac{I}{b}\right)^2}du$$

As $I\rightarrow\infty$, the first term in the denominator becomes negligible:

$$F = \frac{z^3b^2}{I^2}\int_0^{\infty}(u+1)^2e^{-zu}du \qquad (A5.26)$$

Expanding the polynomial yields:

$$\frac{z^3b^2}{I^2}\int_0^{\infty} u^2e^{-zu} + 2ue^{-zu} + e^{-zu}\,du \qquad \text{(A5.27)}$$

Each of the integrals in equation (A5.27) can be evaluated by the method of integration by parts. The result is:

$$F = \frac{b^2}{I^2}(z^2 + 2z+2) \qquad \text{(A5.28)}$$

Part *ii*

The integral to be evaluated is:

$$\frac{z^2}{b}\int_0^{\infty} \frac{(u+1)\,e^{-zu}}{(z[u+1])^2+\left(\frac{I}{b}\right)^2}\,du \qquad \text{(A5.29)}$$

As $I\rightarrow\infty$, the left hand term in the denominator becomes negligible, resulting in the equation:

$$\frac{z^2b}{I^2}\int_0^{\infty}(u+1)\,e^{-zu}\,du \qquad \text{(A5.30)}$$

Equation (A5.30) can be integrated by parts to yield:

$$\frac{z^2b}{I^2}\left(\frac{1}{z^2} + \frac{1}{z}\right) \qquad \text{(A5.31)}$$

Part *iii*

The integral to be evaluated is:

$$\frac{zI}{b^2}\int_0^{\infty}\frac{e^{-zu}}{(z[u+1])^2+\left(\frac{I}{b}\right)^2}\,du \qquad \text{(A5.32)}$$

As I→∞, the left hand term in the denominator becomes negligible, resulting in the equation:

$$\frac{z}{I}\int_0^{\infty}e^{-zu}\,du \qquad \text{(A5.33)}$$

The integration is performed to yield:

$$\Im = -\frac{1}{I} \qquad \text{(A5.34)}$$

Part *iv*

Equations (A5.28), (A5.31), and (A5.34) are substituted into equation (A5.1) to yield:

$$\frac{b(bz^2+(2b-R)z+(2b-R))}{(bz+[b-R])^2} + \frac{I}{bz+(b-R)}j \qquad \text{(A5.35)}$$

Substituting

$$z=\frac{R+a}{b} \qquad \text{(A5.36)}$$

into equation (A5.35) yields:

$$\frac{(a+b)R+a^2+2ab+2b^2}{(a+b)^2} + \frac{I}{a+b}j \qquad \text{(A5.37)}$$

APPENDIX 6: DERIVATION OF THE STOLTZ METHOD WITH FIRST ORDER REGULARIZATION

First order regularization was defined in the literature review as the minimization of the following residual with respect to the output variable:

$$S = \sum_{i=1}^{n} (Y_i - T_i)^2 + \alpha \sum_{i=1}^{n-1} (q_{i+1} - q_i)^2 \qquad (A.6.1)$$

The variable Y represents the solution to the direct problem, which can be obtained by any means. For the Stoltz method, the solution to the direct problem is replaced by Duhammel's equation as follows:

$$T_i = T_0 + q_1 \Delta\Phi_i + q_2 \Delta\Phi_{i-1} + \ldots + q_i \Delta\Phi_0 \qquad (A.6.2)$$

Substituting equation (A.6.2) into equation (A.6.1):

$$S = \sum_{i=1}^{n} (T_0 + q_1 \Delta\Phi_i + q_2 \Delta\Phi_{i-1} + \ldots + q_i \Delta\Phi_0 - Y_i)^2 + \alpha \sum_{i=1}^{n-1} (q_{i+1} - q_i)^2$$

Regularization involves the minimization of equation (A.6.3) with respect to q_k. Because differentiation is a linear operator, the two parts of equation (A.6.3) can be treated seperately. First consider S_1, defined by:

$$S_1 = \sum_{i=1}^{n} (T_0 + q_1 \Delta\Phi_i + q_2 \Delta\Phi_{i-1} + \ldots + q_i \Delta\Phi_0 - Y_i)^2 \qquad (A.6.4)$$

or:

$$S_1 = \sum_{i=1}^{n} \left(T_0 + \sum_{j=1}^{i} q_j \Delta\Phi_{i-j+1} - Y_i \right)^2 \qquad (A.6.5)$$

To minimize equation (A.6.5), the partial derivitives with respect to q_1, q_2,...q_n are

equated to zero. The derivitive with respect to q_k is given by:

$$\frac{\partial S_1}{\partial q_k} = 2\sum_{i=1}^{n}\left(T_1 + \sum_{j=1}^{i} q_j \Delta\Phi_{i-j+1} - Y_i\right)\Delta\Phi_{i-k+1} = 0 \qquad (A.6.6)$$

This is rearranged to:

$$\frac{\partial S_1}{\partial q_k} = \sum_{i=1}^{n}(T_0 - Y_i)\,\Delta\Phi_{i-k+1} + \sum_{i=1}^{n}\left(\sum_{j=1}^{i} q_j \Delta\Phi_{1-j+1}\right)\Delta\Phi_{i-k+1} = 0$$

Equation (A.6.7) represents n equations with n unknowns. In matrix form the solution is:

$$[\Phi]\,[q] = [B] \qquad (A.6.8)$$

Where,

$$[\Phi] = \begin{bmatrix} \sum_{I=1}^{N}\Delta\Phi_i\Delta\Phi_i & \sum_{i=2}^{n}\Delta\Phi_i\Delta\Phi_{i-1} & \sum_{i=3}^{n}\Delta\Phi_i\Delta\Phi_{i-2} & \cdots & \sum_{i=n}^{n}\Delta\Phi_i\Delta\Phi_{i-n-1} \\ & \sum_{i=1}^{n-1}\Delta\Phi_i\Delta\Phi_i & \sum_{i=2}^{n-1}\Delta\Phi_i\Delta\Phi_{i-1} & \cdots & \sum_{i=n-1}^{n-1}\Delta\Phi_i\Delta\Phi_{i-n+1} \\ & & \sum_{i=1}^{n-2}\Delta\Phi_i\Delta\Phi_{i-1} & \cdots & \sum_{i=1}^{n-2}\Delta\Phi_i\Delta\Phi_{i-n+2} \\ & & & \cdots & \cdots\cdots \\ \textit{Symmetric} & & & & \\ & & & & \sum_{i=1}^{1}\Delta\Phi_i\Delta\Phi_i \end{bmatrix}$$

and [B] is given by,

$$[B] = \begin{bmatrix} \sum_{i=1}^{n} (Y_i - T_0)\,\Delta\Phi_i \\ \sum_{i=1}^{n-1} (Y_{i+1} - T_0)\,\Delta\Phi_i \\ \sum_{i=1}^{n-2} (Y_{i+2} - T_0)\,\Delta\Phi_i \\ \cdots\cdots \\ \sum_{i=1}^{1} (Y_{i+n-1} - T_0)\,\Delta\Phi_i \end{bmatrix} \qquad (12.3)$$

The second part of the residual is defined by:

$$S_2 = \alpha \sum_{i=1}^{n-1} (q_{i+1} - q_i)^2 \qquad (A.6.11)$$

The partial derivitive of S_2 is then:

$$\frac{\partial S_2}{\partial q_k} = \alpha\left((q_{k+1} - q_k)(-1) + (q_k - q_{k-1})(1)\right) = 0 \qquad (A.6.12)$$

which simplifies to:

$$\begin{aligned} \frac{\partial S_2}{\partial q_k} &= \alpha(-q_{k+1} + 2q_k - q_{k-1}) && \text{if } k \neq 1, n \\ &= \alpha(q_k - q_{k+1}) && \text{if } k = 1 \\ &= \alpha(q_k - q_{k-1}) && \text{if } k = n \end{aligned} \qquad (A.6.13)$$

Adding together the minimization expressions for S_1 and S_2 yields the regularized solution matrix:

$$\begin{bmatrix} \sum_{i=1}^{N} \Delta\Phi_i\Delta\Phi_i + \alpha & \sum_{i=2}^{n} \Delta\Phi_i\Delta\Phi_{i-1} - \alpha & \sum_{i=3}^{n} \Delta\Phi_i\Delta\Phi_{i-2} & \cdots & \sum_{i=n}^{n} \Delta\Phi_i\Delta\Phi_{i-n-1} \\ & \sum_{i=1}^{n-1} \Delta\Phi_i\Delta\Phi_i + \alpha & \sum_{i=2}^{n-1} \Delta\Phi_i\Delta\Phi_{i-1} - \alpha & \cdots & \sum_{i=n-1}^{n-1} \Delta\Phi_i\Delta\Phi_{i-n+1} \\ & & \sum_{i=1}^{n-2} \Delta\Phi_i\Delta\Phi_{i-1} + \alpha & \cdots & \sum_{i=1}^{n-2} \Delta\Phi_i\Delta\Phi_{i-n+2} \\ & & & \cdots & \cdots\cdots \\ \textit{Symmetric} & & & & \sum_{i=1}^{1} \Delta\Phi_i\Delta\Phi_i + \alpha \end{bmatrix}$$